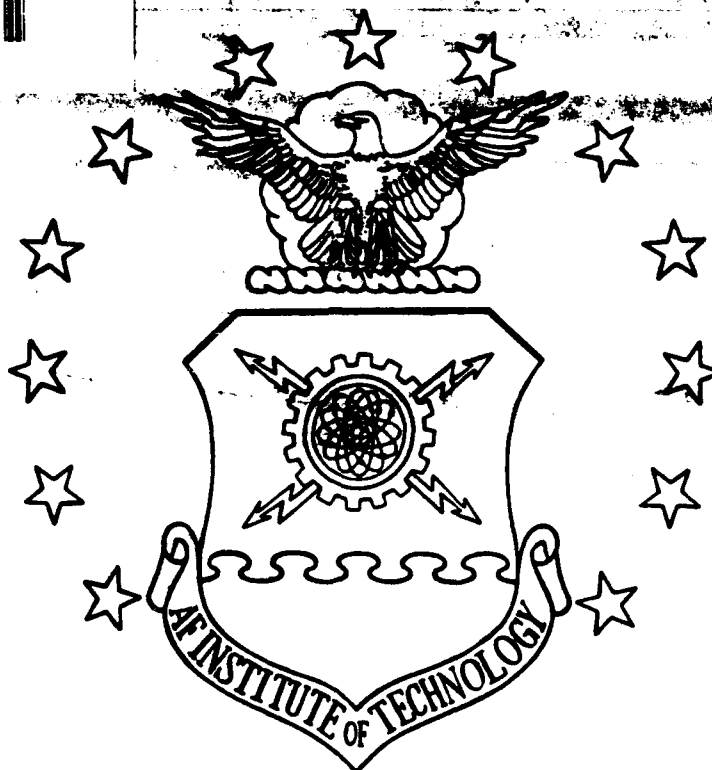


AD-A270 625



1



INVESTIGATION OF THE SENSITIVITY,
SELECTIVITY, AND REVERSIBILITY OF THE
CHEMICALLY-SENSITIVE FIELD-EFFECT
TRANSISTOR (CHEMFET) TO DETECT NITROGEN
DIOXIDE, DIMETHYL METHYLPHOSPHONATE,
AND BORON TRIFLUORIDE

THESIS

Neal Terence Hauschild
Second Lieutenant, USAF

AFIT/GE/ENG/93S-10

DTIC
ELECTE
OCT 12 1993
S B D

93-23815



DISTRIBUTION STATEMENT 2

Approved for public release
Distribution Unlimited

DEPARTMENT OF THE AIR FORCE
AIR UNIVERSITY

AIR FORCE INSTITUTE OF TECHNOLOGY

Wright-Patterson Air Force Base, Ohio

93 10 7 073

AFIT/GE/ENG/93S-10

INVESTIGATION OF THE SENSITIVITY,
SELECTIVITY, AND REVERSIBILITY OF THE
CHEMICALLY-SENSITIVE FIELD-EFFECT
TRANSISTOR (CHEMFET) TO DETECT NITROGEN
DIOXIDE, DIMETHYL METHYLPHOSPHONATE,
AND BORON TRIFLUORIDE

THESIS

Neal Terence Hauschild
Second Lieutenant, USAF

AFIT/GE/ENG/93S-10

Approved for public release; distribution unlimited

AFIT/GE/ENG/93S-10

**INVESTIGATION OF THE SENSITIVITY, SELECTIVITY, AND
REVERSIBILITY OF THE CHEMICALLY-SENSITIVE FIELD-EFFECT
TRANSISTOR (CHEMFET) TO DETECT NITROGEN DIOXIDE,
DIMETHYL METHYLPHOSPHONATE, AND BORON TRIFLUORIDE**

THESIS

Presented to the Faculty of the School of Engineering
of the Air Force Institute of Technology
Air University
In Partial Fulfillment of the
Requirements for the Degree of
Master of Science in Engineering and Environmental Management

Neal Terence Hauschild, BSEE
Second Lieutenant, USAF

September 1993

Approved for public release; distribution unlimited

Acknowledgements

The help and guidance of several individuals aided me to successfully complete this thesis. I would first like to express my gratitude to my thesis advisors, Dr. Victor M. Bright and Dr. Edward S. Kolesar currently at Texas Christian University. Their encouragement, advice, and patience enabled me to accomplish the goals set forth in this difficult project. I also want to thank Maj Mark Mehalic and Maj Paul Ost diek for reviewing my thesis and adding valuable suggestions for improvement. I would also like to thank Mr. William Trop, Capt John Wiseman, Capt Thomas Jenkins, and Capt Dave Sowders for their assistance with using the equipment in the AFIT Electronics and Materials Cooperative Laboratory. Their technical support and interest made this research project possible. I must also thank the members of the Environmental and Engineering Management class and department for their concern and support for me during my time in school.

Neal T. Hauschild

DTIC QUALITY INSPECTED 2

| | |
|--------------------|--------------------------------------------|
| Accession For | |
| NTIS GRA&I | <input checked="checked" type="checkbox"/> |
| DTIC TAB | <input type="checkbox"/> |
| Unannounced | <input type="checkbox"/> |
| Justification | |
| By | |
| Distribution/ | |
| Availability Codes | |
| Dist | Avail and/or Special |
| A-1 | |

Table of Contents

Contents

| | |
|--------------------------------------------------------------------------------------------------------|-----|
| Acknowledgements | 11 |
| List of Figures | v |
| List of Tables | xii |
| List of Chemical Formulas | xiv |
| Abstract | xv |
| | |
| 1 Introduction | 1 |
| 1.1 Background | 1 |
| 1.2 Problem Statement | 6 |
| 1.3 Research Questions | 6 |
| 1.4 Definitions | 7 |
| 1.5 Scope | 10 |
| 1.6 Summary | 13 |
| 1.7 Plan of Development | 13 |
| | |
| 2 Literature Review | 15 |
| 2.1 Introduction | 15 |
| 2.2 Chemical Polymers | 16 |
| 2.3 Solid-State Chemical Sensors | 23 |
| 2.3.1 Piezoelectric Devices | 23 |
| 2.3.2 Surface Acoustic Wave Devices | 26 |
| 2.3.3 Chemiresistor Devices | 29 |
| 2.3.4 Notch Filter | 31 |
| 2.3.5 Charge-Flow Transistor | 33 |
| 2.3.6 IGEFET | 35 |
| 2.4 Significant Findings | 37 |
| 2.5 Summary | 43 |
| | |
| 3 Gas-Delivery System, Phthalocyanine-Gas Interaction, and Electrical Conductivity Modulation | 44 |
| 3.1 Gas-Delivery System | 44 |
| 3.1.1 Mass Flow Controllers | 46 |
| 3.1.2 Test Chamber and Cabinet | 52 |
| 3.2 Phthalocyanine-Gas Interaction | 55 |
| 3.3 Modulation of Electrical Conductivity | 57 |
| 3.4 Summary | 58 |

| | | |
|-------|--------------------------------------------------------------------------------|-----|
| 4 | CHEMFET Design and Evaluation Procedures | 60 |
| 4.1 | Introduction | 60 |
| 4.2 | Design and Fabrication | 60 |
| 4.3 | Evaluation Procedures | 73 |
| 4.3.1 | DC Resistance Measurements | 77 |
| 4.3.2 | Impedance Measurements | 79 |
| 4.3.3 | Gain and Phase Angle Measurements | 80 |
| 4.3.4 | Spectrum Measurements | 80 |
| 4.3.5 | Testing | 82 |
| 4.4 | Summary | 88 |
| 5 | Experimental Results and Analysis | 89 |
| 5.1 | Introduction | 89 |
| 5.2 | Baseline Data | 89 |
| 5.3 | Responses of Copper Phthalocyanine | 97 |
| 5.3.1 | NO ₂ Challenges | 97 |
| 5.3.2 | DMMP Challenges | 111 |
| 5.3.3 | BF ₃ Challenges | 122 |
| 5.3.4 | Other Gases | 128 |
| 5.4 | Responses of Lead Phthalocyanine | 139 |
| 5.4.1 | NO ₂ Challenges | 140 |
| 5.4.2 | DMMP Challenges | 152 |
| 5.4.3 | BF ₃ Challenges | 154 |
| 5.4.4 | Other Gases | 157 |
| 5.5 | Sensitivity | 171 |
| 5.6 | Selectivity | 180 |
| 5.7 | Reversibility | 185 |
| 5.8 | Summary | 187 |
| 6 | Conclusions and Recommendations | 203 |
| 6.1 | Conclusions | 203 |
| 6.2 | Recommendations | 206 |
| | Appendix A: Data Acquisition Software | 209 |
| | Appendix B: Supplemental Graphs for CuPc/NO ₂ Experiments | 216 |
| | Appendix C: Supplemental Graphs for CuPc/DMMP Experiments | 223 |
| | Appendix D: Supplemental Graphs for CuPc/ BF ₃ Experiments | 230 |
| | Bibliography | 237 |
| | Vita | 242 |

List of Figures

| Figure | Title | Page |
|--------|--------------------------------------------------------------------------------------|------|
| 1.1: | Structure of a CHEMFET | 4 |
| 1.2: | Challenge Gas Concentration with Respect to Duration of Exposure | 11 |
| 2.1: | Chemical Structure of Undoped Phthalocyanine | 21 |
| 2.2: | Chemical Structure of Metal-Doped Phthalocyanine | 22 |
| 2.3: | Schematic Diagram of a Quartz Crystal Microbalance | 25 |
| 2.4: | Schematic of a Dual-SAW Delay Line Chemical Vapor Sensor | 28 |
| 2.5: | Schematic of a Chemiresistor Device for Gas Detection | 30 |
| 2.6: | Schematic of a Notch Filter | 32 |
| 2.7: | Schematic of a Modified CFT | 34 |
| 2.8: | Interdigitated Gate Electrode (IGE) Structure .. | 36 |
| 3.1: | Gas Delivery System Used in Previous Research Performed at AFIT | 45 |
| 3.2: | Three Basic Components of a Mass Flow Controller | 50 |
| 3.3: | Improved Gas Delivery System Incorporating Mass Flow Controllers | 53 |
| 3.4: | Diagram of the Test Chamber and Test Cabinet with BNC Connectors for Wiring | 54 |
| 4.1: | Dimensions of an IGE Structure | 62 |
| 4.2: | Optical Photograph of the CHEMFET Device | 64 |
| 4.3: | Optical Photograph of an IGE Structure Coated with 1000 Å of CuPc | 65 |

| | | |
|-------|-----------------------------------------------------------------------------------------------------|-----|
| 4.4: | Bond Pad Diagram | 67 |
| 4.5: | IC Die Layout of Nine Sensing Elements and Connections | 75 |
| 4.6: | Optical Photograph of CHEMFET with Thin-Film Coatings | 76 |
| 4.7: | System Architecture of Instrumentation and GPIB | 78 |
| 4.8: | Voltage Pulse Used for Excitation in the Time Domain and Frequency Domain | 81 |
| 4.9: | Graphical Representation of the Challenge Gas "Plug" | 84 |
| 5.1: | Gain of the CHEMFET Coated with CuPc and PbPc when Exposed to Filtered Air | 94 |
| 5.2: | Change in DC Resistance of IGE Structures Coated with CuPc when Exposed to NO ₂ | 98 |
| 5.3: | Change in Gain at 10 Hz of CuPc CHEMFET when Exposed to NO ₂ | 100 |
| 5.4: | Change in Phase Angle at 10 Hz of CuPc CHEMFET when Exposed to NO ₂ | 102 |
| 5.5: | Time-Domain Response of CuPc CHEMFET Operated at 22°C when Exposed to NO ₂ | 103 |
| 5.6: | Time-domain Response of CuPc CHEMFET Operated at 110°C when Exposed to NO ₂ | 104 |
| 5.7: | Difference Spectra Response of 250 Å Thick CuPc Film when Exposed to NO ₂ | 106 |
| 5.8: | Difference Spectra Response of 550 Å Thick CuPc Film when Exposed to NO ₂ | 107 |
| 5.9: | Difference Spectra Response of 1000 Å Thick CuPc Film when Exposed to NO ₂ | 108 |
| 5.10: | Change in DC Resistance of IGE Structures Coated with CuPc when Exposed to DMMP | 113 |
| 5.11: | Change in Gain at 10 Hz of CuPc CHEMFET when Exposed to DMMP | 115 |

| | |
|---------------------------------------------------------------------------------------------------------------------------------------------|-----|
| 5.12: Change in Phase Angle at 10 Hz of CuPc CHEMFET when Exposed to DMMP | 116 |
| 5.13: Difference Spectra Response of 250 Å Thick CuPc Film when Exposed to DMMP | 118 |
| 5.14: Difference Spectra Response of 550 Å Thick CuPc Film when Exposed to DMMP | 119 |
| 5.15: Difference Spectra Response of 1000 Å Thick CuPc Film when Exposed to DMMP | 120 |
| 5.16: Change in DC Resistance of IGE Structures Coated with CuPc when Exposed to BF_3 | 124 |
| 5.17: Change in Gain at 10 Hz of CuPc CHEMFET when Exposed to BF_3 | 126 |
| 5.18: Change in Phase Angle at 10 Hz of CuPc CHEMFET when Exposed to BF_3 | 127 |
| 5.19: Change in DC Resistance of IGE Structures Coated with CuPc when Exposed to CH_3OH at 70°C | 130 |
| 5.20: Change in Gain at 10 Hz of CuPc CHEMFET when Exposed to CH_3OH at 70°C | 131 |
| 5.21: Change in Phase Angle at 10 Hz of CuPc CHEMFET when Exposed to CH_3OH at 70°C | 132 |
| 5.22: Change in DC Resistance of IGE Structures Coated with CuPc when Exposed to CH_2CHCl at 70°C | 133 |
| 5.23: Change in Gain at 10 Hz of CuPc CHEMFET when Exposed to CH_2CHCl at 70°C | 134 |
| 5.24: Change in Phase Angle at 10 Hz of CuPc CHEMFET when Exposed to CH_2CHCl at 70°C | 135 |
| 5.25: Change in DC Resistance of IGE Structures Coated with CuPc when Exposed to C_2HCl_3 at 70°C | 136 |
| 5.26: Change in Gain at 10 Hz of CuPc CHEMFET when Exposed to C_2HCl_3 at 70°C | 137 |
| 5.27: Change in Phase Angle at 10 Hz of CuPc CHEMFET when Exposed to C_2HCl_3 at 70°C | 138 |

| | |
|--------------------------------------------------------------------------------------------------------------------------|-----|
| 5.28: Change in DC Resistance of IGE Structures Coated with PbPc when Exposed to NO ₂ | 141 |
| 5.29: Change in Gain at 10 Hz of PbPc CHEMFET when Exposed to NO ₂ | 143 |
| 5.30: Change in Phase Angle at 10 Hz of PbPc CHEMFET when Exposed to NO ₂ | 144 |
| 5.31: Time-Domain Response of PbPc CHEMFET Operated at 22°C when Exposed to NO ₂ | 145 |
| 5.32: Time-domain Response of PbPc CHEMFET Operated at 110°C when Exposed to NO ₂ | 146 |
| 5.33: Difference Spectra Response of 300 Å Thick PbPc Film when Exposed to NO ₂ | 148 |
| 5.34: Difference Spectra Response of 650 Å Thick PbPc Film when Exposed to NO ₂ | 149 |
| 5.35: Difference Spectra Response of 1100 Å Thick PbPc Film when Exposed to NO ₂ | 150 |
| 5.36: Change in DC Resistance of IGE Structures Coated with PbPc when Exposed to DMMP | 153 |
| 5.37: Change in Gain at 10 Hz of CuPc CHEMFET when Exposed to DMMP | 155 |
| 5.38: Change in Phase Angle at 10 Hz of PbPc CHEMFET when Exposed to DMMP | 156 |
| 5.39: Change in DC Resistance of IGE Structures Coated with PbPc when Exposed to CH ₃ OH at 70° C | 159 |
| 5.40: Change in Gain at 10 Hz of PbPc CHEMFET when Exposed to CH ₃ OH at 70°C | 160 |
| 5.41: Change in Phase Angle at 10 Hz of PbPc CHEMFET when Exposed to CH ₃ OH at 70°C | 161 |
| 5.42: Change in DC Resistance of IGE Structures Coated with PbPc when Exposed to CO | 162 |
| 5.43: Change in Gain at 10 Hz of PbPc CHEMFET when Exposed to CO | 163 |

| | |
|-------------------------------------------------------------------------------------------------------------------------------------------------------------------------------------------------|-----|
| 5.44: Change in Phase Angle at 10 Hz of PbPc CHEMFET when Exposed to CO | 164 |
| 5.45: Change in DC Resistance of IGE Structures Coated with PbPc when Exposed to CH ₂ CHCl at 70 °C | 165 |
| 5.46: Change in Gain at 10 Hz of PbPc CHEMFET when Exposed to CH ₂ CHCl at 70°C | 166 |
| 5.47: Change in Phase Angle at 10 Hz of PbPc CHEMFET when Exposed to CH ₂ CHCl at 70°C | 167 |
| 5.48: Change in DC Resistance of IGE Structures Coated with PbPc when Exposed to C ₂ HCl ₃ at 70 °C | 168 |
| 5.49: Change in Gain at 10 Hz of PbPc CHEMFET when Exposed to C ₂ HCl ₃ at 70°C | 169 |
| 5.50: Change in Phase Angle at 10 Hz of PbPc CHEMFET when Exposed to C ₂ HCl ₃ at 70°C | 170 |
| 5.51: Normalized Sensitivities Determined from DC Resistance Values for Three Thicknesses of CuPc | 174 |
| 5.52: Normalized Sensitivities Determined from Gain Values for Three Thicknesses of CuPc | 175 |
| 5.53: Normalized Sensitivities Determined from DC Resistance Values for Three Thicknesses of PbPc | 176 |
| 5.54: Normalized Sensitivities Determined from Gain Values for Three Thicknesses of PbPc | 177 |
| 5.55: Difference Spectra Responses of 1100 Å Thick PbPc Film and 1000 Å Thick CuPc Film when Exposed to the Combination of 1 ppm of NO ₂ and 1 ppm of DMMP | 181 |
| 5.56: Difference Spectra Responses of 1100 Å Thick PbPc Film and 1000 Å Thick CuPc Film when Exposed to the Combination of 1 ppm of NO ₂ and 1 ppm of BF ₃ | 182 |

| | |
|-----------------------------------------------------------------------------------------------------------------------------------------------------------------------------|-----|
| 5.57: Difference Spectra Responses of 1100 Å Thick PbPc Film and 1000 Å Thick CuPc Film when Exposed to the Combination of 1 ppm of DMMP and 1 ppm of BF ₃ | 183 |
| 5.58: Reversibility of PbPc Film of Thickness 1100 Å when Exposed to 1 ppm of NO ₂ for Varying Durations | 188 |
| B.1: Low Frequency Response of 1000 Å Thick CuPc Film when Exposed to 10 ppb and 1 ppm of NO ₂ at 22 °C | 217 |
| B.2: Low Frequency Response of 1000 Å Thick CuPc Film when Exposed to 10 ppb and 1 ppm of NO ₂ at 110 °C | 218 |
| B.3: Resistance versus Time of 1000 Å Thick CuPc Film when Exposed to 1 ppm of NO ₂ at 22°C | 219 |
| B.4: Resistance versus Time of 1000 Å Thick CuPc Film when Exposed to 1 ppm of NO ₂ at 110°C | 220 |
| B.5: Resistance Part of the Impedance of 1000 Å Thick CuPc Film when Exposed to 1 ppm of NO ₂ at 22 °C | 221 |
| B.6: Reactance Part of the Impedance of 1000 Å Thick CuPc Film when Exposed to 1 ppm of NO ₂ at 22 °C | 222 |
| C.1: Low Frequency Response of 1000 Å Thick CuPc Film when Exposed to 10 ppb and 1 ppm of DMMP at 22 °C | 224 |
| C.2: Low Frequency Response of 1000 Å Thick CuPc Film when Exposed to 10 ppb and 1 ppm of DMMP at 110 °C | 225 |
| C.3: Resistance versus Time of 1000 Å Thick CuPc Film when Exposed to 1 ppm of DMMP at 22 °C ... | 226 |
| C.4: Resistance versus Time of 1000 Å Thick CuPc Film when Exposed to 1 ppm of DMMP at 110 °C .. | 227 |
| C.5: Resistance Part of the Impedance of 1000 Å Thick CuPc Film when Exposed to 1 ppm of DMMP at 22 °C | 228 |

| | | |
|------|----------------------------------------------------------------------------------------------------------------------------|-----|
| C.6: | Reactance Part of the Impedance of 1000 Å Thick CuPc Film when Exposed to 1 ppm of DMMP at 22 °C | 229 |
| D.1: | Low Frequency Response of 1000 Å Thick CuPc Film when Exposed to 10 ppb and 1 ppm of BF ₃ at 22 °C | 231 |
| D.2: | Low Frequency Response of 1000 Å Thick CuPc Film when Exposed to 10 ppb and 1 ppm of BF ₃ at 110 °C | 232 |
| D.3: | Resistance versus Time of 1000 Å Thick CuPc Film when Exposed to 1 ppm of BF ₃ at 22°C | 233 |
| D.4: | Resistance versus Time of 1000 Å Thick CuPc Film when Exposed to 1 ppm of BF ₃ at 110°C | 234 |
| D.5: | Resistance Part of the Impedance of 1000 Å Thick CuPc Film when Exposed to 1 ppm of BF ₃ at 22 °C | 235 |
| D.6: | Reactance Part of the Impedance of 1000 Å Thick CuPc Film when Exposed to 1 ppm of BF ₃ at 22 °C | 236 |

List of Tables

| Table | Title | Page |
|-------|--------------------------------------------------------------------------------------------------------------------------------------|------|
| 2.1: | Significant Findings on Sensitivity and Reversibility for Given MPC Thin-Films and Challenge Gas Concentrations | 39 |
| 4.1: | Critical Dimensions of the Interdigitated Gate Electrode | 63 |
| 4.2: | Bond Pad Connections for the CHEMFET die | 68 |
| 4.3: | IGEFET Configuration Matrix of the Chemically-Sensitive Thin Films | 74 |
| 4.4: | Challenge Gas Concentration Used | 87 |
| 5.1: | Resistance Values for Uncoated Sensing Elements at 22 °C | 91 |
| 5.2: | Resistance Values for Coated Sensing Elements at 22 °C | 91 |
| 5.3: | Resistance Values for Uncoated Sensing Elements at 110 °C | 93 |
| 5.4: | Resistance Values for Coated Sensing Elements at 110 °C | 93 |
| 5.5: | Sampled Frequency Values for Zero-Crossing Points of the Normalized Difference Spectra of CuPc when exposed to NO ₂ | 109 |
| 5.6: | Sampled Frequency Values for Zero-Crossing Points of the Normalized Difference Spectra of CuPc when exposed to DMMP | 121 |
| 5.7: | Sampled Frequency Values for Zero-Crossing Points of the Normalized Difference Spectra of PbPc when exposed to NO ₂ | 151 |
| 5.8: | Challenge Gases and Their Lowest Detectable Concentration for CuPc and PbPc | 172 |
| 5.9: | Determined Correlations Between Sensitivities .. | 179 |
| 5.10: | Selectivity for Challenge Gas Combinations | 184 |

| | |
|-------------------------------------------------------------------------------------------------------------------------|-----|
| 5.11: Reversibility for the Highest Concentration of the Challenge Gases at 22 °C | 186 |
| 5.12: Reversibility for the Highest Concentration of the Challenge Gases at 110 °C | 186 |
| 5.13: Findings on Sensitivity, Selectivity, and Reversibility for the Investigated CuPc- Coated Microsensor | 190 |
| 5.14: Findings on Sensitivity, Selectivity, and Reversibility for the Investigated PbPc- Coated Microsensor | 196 |

List of Chemical Formulas

| Chemical Compound | Chemical Formula |
|--------------------------------------|-------------------------------------------------------------------------------|
| Hydrogen | H ₂ |
| Chlorine | Cl ₂ |
| Nitrogen | N ₂ |
| Nitrogen Oxide | NO |
| Nitrogen Dioxide | NO ₂ |
| Sulfur Dioxide | SO ₂ |
| Ammonia | NH ₃ |
| Dimethyl Methylphosphonate (DMMP) | C ₃ H ₉ PO ₃ |
| Diisopropyl Methylphosphonate (DIMP) | C ₅ H ₁₅ C ₂ H ₂ PO ₃ |
| Diisopropyl Fluorophosphate (DFP) | C ₄ H ₁₂ C ₂ H ₂ PFO ₃ |
| Boron Trifluoride | BF ₃ |
| Methanol | CH ₃ OH |
| Carbon Monoxide | CO |
| Chloroethylene (vinyl chloride) | CH ₂ CHCl |
| Trichloroethylene (TCE) | C ₂ HCl ₃ |
| Tetrachlorethylene (PCE) | C ₂ Cl ₄ |
| Copper | Cu |
| Lead | Pb |
| Nickel | Ni |
| Magnesium | Mg |
| Cobalt | Co |
| Copper Phthalocyanine (CuPc) | C ₃₂ H ₁₈ N ₈ Cu |
| Lead Phthalocyanine (PbPc) | C ₃₂ H ₁₈ N ₈ Pb |

Abstract

This study investigated the sensitivity, selectivity, and reversibility of a chemically-sensitive field-effect transistor (CHEMFET) gas microsensor. The sensitivity, selectivity, and reversibility were computed from response changes generated from electrical conductivity modulations. Various physical operating parameters were tested to determine which produced the most significant sensitivity, selectivity, and reversibility when exposed to challenge gases. The variable operating parameters included: thin-film material, thin-film thickness, challenge gas specie, challenge gas concentration, and operating temperature. Copper phthalocyanine (CuPc) and lead phthalocyanine (PbPc) were used as thin-films which ranged in thicknesses from 250Å to 1100Å. The challenge gases included: nitrogen dioxide (NO₂), dimethyl methylphosphonate (DMMP), boron trifluoride (BF₃), methanol (CH₃OH), carbon monoxide (CO), vinyl chloride (CH₂CHCl), and trichloroethylene (C₂HCl₃). The concentrations of the gases ranged from 10 parts per billion (ppb) to 50 parts per million (ppm). Tests performed at 22°C and 110°C (70°C for the latter four gases) revealed that CuPc was the most sensitive to DMMP and BF₃, whereas PbPc was the most sensitive to NO₂, CH₃OH, CO,

CH_2CHCl , and C_2HCl_3 . The thin films were most selective to NO_2 followed by DMMP. The CHEMFET was not very selective for BF_3 when combined with other challenge gases. The CHEMFET was fully reversible for both thin-film types and all challenge gases. The time duration for full reversibility increased with increasing challenge gas concentrations and increasing time of exposure. At higher operating temperatures, the reversibility improved; however, the sensitivity and selectivity responses were diminished.

INVESTIGATION OF THE SENSITIVITY, SELECTIVITY, AND
REVERSIBILITY OF THE CHEMICALLY-SENSITIVE FIELD-EFFECT
TRANSISTOR (CHEMFET) TO DETECT NITROGEN DIOXIDE,
DIMETHYL METHYLPHOSPHONATE, AND BORON TRIFLUORIDE

CHAPTER 1

1 Introduction

Our rapidly developing world is faced with many environmental challenges. The efforts to maintain and improve the world's "standard of living" from a technological perspective has resulted in the contamination of the air, water, and land. Exposing the environment to toxic chemicals has threatened the living and working conditions of man. Prior to the past three decades, technological innovations for monitoring and protecting the environment have been limited.

1.1 Background

Increased concern for the health and safety issues involved with degrading environment has prompted the development of technologies to detect, quantify, monitor,

and remediate environmental toxins. As progress is made in some areas, new problems are discovered; these new environmental challenges tend to involve less visible pollutants that are also more persistent. Emissions into the air and water may persist for decades. Furthermore, various chemical compounds once thought to be harmless have now been determined to be toxic, even in trace amounts.

Many chemical compounds which have been determined to be hazardous are in the form of gases or vapors. The detection and measurement of these gases and vapors in the atmosphere, as well as in closed ecological systems, have merited significant attention. Much of this attention has been focused on health and safety issues, primarily through additional restrictive federal regulations, and the economic liabilities for non-compliance are becoming more influential.

The military is particularly interested in detecting and monitoring regulated toxic gases or corrosive vapors that pose a threat to personnel and electronic systems. In this time of budget constraints, the military needs to find economical, as well as reliable devices to detect and quantify toxic gases. Chemical sensors will have widespread applications in the military, such as detecting chemical-warfare nerve agents, monitoring emissions from point sources, such as air strippers and coke ovens, and

monitoring the concentrations of corrosive vapors around aircraft maintenance centers.

Solid-state chemical sensors are projected to be a promising technology for detecting toxic gas species. These devices have several potential advantages compared to the current detection instrumentation. Solid-state chemical sensors would be less expensive, smaller, and easier to operate. Many studies are presently being performed on solid-state chemical sensor technologies.

One such device used to sense gaseous compounds, the chemically-sensitive field-effect transistor (CHEMFET), has been investigated at the Air Force Institute of Technology (AFIT) [8, 9, 14, 20, 23, 35]. The CHEMFET (Figure 1.1) is a conventional metal-oxide-semiconductor field-effect transistor (MOSFET) which has an interdigitated gate electrode (IGE) structure, as opposed to a typical solid polysilicon gate. The IGE structure consists of a driven gate electrode and a floating gate electrode. A chemically-sensitive film deposited over these two electrode structures electrically couples the system.

The chemical state of the thin-film IGE coating determines its electrical conductivity which is subsequently transduced as a change in the MOSFET's drain current. If the driven gate electrode of the IGE structure is excited with a pulsed voltage, it will produce a corresponding

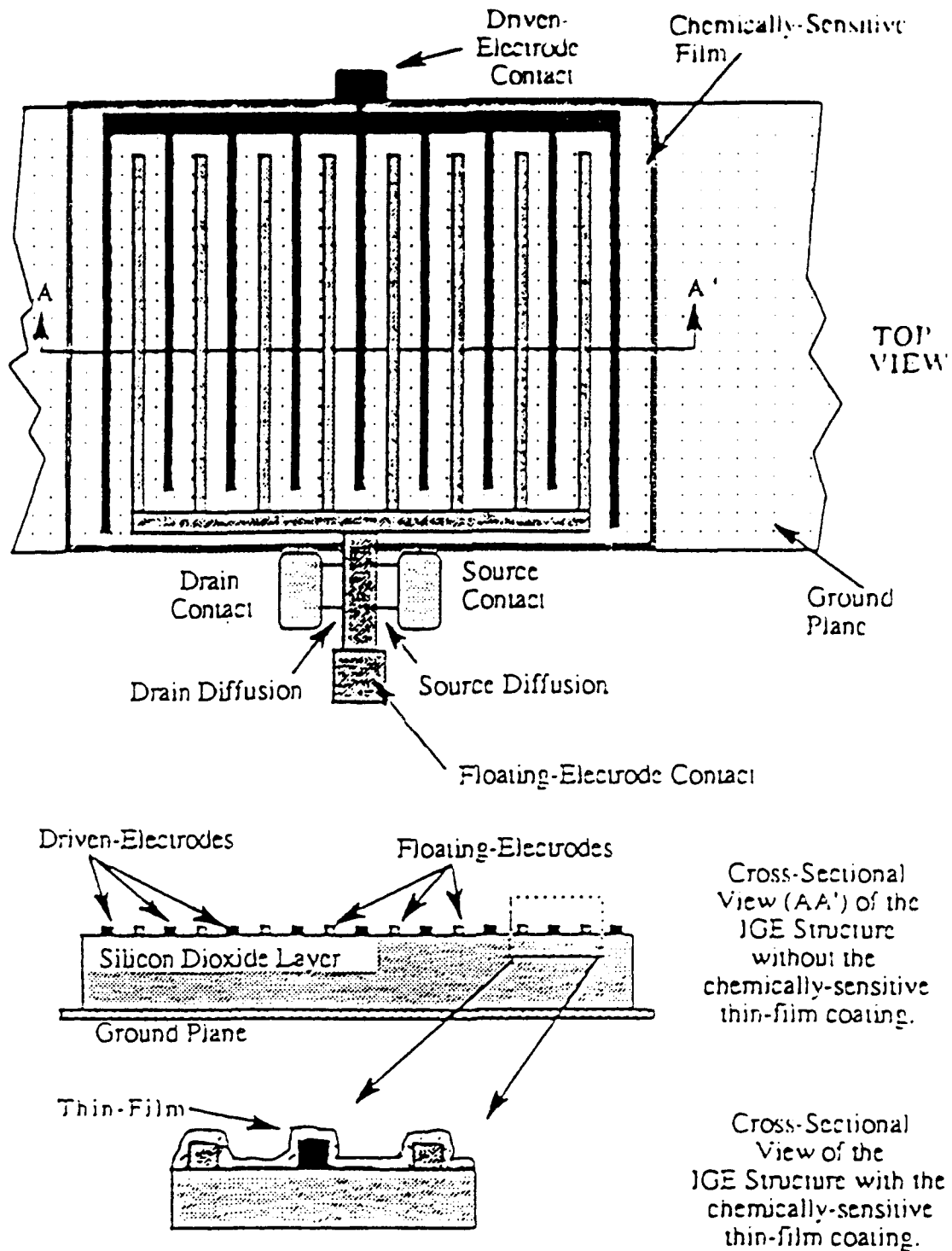


Figure 1.1: Structure of a CHEMFET [8].

response characteristic in the drain current of the MOSFET. In the presence of a detectable gas or vapor, the chemical state of the thin film is altered; thus, the film's electrical conductivity change induces a corresponding change in MOSFET's drain current. Hence, the changes in the gas-sensitive thin-film's electrical impedance can be detected via the corresponding changes in the drain current of the CHEMFET.

The CHEMFET has been demonstrated to detect oxides of nitrogen and organophosphorus compounds [8, 9, 14, 20, 23, 35]. These two groups of chemical compounds are of particular interest to the United States Air Force. Nitrogen oxides (NO_x), particularly nitric oxide (NO) and nitrogen dioxide (NO_2), are known to be corrosive to electrical circuits [24]. In modern weapon systems, an electrical malfunction can be detrimental and even fatal. The family of organophosphorus compounds include chemical-warfare nerve agents, as well as less toxic pesticides which are also harmful to humans [21]. Both species of organophosphorus compounds can severely impair personnel. The detection of low levels of these gases enables protective measures to be taken to minimize their potential damage to personnel and electronic equipment.

Another critical group of contaminants are the volatile organic compounds (VOCs). Vinyl chloride (CH_2CHCl) and

trichloroethylene (C_2HCl_3) are two examples of VOCs which are by-products of operations performed by the Air Force, and they are known to be toxic to humans. Furthermore, the emission of VOCs is Federally regulated. Thus, it is necessary to be able to detect the presence of small quantities of these chemical compounds.

1.2 Problem Statement

The purpose of this thesis is to evaluate the sensitivity, selectivity, and reversibility of a CHEMFET, which can be used to detect toxic gases *in situ*.

1.3 Research Questions

1. Which chemically-sensitive film and physical operating parameters produce the most significant sensitivity when exposed to the challenge gases?
2. Which chemically-sensitive film and physical operating parameters display the most significant selectivity when exposed to the challenge gases?
3. Which chemically-sensitive film and physical operating parameters exhibit the most complete degree of reversibility when exposed to the challenge gases?

1.4 Definitions

The CHEMFET is coated with a chemically-sensitive thin film. This film is a metal-doped phthalocyanine (MPc) compound. Two thin-film candidates will be used in this research effort: copper phthalocyanine (CuPc) and lead phthalocyanine (PbPc). These thin films are anticipated to chemically react with the challenge gases, which represent the toxic or corrosive vapors that need to be detected. The gases that will be screened in this research include: nitrogen dioxide (NO_2), dimethyl methylphosphonate (DMMP), boron trifluoride (BF_3), carbon monoxide (CO), methanol (CH_3OH), trichloroethylene (C_2HCl_3), and chloroethylene (CH_2CHCl).

Given a well-defined pulsed-voltage waveform (for example, a pulse that is 2 to 5 μsec in duration, 2 to 6 volts in amplitude, and a repetition frequency ranging from 200 to 1000 Hertz) as the electrical excitation for the CHEMFET, the variables which have an effect on the electrical output characteristics will include the type of film and the physical operating parameters. These operating parameters include at least four independent variables: the film thickness, the operating temperature, the type of challenge gas, and the concentration of the challenge gas. All possible combinations of these variables will be

evaluated to determine which combination produces optimal sensitivity, selectivity, and reversibility of a CHEMFET.

The sensitivity, selectivity, and reversibility can be defined in terms of the measurable parameters produced by the CHEMFET. The measurable response parameters include the gain and phase of the device, the electrical impedance of the IGE, the direct current resistance of the IGE, and the CHEMFET's voltage-pulse response in the time domain and the frequency domain.

The mean value of each measurable response parameter will be used to describe the behavior (i.e., sensitivity, selectivity, and reversibility) for a specific set of physical operating variables (i.e., film type, film thickness, temperature, challenge gas, and challenge gas concentration). Equation (1.1) calculates the mean value (x) of a particular measured parameter (p) from the collected data points:

$$x(p) = \left(\frac{1}{N}\right) \sum_{i=1}^N p_i \quad (1.1)$$

where N is the number of data points, and p_i is a discrete measured parameter. Using the calculated mean values of the measurable parameters, a comparison can be made between the challenge gas values and the baseline values to determine

the CHEMFET's relative sensitivity, selectivity, and reversibility.

The sensitivity of the CHEMFET is a relative measure of the lowest concentration of a challenge gas that can be detected [8]. The sensitivity can be calculated with respect to the mean baseline response of the sensor when exposed to room air relative to a particular challenge gas concentration. Equation (1.2) formulates the normalized sensitivity of the CHEMFET operating under a set of particular variables:

$$\text{Sensitivity}_{x(p)} = \frac{[X_{\text{baseline}} - X_{\text{challenge gas}}]}{X_{\text{baseline}}} \quad (1.2)$$

Selectivity is the CHEMFET's ability to distinguish among various challenge gases [2]. The selectivity of the CHEMFET can be determined by comparing the measurable parameters for each challenge gas. Equation (1.3) quantitatively describes the selectivity of the CHEMFET for a particular challenge gas (b) relative to another challenge gas (a) with the same concentration:

$$\text{Selectivity}_{x(p)} = \frac{[X_{\text{challenge gas(a)}} - X_{\text{challenge gas(b)}}]}{X_{\text{challenge gas(a)}}} \quad (1.3)$$

The reversibility parameter describes the system's ability to return to its initial state after being exposed to a particular challenge gas. The value for the reversibility of the CHEMFET will be quantified relative to time. For this relative measure, the challenge gas type will be the same, but the concentration will be varied. This relationship can be expressed mathematically as Equation (1.4):

$$\text{Reversibility}_{\text{gas}} = \frac{[x_1(c_1, t_1) - x_2(c_2, t_2)]}{[x_3(c_1, t_3) - x_2(c_2, t_2)]} \quad (1.4)$$

where c_1 is the initial concentration of the challenge gas, and c_2 is the concentration of the challenge gas "plug". A generic relationship between challenge gas concentration and time is shown in Figure 1.2. The points in time when the measurements are collected are represented by t_1 , t_2 , and t_3 . Time t_1 and t_3 represent the purge cycle for the CHEMFET, and t_2 corresponds to an instant of time during the exposure portion of the challenge gas cycle.

1.5 Scope

The work in this thesis involved the evaluation of CuPc and PbPc as the chemically-sensitive thin-film candidates. The challenge gases were limited to NO_2 , DMMP, and BF_3 .

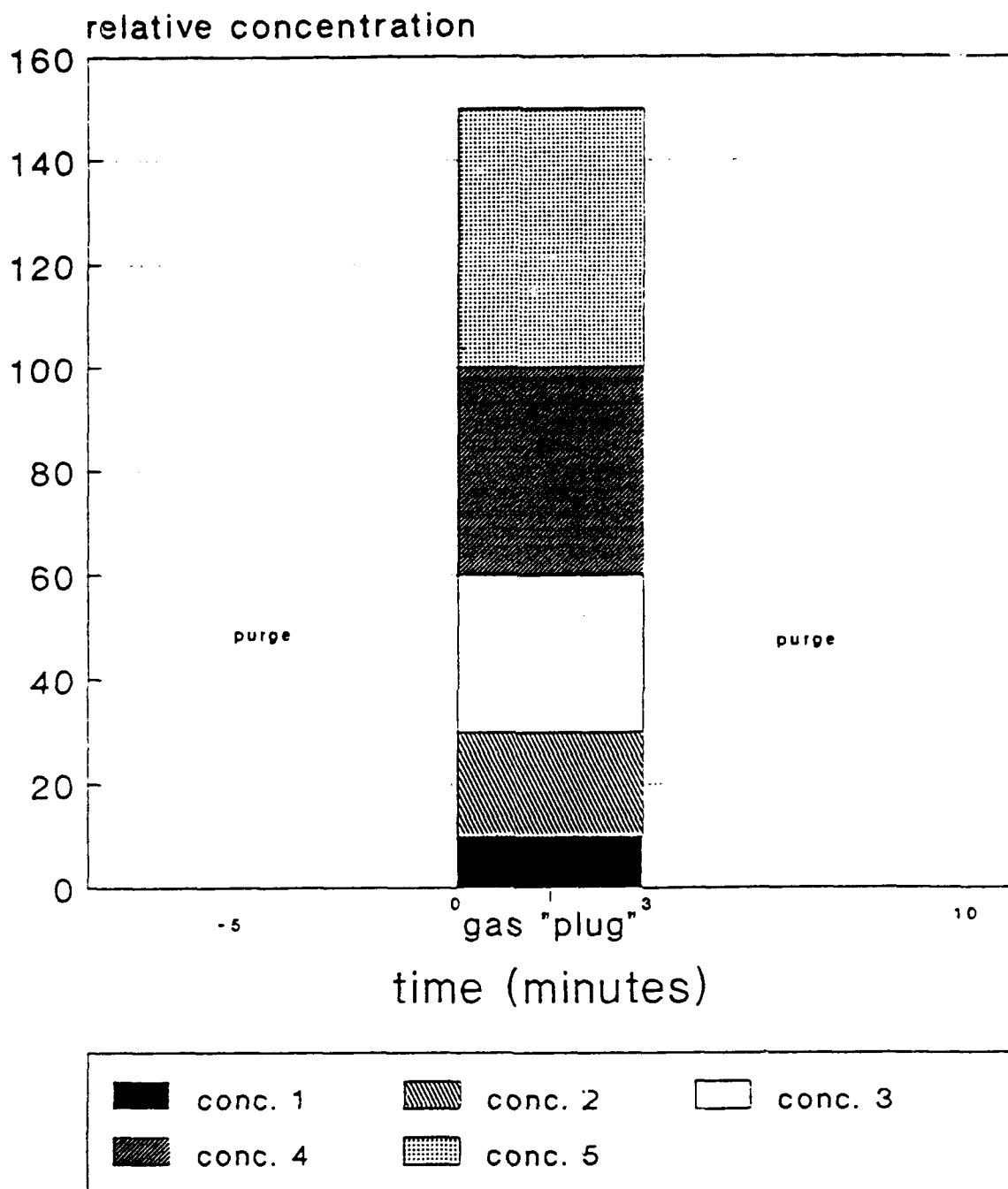


Figure 1.2: Challenge Gas Concentration with Respect to Duration of Exposure.

Single concentrations of CH_3OH , CO , C_2HCl_3 , and CH_2CHCl were screened to determine if the CHEMFET can detect these environmentally toxic gases. The CHEMFET's response was measured with respect to three different film thicknesses, two operating temperatures, and three to five challenge gas concentrations. This research effort used a 3×3 array of CHEMFET sensing elements based on the IGE structure designed, developed, and tested in previous research projects at AFIT [8, 9, 14, 20, 23, 35].

Similar to previous experiments which investigated the CHEMFET [8, 9, 14, 20, 23, 35], it was assumed that the CHEMFET is a pseudo-linear, time-invariant system for small ranges of input values. This assumption enabled the responses from two input signals to be summed to equal the net response of the corresponding summed inputs. For a time-invariant system, the transfer function is a constant with respect to time. The CHEMFET can only be considered as a time-invariant system since the sensor's transfer function is only known to change with respect to the chemical state of the thin film, which itself is time dependent. Maintaining a short time period between measurements relative to the rate of change in the chemically-sensitive film, (pseudo) time-invariant principles could be applied to the CHEMFET.

1.6 Summary

The synergistic combination of microelectronics and organic chemistry affords a unique opportunity to develop a simple and rugged, yet sensitive and selective, device to detect gas compounds that are known to pose a threat to the health and safety of personnel and/or cause damage to electronic systems. The CHEMFET sensor is designed to detect trace concentrations of nitrogen oxides and organophosphorus compounds. It utilizes metal-doped phthalocyanines, such as CuPc and PbPc, as the chemically-sensitive component of the gas sensor.

For each challenge gas (NO_2 , DMMP, and BF_3), this research effort attempted to identify the most sensitive, selective, and reversible combination of chemically-sensitive film, film thickness, operating temperature, and challenge gas concentration. Furthermore, the CHEMFET's ability to detect a fixed concentration of CH_3OH , CO , C_2HCl_3 , and CH_2CHCl was investigated.

1.7 Plan of Development

This chapter reviewed the background and motivation for this investigation. The research objectives and goals were stated and carried out hence-forth. Chapter 2 reviews the current literature concerning gas-sensing devices incorporating chemically-sensitive polymers with

microelectronic technology. Significant findings are presented as a basis for the development of test parameters for the research conducted in this thesis. Chapter 3 discusses the design of the gas-delivery system. The physical characteristics of the gas-phthalocyanine interactions which modulate the film's electrical conductivity are also discussed. Chapter 4 describes the experimental methodology which includes the design and fabrication of the CHEMFET, the electrical parameters which were measured, and the instruments used to collect and record these measurements. Analysis of the data and significant findings are presented in Chapter 5. Chapter 6 presents the conclusions for this investigation and recommendations for further research.

Chapter 2

2 Literature Review

2.1 Introduction

Significant attention has been focused on the development of compact and inexpensive gas-sensing devices which possess a high degree of sensitivity, selectivity, reversibility, and reliability. A variety of solid-state chemical sensors have been investigated over the past decade, and several technologies have shown themselves to be feasible candidates to replace the "traditional" technologies employed for gas detection and quantification. Two of the traditional technologies include gas chromatography (GC) and mass spectrometry (MS) [26].

A variety of chemical sensors have been developed that use microelectronics as the basic technology. A major feature of these devices is that they incorporate a chemically-sensitive polymer or metal oxide to detect the gaseous compounds of interest and to transduce the presence of the chemical moiety into a useful electronic signal [10]. Numerous quantitative gas sensor studies have been successfully accomplished to detect organic and inorganic gas species [27]. The chemical polymers and metal oxides have been used with thick-film and thin-film morphologies.

At least six devices that incorporate chemically-sensitive films have been successfully used to detect nitrogen dioxide and one or more organophosphorus compounds [10, 17, 28]. The chemically-sensitive devices that will be critically reviewed include: piezoelectric sensors [10, 19], surface acoustic wave (SAW) detectors [24], chemiresistors [11, 12], notch filters [13], the charge-flow transistor (CFT) [9], and the interdigitated gate electrode field-effect transistor (IGFET) [8, 9, 14, 23, 35].

This chapter focuses upon and presents a review of the current literature concerning the chemical polymers and metal oxides used to react with specific challenge gases and the theory and operation of the particular solid-state chemical sensor technology. The gas detectors reviewed differ primarily by the mechanisms employed to detect a change in electrical conductivity, the bulk dielectric constant, or the bulk permeability. The literature review summarizes the significant findings and concludes with the historical basis for using the IGFET sensor that is coated with a metal-doped phthalocyanine thin-film to realize a sensitive, selective, and reversible gas detector.

2.2 Chemical Polymers

Various polymers have been used with solid-state chemical sensors. The chemical state of the polymer is

altered when an interaction occurs with another chemical specie that causes a physical interaction or chemical reaction to occur. A change in the structure of the polymer leads to detectable deviations in the polymer's electrical conductivity [10]. However, there is a lack of experimental data and theoretical analyses concerning the relationship between the surface adsorption of gases on a polymer and the subsequent electrical changes that can be measured. To study gas adsorption and electrical changes, limited studies have been performed with single crystals and compressed discs made of metal oxides [27]. However, the reliability of the measured results is questionable. The primary problem with the single crystals and the compressed discs is ensuring that a good electrical contact exists between the organic materials and the metal electrodes. To overcome this limitation, thin films, which are easier to use and deposit on an electrode array, can be used [27]. Furthermore, these thin films are not limited to organic materials, but can also be realized from metal oxides and organic semiconducting materials [7].

Chemically-sensitive films can either have a thick-film or thin-film morphology. The role of metal oxides and organic semiconducting polymers as chemically-sensitive films deposited on physical and chemical sensors has been shown to be reliable and accurate [7]. Thick-film

technology (TFT) offers flexibility with choice of materials, such as organic and inorganic materials, flexibility with the choice of design and deposition procedures, and easy integration with electronic circuits and packaging [31]. A major disadvantage to the TFT is the lack of sensitivity to small concentrations of challenge gases due to the layering effect of the individual molecules. On the other hand, thin-films can be used to improve the sensitivity of a gas sensor. However, the choice of materials and the method of deposition on the electronic device are more limited. For example, the Langmuir-Blodgett (LB) or vacuum sublimation [27] techniques are the most practical, but the techniques of spraying, dipping, and sputtering are also viable. Not only can thin-films detect very small gas concentrations, but the resulting effects on the film when exposed to an analyte gas can be more quickly reversed at a lower temperature compared to that associated with a thick-film [27].

Inorganic and organic chemically-sensitive films have been used in experiments to detect particular gases. Schiede and Guilbault evaluated chemically-sensitive coatings of inorganic salts such as ferric chloride to detect organophosphorus compounds [19]. However, a more sensitive and selective family of film candidates incorporates metal oxides. Tin dioxide, zinc oxide, and

cuprous oxide films have been successfully evaluated to detect organophosphorus compounds [4, 11, 13, 18]. A variety of the studies have been conducted in relation to gas adsorption on binary metal oxides. The chemical sensor technologies presently available are based on polycrystalline thick films of oxides which are doped with minute levels of metals such as platinum, copper, silver, or gold [16]. These inorganic semiconductors are highly sensitive to analyte gases, have good reversibility, are relatively cheap, and are easy to use. However, the experimental results from the conductance-modulating oxides have been plagued with problems of reproducibility, stability, and selectivity [32]. This lack of selectivity prevents these materials from being used in practical applications.

The use of organic materials has been shown to possess the same advantages as the inorganic oxide films, but the organic materials can easily be modified to improve selectivity [1, 32]. A reactive group can readily be substituted onto the parent molecule which can then interact selectively with certain atmospheric contaminants [3]. These reactive groups are commonly substituted onto the polycyclic ring structures. These substitutions alter the surface chemistry of the material and modify the electron distribution, thereby changing the electrical properties of

the film [18]. The primary disadvantages of organic materials are that they are generally insulators and do not conduct electricity well, and they are thermally unstable at temperatures which are typically required for practical applications [18].

Phthalocyanines are one group of organic materials which are considered to be good conductors and are thermally stable [27]. These materials have been some of the most widely studied organic compounds to sense gases. The metal-free phthalocyanine molecule is shown in Figure 2.1. The central hydrogen atoms in this structure can be replaced with a metallic element. The metal-doped phthalocyanines are typically p-type semiconductors [32]. Additionally, the chemical structure of a metal-doped phthalocyanine is shown in Figure 2.2. The practical gas sensing temperature range is typically 100°C to 300°C which produces favorable polymeric electrical conductivity characteristics [27]. Furthermore, these organic polymers can be deposited as thin films with a vacuum sublimation process, which, as mentioned earlier, is a practical and reliable method of depositing a thin film.

The investigation of phthalocyanine materials and their use in gas detection systems have concentrated on their electrical conductivity changes. These conductivity changes

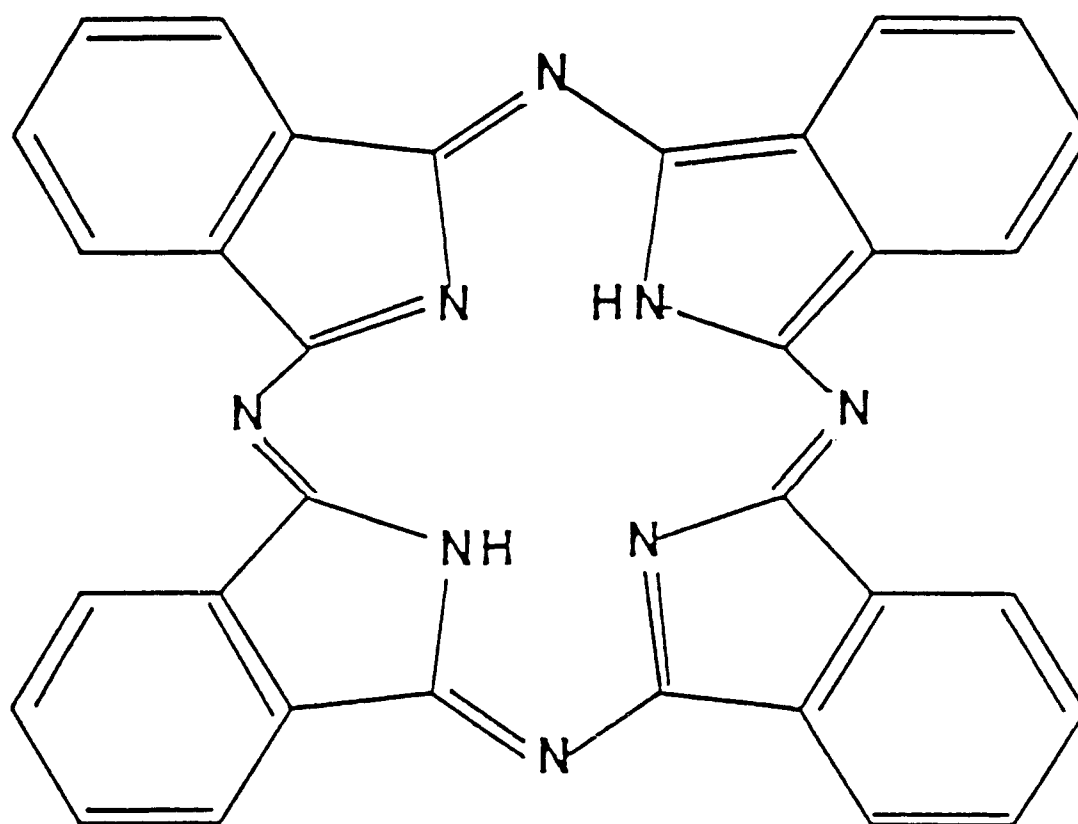


Figure 2.1: Chemical Structure of Undoped Phthalocyanine [22].

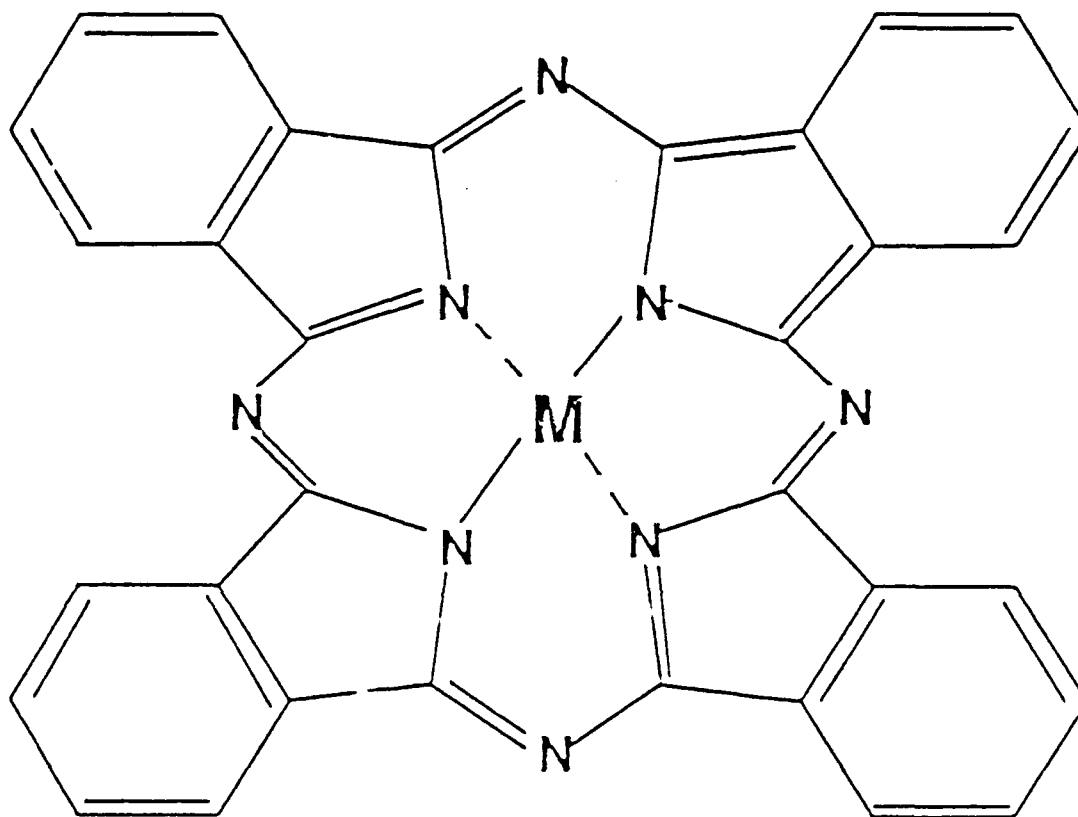


Figure 2.2: Chemical Structure of Metal-Doped Phthalocyanine [3].

have been predominantly observed with copper phthalocyanine (CuPc) and lead phthalocyanine (PbPc) [1, 11, 12]. CuPc, PbPc, and several other metal phthalocyanine thin films have been shown to be highly sensitive to strong electron-acceptor gases, such as nitrogen dioxide and chlorine [8, 9, 12, 16]. The detailed mechanism of charge transfer between a challenge gas and a metal-doped phthalocyanine is far from being understood. The mechanism may actually depend upon the type of phthalocyanine and the type of challenge gas. Research continues to be performed in this area.

2.3 Solid-State Chemical Sensors

Chemically-sensitive thin films, specifically the metal-doped phthalocyanines, have been used to detect the presence of various gases via the corresponding change in the electrical properties of these thin films. The gas sensors reviewed differ with respect to the electrical response mechanisms involved in detecting the changes in the electrophysical characteristics (conductivity, dielectric constant, etc.) of these films. A description of each microsensor technology is presented in the following sections.

2.3.1 Piezoelectric Devices. A piezoelectric gas detector is typically manifested by a piezoelectric crystal

which mechanically oscillates at a characteristic frequency when a time-dependent electric field is applied to it. To make use of the piezoelectric effect for gas sensing, the crystal is coated with a chemically-sensitive material [19]. This material reacts either physically or chemically with atmospheric gases through the processes of adsorption and/or absorption [10].

The piezoelectric crystal with the deposited chemically-sensitive film will also oscillate by applying a harmonic potential to the electrodes attached to the device. A change in the film's mass or visco-elastic properties can alter the resonant frequency of the crystal [10, 19]. The resonant frequency shift relates to the presence of a binding molecule on the chemically-sensitive thin-film coating.

The simplest piezoelectric device is the quartz crystal microbalance (QCM) (shown in Figure 2.3). Lucklum et al. reported that the QCM can be used to detect specific gases [15]. The QCM has been used to detect polar and non-polar organic and inorganic gas compounds, including carbon dioxide, carbon monoxide, and nitrogen dioxide. As the mass of the chemically-sensitive film changes due to adsorbed molecules, the resonant frequency of the crystal shifts [28]. The change in the resonant frequency, for chemically-sensitive films when exposed to a challenge gas, can be

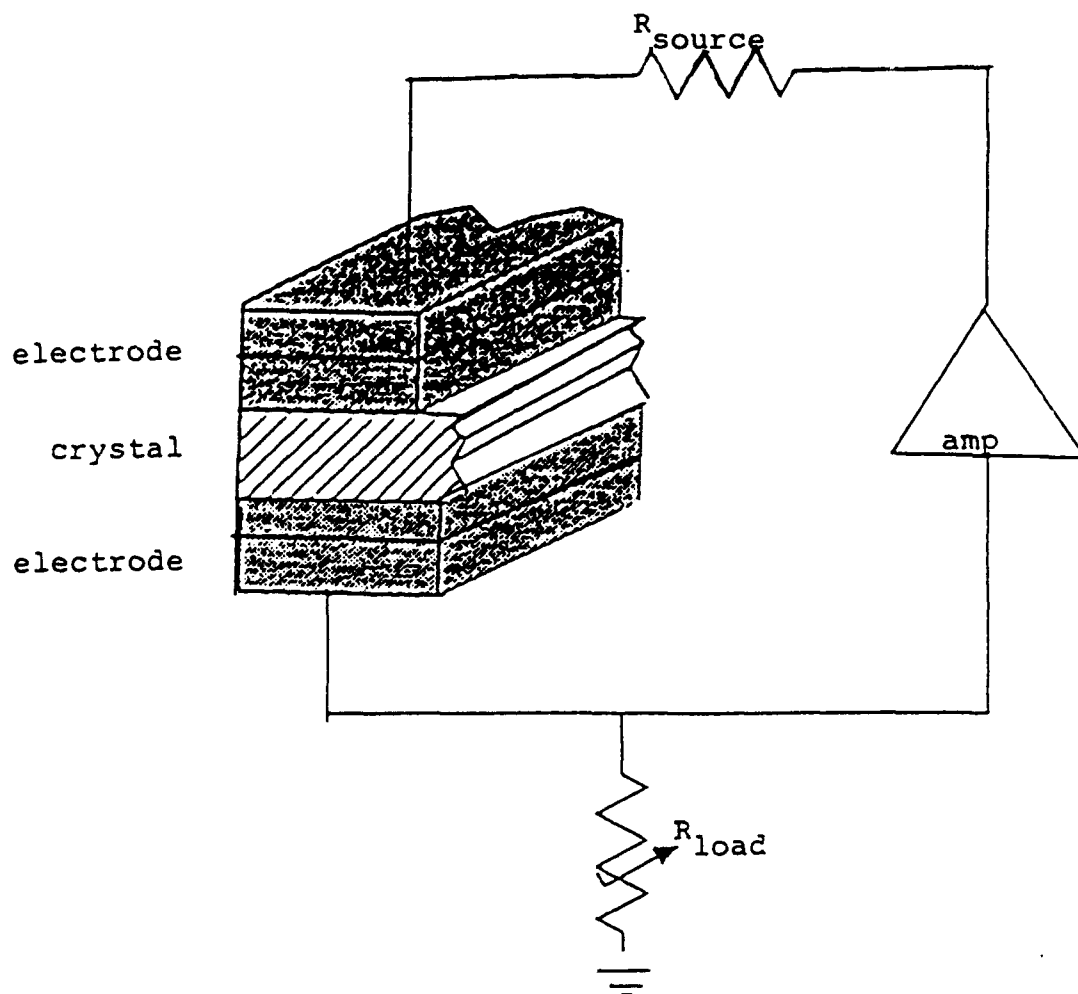


Figure 2.3: Schematic Diagram of a Quartz Crystal Microbalance [19].

calculated by using the following empirical formula [33]:

$$\delta f = -2.3 * 10^6 * f^2 * \Delta m/A \quad (2.1)$$

where, δf is the change in the resonant frequency measured in Hertz, f is the crystal's natural resonant frequency measured in Hertz, Δm is the change in the crystal's mass measured in grams, and A is the surface area of the coating measured in cm^2 .

The advantages of the QCM is its simplicity of operation and its sensitivity. Unfortunately, the QCM is not selective to a mixture of gases and it is not highly reliable since the response of the QCM is based solely on the change in the crystal's mass.

2.3.2 Surface Acoustic Wave Devices. Another class of sensors has been designed based upon the principle of a surface acoustic wave (SAW). Similar to the QCM, the SAW device measures the presence of a gas by measuring the deviations in the detector's resonant frequency. The device's resonant frequency depends upon the crystal's wave velocity, the surface electrode spacing, and the type of thin film coating used. Wohltjen et al. reported sensitivities at the parts-per-million (ppm) concentration

level by using dual-SAW delay-lines [24]. Figure 2.4 shows the configuration of a dual-SAW delay-line gas detector. The change in oscillating frequency (δf) is given as [24]:

$$\delta f = (k_1 + k_2)f^2\eta p - k_2f^2\eta[(4\mu/V_R^2)(\epsilon + \mu/\epsilon + 2\mu)] \quad (2.2)$$

where, k_1 and k_2 are the material constants for the selective and reference coatings (films), f is the unperturbed resonant frequency, η is the thickness of the selective coating, p is the density of the selective coating, V_R is the unperturbed Raleigh wave velocity, ϵ is the Lamé constant, and μ is the frequency modulus of the film.

The comparison of equations (2.1) and (2.2) reveals that unlike the QCM, the resonant frequency shift of a SAW gas detector cannot be exactly attributed to variations in the mass of the films or chemical reaction causing electromechanical perturbations. The shift in resonant frequency for the SAW is also accounted for by the thickness and modulus of the film. Even though the SAW is more sensitive than the QCM, its reliability is worse. Neither device is selective for a mixture of challenge gases.

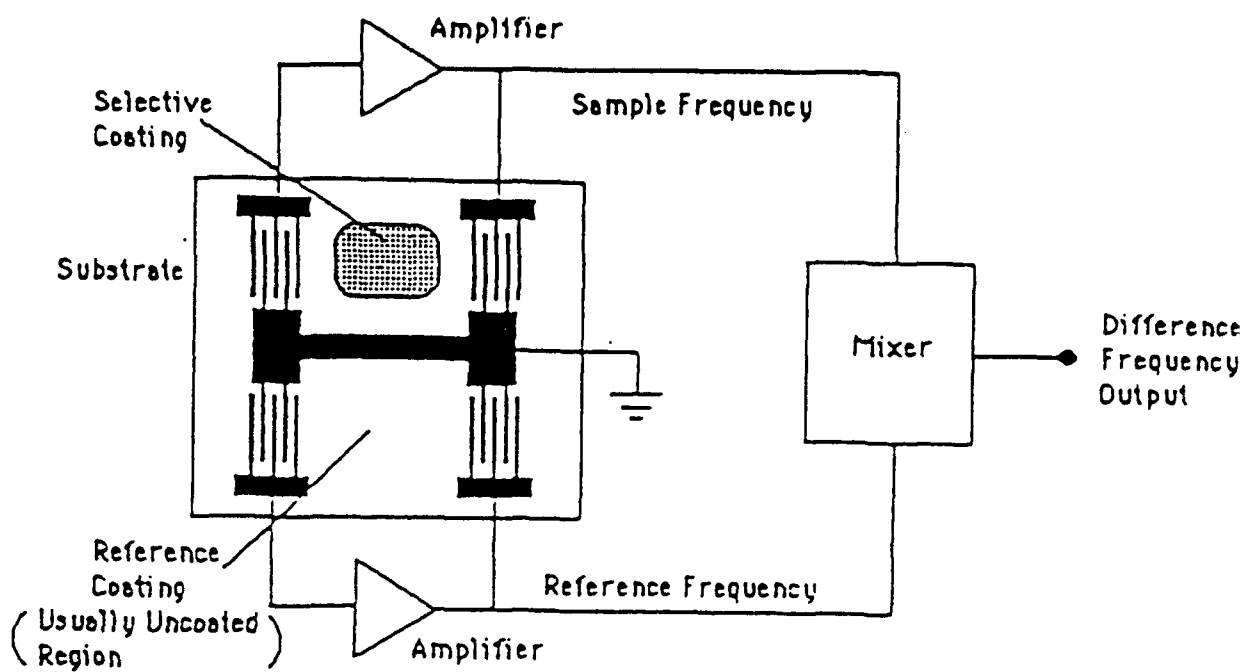


Figure 2.4: Schematic of a Dual-SAW Delay Line Chemical Vapor Sensor [7].

2.3.3 Chemiresistor Devices. Chemiresistors are commonly employed to transduce a response change in the alternating current (ac) impedance and direct current (dc) resistance of a chemically-sensitive thin-film coating when exposed to certain gases. These devices are small, planar, interdigitated electrode structures that are coated with a chemically-sensitive material. An example of a chemiresistor gas-sensing device is shown in Figure 2.5. Challenge gases donating electrons, accepting electrons, or polarizing charge carriers in the thin film produce changes in the material's bulk resistance.

One type of chemiresistor is the tin oxide (SnO_2) microsensor. The operating principle of the tin oxide microsensor involves monitoring the change in the thin film's electrical conductivity due to the chemisorption of a gas molecule of interest [5]. However, the inability of conductance-modulating oxides such as SnO_2 to offer reproducibility and stability has limited their practical applications.

Chemiresistors have also been fabricated by using metal-doped phthalocyanine as the chemically-sensitive material coating the electrodes. Jones and Bott reported having developed a chemiresistor device using PbPc as the chemically-sensitive selective coating [11, 12]. This

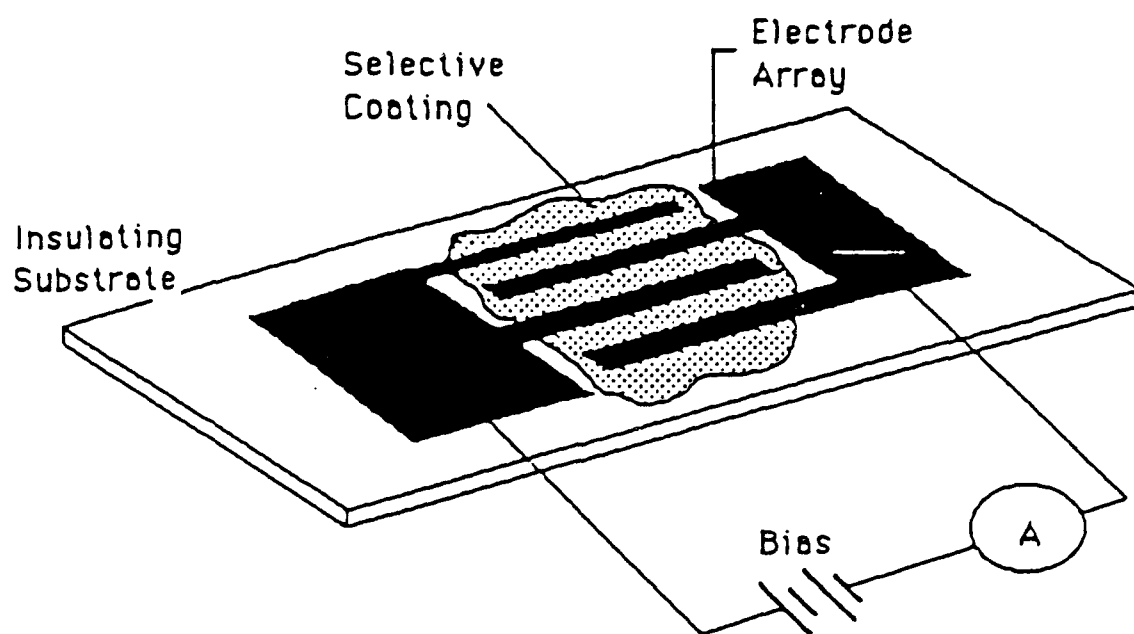


Figure 2.5: Schematic of a Chemiresistor Device for Gas Detection [25].

device was sufficiently sensitive to detect NO₂ at 44 parts-per-billion (ppb) [12]. Similar to the SAW and the QCM, this device has problems with interferants in the challenge gas atmosphere.

2.3.4 Notch Filter. The fundamental principle of gas detection for the notch filter is similar to that of the chemiresistor. A chemically-sensitive notch filter was developed by Kolesar [13]. The notch filter is realized by establishing a frequency dependent electrical network in which a component's resistive value is sensitive to a specific gas compound. Upon exposure to this gas compound, the conductance of the gas sensitive component changes. As a result, the notch characteristic of the filter shifts.

The notch filter is fabricated by incorporating a conductive ground-plane electrode, a dielectric layer, and a chemically-sensitive, electrically-resistive, thin-film surface electrode. Figure 2.6 shows the implementation of a notch filter used for gas detection. The chemically-sensitive thin film used by Kolesar was a discontinuous copper and copper oxide layer. This sensor was able to detect organophosphorus compounds at concentrations less than 10 ppm [13].

This device is very sensitive and reliable with the discontinuous copper and copper oxide layer. This device is

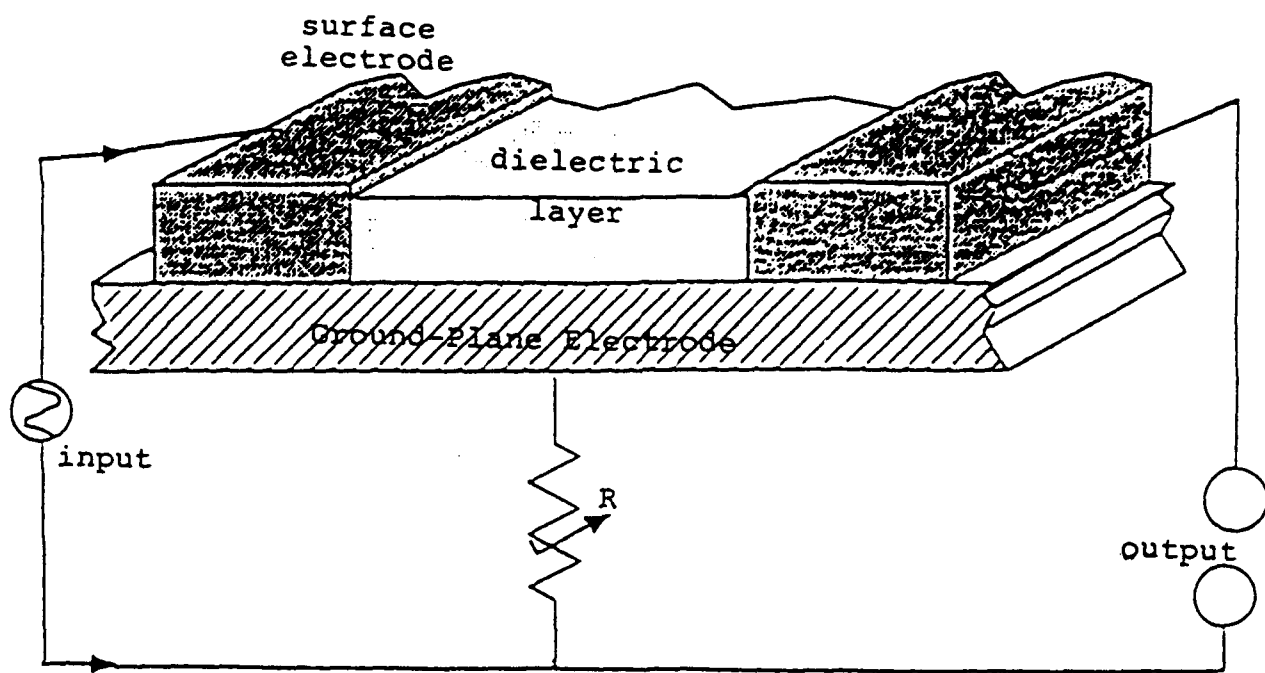


Figure 2.6: Schematic of a Notch Filter [13].

irreversible when exposed to high concentrations of challenge gases. Also, individual gases from a mixture cannot be selected.

2.3.5 Charge-Flow Transistor. This device, also known as the CFT, is an extension of the conventional metal-oxide semiconductor field-effect transistor (MOSFET). The distinctive resistance and capacitance (RC) network of this device allows current to flow through a split-gate electrode. To establish this device as a gas sensor, a chemically-sensitive film is deposited on and between the split electrode arrangement. The electrical potential across the complete gate electrode causes a flow of charge which results in a characteristic delay in the gas sensor's response. The primary application for this device was to determine the rate of cure for an epoxy resin. The sensor's response was not linear, and this feature posed many measurement problems [9].

Modifications to the CFT structure improved its linearity and reduced the parasitic impedances. The metal gate electrodes were moved to a position directly above the source and drain diffusions of the MOSFET. The modified CFT is shown in Figure 2.7. With this modification, the carrier channel was predominantly influenced by the thin-film

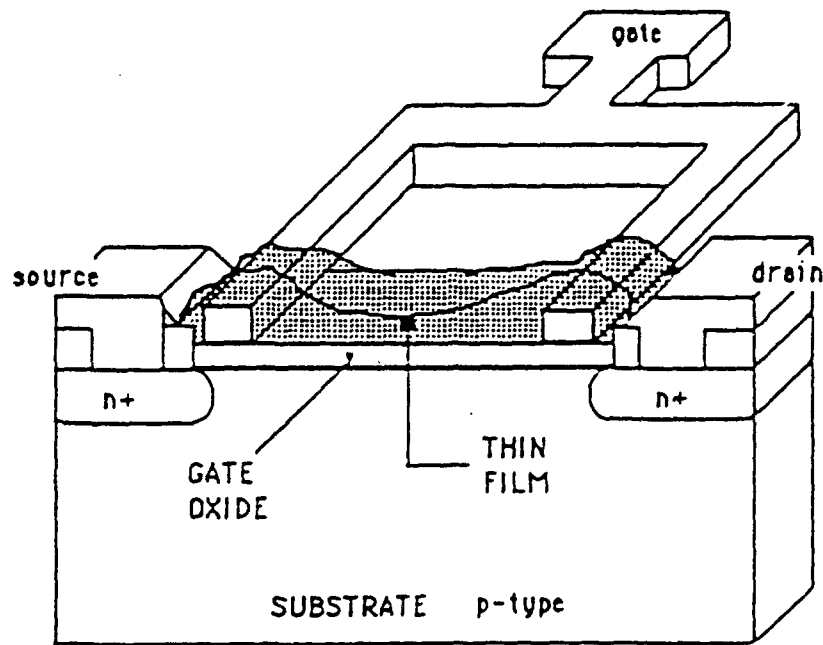


Figure 2.7: Schematic of a Modified CFT [9].

coating and not significantly by the electromagnetic flux between the metal gate electrodes [9].

2.3.6 Interdigitated Gate Electrode Field-Effect Transistor. The CFT forms the basis for the design of the interdigitated gate electrode field-effect transistor (IGEFET). The interdigitated gate electrode (IGE) configuration in an IGEFET consists of a metallized driven-gate electrode which is physically isolated from the floating-gate electrode that is connected to the gate oxide of the MOSFET. An IGEFET is depicted in Figure 2.8. The IGE structure is typically coated with a chemically-sensitive thin film forming a chemically-sensitive field-effect transistor (CHEMFET). When a voltage pulse is applied to the driven-gate electrode, the characteristic response of the CHEMFET is found to change as a function of the challenge gases and the material used to coat the electrodes.

The conductive properties of the film can be affected upon exposure to specific gaseous compounds, and the *in situ* MOSFET amplifier provides a sufficient level of gain to ensure a proper signal-to-noise ratio for processing the sensor's response signal. The time domain and frequency domain of the sensor's electrical response are valuable indicators of its gas sensitivity and selectivity. As the

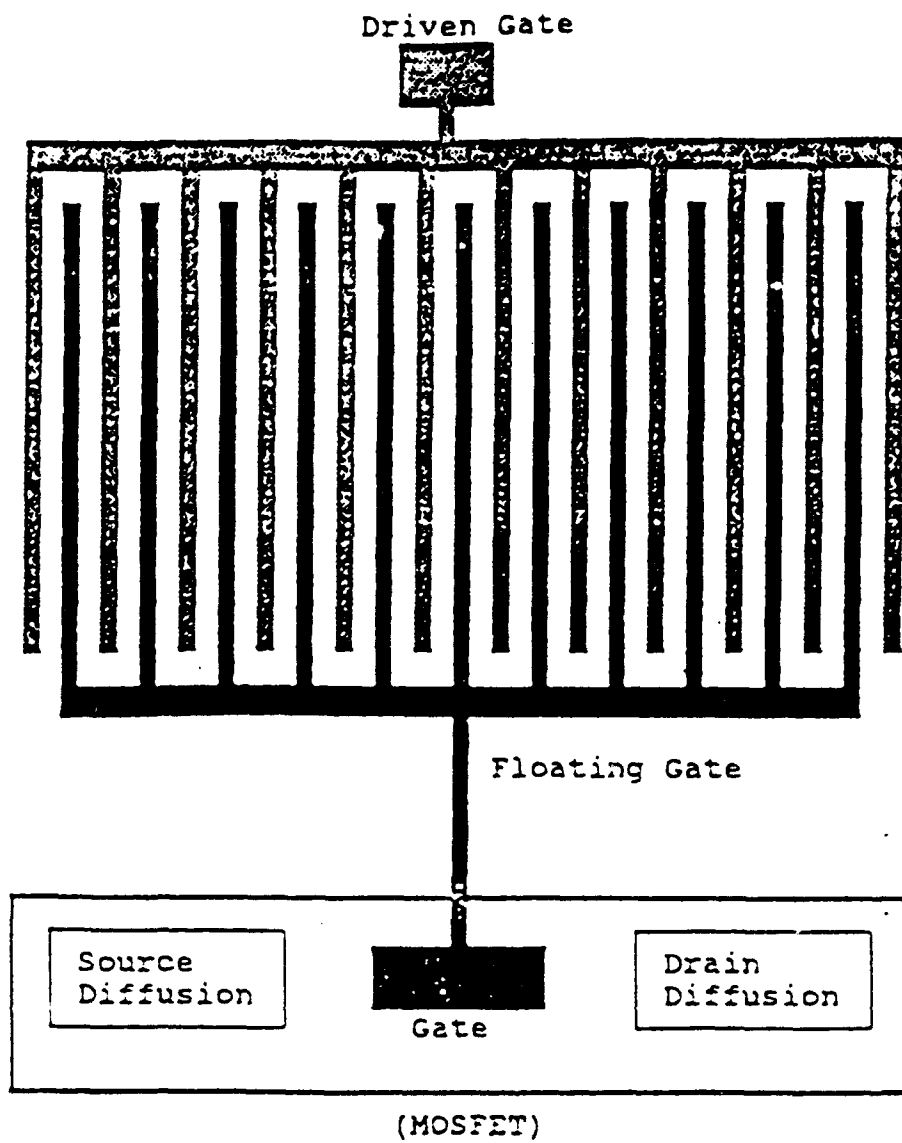


Figure 2.8: Interdigitated Gate Electrode (IGE) Structure [23].

charge levels change on the floating-gate electrode, variations in the MOSFET's source-to-drain electrical conductivity are induced [14, 28-30]. These changes are amplified and detected.

The CHEMFET microsensor becomes useful for detecting gases such as NO₂ and organophosphorus compounds when the IGE structures are coated with a metal-doped phthalocyanine compound (MPc) [8, 9, 14, 20, 23, 28-30, 35]. The sensitivity, selectivity, and reversibility of this device has been studied using a variety of phthalocyanine thin-films. These characteristics depend upon the transconductance of the device as well as the altered electrical characteristics of the phthalocyanine film. Gases, NO₂ in particular, have been detected at a concentration level of less than 25 ppb [9, 14, 23, 35]. However, the CHEMFET still has problems with stability and reproducibility.

2.4 Significant Findings

Sensor technology research is currently playing an increasingly vital role in the integration of systems and sensors. Considering the advances in information processing already achieved by integrated circuits, the field of integrated sensors can profit from integrated circuit process technology to realize enhanced sensitivities,

selectivities, and reversibilities. The advantages offered by such proven, powerful, and versatile technologies have been used to contribute to further success in the gas sensing field. Gas sensors using chemically-sensitive thin-films of metal-doped phthalocyanines have been studied for numerous gases. Most data for sensitivity and selectivity of a gas sensing device have arbitrary correlation with challenge gas concentrations and may be skewed by the selection of an electronic baseline. Table 2.1 depicts the sensitivity, selectivity, and reversibility (when applicable) in terms of vapor type and concentration, film type and thickness, and operating temperature for CHEMFET devices. The values of sensitivity given in Table 2.1 are defined as the initial resistance of the device prior to exposure (R_0) divided by the resistance of the device after being exposed to a challenge gas (R). The reversibility shown depicts the amount of time needed for the resistance of the CHEMFET to return to within 90% of its initial value.

It can be seen from Table 2.1 that the sensitivity and reversibility of a gas sensor using MPC thin-films is dependent upon the type of metal used to dope the phthalocyanine and the thickness of the thin-film, the exposure gas and its concentration, and the operating temperature of the system. In the MPC series, lead (Pb), copper (Cu), and cobalt (Co) phthalocyanine films have the

Table 2.1: Significant Findings on Sensitivity and Reversibility for Given MPc Thin-Films and Challenge Gas Concentrations

| reference | thin-film/ thickness | gas/ concen. | temp. (°C) | sensitivity (R_0/R) | revers- ibility |
|-----------|-------------------------|----------------------------|---------------|----------------------------|--------------------|
| 36 | CoPc 200 nm | NH ₃ 1000ppm | 170 | 4.94 | 30 seconds |
| | NiPc 200 nm | NH ₃ 1000ppm | 170 | 1.53 | 30 seconds |
| | PtPc 200 nm | NH ₃ 1000ppm | 170 | not sensitive | |
| 37 | PbPc | H ₂ 5600ppm | 200 | 8.0 | |
| | NiPc | H ₂ 5600ppm | 200 | 1.5 | |
| | CoPc | H ₂ 5600ppm | 200 | 1.3 | |
| | MgPc | H ₂ 5600ppm | 200 | 0.8 | |
| | ZnPc | H ₂ 5600ppm | 200 | 0.6 | |

TABLE 2.1 (continued)

| reference | thin-film/ thickness | gas/ concen. | temp. (°C) | sensitivity (R_0/R) | revers- ibility |
|-----------|-------------------------|----------------------------|---------------|----------------------------|--------------------|
| 37 | PbPc | CO 280ppm | 200 | 0.9 | |
| | NiPc | CO 280ppm | 200 | 1.1 | |
| | CoPc | CO 280ppm | 200 | 1.0 | |
| | MgPc | CO 280ppm | 200 | 0.9 | |
| | ZnPc | CO 280ppm | 200 | 0.5 | |
| 38 | PbPc 1000 nm | NO ₂ 100ppb | 25 | 0.8 | > 3600 seconds |
| | PbPc 1000 nm | NO ₂ 100ppb | 150 | 0.4 | > 3600 seconds |
| 39 | PbPc 200 nm | NO ₂ 1ppm | 160 | high | |
| | PbPc 200 nm | CO 100ppm | 160 | < NO ₂ | |
| | PbPc 200 nm | SO ₂ 2000ppm | 160 | not sensitive | |
| 40 | PbPc | Cl ₂ 9ppm | | -2 | 120 seconds |
| | PbPc | NO ₂ 9ppm | | 1 | 120 seconds |
| 41 | PbPc | PCE 4ppm | 25 | | > 3600 seconds |
| | PbPc | PCE 4ppm | 100 | | 3000 seconds |
| | PbPc | PCE 4ppm | 180 & 275 | | 1200 seconds |
| 42 | CuPc | NH ₃ 300ppm | 65 | 0.3 | 2220 seconds |

Table 2.1 (continued)

| reference | thin-film/ thickness | gas/ concen. | temp. (°C) | sensitivity (R_0/R) | revers- ibility |
|-----------|-------------------------|----------------------------|---------------|----------------------------|--------------------|
| 42 | CuPc | NH ₃ 600ppm | 65 | 0.4 | 1500 seconds |
| | CuPc | NH ₃ 900ppm | 65 | 0.4 | 600 seconds |
| 35 | CuPc 200 nm | DIMP 100ppb | 30 | 0.8 | > 3600 seconds |
| | CuPc 200 nm | DMMP 100ppb | 30 | 0.95 | > 3600 seconds |
| | CuPc 200 nm | DFP 100ppb | 30 | 0.35 | > 3600 seconds |
| 8 | CuPc 1600 nm | BF ₃ 24ppm | 150 | 1.28 | |
| | CoPc 540 nm | BF ₃ 24ppm | 150 | 0.2 | |
| | NiPc 1250 nm | BF ₃ 24ppm | 150 | 1.11 | |
| | CuPc 210 nm | NH ₃ 500ppm | 150 | 3.33 | |
| | CoPc 540 nm | NH ₃ 500ppm | 150 | 1.8 | |
| | NiPc 1250 nm | NH ₃ 500ppm | 150 | 1.33 | |
| | CuPc 320 nm | DIMP 3ppm | 150 | 0.96 | |
| | NiPc 680 nm | DIMP 3ppm | 150 | 0.93 | |
| | CuPc 160 nm | NO ₂ 1000ppb | 150 | 0.43 | 900 seconds |
| | CoPc 250 nm | NO ₂ 1000ppb | 150 | 0.29 | > 3600 seconds |
| | NiPc 260 nm | NO ₂ 1000ppb | 150 | 0.10 | 3600 seconds |

largest sensitivity ranges. Other metal-phthalocyanine films such as nickel (Ni) and magnesium (Mg) have significantly smaller sensitivities toward organic and inorganic gases. Vapors which are strong electron-acceptors or strong electron-donors have been shown to have significant responses with MPC thin-films. Gases which are not strong, or even moderate, electron-acceptors or -donors, such as carbon monoxide (CO), sulfur dioxide (SO₂), and hydrogen (H₂), have negligible responses.

Reversibility is a measure of how well a response signal of a gas sensor can return to its initial equilibrium state. The reversibility, or recovery time, of a sensor not only depends on the thin-film type and thickness, but also depends on the operational temperature and the strength of the interaction between the challenge gas and the thin-film. NO₂ is a strong electron-acceptor and, therefore, NO₂ is strongly absorbed by thin-films of copper, lead, and cobalt phthalocyanine. It is evident from the studies presented in Table 2.1 that operational temperatures below 100°C require several hours for the sensor's signal to return to its original equilibrium state. For temperatures over 100°C, the gas sensors are either partially or fully reversible.

Selectivity is not included in Table 2.1 because of the limited references to this feature of gas sensors. Heilman et al. [39] discussed the selectivity of PbPc relative to

NO_2 , CO , and SO_2 . The gas sensor is selective toward NO_2 relative to the other two gases, CO and SO_2 . Unwin and Walsh [41] also investigated the selectivity of PbPc. The gases compared in this study were chlorine (Cl_2), 1,1,1-trichloroethane, trichloroethylene (TCE), and tetrachloroethylene (PCE). The gas sensor selected Cl_2 relative to 1,1,1-trichloroethane, but TCE and PCE were both selected relative to Cl_2 .

2.5 Summary

At the present time, the surface acoustic wave device is considered to be the most advanced technology for solid-state gas detection. The chemiresistor, the notch filter, and the charge-flow transistor have led to the development of the interdigitated gate electrode field-effect transistor and ultimately, the CHEMFET. This device has the potential for detecting minute concentrations of gaseous compounds. With the use of metal-doped phthalocyanines with this device, favorable sensitivity, selectivity, and reversibility should be obtainable.

Chapter 3

3 Gas-Delivery System, Phthalocyanine-Gas Interaction, and Electrical Conductivity Modulation

3.1 Gas-Delivery System

The gas generation and delivery system is used to generate, control, and transport small concentrations of the challenge gases to the test chamber containing the CHEMFET microsensor. Previous studies at AFIT using the CHEMFET coated with chemically-sensitive thin films have used a manual gas-delivery system [8, 9, 20, 23, 35]. The challenge and purge gases delivered to the CHEMFET microsensor test-chamber in this investigation were controlled by the system depicted in Figure 3.1.

Pressurized laboratory air or ultra-high purity nitrogen (N_2) were supplied to the gas delivery system to serve as the carrier and diluent gas. The filtered carrier and diluent gas was passed through a silica-gel bed to remove moisture and, thus, regulate the humidity of the challenge gas generating and delivery system. The relative humidity level was precisely controlled by passing the carrier and diluent gas through a deionized water bubbler. The carrier and diluent gas was then passed through an activated charcoal filter to remove any residual organic

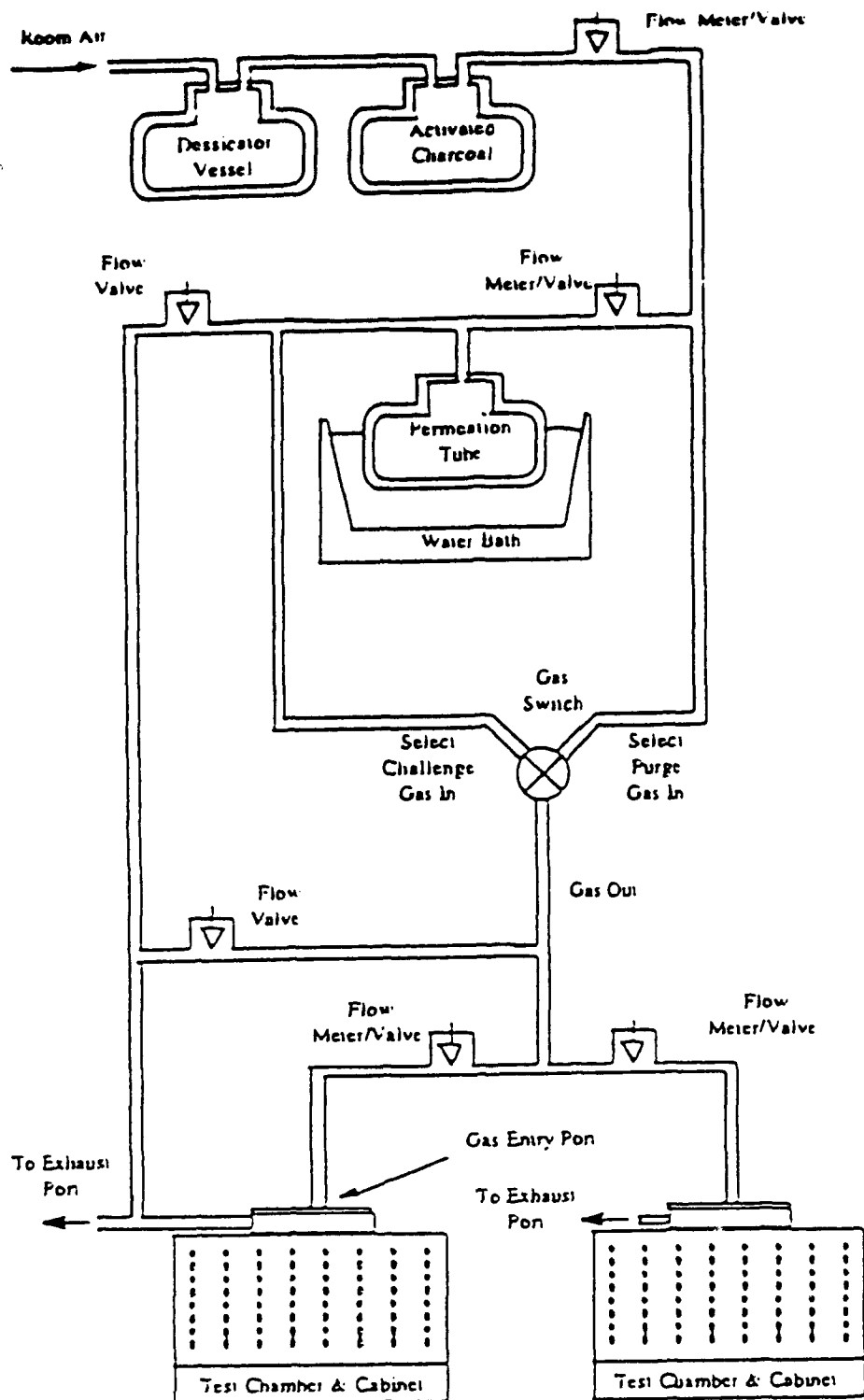


Figure 3.1: Gas Delivery System Used in Previous Research at AFIT [8].

contaminants. Depending upon the gas delivery requirements, the carrier and diluent gas was passed to the challenge gas path or to the purge path. The flow of the carrier gas along either path was controlled with calibrated flowmeters fitted with micrometer valve assemblies (Gilmont Instruments, Model F-7660, Great Neck, NY). To generate the desired concentrations of a challenge gas, permeation tubes were used (G-Cal Permeation Devices, GC Industries, Chatsworth, CA). These permeation tubes allow the challenge gas to permeate through an orifice at a constant rate when isothermally operated. The ultimate challenge gas concentration is determined by the gas mixture formed with the carrier and diluent gas flow rates. The manual interaction with the flowmeters inevitably creates a restriction on the range of achievable challenge gas concentrations.

3.1.1 Mass Flow Controllers. The design and development of a semi-automatic test chamber for characterizing the microelectronic gas sensors has been realized [34]. As a result, the automated characterization of gas microsensors has been accomplished under precisely controlled conditions concerning relative humidity and temperature. Also, the completely automated gas delivery system can deliver small, precisely-controlled

concentrations of the challenge gas to the test chamber over a designated period of time. The most common automated gas delivery systems include mass-flow controllers [34]. A mass-flow controller is designed to minimize the fluctuations between the desired and measured mass flow rates of a gas by incorporating a computer controlled interface. The ease of interfacing with a computer enables the mass flow controllers to continuously monitor and adjust the flow rate to the determined level. As a result, the concentration of the gas should be more precise with the use of mass-flow controllers in conjunction with the permeation tubes.

To determine the mass flow of a gas through a mass flow controller, a ratio is made between two distinct gases and their respective correction factors. In this investigation, the mass flow controllers (Tylan General, Model FM-280AD) were calibrated with N_2 which has a correction factor of 1.00. The correction factors for several other gases relative to N_2 is published by Tylan General [44]. Equation (3.1) describes the mass flow controller relationship involving the flow rates and the correction factors for two distinct gases [44]:

$$\frac{C_1}{C_2} = \frac{w_1}{w_2} \quad (3.1)$$

where w_1 is the flow rate for N_2 through the mass flow controller, w_2 is the flow rate of the desired challenge gas, and C_1 and C_2 are the respective correction factors. The flow rates of individual gases are determined by their molecular and chemical properties.

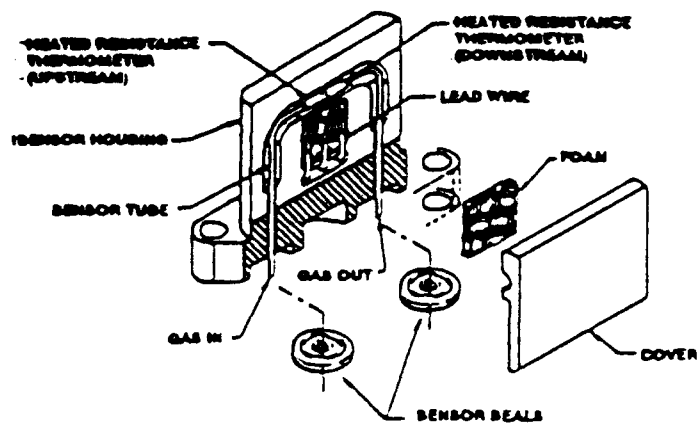
The flow rates of the gases passed through the mass flow controllers are regulated by an electrical control valve. The voltage level applied to the control valve regulates the size of the aperture through which the gases pass. For example, when the voltage level is set at 0 volts, the control valve is closed, allowing no gas to pass through the mass flow controller. If the voltage level is set at 5 volts, the control valve allows 100% of the entering gas to exit the mass flow controller. At intermediate voltages, the control valve is only proportionately opened, thus allowing proportional amounts of the gas to flow through the mass flow controller. The flow rate of a gas depends upon the molecular structure of the gas, the density of the gas, and the specific heat of the challenge gas. In this research, the mass flow controllers were calibrated with N_2 . The flow rates of N_2 through the mass flow controllers were determined. The correction factors for other gases in relation to N_2 were supplied by Tylan General [44]. For equal voltage levels determined from the calibration of the mass flow controllers

with N_2 , Equation (3.2) shows the relationship between the properties of a challenge gas and its rate of flow (w) in cubic centimeters/minute [44]:

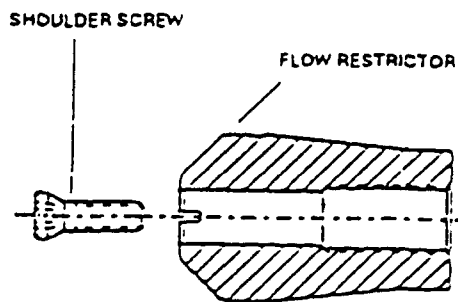
$$w = \frac{KN}{pC_p} \quad (3.2)$$

where K is an empirical constant for a particular mass flow controller (vendor provided), N is a correction factor for the molecular structure of a gas, p is the density of the gas at 0°C , and C_p is the specific heat of the gas.

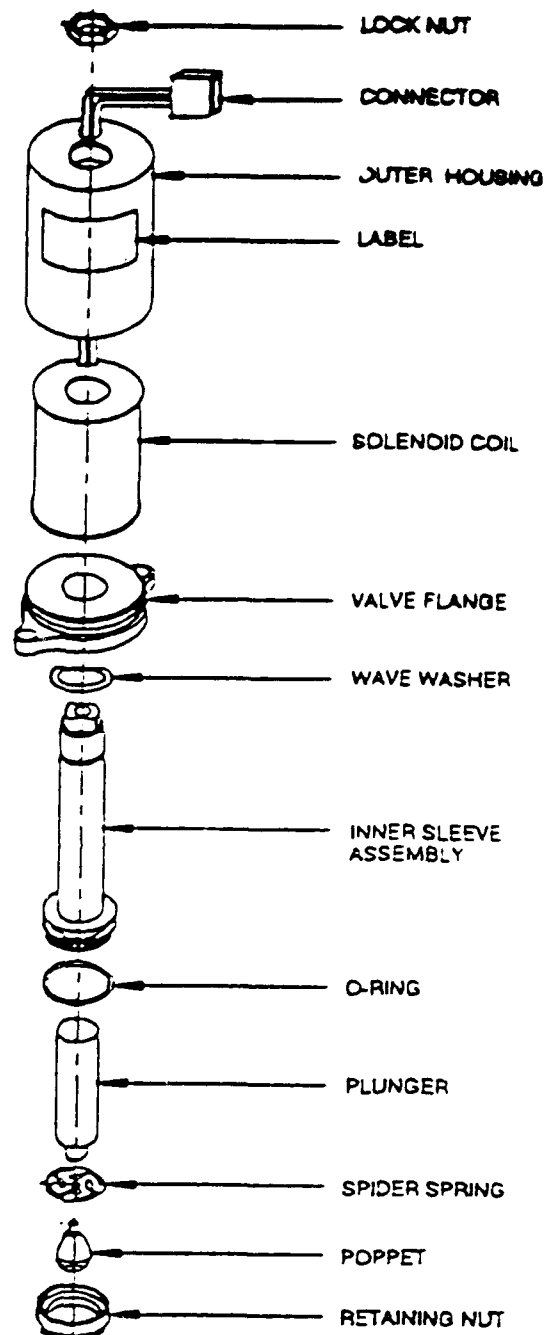
A mass-flow controller consists of four basic elements: the flow sensor, the bypass, which determines the full-scale flow range of the measuring section, the control valve, and the electronics that condition the mass flow control signal and drive the control valve [44]. Figure 3.2 shows three of the four basic units of a mass flow controller. The flow sensor typically consists of two self-heated resistance thermometers wound around the outside wall of the capillary tube through which the gas flows. When there is no gas flow, heat is symmetrically distributed along the entire length of the tube; however, when gas is flowing through the capillary tube, heat is transferred downstream. A temperature gradient is created between the upstream thermometer and the downstream thermometer. The temperature



(a) Flow Sensor



(b) Bypass



(c) Solenoid Valve

Figure 3.2: Three Basic Components of a Mass Flow Controller (Electronics Not Shown) [44].

gradient (and its corresponding electrical resistance gradient) is directly proportional to the mass flow rate of the gas through the capillary tube. The bypass, or flow-splitter, generally consists of a flow restrictor, and it serves to produce a linear pressure drop versus flow rate which allows the mass-flow controller to establish the sensor's flow through its full operational range from 0% to 100% flow. The control valve is frequently a solenoid valve with a rapid shutoff response time. This solenoid valve typically replaces the manually adjustable valve in a conventional laboratory flowmeter, thereby imparting the automated feature to this technology. The entire system is powered and driven by electrical impulse signals. The thermal resistor bridge supply circuit consists of an operational amplifier which generates an output signal which is proportional to the desired flow rate.

The desired flow rate of the challenge gas into the test chamber can be regulated automatically with the combination of a mass-flow controller and a permeation tube. The desired concentration within the test chamber (C_g) can be quantitatively expressed by Equation (3.3) [34]:

$$C_g = (Fr\dot{U}/v) * 10^6 \text{ ppm} \quad (3.3)$$

where F is the flow rate in milliliters per second, r is the

time duration of the gas pulse in seconds, \bar{U} is the dilution ratio, and v is the volume of the test chamber in milliliters. With this technology, it is possible to generate challenge gas concentration levels at the parts-per-billion (ppb) and the parts-per-million (ppm) levels. The configuration of the revised gas generation and delivery system is shown in Figure 3.3.

3.1.2 Test Chamber and Cabinet. The challenge gas is distributed equally to two test chambers. The test chambers and the test cabinets were designed and fabricated at AFIT, and the schematic diagram for this hardware is depicted in Figure 3.4. The test chamber is a rectangular box constructed of stainless steel set atop the aluminum test cabinet. The bottom of the test chamber consists a 64-pin zero-insertion-force (ZIF) receptacle and socket mounted on a printed circuit board. The ZIF socket serves to hold the 64-pin CHEMFET dual in-line package (DIP) in place. The internal temperature of the test chamber is regulated with an external power supply and control circuit. The leads for the dc power supply for the heater strip and the leads for the thermocouple enter the test chamber through the printed circuit board located on the floor of the test chamber. The other leads necessary for the test measurements are connected to the 64-pin ZIF receptacle and socket. The

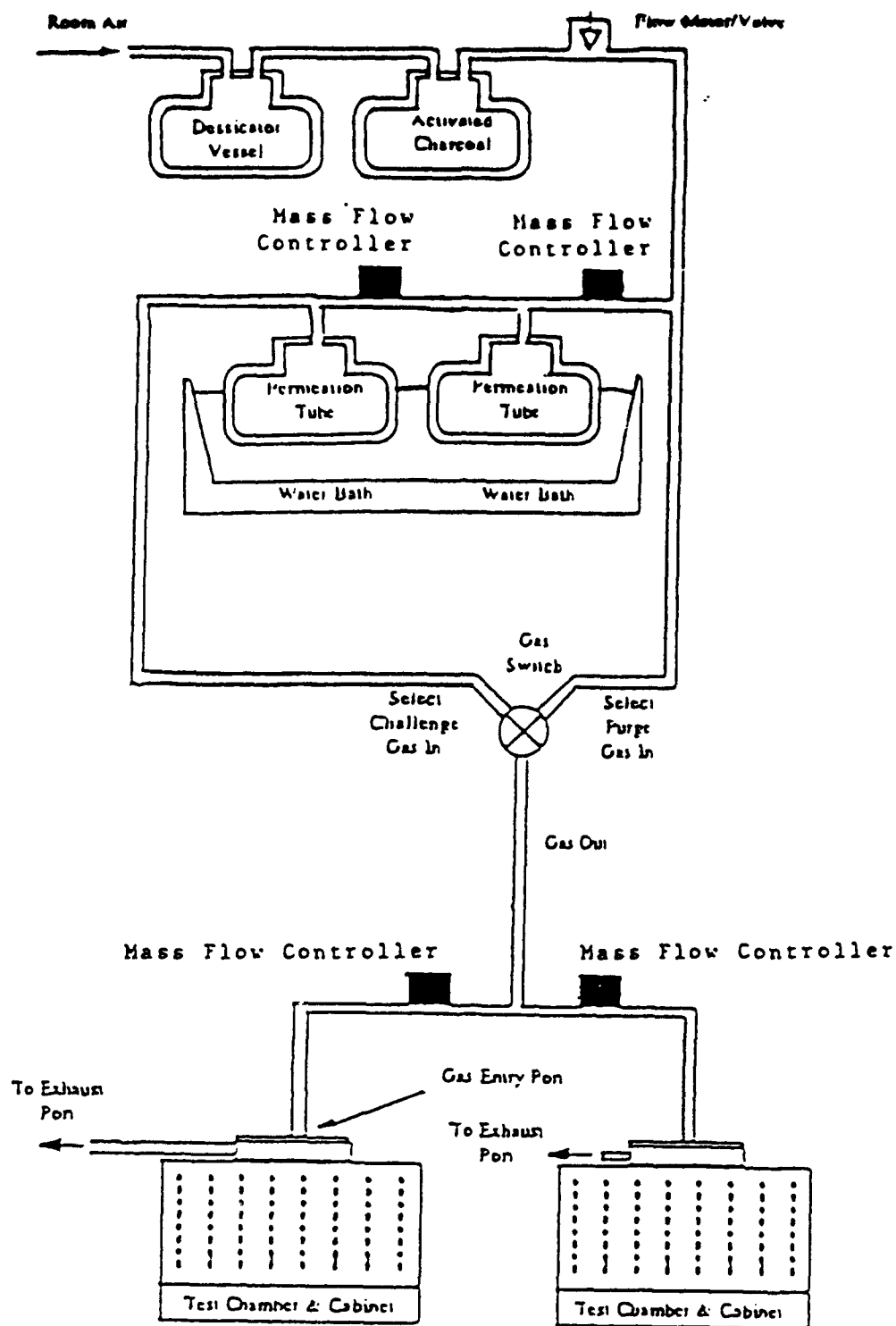


Figure 3.3: Improved Gas Delivery System Incorporating Mass Flow Controllers.

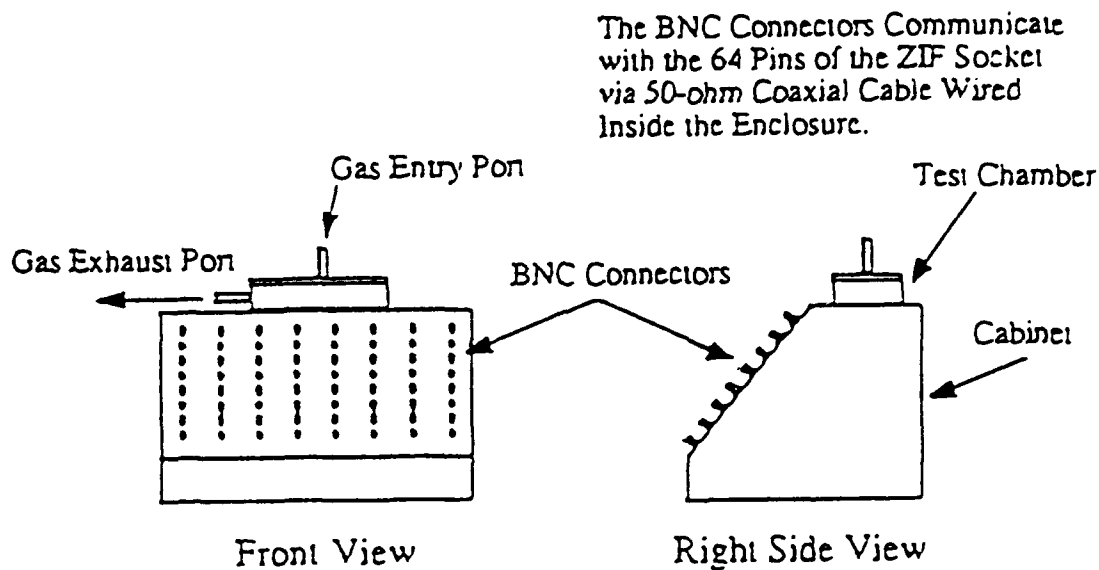
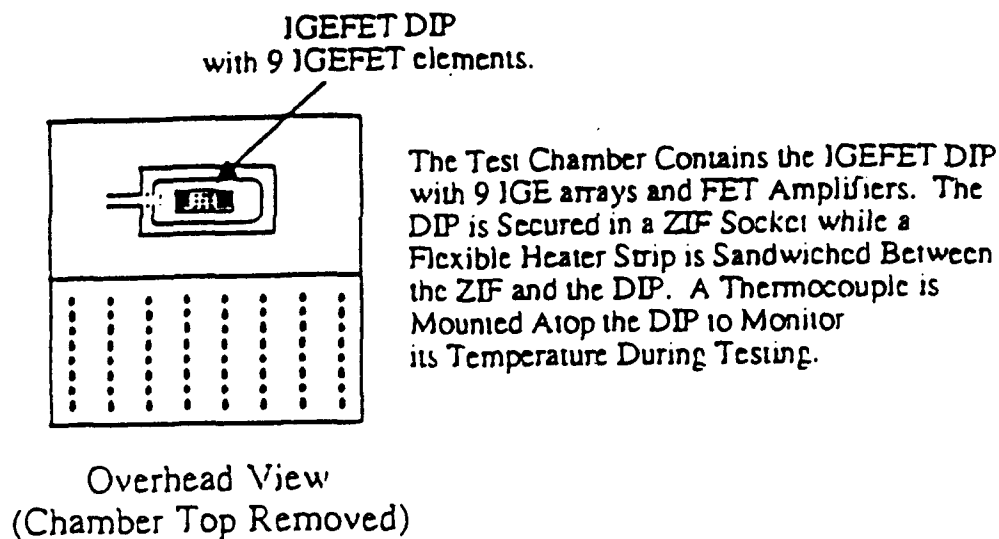


Figure 3.4: Diagram of the Test Chamber and Test Cabinet with BNC Connectors [8].

individual test leads run through the test cabinet and are terminated to the body of the test cabinet with BNC bulkhead connectors. Both the test chamber and the test cabinet ground ties are isolated from the dc power supply to limit electrical crosstalk and noise problems.

3.2 Phthalocyanine-Gas Interaction

The advantageous chemical and physical properties of the MPC compounds include the large delocalized π -electron system, low ionization energies, and high polarization energies. The delocalized π -electron system has been postulated to contribute to strong van der Waals interactions with small gas molecules [43]. The low ionization energy and high polarization energy of the MPC compounds leads to a small energy requirement to form a charge-transfer complex; thus, charge-transfer interactions between the metal-doped phthalocyanine thin-film compounds and adsorbed gas molecules may readily occur.

The adsorption of gas molecules onto the metal-doped phthalocyanine thin-film is necessary to observe the modulation of the film's electrical conductivity. The concentration of gas molecules that adsorb (C_a) on a metal-doped phthalocyanine thin-film has been characterized by

Equation (3.4) [45]:

$$C_s = \bar{n} t_{av} \quad (3.4)$$

where \bar{n} is the number of gas molecules interacting with the phthalocyanine thin-film, and t_{av} is the average time a gas molecule remains adsorbed on the phthalocyanine thin-film. However, due to different crystal faces, edges, and corners, as well as structural defect sites, there is a distribution of adsorption sites and associated activation energies [43]. Thus, the adsorption interactions between the phthalocyanine thin films and the gas molecules will vary in number and strength.

Theoretically, adsorption initially occurs with a maximum heat of adsorption which decreases with an increase in surface coverage by the gas molecules. As the number of available adsorption sites on a clean and uniform MPC thin-film surface decreases, the activation energy for further adsorption of gas molecules increases. However, under ambient conditions, most phthalocyanine thin-films are covered with adsorbed background gas species; for example, oxygen and water molecules [43]. For the adsorption of a different gas species, the background species may need to be desorbed. Thus, the desorption energy (which is usually greater than the activation energy) determines the rate of

adsorption of the challenge gas onto the metal-doped phthalocyanine thin-film.

3.3 Modulation of Electrical Conductivity

When a gas molecule is adsorbed onto a phthalocyanine thin-film, surface charge-transfer interactions occur. These charge-transfer interactions cause a net change in the surface electrical conductivity of the phthalocyanine material. The electrical conductivity is modulated due to the change in the number of charge carriers available for transport. The charge carriers may be electrons or holes (holes make up the majority of the charge carriers in metal-doped phthalocyanine p-type semiconductors). The number of adsorbed gas molecules (Equation 3.4) is linearly related to the change in the number of charge carriers and the change in the electrical conductivity. This linear relationship is expressed by [46]:

$$\sigma(P) - \sigma(0) = kA_s \quad (3.5)$$

where A_s is the fraction of the phthalocyanine surface area covered with gas molecules at some challenge gas partial pressure (P), k is a constant, $\sigma(P)$ is the phthalocyanine thin-film electrical conductivity at some gas partial pressure, and $\sigma(0)$ is the phthalocyanine thin-film

electrical conductivity prior to gas exposure. At small challenge gas concentration levels and at a specific temperature, the electrical conductivity (σ) of the phthalocyanine thin-film can be approximated by [47]:

$$\sigma = K_1 C_0^\alpha \quad (3.6)$$

where K_1 and α are constants, and C_0 is the challenge gas concentration in the test chamber. The morphology of the phthalocyanine film, as well as the challenge gas concentration, play an important role in establishing the film's electrical conductivity and challenge gas response. The charge-transfer interactions and the charge-carrier transport influence the changes in the electrical conductivity of the metal-doped phthalocyanine thin-films which can be documented through the electrical characterization measurements.

3.4 Summary

Attention has been afforded to the development of an automated gas generation and delivery system. An automated system should improve the accuracy of regulating the challenge gas concentration and its rate of flow to the microsensor's test chamber. The use of a computer-controlled, self-contained, closed-loop system should vastly

improve the process of measuring the mass flow rate of the challenge gas flow. Furthermore, permeation tubes provide accurate concentrations of the challenge gases.

The pertinent electrical and molecular properties of the metal-doped phthalocyanine thin-films were presented. Due to these properties, metal-doped phthalocyanine thin-films can be used to detect gas species. The presence of a challenge gas that adsorbs onto the surface of the phthalocyanine thin-film with a charge-transfer bond causes a net change in the number of charge carriers, which correspondingly changes the electrical conductivity of the thin-film.

Chapter 4

4 CHEMFET Design and Evaluation Procedures

4.1 Introduction

This chapter discusses the design and fabrication, as well as the experimental and evaluation processes, involved with the chemically-sensitive field-effect transistor (CHEMFET) microsensor. The design and fabrication section of this chapter presents the layout of the integrated circuit (IC), the structural components of the CHEMFET, and the fundamental electrical characteristics of the microsensor. The critical experiments and data evaluation techniques are described in the experimental and evaluation processes section. This section also describes the configuration of the test instrumentation and the methods implemented to accomplish data collection.

4.2 Design and Fabrication

The gas sensing microsensor used in this investigation is similar to those used previously at AFIT [8, 9, 14, 20, 23, 35]; however, several improvements have been made by Jenkins. The interdigitated gate electrode (IGE) Field-Effect Transistor (FET) was constructed by the Metal-Oxide-Semiconductor Implementation System (MOSIS) (University of

California, Berkeley, California). ORBIT fabricated the IGEFET-based microsensor using the scalable 2-micron, double-metal, double-poly silicon, p-well technology [9] with the dimensions shown in Figure 4.1 and summarized in Table 4.1.

The IGE structure was fabricated with a second-level metal (aluminum), while a first-level metal was used to form the ground plane. The CHEMFET IC die was configured as a symmetric array of nine, independently-operated sensors (Figure 4.2).

Each IGEFET is integrated with its own impedance-matching, differential-input amplifier which consists of serially connected MOSFET inverters. A photograph of the IGE structure and the amplifier is shown in Figure 4.3. The amplifier section for each individual IGEFET reduces the complexity of the IC die analog signal paths.

To further improve the design of the CHEMFET, an independent MOSFET amplifier (similar to those serially connected to the IGE structures) was included in the design of the IC die (64-pin package) to compensate for temperature variations. Another feature of the improved microsensor design is the layout of the bond pads. It was observed in the previous studies [8, 9, 14, 20, 23, 35] that parasitic effects exist due to the configuration of the bond pads.

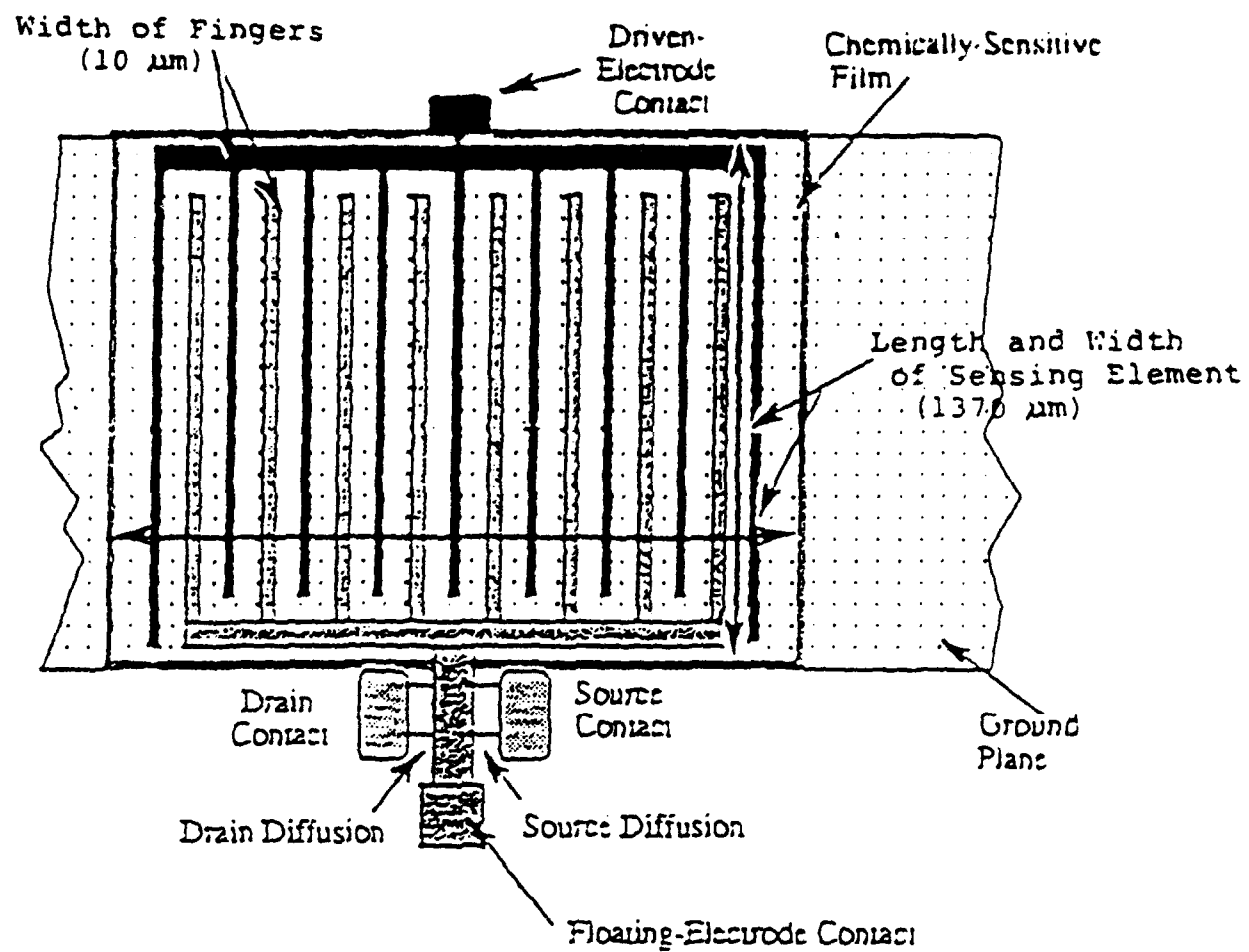


Figure 4.1: Dimensions of an IGE Structure.

Table 4.1: Critical Features and Dimensions of the Interdigitated Gate Electrode Structure.

| IGEFET Component | Value |
|-------------------------------------------|-------------------------|
| Number of Driven-Gate Electrode Fingers | 35 |
| Number of Floating-Gate Electrode Fingers | 34 |
| Total Area of Driven-Gate Electrodes | 479,500 μm^2 |
| Total Area of Floating-Gate Electrodes | 465,800 μm^2 |
| Width of Individual Electrode Fingers | 10 μm |
| Separation Between Electrode Fingers | 10 μm |
| Sensing Element Length | 1370 μm |
| Sensing Element Width | 1370 μm |

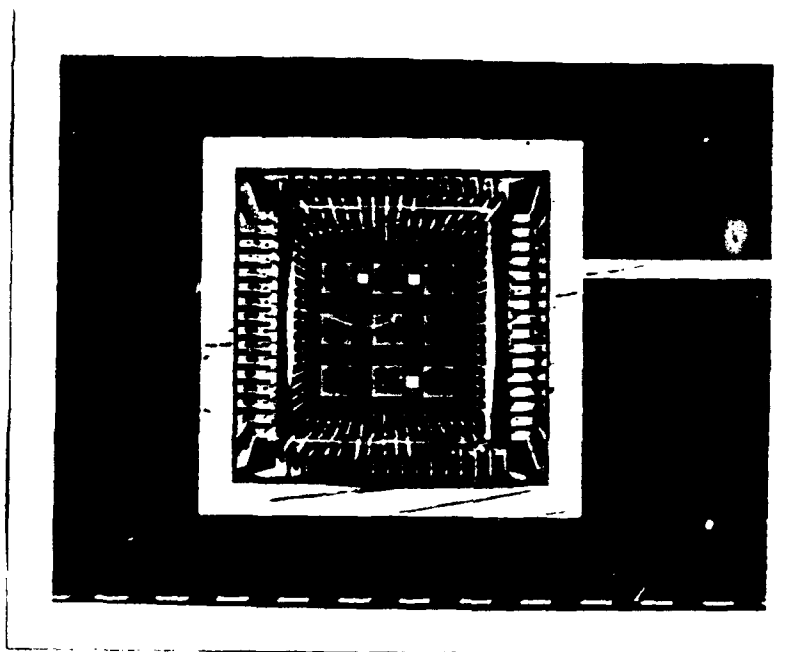


Figure 4.2: Optical Photograph of the CHEMFET Microsensor.

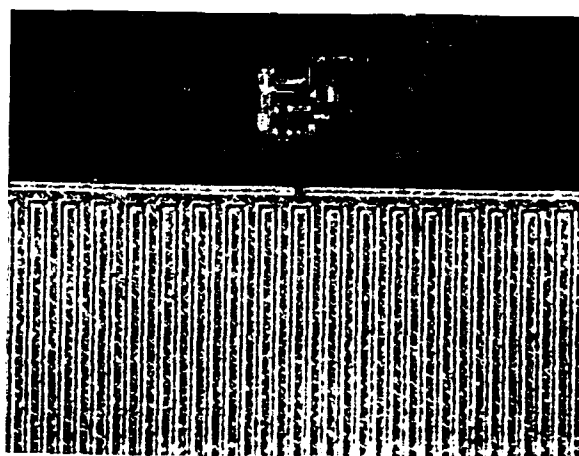


Figure 4.3: Optical Photograph of an IGE Structure Coated with 1000 Å of CuPc.

Originally, no two array elements shared any pins on the microsensor; the routing of the metal lines used single metal layers with no cross-overs. This layout ensured that if any individual element failed, the performance of the entire 3 x 3 array would not be compromised. To further minimize the electrical coupling, an improvement in the bond pad configuration was implemented in the revised IC design; the driven-gate bond pads were isolated from the floating-gate bond pads, and the amplifier input bond pads were isolated from the amplifier output bond pads. The bond pad diagram is shown in Figure 4.4, and the bond pad connections are listed in Table 4.2. In Table 4.2, V_{out} is the voltage follower output of the amplifier; V_{dd} is the voltage follower power supply, which is high (+5V); V_{ss} is the voltage follower power supply, which is low (0V); and V_{bias} is the voltage follower bias-control line used to center the amplifier's output relative to its operational range.

The IGE structure consists of two primary components: a floating-gate electrode and a driven-gate electrode. An input signal is applied to the driven-gate electrode, and it is coupled to the floating-gate electrode with the chemically-sensitive thin-film coating which covers the IGE structure. Metal-doped phthalocyanine (MPc) organic semiconductor compounds were used as the chemically-sensitive thin-films in this research study; more

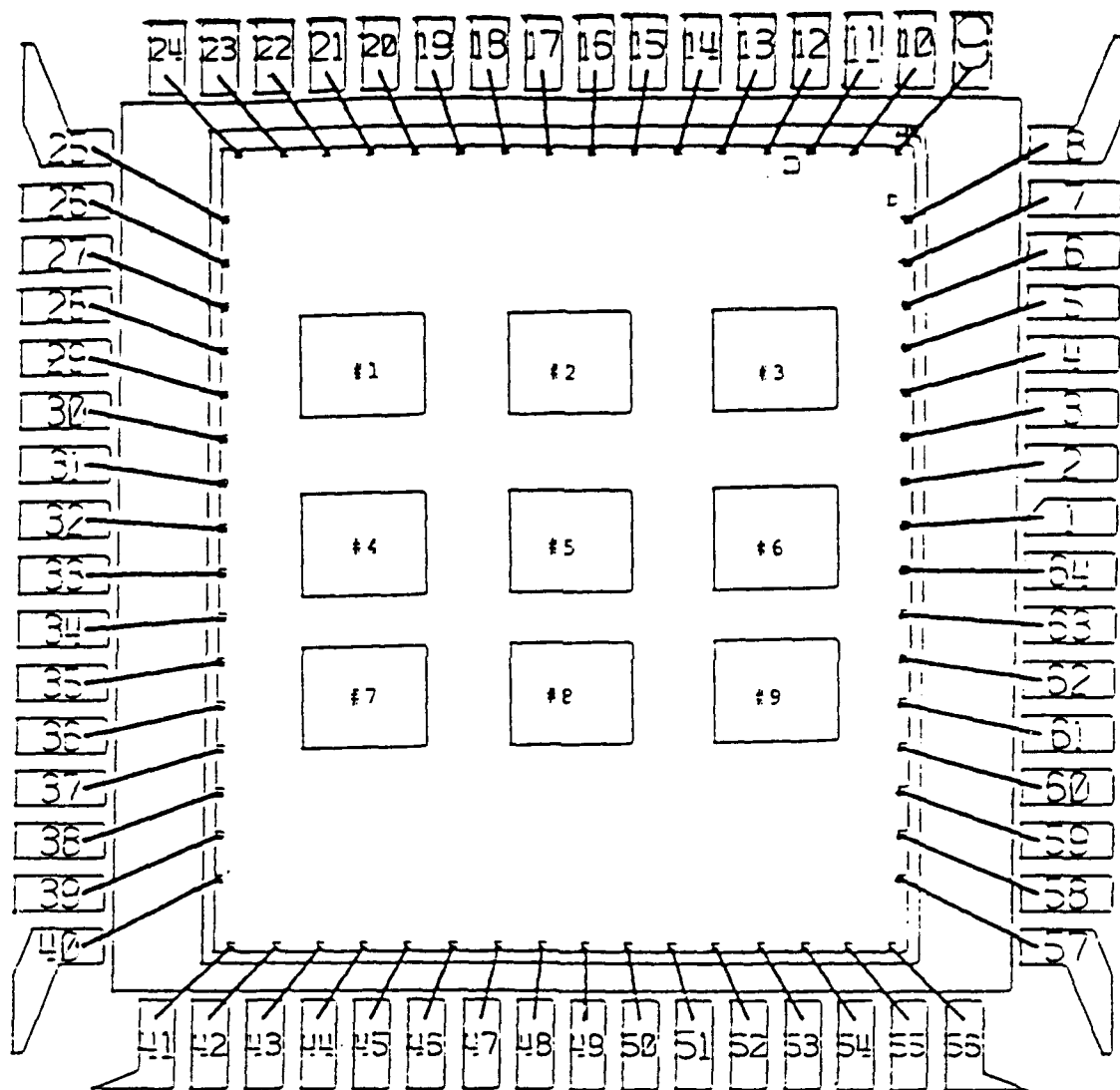


Figure 4.4: IGEFET IC Die Bond Pad Diagram.

Table 4.2: Bond Pad Connections for the IGEFET Microsensor.

| Bond Pad Number | Function |
|-----------------|----------------------------|
| 1 | Vbias, Amplifier #6 |
| 2 | Vss #6 |
| 3 | Vout, Amplifier #6 |
| 4 | not used |
| 5 | Floating-Gate Electrode #6 |
| 6 | not used |
| 7 | Driven-Gate Electrode #3 |
| 8 | not used |
| 9 | Vbias, Amplifier #3 |
| 10 | not used |
| 11 | Vout, Amplifier #3 |
| 12 | not used |
| 13 | Floating-Gate Electrode #3 |
| 14 | not used |
| 15 | Vbias, Amplifier #2 |
| 16 | Vss #1, #2, #3 |
| 17 | Vout, Amplifier #2 |
| 18 | Vdd, Amplifier #1, #2, #3 |
| 19 | Floating-Gate Electrode #2 |
| 20 | not used |
| 21 | Vbias, Amplifier #1 |
| 22 | not used |
| 23 | Vout, Amplifier #1 |
| 24 | not used |
| 25 | Floating-Gate Electrode #1 |
| 26 | not used |
| 27 | Driven-Gate Electrode #2 |

Table 4.2: (continued)

| Bond Pad Number | Function |
|-----------------|----------------------------|
| 28 | Driven-Gate Electrode #5 |
| 29 | Driven-Gate Electrode #4 |
| 30 | Driven-Gate Electrode #1 |
| 31 | Vbias, Amplifier #4 |
| 32 | Vss #4, #5 |
| 33 | Vout, Amplifier #4 |
| 34 | Vdd, Amplifier #4 |
| 35 | Floating-Gate Electrode #4 |
| 36 | not used |
| 37 | Vbias, Amplifier #5 |
| 38 | not used |
| 39 | Driven-Gate Electrode #8 |
| 40 | Driven-Gate Electrode #7 |
| 41 | not used |
| 42 | Vbias, Amplifier #7 |
| 43 | not used |
| 44 | Vout, Amplifier #7 |
| 45 | not used |
| 46 | Floating-Gate Electrode #7 |
| 47 | not used |
| 48 | Vbias, Amplifier #8 |
| 49 | Vss #7, #8, #9 |
| 50 | Vout, Amplifier #8 |
| 51 | Vdd, Amplifier #7, #8, #9 |
| 52 | Floating-Gate Electrode #8 |
| 53 | not used |
| 54 | Vbias, Amplifier #9 |

Table 4.2: (continued)

| Bond Pad Number | Function |
|-----------------|-------------------------------|
| 55 | not used |
| 56 | Vout, Amplifier #9 |
| 57 | not used |
| 58 | Floating-Gate Electrode #9 |
| 59 | Ground Plane Under Electrodes |
| 60 | Driven-Gate Electrode #9 |
| 61 | Vout, Amplifier #5 |
| 62 | Vdd, Amplifier #5, #6 |
| 63 | Floating-Gate Electrode #5 |
| 64 | Driven-Gate Electrode #6 |

specifically, CuPc and PbPc thin-films were used. CuPc and PbPc were utilized because of their known p-type semiconducting properties, and their ability to absorb and desorb NO₂ [8, 9, 38, 39, 40], DMMP [20, 25, 35], BF₃ [8], CO [37, 39], and C₂HCl₃ [41].

Prior to the deposition of the CuPc and PbPc thin films on the IGE structures, each of the nine sensors were electronically evaluated to ensure proper functioning of the IGE structure and the corresponding MOSFET amplifier. The deposition of the MPC compounds onto the nine sensors was accomplished via a sublimation process which utilized a thermal evaporation vacuum deposition system (Denton Vacuum Corp., Model DV-602) located in the AFIT Cooperative Electronics and Materials Processing Laboratory at Wright-Patterson AFB.

The first step implemented to deposit the chemically-sensitive thin films onto the IGE structures was to prepare a mask which would shadow all the elements that were not to be exposed to a particular phthalocyanine compound. The masks for this research were fabricated by using a hard steel punch to form square-shaped holes in strips of a copper sheet. A mask with the desired pattern of holes was placed over the IC die and secured to the dual-in-line package (DIP) with adhesive tape. The 64 pins of the DIP were then covered with aluminum foil to prevent MPC deposits

on the pins and the remaining DIP surfaces were covered to reduce the risk of damaging the IC.

Next, the masked DIP packages were positioned in the vacuum chamber of the deposition system at a location 20 centimeters above the thermal evaporation boat. A silicon wafer was also positioned in the vacuum chamber at the same height above the thermal evaporation boat as the IC packages. This silicon wafer was used to determine the thickness of the deposited MPC materials. The thermal evaporation boat was filled with the desired MPC material (i.e., CuPc (Pfaltz & Bauer, Inc., Stock L02080, Waterbury, CT) or PbPc (Pfaltz & Bauer, Inc., Stock C25430, Waterbury, CT)). The vacuum chamber was sealed and pumped to a vacuum level of 10^{-5} Torr. The chosen MPC was then slowly heated for 3 minutes prior to deposition by gradually increasing the current to 180 amperes to the thermal evaporation boat charged with the MPC. This process resulted in a controllable sublimation of the MPC. The sublimed MPC was then deposited onto the unmasked portion of the IC package.

The vacuum chamber contained a piezoelectric quartz crystal microbalance (QCM) which monitored the thickness of the deposited MPC. Unfortunately, due to the chemical unknowns of the MPCs used in this research, such as the exact molecular density of the sublimed MPC, the accuracy of the QCM was questionable. Therefore, to ensure accurate

deposition thicknesses, the silicon wafer, which was co-located in the vacuum chamber with the DIP, and thus deposited with essentially the same thickness of the MPC material, was measured with a stylus profilometer (Sloan Technology Corp., Model Dek-Tak 900051). The measured thicknesses of the CuPc and the PbPc are shown in Table 4.3. The arrangement of the sensing elements within the array is shown in Figure 4.5. The thin-film coatings deposited on the sensing elements are shown in Figure 4.6. A batch of six CHEMFET IC die were fabricated with the specified metal-doped phthalocyanines and the specified thicknesses.

4.3 Evaluation Procedures

The specific electrical and ambient parameters were chosen to yield the most favorable performance measurements for the CHEMFET. Several electrical measurements were conducted during this research investigation. The IGE structure's dc resistance, its ac impedance, and the sensor's frequency- and time-domain responses were investigated.

The electronic measuring instrumentation used to accumulate the required data included: an electrometer, an impedance analyzer, a gain/phase analyzer, a spectrum analyzer, and a digital storage oscilloscope. To efficiently collect data from these instruments, a

Table 4.3: IGEFET Configuration Matrix of the Chemically-Sensitive Thin Films.

| Element Number | MPC Compound | Thickness (Å) |
|----------------|--------------|---------------|
| 1 | PbPc | 300 |
| 2 | CuPc | 250 |
| 3 | PbPc | 300 |
| 4 | PbPc | 650 |
| 5 | CuPc | 550 |
| 6 | PbPc | 650 |
| 7 | PbPc | 1100 |
| 8 | CuPc | 1000 |
| 9 | PbPc | 1100 |

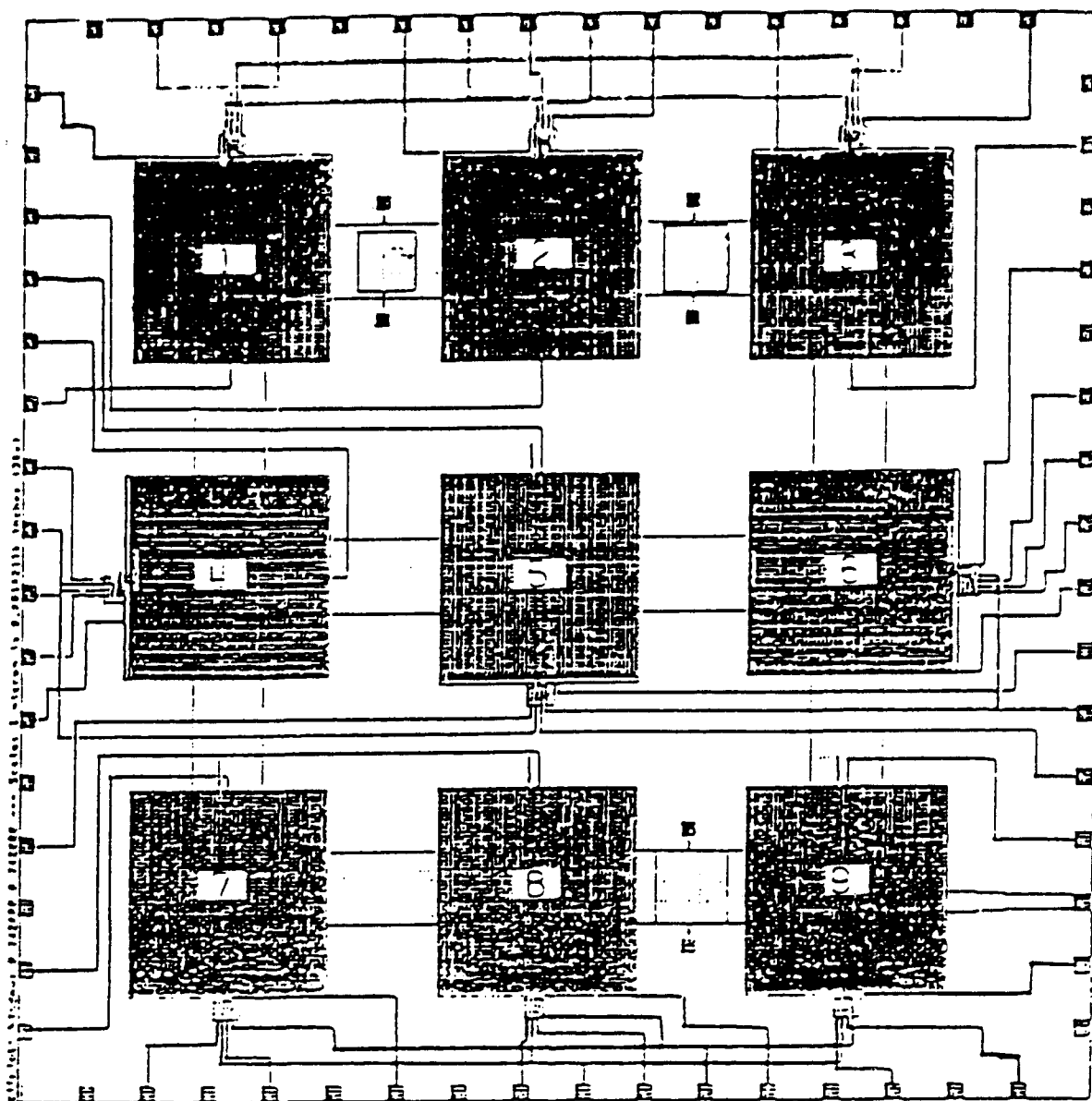


Figure 4.5: IC Die Layout of Nine Sensing Elements and Connections.

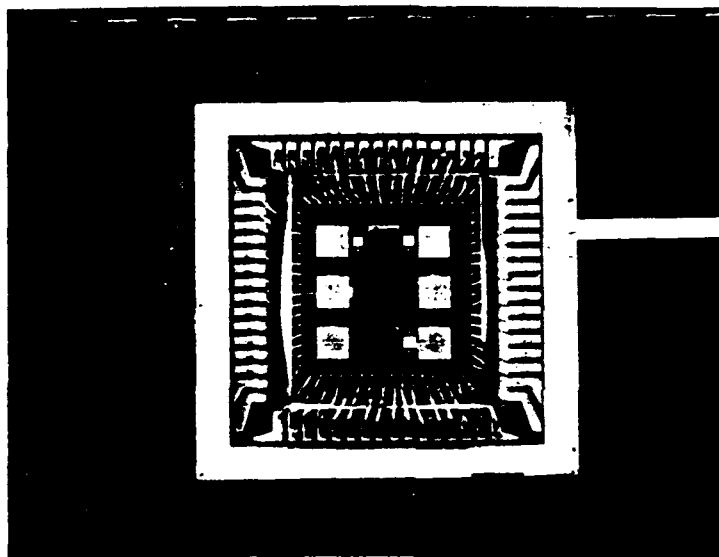


Figure 4.6: Optical Photograph of CHEMFET with Thin-Film Coatings.

General Purpose Instrumentation Bus (GPIB) card (Capital Equipment Corp., Model PC-488, Burlington, MA) was used in conjunction with a Zenith 248 personal computer (Zenith Data Systems, St. Joseph, MI). The general layout of the instrumentation is shown in Figure 4.7. Software programs written in PASCAL were used to initialize, trigger, and reset the instruments, as well as to measure and store the data for subsequent off-line processing. The program listings are located in Appendix A.

4.3.1 DC Resistance Measurements. An electrometer (Keithley Instruments Inc., Model 617, Cleveland, OH) was used to measure the dc resistance of the IGE structure. The dc resistance for each thin-film specie was measured between the driven-gate and floating-gate electrode contacts. The electrometer was used in the voltage/ampere (V/I) mode. This mode facilitated the measurement of resistance magnitudes on the order of 10^{16} ohms (resistance values for phthalocyanine thin-films can be as great as $10^{16} \Omega$). Furthermore, the (V/I)-mode minimizes the adverse effects of the IGE structure's distributed capacitance and resistance leakage. The dc resistance was measured and recorded as a function of time. In order to establish the dc measurements across the IGE structure, the electrometer uses a bias voltage to drive a current through the driven-gate

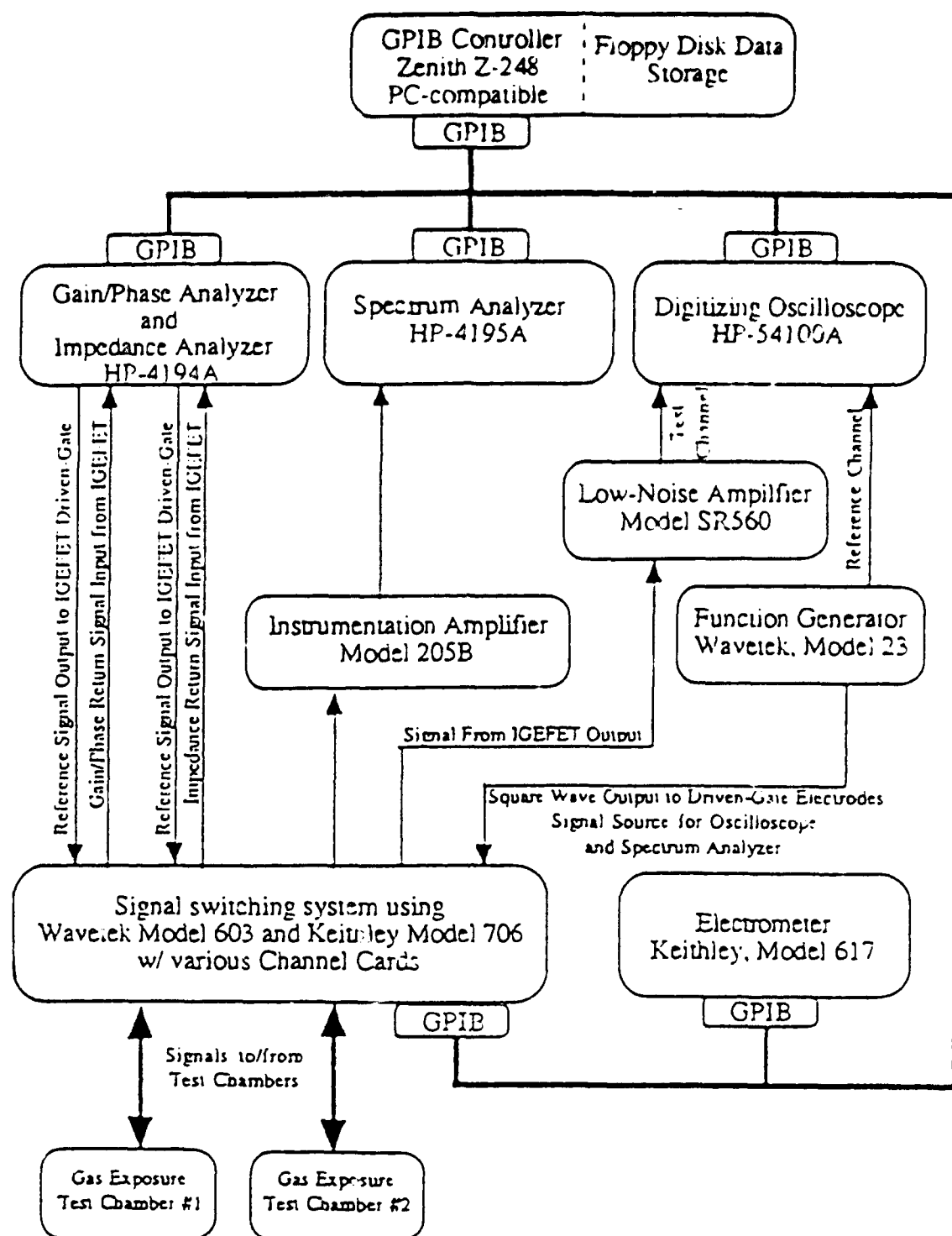


Figure 4.7: System Architecture of Instrumentation and GPIB [8].

and floating-gate electrodes. The most favorable operating bias-voltage was determined from previous studies [8, 9], and it yielded a region which most closely approximated the linear response of the CuPc and PbPc thin films. The dc resistance was measured, averaged, and recorded every 20 seconds for each IGE structure, and this situation resulted in a temporal period of 3 minutes to characterize the entire IC die.

4.3.2 Impedance Measurements. The ac impedance of the interdigitated gate electrodes was measured across the driven-gate and floating-gate electrodes and recorded with an impedance-gain/phase analyzer (Hewlett Packard, Model HP4194A, Palo Alto, CA). The analyzer was used in the impedance measurement mode with the level of oscillation set at 1 volt peak-to-peak. The impedance was measured as a function of frequency (10 Hz to 1 MHz). Both the real and the imaginary components of the impedance were derived from Equation (4.1) and Equation (4.2), respectively:

$$\text{Re}(Z) = |Z| \cos(\phi) \quad (4.1)$$

$$\text{Im}(Z) = |Z| \sin(\phi) \quad (4.2)$$

where $|Z|$ is the magnitude of the impedance, and ϕ is the phase angle of the impedance.

4.3.3 Gain and Phase Angle Measurements. The impedance-gain/phase analyzer was also used to collect the gain and phase data for the microsensor's performance. The analyzer compares the reference (excitation) signal of the CHEMFET with its response (output) signal. The gain/phase mode of the analyzer was used with the level of oscillation established to obtain a measurement with the least amount of noise interference. The oscillation level varied (peak-to-peak) from 0.2 to 0.4 volts. The voltage gain and the phase difference were measured over a frequency range of 10 Hz to 1 MHz.

4.3.4 Spectrum Measurements. The voltage-pulse response was measured and recorded in the time domain and the frequency domain. The time-domain response measurements were accomplished by applying a voltage pulse from a function generator (Wave-Tek Corp., Model 148, San Diego, CA) and measuring the output response with a digital storage oscilloscope (Hewlett Packard, Model HP54100A, Palo Alto, CA). The function generator produced a square-wave pulse which had a period of 1 millisecond, a width of 5 microseconds, and an amplitude of 2.5 volts. The pulse shape is shown in Figure 4.8. The function generator was also used to enable sampling the spectral response with the

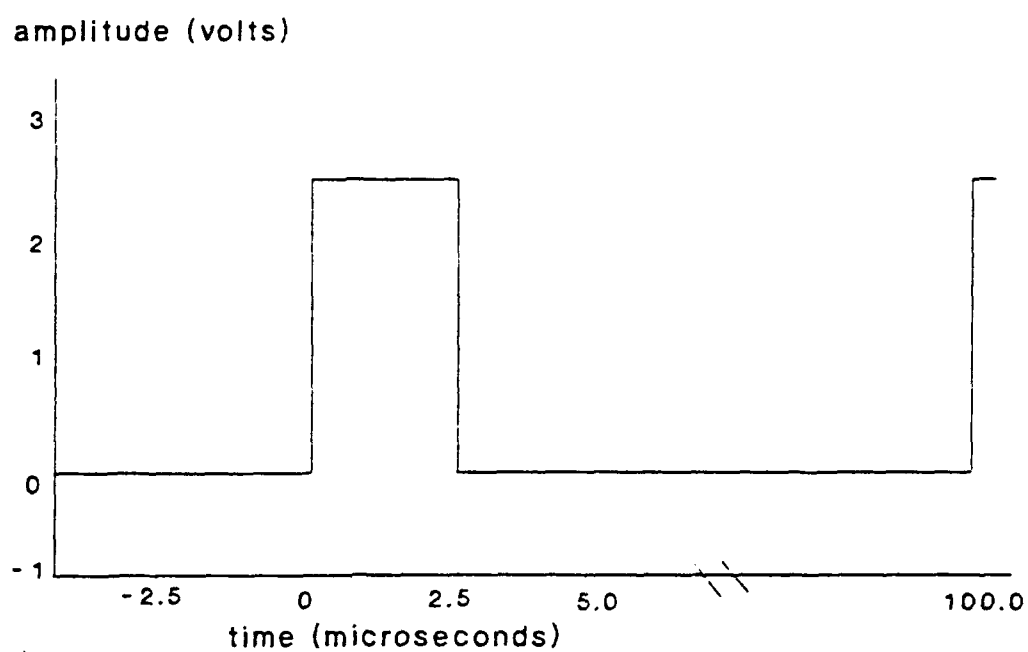


Figure 4.8: Voltage Pulse Used to Establish the Time- and Frequency-Domain Responses of the IGEFET.

spectrum analyzer (Hewlett Packard, Model 4195A, Palo Alto, CA) in order to gather measurements in the frequency domain. The output signal from the CHEMFET was passed through a low-noise amplifier (Stanford Research Systems, Model SR560, Sunnyvale, CA) before being sent to the spectrum analyzer. The spectrum analyzer was initialized to measure the microsensor's response over a frequency range of 10 Hz to 200 KHz, which coincides with the bandwidth (3 dB) of the signal.

4.3.5 Testing. Preliminary tests were performed prior to exposing the CHEMFET to the challenge gases to obtain a baseline response of the system from which a comparison could be made with the subsequent challenge gas exposure data. The electrical test parameter ranges and physical test conditions, such as operating temperature, thin-film thicknesses, and challenge gas concentrations, were formulated from the pertinent previous studies [8, 9, 11, 23, 41]. One of the primary interests of this research effort was to investigate what effects the exposure time had on the characteristics (specifically the microsensor's reversibility) of the CHEMFET. Previous studies performed at AFIT [8, 9, 20, 23, 35] used challenge gas exposure durations spanning 15 to 90 minutes. This investigation, however, exposed the chemically-sensitive thin-films to

small concentrations of the challenge gases for much shorter durations (i.e., the gas "plug" had a time duration spanning 2 to 6 minutes). The challenge gas concentration and the time duration for an exposure was accurately controlled by utilizing electrically-triggerable mass flow controllers.

The timing of the carrier and diluent gas (filtered air), relative to the activation of the instrumentation, was of primary importance. For a one hour period prior to the data collection process, the test chamber and the IC packages were heated to the desired operating temperature. The carrier and diluent gas (room air with a relative humidity (RH) of 2%) was allowed to flow through the test chamber at a rate of 100 ml/min. After this initial period of achieving a stabilized temperature and baseline, the data collection process was initiated. After period of 15 minutes, a challenge gas "plug" was introduced into the test cell. The challenge gas "plug" was a pulse of gas having a time duration of 3 minutes (the amount of time for the instrumentation to assay all nine elements) and an amplitude equal to that of the desired concentration. After the exposure to the challenge gas "plug", the CHEMFET was purged with room air at 100 ml/min until equilibrium (reversibility to within 90% of the original baseline response) was achieved. Figure 4.9 graphically displays the concept of the challenge gas "plug" and the associated purge time.

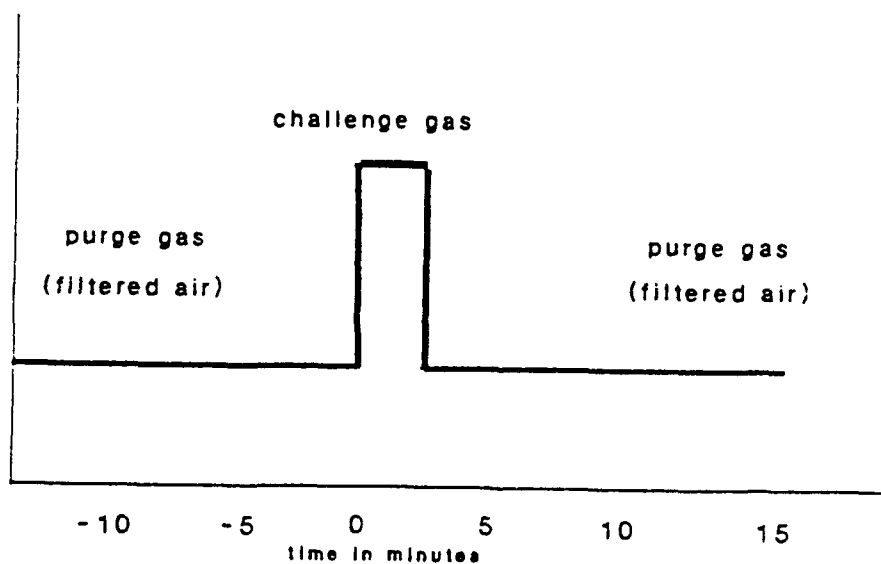


Figure 4.9: Graphical Representation of the Challenge Gas "Plug".

The challenge gases used for detection and quantification purposes included: NO_2 , DMMP, and BF_3 . NO_2 is an electron acceptor gas, and it was used as a representative pollutant for the oxides which corrode electronic equipment. DMMP is an organophosphorus compound which has a molecular structure closely resembling chemical-warfare nerve agents and pesticides. BF_3 is a strong electron acceptor gas similar to NO_2 , and this gas compound is also toxic to living organisms. These challenge gases are available in permeation tubes (GC Industries, Inc., Chatsworth, CA). These permeation tubes are designed to continuously emit a fixed rate of the challenge gas when heated to a specific operating temperature. The challenge gas can then be mixed with the carrier gas (room air at a specific flow rate) to generate the required concentration of the challenge gas. In this research investigation, the following formula was used to determine the challenge gas concentration:

$$C = \frac{K * P}{F} \quad (4.3)$$

where C is the challenge gas concentration in ppm, K is the gas permeability constant (i.e., for NO_2 , $K=0.532$; for DMMP,

$K=0.197$; for BF_3 , $K=0.361$), and P is the permeation rate in nanograms/minute at a given temperature (i.e., at 50°C , $P=6200$ for NO_2 , $P=1100$ for DMMP, and $P=2070$ for BF_3), and F is the carrier gas flow rate in milliliters/minute.

Another similar series of electrical tests were accomplished whose purpose was to screen several challenge gas candidates for their detectability properties. The gases used for these experiments included: CH_3OH , CO , CH_2CHCl , and C_2HCl_3 . These four gases are volatile organic compounds (VOCs), and they pose a threat to the environment. CH_3OH and CO are available in permeation tubes. However, CH_2CHCl and C_2HCl_3 are not available in permeation tubes; the delivery system for exposing the CHEMFET to these two gases was modified. At room temperature, CH_2CHCl and C_2HCl_3 are liquids. When heated to their respective equilibrium vaporization points, a specific concentration of each challenge gas was collected in a heated syringe. The gas molecules were then injected into the test chamber, and the electrical characteristics were measured and recorded by the computer-controlled instrumentation.

Table 4.4 summarizes the challenge gases and the concentrations that were used in this investigation.

Table 4.4: Challenge Gases and Concentrations Utilized.

| Challenge Gas | Concentration (ppb) |
|---------------------------------|---------------------|
| NO ₂ | 10 |
| | 50 |
| | 100 |
| | 500 |
| | 1000 |
| DMMP | 50 |
| | 100 |
| | 500 |
| | 1000 |
| | 10000 |
| BF ₃ | 50 |
| | 100 |
| | 1000 |
| | 10000 |
| | 20000 |
| CH ₃ OH | 1000 |
| | 5000 |
| | 10000 |
| CO | 10000 |
| | 20000 |
| | 50000 |
| CH ₂ CHCl | 30 |
| | 100 |
| | 1000 |
| C ₂ HCl ₃ | 10 |
| | 50 |
| | 100 |

4.4 Summary

This chapter presented a brief discussion of the redesign and characteristics of the CHEMFET IC. The die consists of nine sensing elements based upon an IGE structure coupled to an inverting MOSFET amplifier. The IGE structures were coated with different thicknesses of the metal-doped phthalocyanine thin-films (CuPc and PbPc). The electrical conductivity modulation of these devices was measured and recorded with a series of instruments controlled by a personal computer and GPIB. The experimental test equipment configuration and the evaluation protocol were explained. The mean values of the test parameters were recorded to be used off-line for evaluation of the sensitivity, selectivity, and reversibility of the CHEMFET subject to the established operating conditions.

Chapter 5

5 Analysis of the Experimental Performance Results and Discussion

5.1 Introduction

This chapter presents the experimental results and an analysis of the performance of the CHEMFET. The first section details the baseline performance data for the uncoated and coated microsensor. The second and third sections present the analysis and comparison of data obtained from the microsensor CHEMFET elements that were coated with CuPc and PbPc, respectively. The final three sections discuss the sensitivity, selectivity, and reversibility of the CHEMFET relative to the film type, film thickness, challenge gas, the concentration of the challenge gas, and the operating temperature.

5.2 Baseline Data

A visual and electrical inspection of the CHEMFET was accomplished to ensure that the microsensor functioned properly and to acquire the baseline performance data. Only one die (#6) was determined to be damaged, and it was eliminated from the group of IC's that were tested. Baseline data was established for the microsensors prior to the deposition of the MPC thin-films, as well as after the

CuPc and the PbPc coatings were deposited on the IGE structures of the microsensors. The baseline data for the five functioning CHEMFET die were used to compare and establish for the reproducibility of the electrical characteristics of each sensing element. Table 5.1 presents the dc electrical resistance values measured at room temperature (22°C) for each of the nine sensing elements on each die before the deposition of the MPC thin-films. Correspondingly, Table 5.2 contains the dc electrical resistance values measured at room temperature (22°C) for the nine sensing elements that were coated with different thicknesses of CuPc or PbPc. A comparison of the dc resistance values between the uncoated and the coated IGE structures reveals that a measurable decrease (ranging from one to three orders of magnitude) occurs when either PbPc or CuPc is deposited on the IGE structure. This decrease in dc resistance can be deduced from the electrical properties of the metal-doped phthalocyanines. On the basis of the fundamental response to donor and acceptor gases, CuPc and PbPc are classified as p-type semiconductors. Due to the fact that the family of phthalocyanine compounds are semiconductors, the internal dc electrical resistance of the individual dielectrically-supported (SiO_2) IGEFET sensing elements should decrease since a greater amount of electrical current can flow through the system due to the

Table 5.1: DC Resistance Values ($\times 10^{12} \Omega$) for Uncoated Sensing Elements at 22°C

| Device Number | Element | | | | | | | | |
|---------------|---------|-----|-----|-----|-----|-----|-----|-----|-----|
| | 1 | 2 | 3 | 4 | 5 | 6 | 7 | 8 | 9 |
| 1 | 4.7 | 3.9 | 3.7 | 4.1 | 3.9 | 4.5 | 4.5 | 4.0 | 3.9 |
| 2 | 3.8 | 4.1 | 3.7 | 3.3 | 3.8 | 4.0 | 4.1 | 3.8 | 4.2 |
| 3 | 4.6 | 4.8 | 4.2 | 4.7 | 4.1 | 5.0 | 4.6 | 4.6 | 4.7 |
| 4 | 3.9 | 4.2 | 5.1 | 4.3 | 4.4 | 4.3 | 5.0 | 4.2 | 4.0 |
| 5 | 5.1 | 3.9 | 4.2 | 4.2 | 3.9 | 3.7 | 4.5 | 3.8 | 4.0 |
| 6 | 4.2 | 4.7 | 3.9 | 4.4 | 4.7 | 4.9 | 3.6 | 4.1 | 4.3 |

Table 5.2: DC Resistance Values ($\times 10^{10} \Omega$) for Coated Sensing Elements at 22°C

| Device Number | Element/ Coating/ Thickness (Å) | | | | | | | | |
|---------------|---------------------------------|-------------|-------------|-------------|-------------|-------------|--------------|--------------|--------------|
| | 1 | 2 | 3 | 4 | 5 | 6 | 7 | 8 | 9 |
| | PbPc 300 | CuPc 250 | PbPc 300 | PbPc 650 | CuPc 550 | PbPc 650 | PbPc 1100 | CuPc 1000 | PbPc 1100 |
| 1 | 0.25 | 3.07 | 0.31 | 1.47 | 5.36 | 1.22 | 7.28 | 24.1 | 8.00 |
| 2 | 0.43 | 2.59 | 0.28 | 2.01 | 5.10 | 2.17 | 6.44 | 30.2 | 8.29 |
| 3 | 0.88 | 1.87 | 0.59 | 1.63 | 4.92 | 1.90 | 6.39 | 29.1 | 7.85 |
| 4 | 0.51 | 2.89 | 0.85 | 1.89 | 5.75 | 2.01 | 7.11 | 24.9 | 7.99 |
| 5 | 0.60 | 2.77 | 0.55 | 1.48 | 5.39 | 1.45 | 6.93 | 27.3 | 8.41 |
| 6* | --- | --- | --- | --- | --- | --- | --- | --- | --- |

* Device 6 was damaged in the course of depositing the MPc thin films.

conductive path provided by the MPC coating. The dc electrical resistance values measured at 110°C for the uncoated and the coated sensing elements are shown in Table 5.3 and Table 5.4, respectively.

As shown in Tables 5.1 - 5.4, the dc electrical resistance values varied according to the thin-film type, thin-film thickness, and the operating temperature. The dc electrical resistance values were statistically similar for the uncoated IGEFETs. However, a measurable difference was observed between the dc electrical resistance values for the PbPc and CuPc thin-films. An increase in the dc electrical resistance was noted with an increase in the thin-film thickness, and a decrease in the dc electrical resistance was noted with an increase in the operating temperature.

Temperature testing of the CHEMFET revealed that PbPc and CuPc have unique baseline gain characteristics (Figure 5.1) when exposed to filtered air at 22°C and 110°C. The decrease in the gain of the CHEMFET at the higher operating temperature was expected due to the temperature sensitivity of the inverting MOSFET amplifier design, which contains diffused load resistors, the values of which decrease with an increase in temperature.

Table 5.3: DC Resistance Values ($\times 10^{11} \Omega$) for Uncoated Sensing Elements at 110°C

| Device Number | Element | | | | | | | | |
|---------------|---------|------|------|-----|------|------|------|------|-----|
| | 1 | 2 | 3 | 4 | 5 | 6 | 7 | 8 | 9 |
| 1 | 8.9 | 10.1 | 9.4 | 9.3 | 7.9 | 8.5 | 8.7 | 10.0 | 8.6 |
| 2 | 7.7 | 8.6 | 9.1 | 8.9 | 8.3 | 10.3 | 9.6 | 9.6 | 9.2 |
| 3 | 7.4 | 8.9 | 7.7 | 8.3 | 10.2 | 10.0 | 10.2 | 9.9 | 8.9 |
| 4 | 10.1 | 7.9 | 10.7 | 9.6 | 9.1 | 9.3 | 9.4 | 9.1 | 9.6 |
| 5 | 10.4 | 9.3 | 9.1 | 8.6 | 8.2 | 9.0 | 8.9 | 8.5 | 8.9 |
| 6 | 8.8 | 8.4 | 10.0 | 9.2 | 10.4 | 9.3 | 8.7 | 9.1 | 8.9 |

Table 5.4: DC Resistance Values ($\times 10^9 \Omega$) for Coated Sensing Elements at 110°C

| Device Number | Element/ Coating/ Thickness (Å) | | | | | | | | |
|---------------|---------------------------------|------------------|------------------|------------------|------------------|------------------|-------------------|-------------------|-------------------|
| | 1 PbPc 300 | 2 CuPc 250 | 3 PbPc 300 | 4 PbPc 650 | 5 CuPc 550 | 6 PbPc 650 | 7 PbPc 1100 | 8 CuPc 1000 | 9 PbPc 1100 |
| 1 | 0.91 | 1.34 | 1.02 | 3.41 | 4.99 | 2.89 | 8.31 | 56.1 | 9.27 |
| 2 | 1.13 | 1.98 | 0.99 | 4.02 | 6.07 | 3.17 | 9.14 | 62.9 | 9.35 |
| 3 | 0.98 | 3.01 | 1.51 | 3.82 | 6.12 | 4.31 | 7.99 | 61.4 | 8.79 |
| 4 | 0.89 | 3.58 | 1.22 | 4.53 | 5.99 | 3.18 | 9.00 | 50.7 | 8.41 |
| 5 | 1.52 | 4.00 | 1.03 | 4.10 | 5.79 | 5.01 | 7.51 | 68.0 | 9.42 |
| 6* | --- | --- | --- | --- | --- | --- | --- | --- | --- |

* Device 6 was damaged in the course of depositing the MPC thin film.

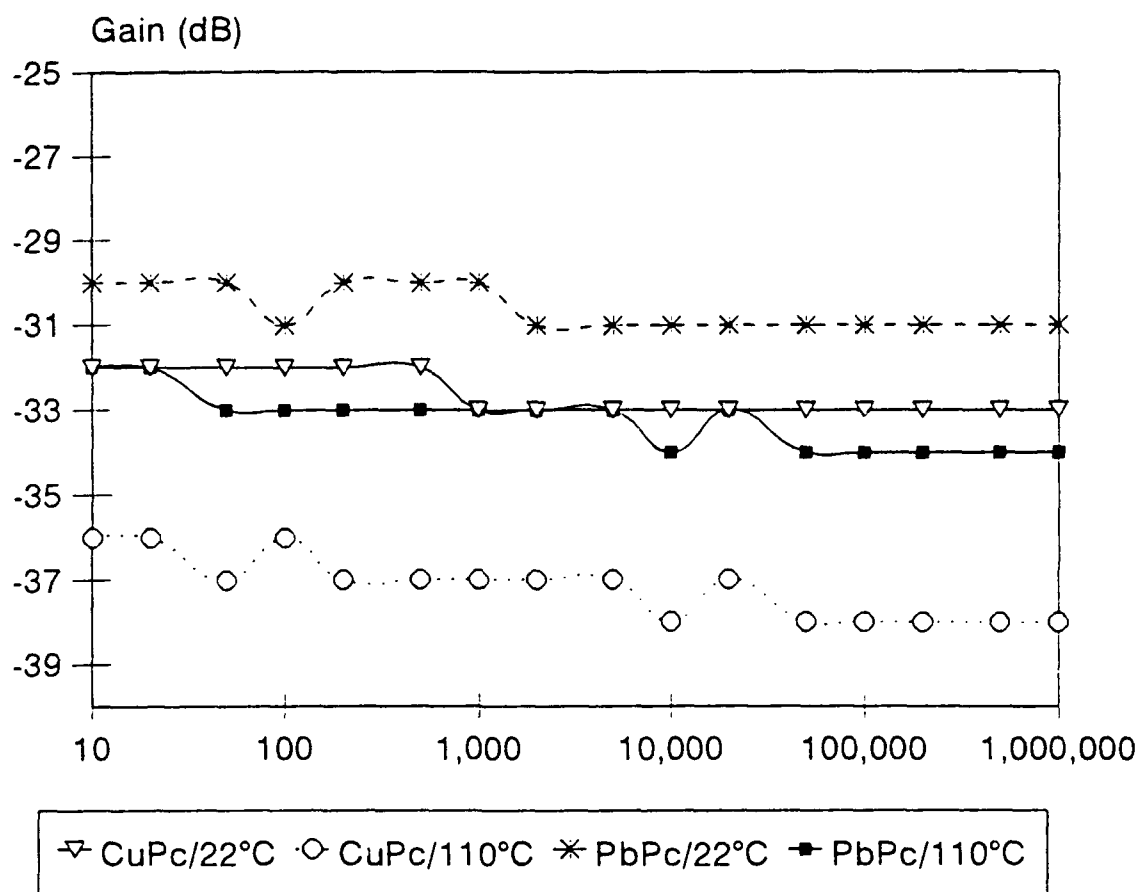


Figure 5.1: Gain of the CHEMFET Coated with CuPc and PbPc when Exposed to Filtered Air.

Measurable changes in the dc electrical resistance of the IGE structures were observed for the baseline performance data. First, a measurable decrease was observed in the dc electrical resistance for the IGE structures that were coated with a metal-doped phthalocyanine thin-film. This was expected since MPc compounds are semiconducting materials which allows a greater amount of current to flow through the driven-gate and floating-gate electrodes. Second, a measurable increase in the dc electrical resistance was observed for IGE structures coated with CuPc films versus the IGE structures coated with PbPc films. It has been shown that PbPc undergoes thermal fragmentation when heated over 300°C [43]. Thermal fragmentation increases the amount of surface oxides that bind to the absorption sites of the PbPc compound, which reduces the conductive properties of the material. Even though thermal fragmentation of the PbPc film was not investigated, the PbPc was heated to approximately 400°C during the thermal evaporation process used to deposit the film onto the IGE structures. Therefore, by heating the PbPc at a high temperature, thermal fragmentation could possibly be assumed to have occurred resulting in a lower resistance of the PbPc film when compared to the CuPc film. Third, a decrease in the dc electrical resistance was observed when the IGE structure was operated at a higher temperature. The

decrease in resistance is a result of the increase in conductivity due to an increase in the available thermal energy. Lastly, the dc resistance increased with increasing film thicknesses. Typically, as the amount of semiconductor material is increased, the resulting resistance decreases. Previous studies have shown CuPc and PbPc to behave as typical semiconductors; a decrease in dc electrical resistance was observed with increasing film thicknesses [8, 9, 25]. In this investigation, numerous measurements were accomplished, all of which revealed an increase in the film's resistance for increasing film thicknesses. The anomaly in this investigation could possibly be attributed to the use of impure MPC compounds or morphologically different films (α -phase versus β -phase) [42].

Changes in the gain were observed. The greater magnitude of gain for CuPc versus PbPc could be expected due to the possibility of thermal fragmentation of the PbPc films at high temperatures. Since CuPc does not undergo thermal fragmentation, it would have a higher magnitude of gain. A higher magnitude of gain was also observed at the higher operating temperature. This characteristic is caused by the inverting MOSFET amplifier design which has a net decrease in resistance at higher operating temperatures. This resistance reduction allows for a greater magnitude of gain to occur.

5.3 Responses of Copper Phthalocyanine

A matrix of CuPc thin-films with different thicknesses and several concentrations of the challenge gases were used in this research effort to verify the measurement methods and to collect gas-sensitivity data. The collected data was compared to data reported in several previous studies [8, 9, 23, 29, 35]. The data from this research indicated that CuPc is sensitive to the three challenge gases investigated: NO₂, DMMP, and BF₃. Furthermore, CuPc is potentially sensitive to CH₃OH, C₂HCl₃, and CH₂CHCl. The CuPc thin-film's response was evaluated by measuring the dc and ac electrical performance characteristics of the CHEMFET.

5.3.1 NO₂ Challenges. The NO₂ gas challenges produced measurable changes in the dc electrical resistance of the IGE, the gain and phase of the CHEMFET, the CHEMFET's voltage-pulse response in the time-domain and the frequency-domain, and the CHEMFET's spectral response when normalized and linearized. Appendix B contains supplemental plots of the electrical responses of the CHEMFET exposed to NO₂.

The dc electrical resistance of the IGE structures coated with CuPc decreased upon exposure of the CHEMFET to NO₂. The percent change in the dc resistance varied with the film's thickness, the concentration of the challenge gas, and the operating temperature. Figure 5.2 shows the change of the dc resistance of three different thicknesses

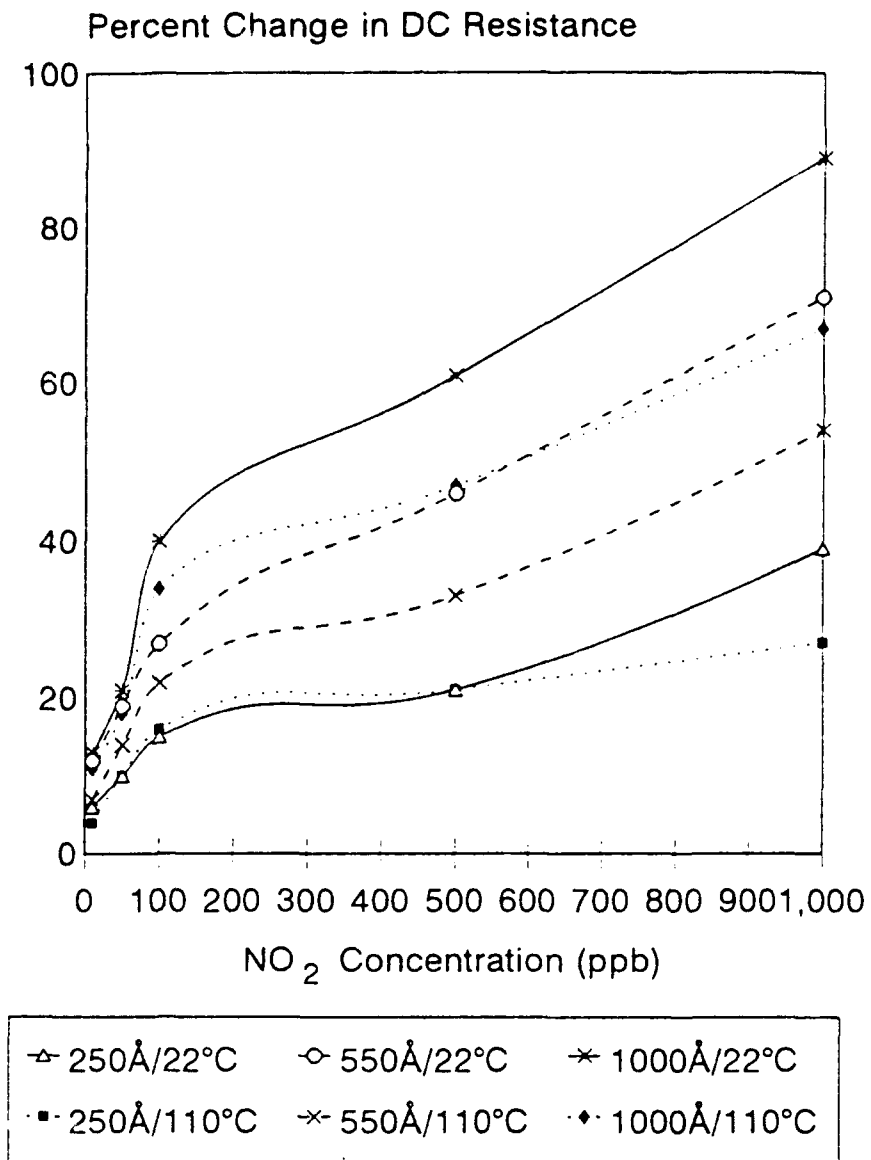


Figure 5.2: Change in DC Resistance of IGE structures coated with CuPc when Exposed to NO₂.

of the CuPc thin-films for the five test gas concentrations at two operating temperatures. It can be observed from the plot that the change in the dc electrical resistance becomes more pronounced with an increase in the gas concentration or an increase in the thin-film thickness. However, as the operating temperature is increased, the overall change in dc electrical resistance decreases.

During the same exposure period for each of the five challenge gas concentrations, the gain for each of the film thicknesses increased. Supplemental graphs in Appendix B show the CHEMFET's gain versus its low frequency response upon exposure to different concentrations of NO_2 . The most dramatic changes in the gain occurred in the low frequency range ($< 10 \text{ KHz}$). Besides being a function of frequency, the changes in the gain appeared to be a function of film thickness, concentration of the challenge gas, and operating temperature. Figure 5.3 shows the change in the gain relative to these influencing factors at 10 Hz. As the frequency is increased, the change in the gain decreases. This behavioral performance trend also occurs as the operating temperature increases. On the other hand, as the thin-film thickness and the challenge gas concentration are increased, the change of the gain increases. Similar to the behavior of the gain at low frequencies, the magnitude of the phase angle of the CHEMFET increases when challenged

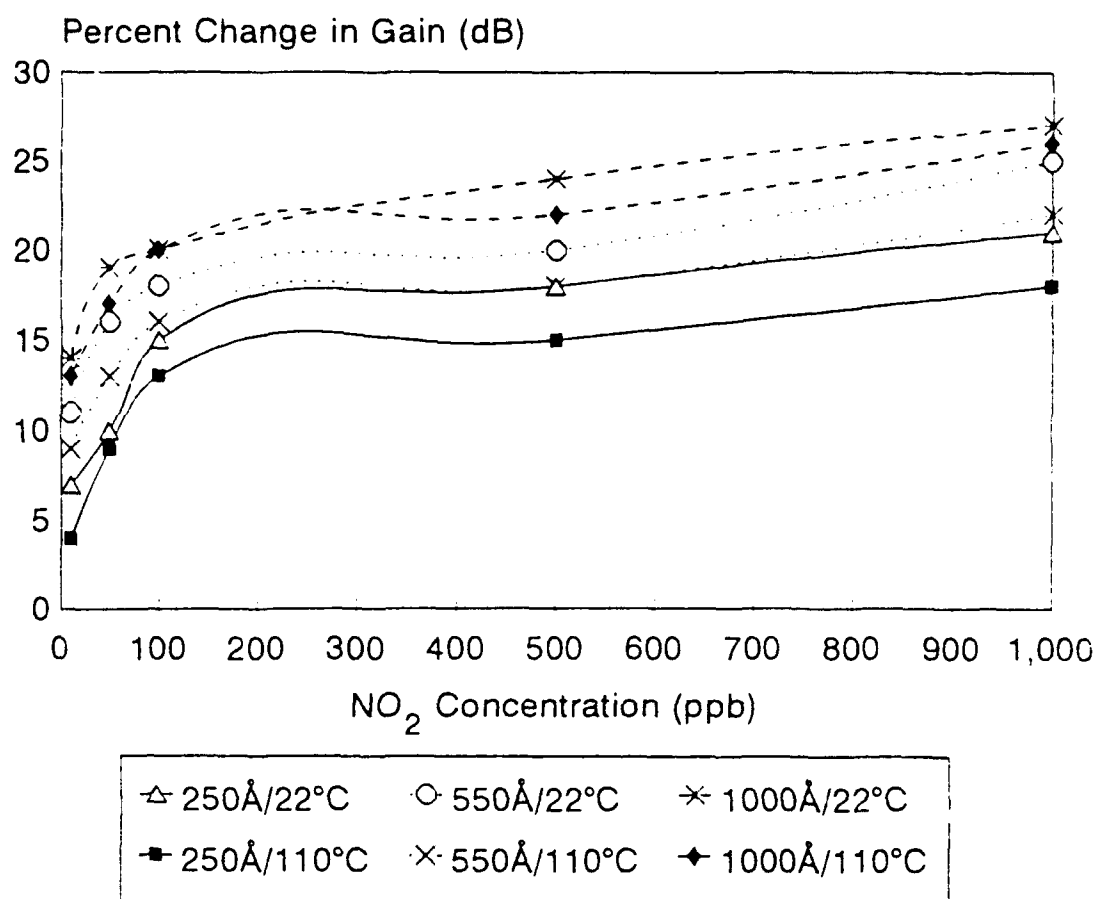


Figure 5.3: Change in Gain at 10 Hz of CuPc CHEMFET when Exposed to NO₂.

with NO_2 . The change in the phase angle is primarily caused by the operating temperature and the challenge gas concentration. However, unlike changes in the gain, the variations in thin-film thickness did not seem to alter the phase angle characteristics. Figure 5.4 represents the change in the phase of the CHEMFET versus gas concentration at 10 Hz.

The time-domain voltage-pulse response of the CHEMFET upon exposure to NO_2 is shown in Figure 5.5 and Figure 5.6 for 22°C and 110°C , respectively. The input excitation pulse for the time-domain response was the 2.5-volt, 5-microsecond duration pulse depicted in Figure 4.8. An identical pulse was used to excite the CHEMFET to extract the spectral response in the frequency domain.

Supplemental graphs in Appendix B show the frequency-domain response in the form of the electrical impedance of the IGE structure (resistive and reactive components) versus frequency (10 Hz to 1 MHz).

The spectral response of the CuPc CHEMFET when exposed to NO_2 indicated a decrease in the electrical conductivity throughout the measured frequency range (10 Hz to 1 MHz). It was convenient to normalize the spectral response to facilitate the analysis of this electrical information. The details of the process for normalizing the spectral response is described by Shin [20].

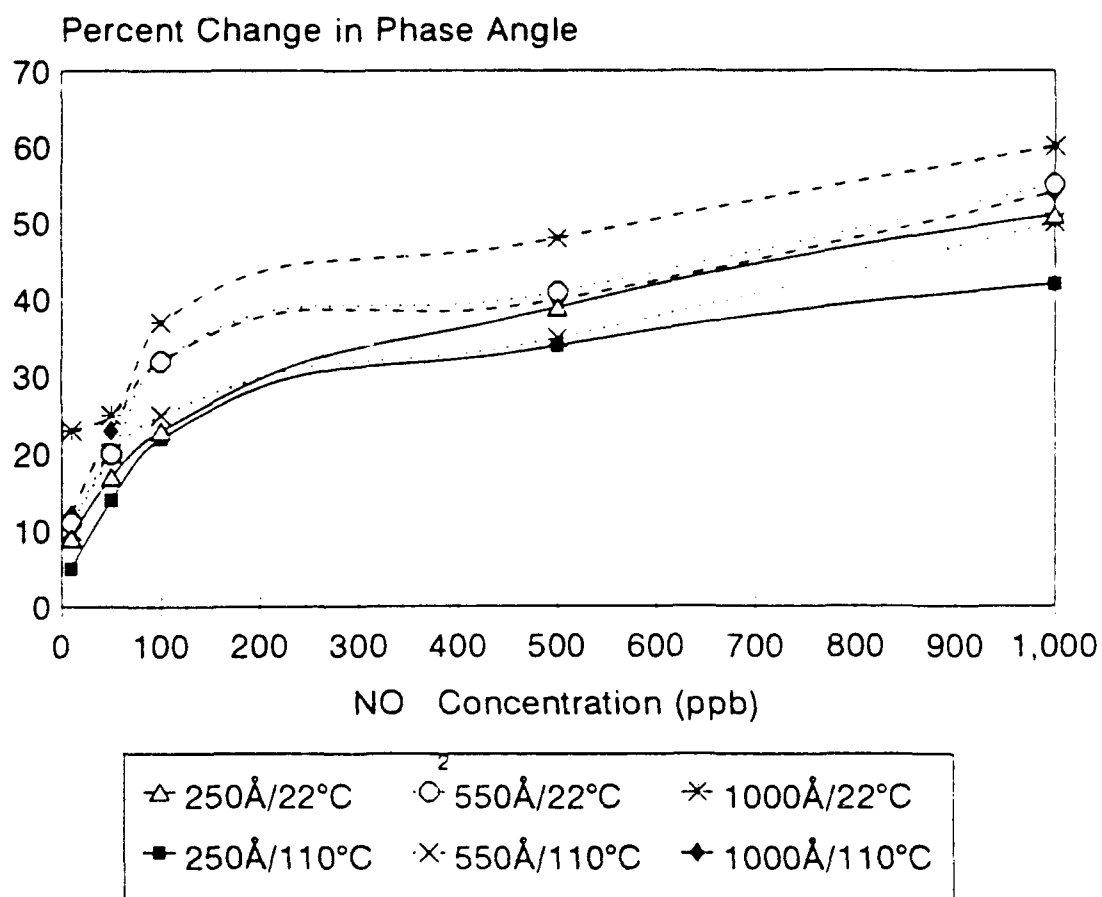


Figure 5.4: Change in Phase Angle at 10 Hz of CuPc CHEMFET when Exposed to NO_2 .

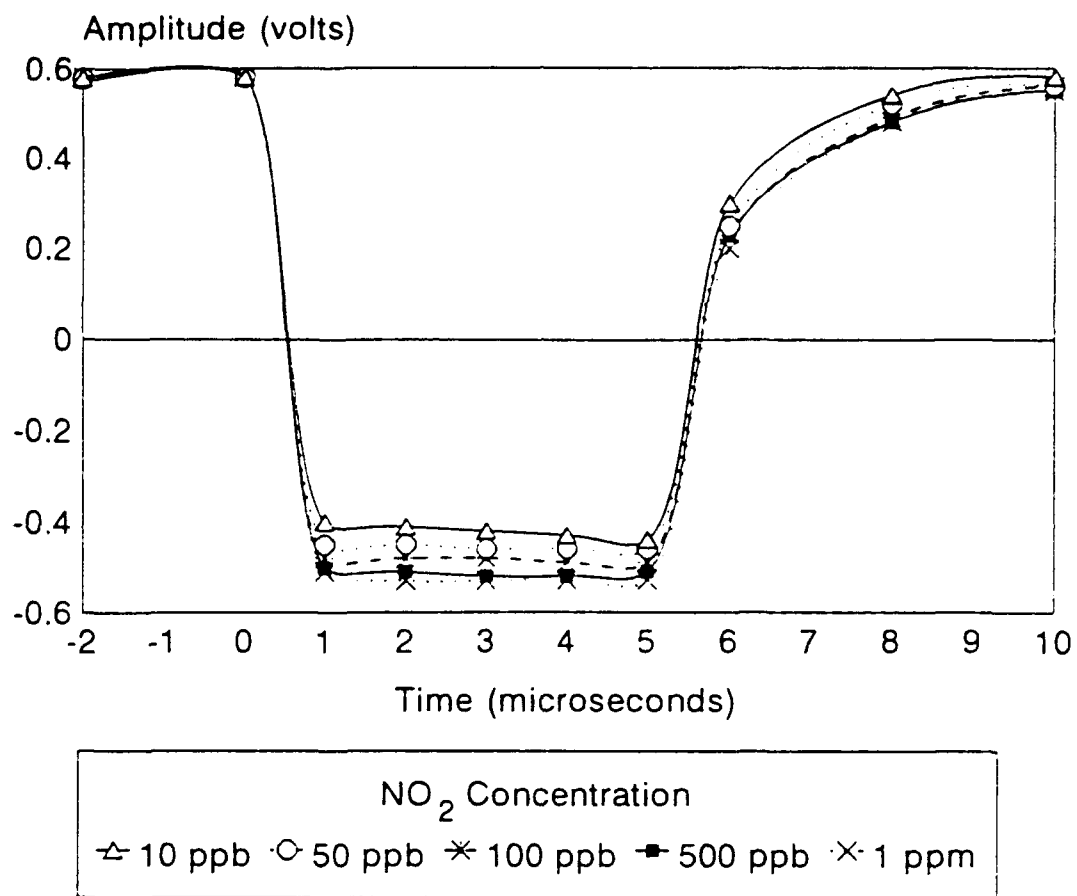


Figure 5.5: Time-Domain Response of CuPc CHEMFET Operated at 22°C when Exposed to NO₂.

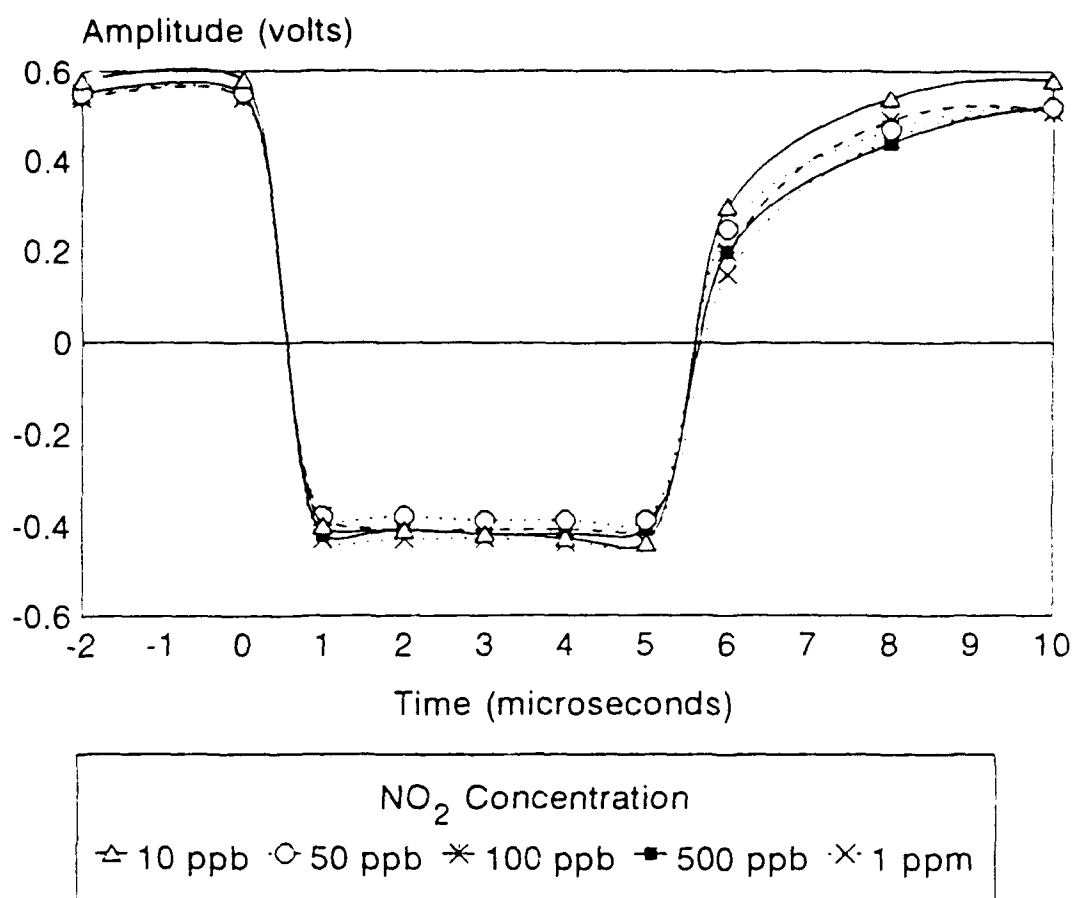


Figure 5.6: Time-domain Response of CuPc CHEMFET Operated at 110°C when Exposed to NO₂.

Figures 5.7 through 5.9 show the normalized, difference spectra for the three CuPc thin-film thicknesses used in this investigation. Varying the operating temperature did not significantly affect the normalized difference spectrum curves; the challenge gas concentration and the film thickness were the predominant factors which caused the variations in responses. While, the magnitude of the normalized difference spectrum is important, the slope of the difference spectrum is unique for each concentration of NO_2 . The combination of the magnitude of the normalized difference spectrum and the unique slope yields a unique zero-crossing point with respect to the sampling frequency for each concentration at each film thickness. The zero-crossing points are depicted in Table 5.5. These unique zero-crossing points were shown to be reproducible by repeating the experimental and evaluation processes and obtaining similar results. The value of the sampling frequency relative to the zero-crossing points of the normalized difference spectral response increases as the concentration of the challenge gas is increased. Likewise, the value of the sampling frequency also increases as the film thickness is increased.

Exposing the CHEMFET coated with CuPc films to different concentrations of NO_2 gas resulted in measurable changes in the dc electrical resistance, gain and phase

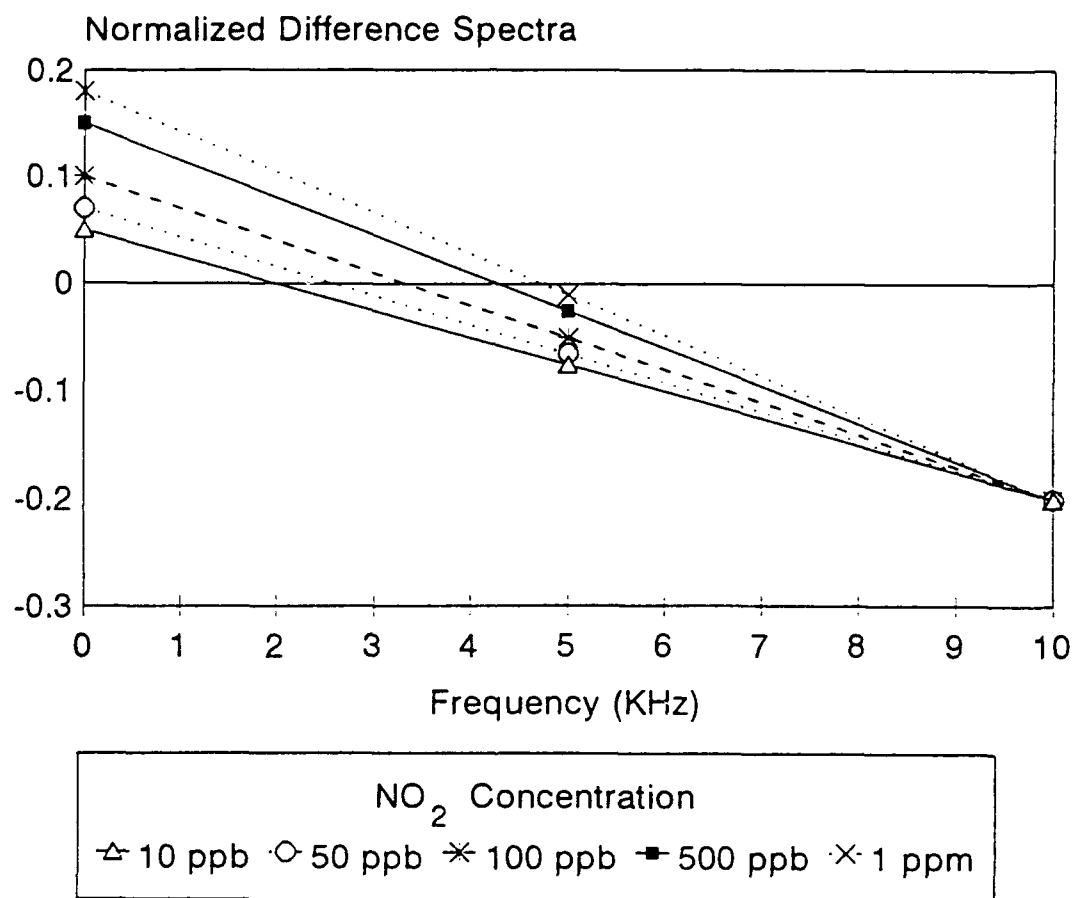


Figure 5.7: Difference Spectral Response of 250 Å Thick CuPc Film when Exposed to NO₂.

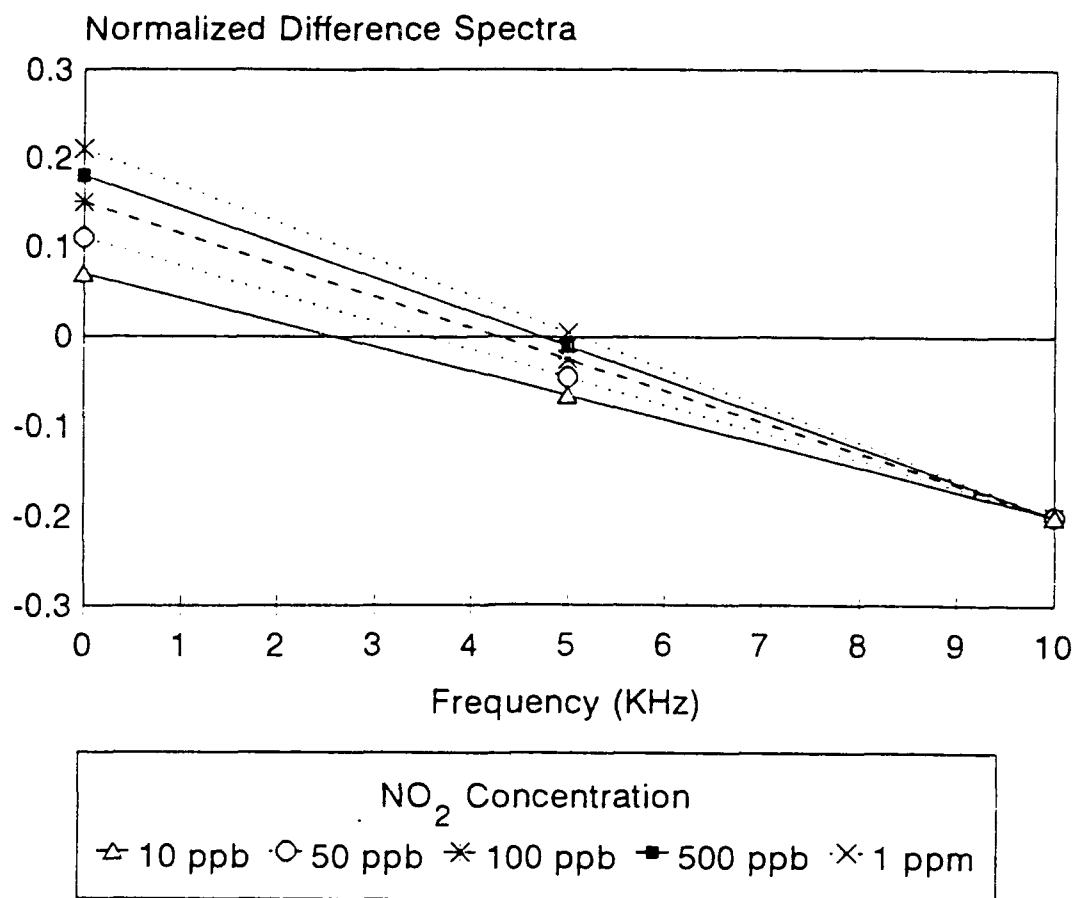


Figure 5.8: Difference Spectral Response of 550 Å Thick CuPc Film when Exposed to NO₂.

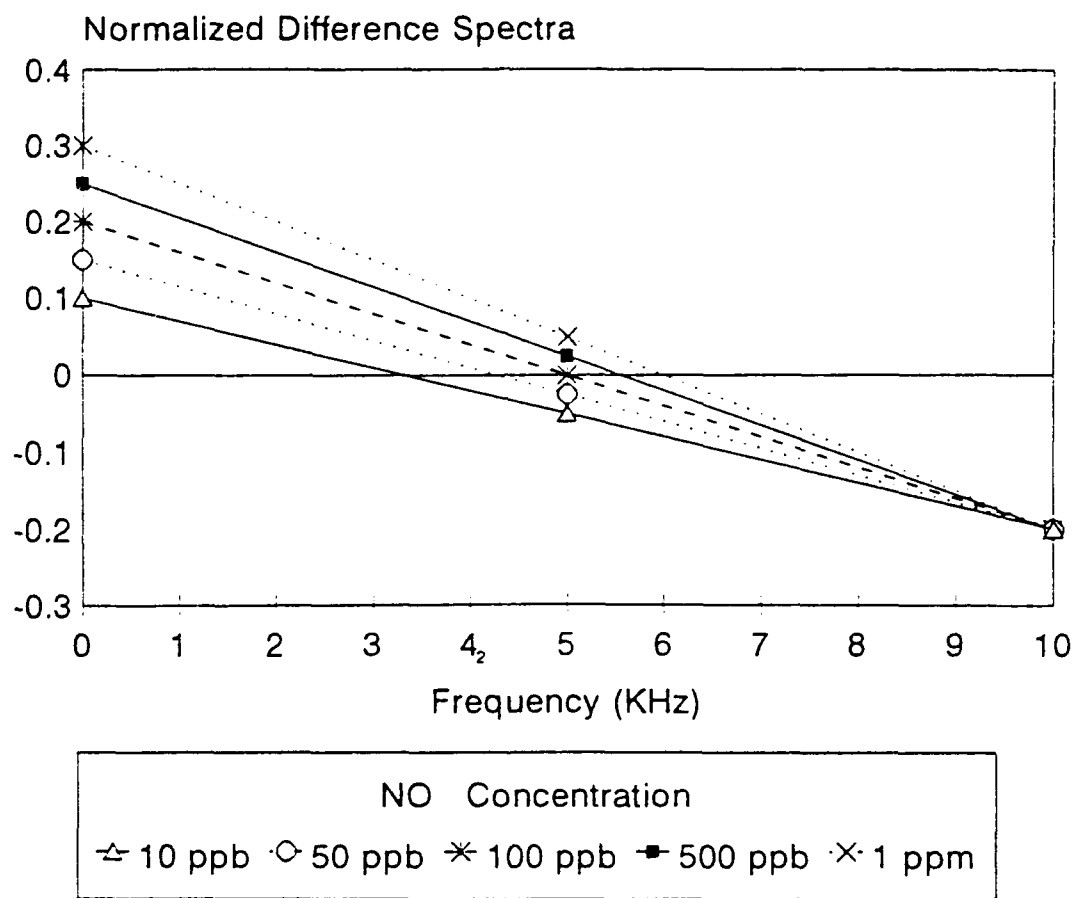


Figure 5.9: Difference Spectral Response of 1000 Å Thick CuPc Film when Exposed to NO₂.

Table 5.5: Sampled Frequency Values for Zero-Crossing Points of the Normalized Difference Spectra of CuPc when Exposed to NO₂.

| NO ₂ Concentration (ppb) | Thin-Film Thickness Å | Sampling Frequency (KHz) |
|-------------------------------------|-----------------------|--------------------------|
| 10 | 250 | 2.05 |
| | 550 | 2.44 |
| | 1000 | 3.21 |
| 50 | 250 | 2.61 |
| | 550 | 3.79 |
| | 1000 | 4.18 |
| 100 | 250 | 3.23 |
| | 550 | 4.12 |
| | 1000 | 5.00 |
| 500 | 250 | 4.30 |
| | 550 | 4.79 |
| | 1000 | 5.46 |
| 1000 | 250 | 4.91 |
| | 550 | 5.15 |
| | 1000 | 6.03 |

angle, and spectral responses. For the dc electrical resistance, it was observed that the percent of change for this electrical characteristic was greater for increasing challenge gas concentrations, increasing film thicknesses, and lower operating temperatures. These characteristic changes in the dc electrical resistance can be attributed to the charge-transfer process between the metal-doped phthalocyanine film and the NO₂ gas molecules, the reactive substances. As the thickness of the CuPc film is increased, more adsorption sites are made available for binding to occur by the challenge gas. As the concentration of the NO₂ challenge gas is increased, more electron-acceptor molecules adsorb to the MPC film. Thus, the increase in adsorption sites and/or the increase in challenge gas molecules results in an decrease in the dc electrical resistance of the IGE structure of the microsensor. The percent of change in the dc electrical resistance increased with increasing NO₂ gas concentration and increasing CuPc film thickness.

Likewise, the percent change in the dc electrical resistance was greater for the low operating temperature (22°C). This is expected since the baseline responses for the dc electrical resistance at the high operating temperature (110°C) are significantly less. Due to the electrical performance boundaries of the microsensor and the

lower baseline dc resistance values, the resulting percent of change in the dc electrical resistance at the high operating temperature was significantly less than the percent of change at 22°C. The most dramatic decreases, and thus the greater percent of change, in the dc resistance were observed when the thickest CuPc film (1000 Å) was exposed to the highest experimental concentration level of NO₂ gas (1 ppm) at 22°C.

A similar analysis can be applied to the characteristic behaviors of the gain, phase angle, and spectral responses for the microsensor coated with different thicknesses of CuPc. For the gain and phase angle responses, greater percents of change were observed for higher challenge gas concentrations, thicker CuPc films, and a lower operating temperature. Also, the percent of change was greater at low frequencies (less than 100 KHz). This behavior is caused by the bandwidth of the response signal, which is on the order of 3 dB (20 KHz), relative to the sampling frequency. The percent of change for the spectral responses were also more prominent at lower frequencies, higher challenge gas concentrations, and thicker films.

5.3.2 DMMP Challenges. The DMMP challenges produced measurable changes in the dc electrical resistance of the IGE structure, the gain and phase angle of the CHEMFET, and

its spectral response. Minimal change was noticed for the CHEMFET's voltage-pulse response in the time domain and the frequency domain. Appendix C contains supplemental plots of the electrical responses of the CHEMFET when exposed to DMMP.

The dc electrical resistance of the IGE structures coated with CuPc decreased during the exposure of the CHEMFET to DMMP. The percent of change in the dc electrical resistance varied with the CuPc film's thickness, the concentration of the DMMP challenge gas, and the operating temperature. Figure 5.10 shows the change of the dc resistance of three different thicknesses of the CuPc films for the five test gas concentrations at two operating temperatures. The greatest change in the dc electrical resistance occurred at the higher concentrations of DMMP and/or with the thicker films. Similar to the response generated by exposing the CHEMFET to NO_2 , the change in the response to the DMMP challenge gas decreased as the operating temperature is increased.

The gain for the CHEMFET when exposed to DMMP displayed a similar pattern to that of the NO_2 response. The gain increased as the thickness of the film increased. Supplemental graphs in Appendix C show the gain versus the frequency (10 Hz to 1 MHz) of the CHEMFET's response upon exposure to different test gas concentrations of DMMP. The

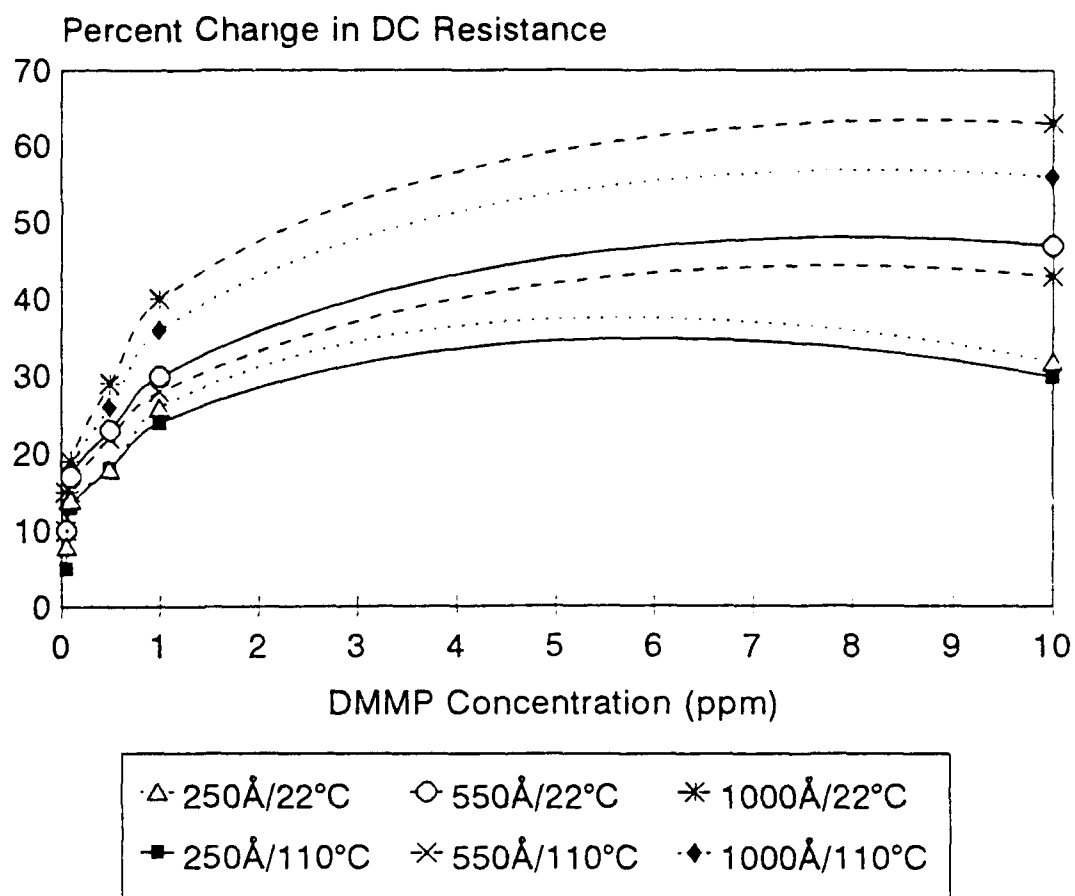


Figure 5.10: Change in DC Resistance of IGE structures coated with CuPc when Exposed to DMMP.

gain predominantly changes in the region of lower frequencies (i.e., 10 Hz to 10 KHz). At higher frequencies (i.e., greater than 10 KHz), the gain stabilizes and manifests a negligible change for variations in the challenge gas concentrations and operating temperature. However, the change in gain appeared to be a function of film thickness, concentration of the challenge gas, and operating temperature at the lower frequencies. Figure 5.11 shows the change of the gain relative to these influencing factors at 10 Hz. These same influencing factors also affect the phase angle of the CHEMFET's response in a similar manner as that of the gain. The change in phase angle of the CHEMFET increases when challenged with DMMP. The phase angle characteristics did not seem to be significantly affected by the variations in the CuPc film thickness. With respect to the operating temperature, Figure 5.12 shows the change in the phase angle of the CHEMFET versus gas concentration at 10 Hz.

The time-domain and the frequency-domain voltage-pulse responses provide very little information concerning the CHEMFET's detection capability of DMMP gas. Plots resistance and reactance components of the impedance of the IGE structure are shown as frequency-domain responses in Appendix C.

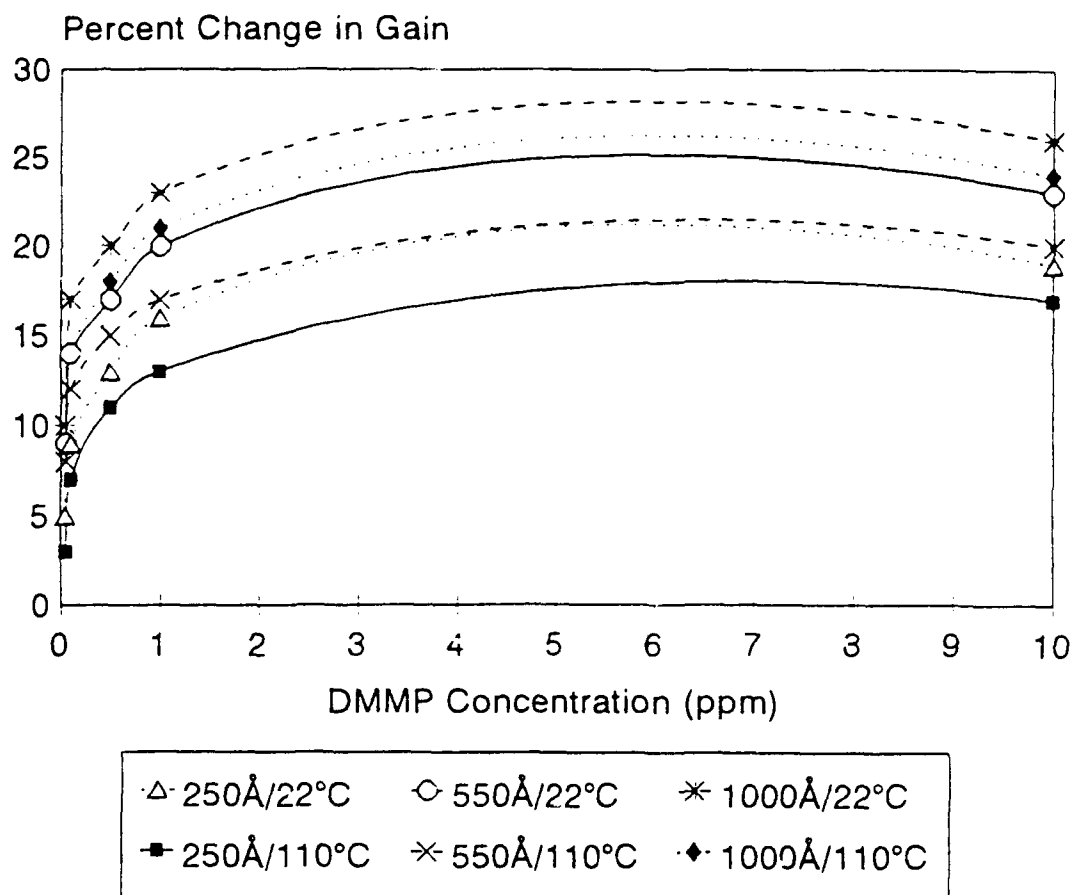


Figure 5.11: Change in Gain at 10 Hz of CuPc CHEMFET when Exposed to DMMP.

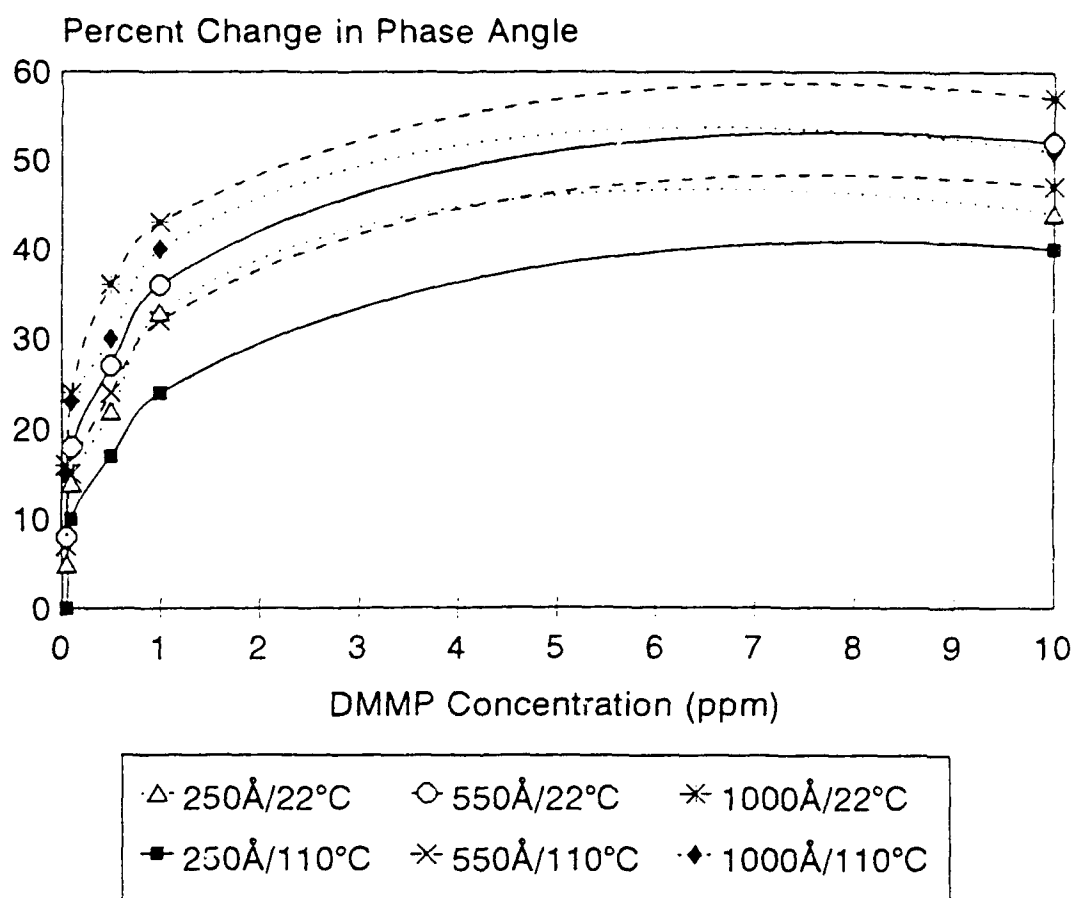


Figure 5.12: Change in Phase Angle at 10 Hz of CuPc CHEMFET when Exposed to DMMP.

The spectral response of the CuPc-coated CHEMFET upon exposure to DMMP indicated a slight decrease in the electrical conductivity of the IGE structure when measured over the frequency range of 10 Hz to 1 MHz. Figures 5.13 through 5.15 show the average difference of the spectra for the three thicknesses of the CuPc thin-films used in this investigation. The average difference of the spectra in the graphs have been normalized and linearized to clearly display the characteristic responses of the five challenge gas concentrations and the three film thicknesses. Similar to the response generated from the NO₂ challenge gas, the increase in operating temperature from 22°C to 110°C did not affect the normalized, linearized, difference spectral curves. However, once again, the magnitude and the slope of the spectral response offer valuable information about the DMMP gas concentration. The zero-crossing points are depicted in Table 5.6. Similar to the behavior observed for the NO₂ spectral response, the value of the sampling frequency relative to the zero-crossing points of the normalized difference spectral response increases as the concentration of the DMMP challenge gas is increased. Likewise, the value of the sampling frequency also increases as the film thickness is increased. However, it was observed that the corresponding sampling frequency values for the zero-crossing points were significantly less for

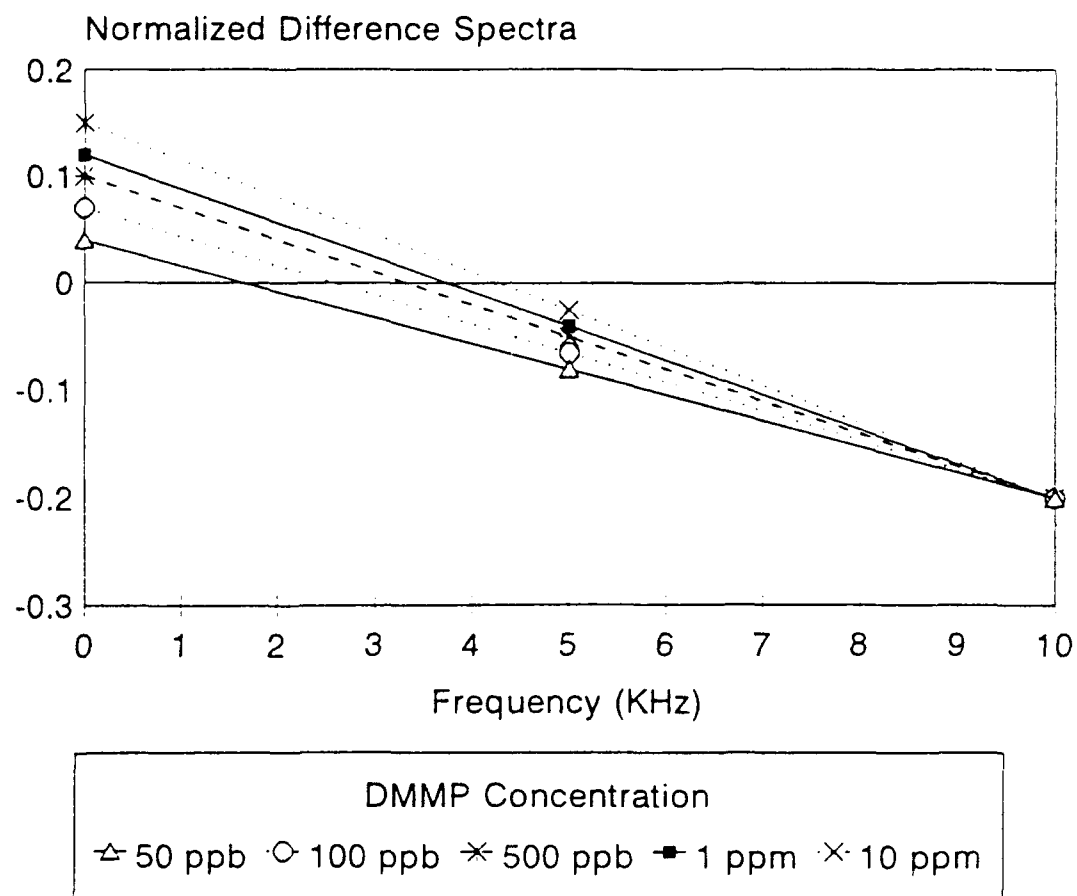


Figure 5.13: Difference Spectral Response of 250 Å Thick CuPc Film when Exposed to DMMP.

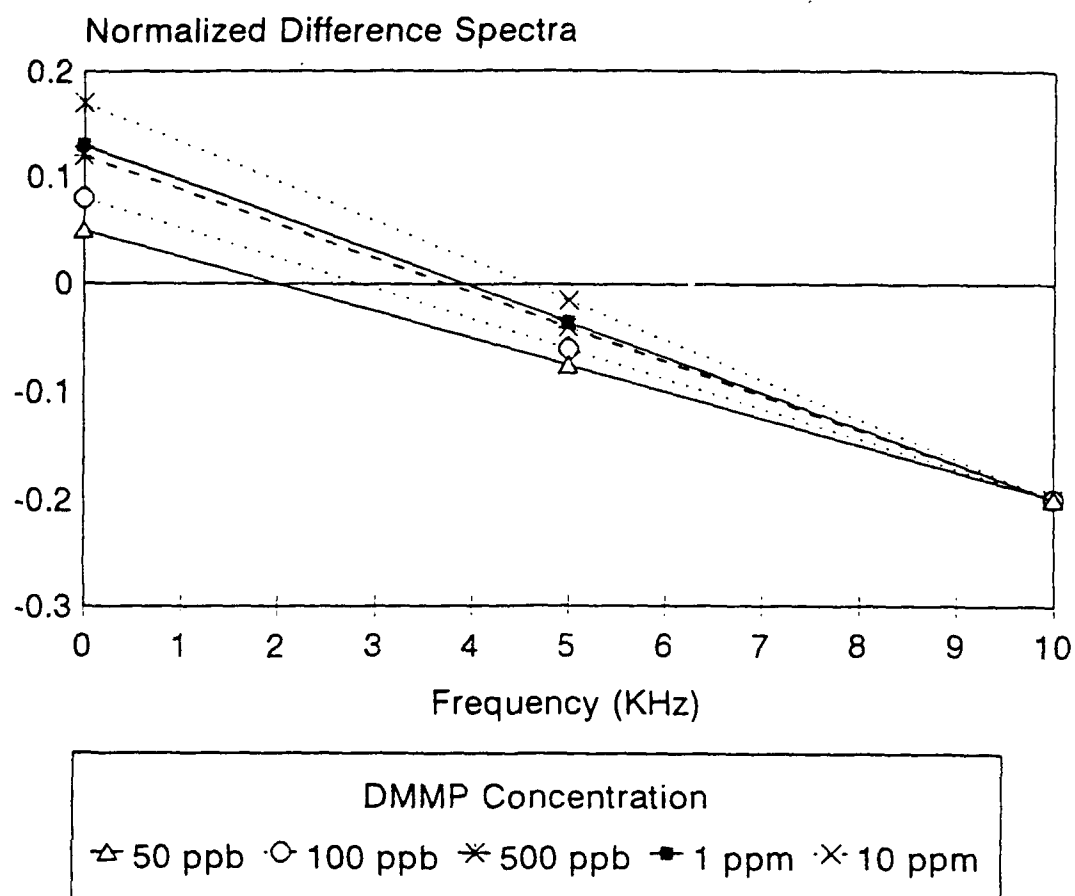


Figure 5.14: Difference Spectral Response of 550 Å Thick CuPc Film when Exposed to DMMP.

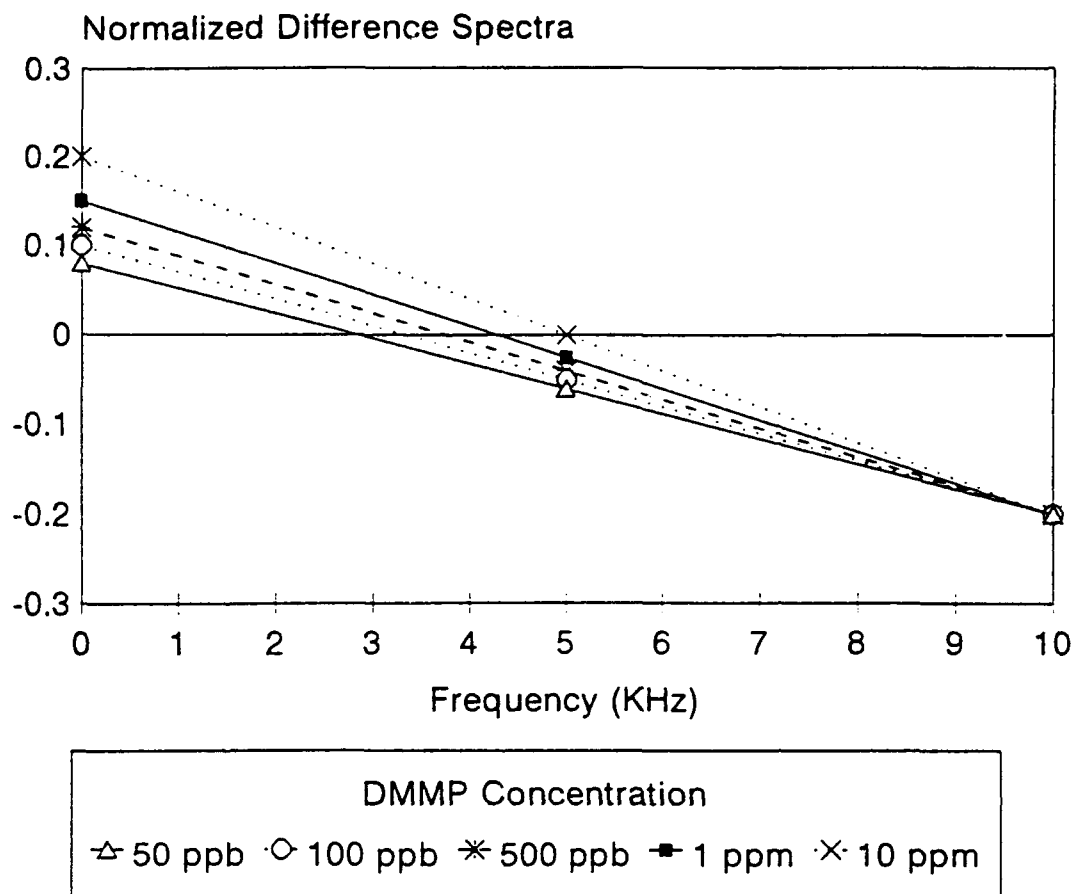


Figure 5.15: Difference Spectral Response of 1000 Å Thick CuPc Film when Exposed to DMMP.

Table 5.6: Sampled Frequency Values for Zero-Crossing Points of the Normalized Difference Spectra of CuPc when Exposed to DMMP.

| DMMP Concentration (ppb) | Thin-Film Thickness Å | Sampling Frequency (KHz) |
|--------------------------|-----------------------|--------------------------|
| 50 | 250 | 1.87 |
| | 550 | 2.03 |
| | 1000 | 2.97 |
| 100 | 250 | 2.80 |
| | 550 | 2.99 |
| | 1000 | 3.55 |
| 500 | 250 | 3.41 |
| | 550 | 3.78 |
| | 1000 | 3.86 |
| 1000 | 250 | 3.90 |
| | 550 | 4.01 |
| | 1000 | 4.45 |
| 10000 | 250 | 4.57 |
| | 550 | 4.76 |
| | 1000 | 5.00 |

DMMP challenge gas exposures than the sampling frequency values for NO₂ challenge gas exposures. The smaller sampling frequency values for the DMMP gas exposures are attributed to the weakness of the electron accepting characteristics associated with DMMP gas molecules.

Exposing the CHEMFET coated with CuPc films to different concentrations of NO₂ gas resulted in measurable changes in the dc electrical resistance, gain and phase angle, and spectral responses. Similar changes resulted upon exposures to different concentrations of DMMP gas. The behavioral characteristics of the DMMP exposures are congruent with those of the NO₂ gas exposures. However, DMMP gas is not a strong electron acceptor (like NO₂), and thus the dc electrical resistance, gain and phase angle, and spectral responses are not as great as the responses produced from exposure to NO₂. Since the overall responses of the DMMP gas exposures are compared with the same baseline performance data as the responses to NO₂ gas exposure, the percent of changes for the measured electrical parameters were smaller.

5.3.3 BF₃ Challenges. Challenges with the BF₃ gas produced no measurable changes in the electrical conductivity of the CHEMFET at concentration levels less than 10 ppm. For concentrations of 10 ppm and 20 ppm, small

changes in the dc electrical resistance of the IGE and the gain and phase of the CHEMFET were observed. The other electrical measurements did not result in adequate information to characterize the CHEMFET's voltage-pulse response and spectral response. Therefore, due to the limited amount of informative data, only responses measured at 10 ppm and 20 ppm are presented.

Unlike NO_2 and DMMP, the dc electrical resistance of the IGE structures coated with CuPc increased during the exposure to BF_3 . This observed behavior of BF_3 is supported by the investigation accomplished by Howe [8]. The change in the dc electrical resistance varied with the film's thickness, the concentration of the challenge gas, and the operating temperature. However, these changes were much smaller when compared to the magnitude of the change manifested for the NO_2 and DMMP exposures. Figure 5.16 shows the change of the dc electrical resistance for the three different thicknesses of the CuPc films for the two BF_3 challenge gas concentrations at the two operating temperatures. The change in the dc electrical resistance occurs only after an increase in the BF_3 challenge gas concentration above a particular level or an increase in the thin-film thickness. As the operating temperature is increased, the rate of change in the dc electrical resistance is reduced.

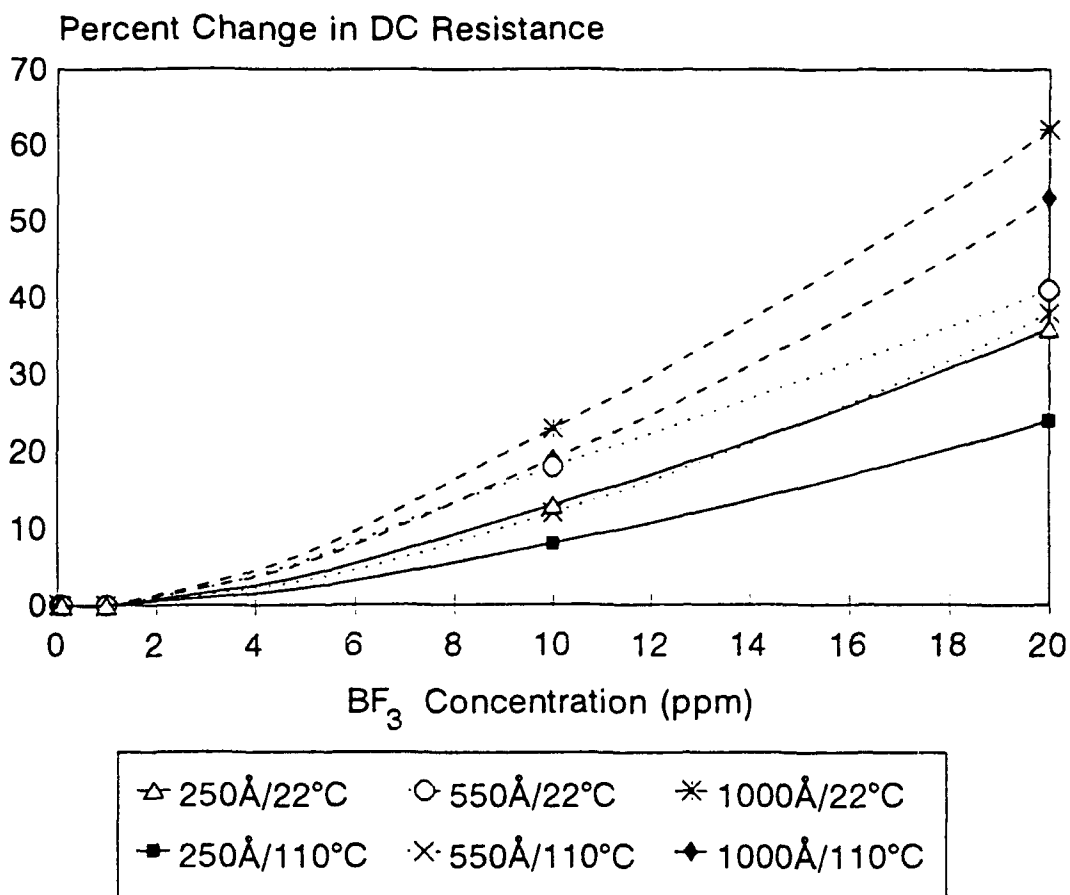


Figure 5.16: Change in DC Resistance of IGE Structures coated with CuPc when Exposed to BF₃.

The weakness of the response to BF_3 makes it difficult to formulate a definitive characteristic response of the CHEMFET.

The gain and the phase angle of the CHEMFET increased with increasing thin-film thickness and increasing challenge gas concentration. The plots in Appendix D show the gain versus frequency upon exposure to 50 ppb and 20 ppm of the BF_3 challenge gas. In addition to being a function of the frequency, the change in gain appears to be a function of film thickness, concentration of the challenge gas, and operating temperature. The impact of these test parameters on the gain and the phase angle at 10 Hz are shown in Figure 5.17 and Figure 5.18, respectively. At low frequencies, the increase in the film's thickness or the challenge gas concentration caused an increase in both the gain and the phase angle. At high frequencies, the gain and the phase angle stabilized and approached the characteristic response manifested with conventional filtered air.

The voltage-pulse response and the spectral response to the BF_3 challenge gas exposures were inconclusive. Meaningful data for characterizing a unique signature of BF_3 using these electrical measurements was not generated in this investigation.

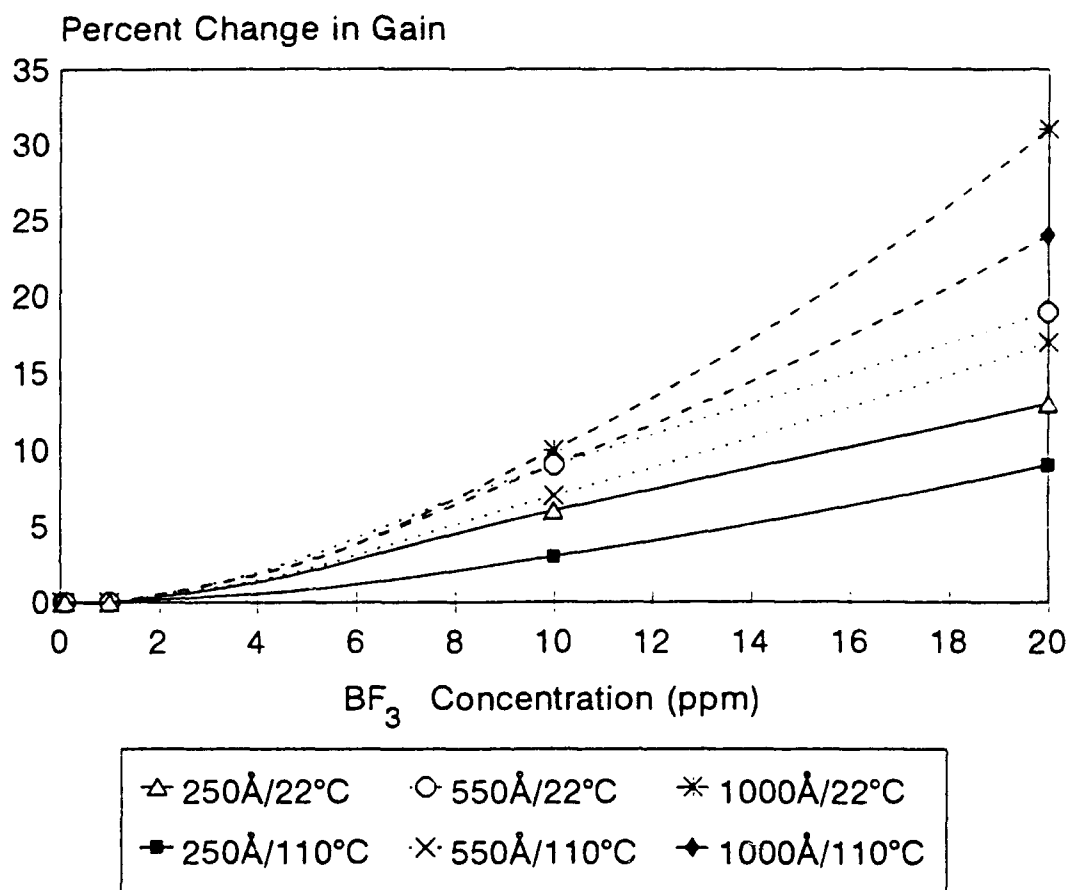


Figure 5.17: Change in Gain at 10 Hz of CuPc CHEMFET when Exposed to BF₃.

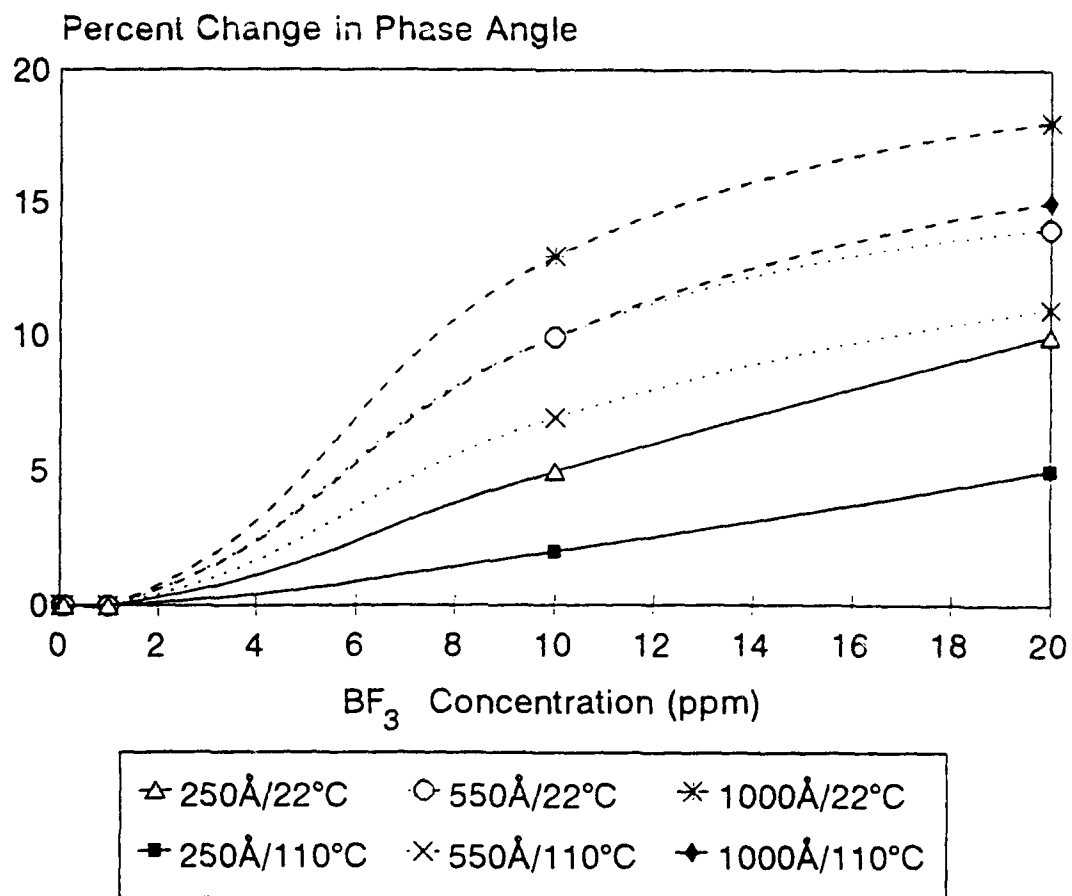


Figure 5.18: Change in Phase Angle at 10 Hz of CuPc CHEMFET when Exposed to BF₃.

5.3.4 Other Gases. CH_3OH , CO , CH_2CHCl , and C_2HCl_3 were only used to screen the detection capability of the CHEMFET. The electrical tests used to gather data for the CHEMFET's response were limited to the dc electrical resistance measurements and the gain/phase angle measurements. These challenge gases were only evaluated at one operating temperature (70°C) so as to maintain all of the substances in a gaseous form.

The range of the responses for these screening gases was quite large. The reliability of the data gathered from CH_3OH and CO was significantly greater compared to that for CH_2CHCl and C_2HCl_3 . The accuracy in obtaining the desired concentrations for CH_3OH and CO was higher since these gases were generated from a calibrated permeation tube. The actual concentrations of CH_2CHCl and C_2HCl_3 that were delivered to the test chamber with a syringe can be questioned. On occasion, condensation was noticed in the syringe after re-injecting the gas molecules into the test chamber. The problem of condensation was subsequently resolved by heating the syringe to 70°C prior to filling it with the challenge gas.

Weak responses for the dc electrical resistance and the gain/phase angle were gathered from the CH_3OH exposures. The magnitude of the changes in the dc electrical resistance and gain/phase angle correlated to the film thickness. The

increase in the dc electrical resistance relative to the challenge gas concentration and the film thickness is shown in Figure 5.19. Figures 5.20 and 5.21 show the change in the gain and the phase angle at 10 Hz, respectively.

No change in the electrical characteristics were observed from the exposures to filtered air and 10 ppm, 20 ppm, and 50 ppm of the CO challenge gas.

The dc electrical resistance and the gain/phase angle responses of the CHEMFET for both CH_2CHCl and C_2HCl_3 were very strong. Even at small concentrations (i.e., 30 ppb of the CH_2CHCl challenge gas and 10 ppb of the C_2HCl_3 challenge gas) the electrical characteristics of the CuPc thin-film differed from the exposures to filtered air. The measured electrical characteristics of the CH_2CHCl challenge gas at concentrations of 30 ppb, 100 ppb, and 1 ppm were plotted relative to the thin-film thickness; the dc electrical resistance, and the gain and phase angle at 10 Hz are shown in Figures 5.22, 5.23, and 5.24, respectively. Similarly, for exposures to 10, 50, and 100 ppb of the C_2HCl_3 challenge gas, the dc electrical resistance, and the gain and phase angle at 10 Hz are shown in Figures 5.25, 5.26, and 5.27, respectively.

The ability of these challenge gases to be detected by CuPc films is attributed to the molecular structure of these VOCs. The four VOCs evaluated in this investigation are all

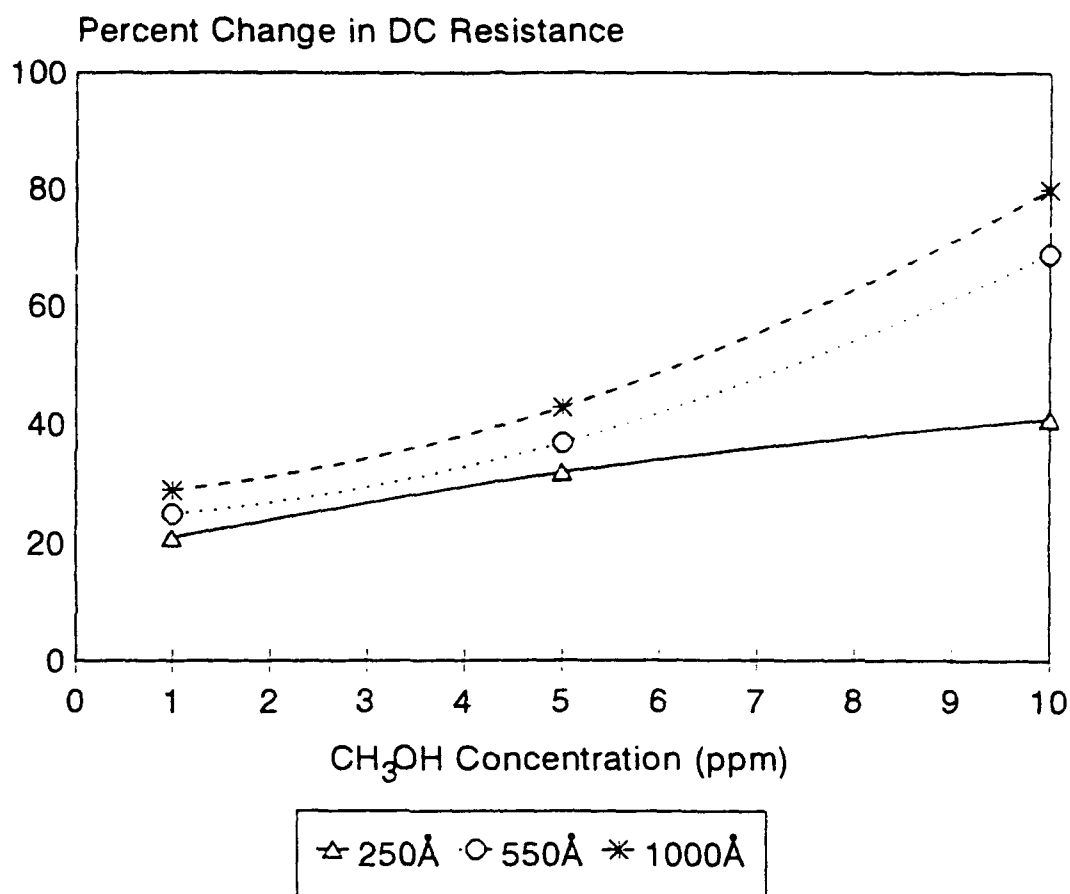


Figure 5.19: Change in DC Resistance of IGE Structures coated with CuPc when Exposed to CH₃OH at 70°C.

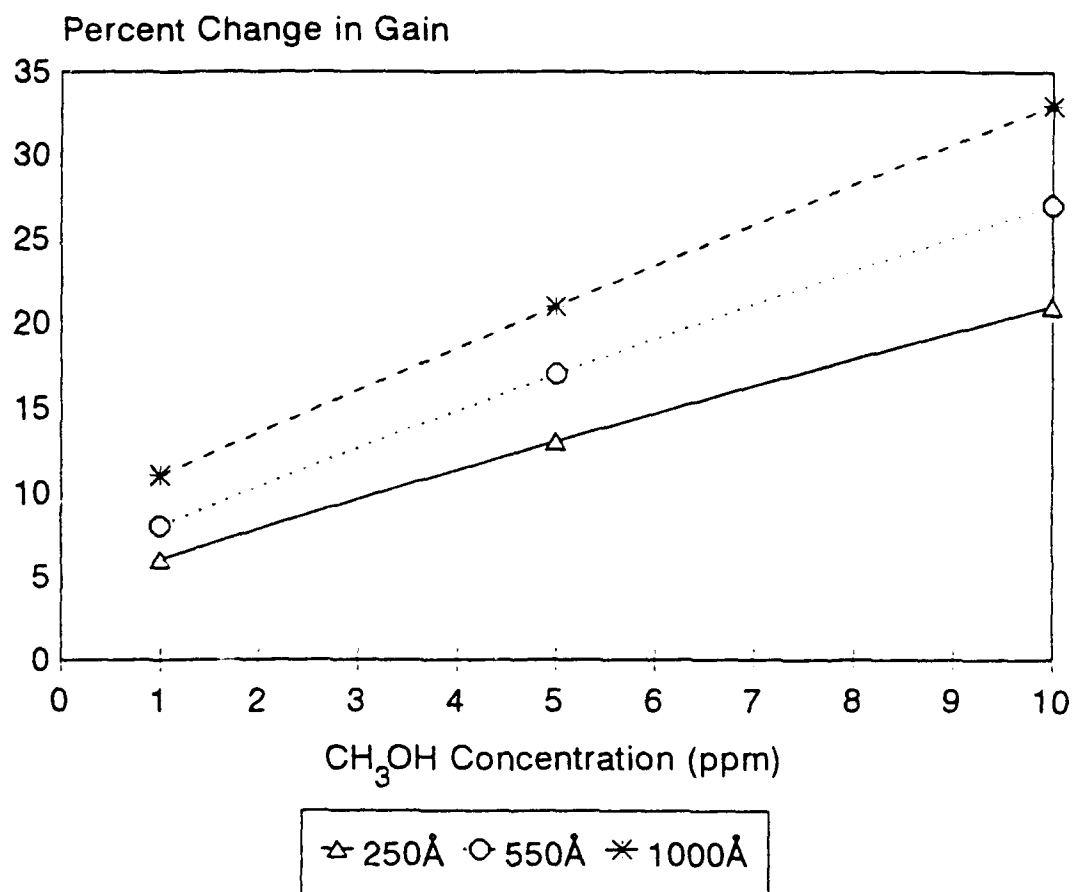


Figure 5.20: Change in Gain at 10 Hz of CuPc CHEMFET when Exposed to CH₃OH at 70°C.

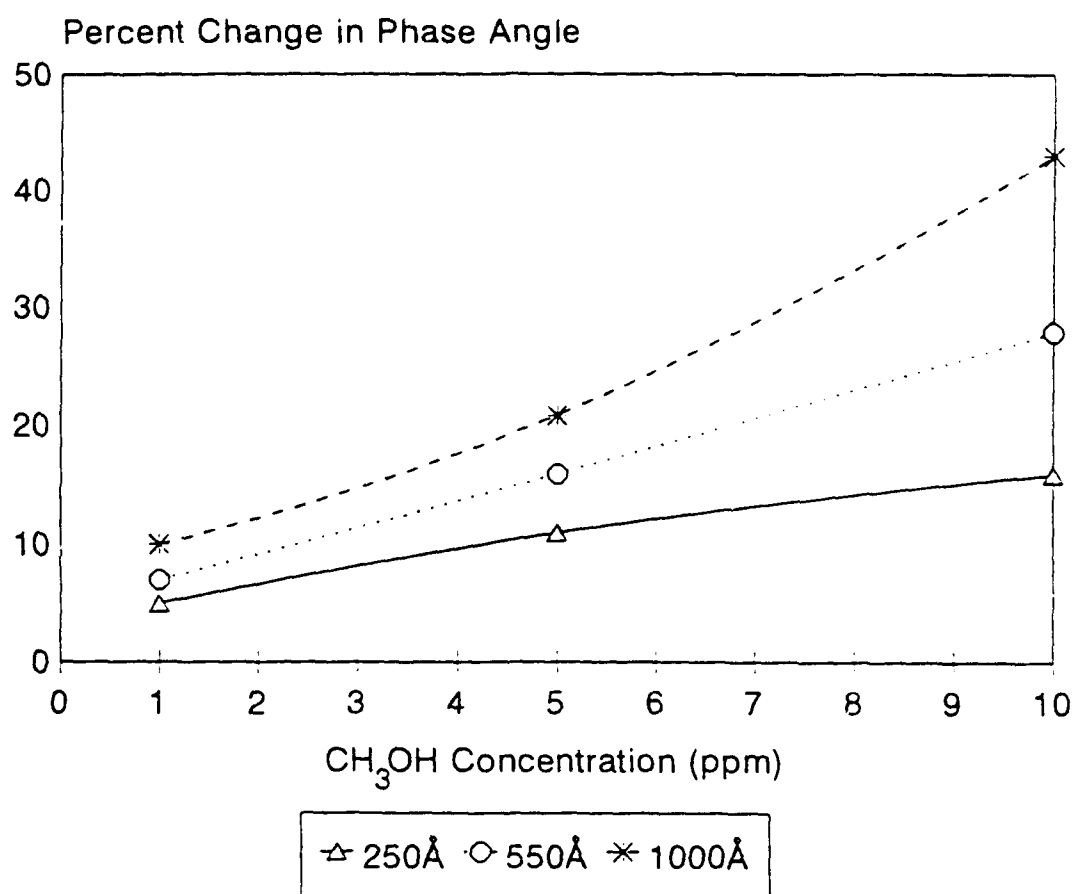


Figure 5.21: Change in Phase Angle at 10 Hz of CuPc CHEMFET when Exposed to CH₃OH at 70°C.

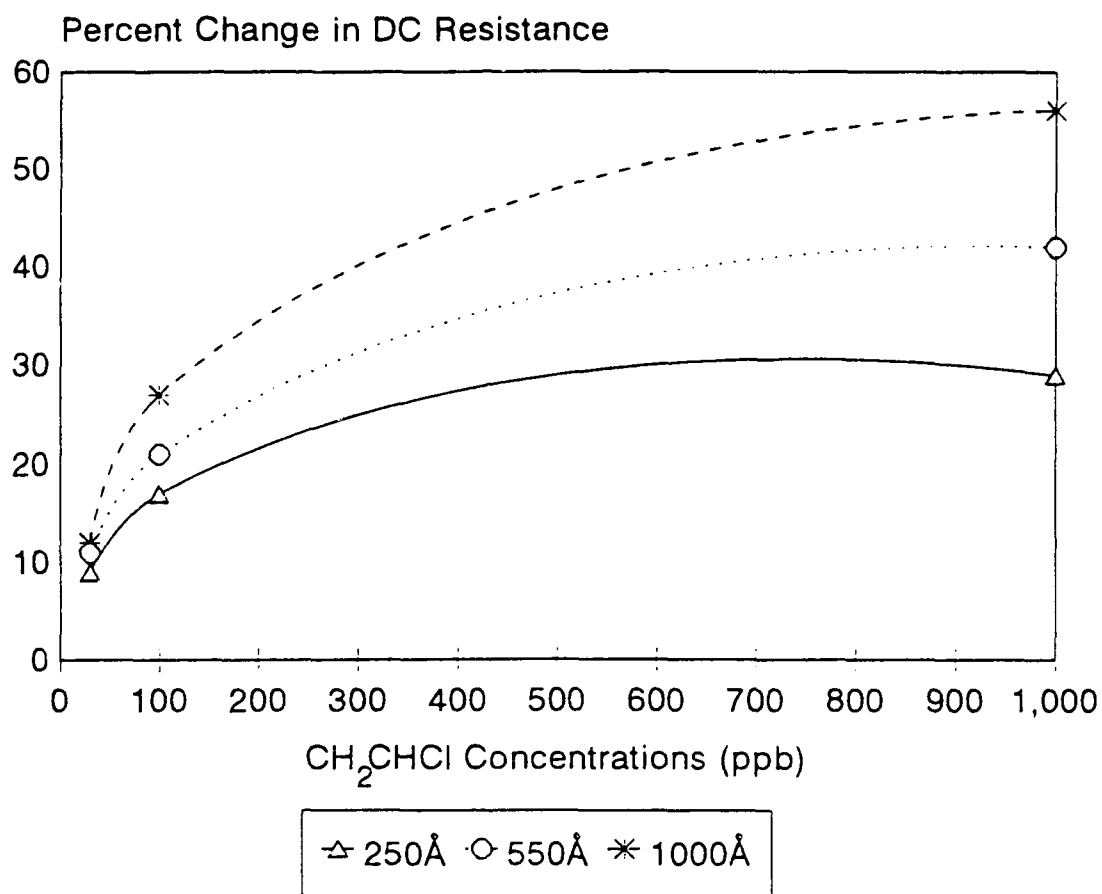


Figure 5.22: Change in DC Resistance of IGE Structures coated with CuPc when Exposed to CH₂CHCl at 70°C.

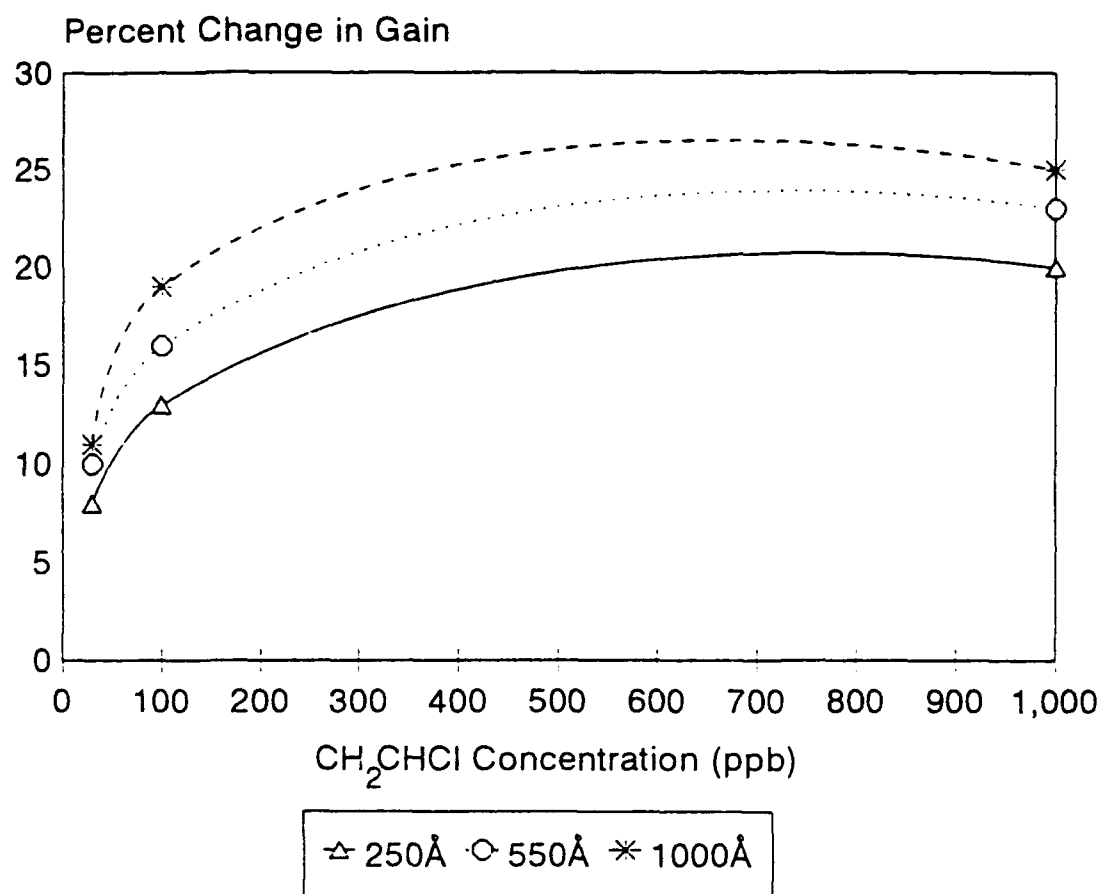


Figure 5.23: Change in Gain at 10 Hz of CuPc CHEMFET when Exposed to CH₂CHCl at 70°C.

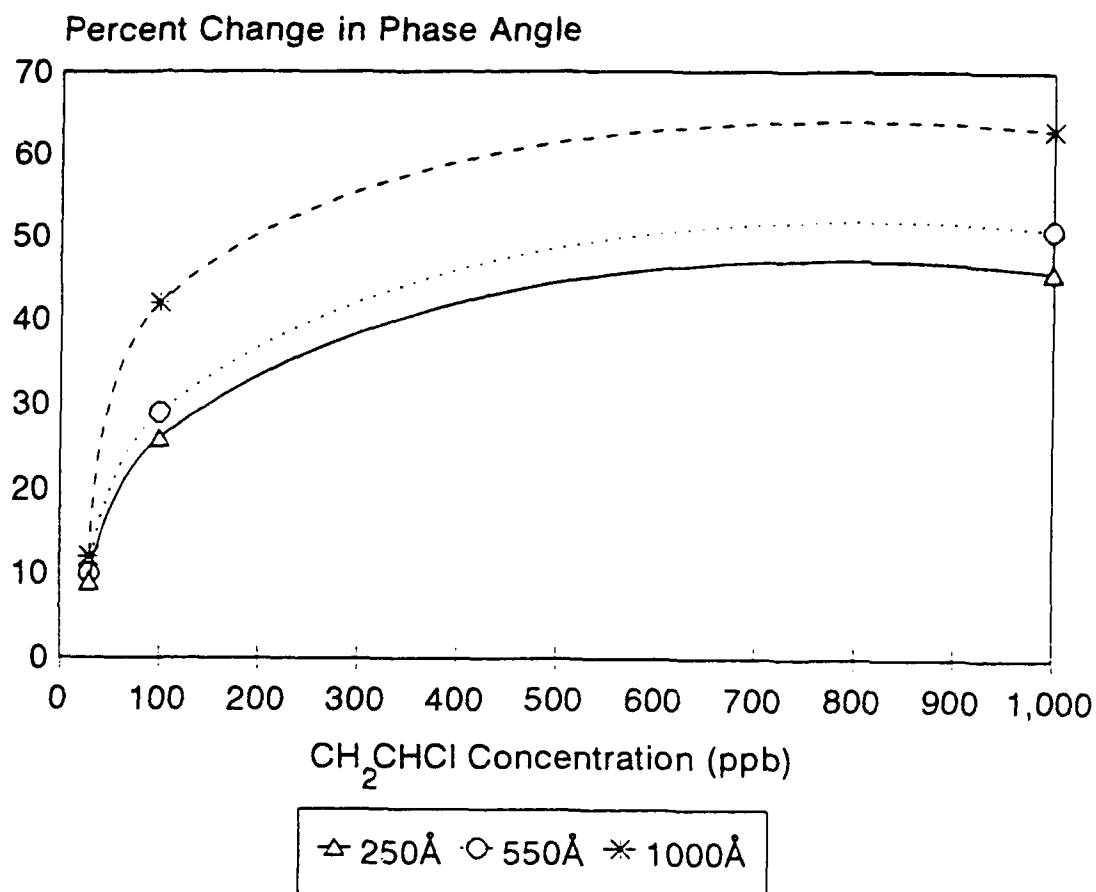


Figure 5.24: Change in Phase Angle at 10 Hz of CuPc CHEMFET when Exposed to CH₂CHCl at 70°C.

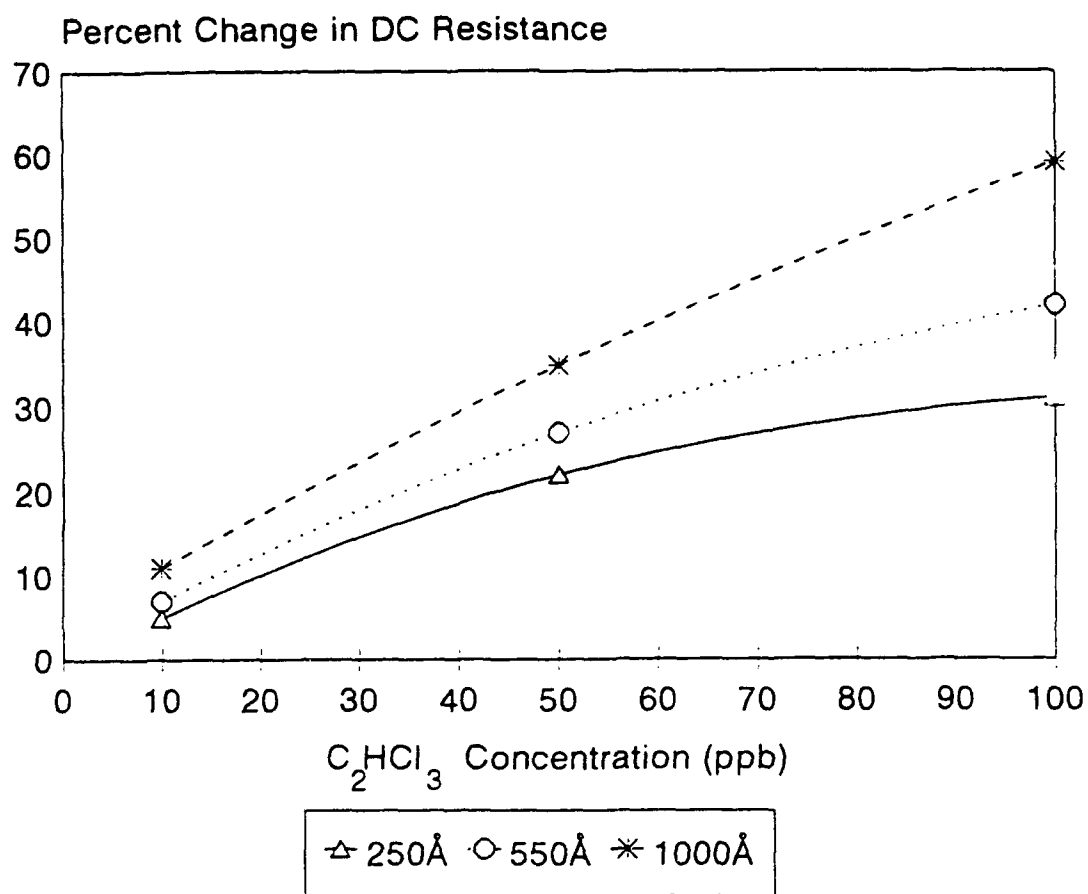


Figure 5.25: Change in DC Resistance of IGE Structures coated with CuPc when Exposed to C_2HCl_3 at 70°C.

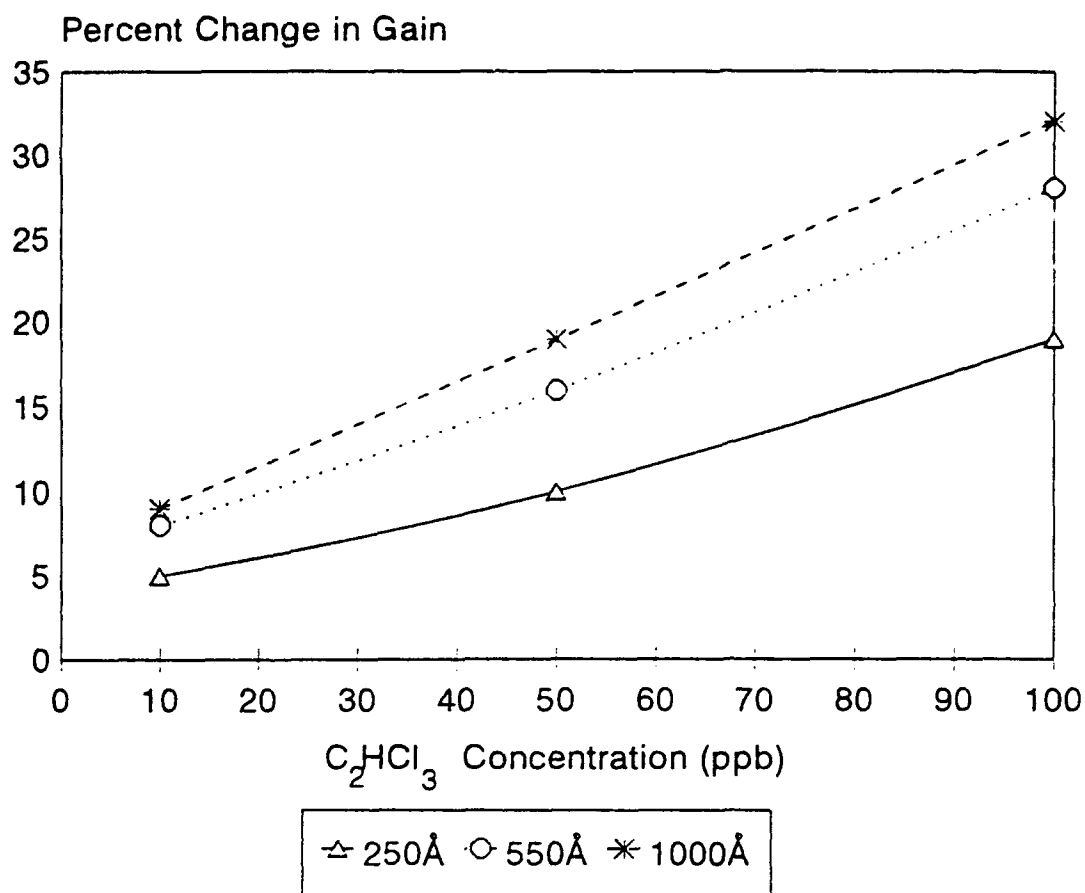


Figure S.26: Change in Gain at 10 Hz of CuPc CHEMFET when Exposed to C_2HCl_3 at 70°C.

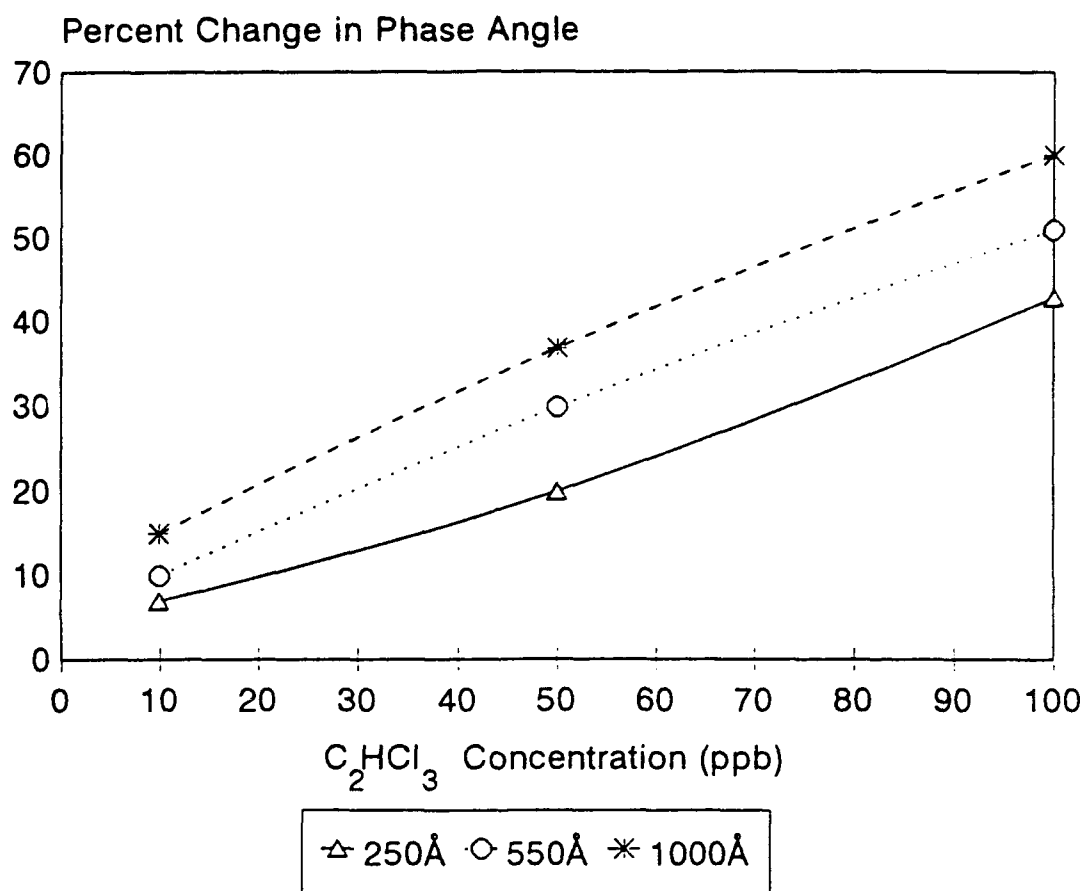


Figure 5.27: Change in Phase Angle at 10 Hz of CuPc CHEMFET when Exposed to C_2HCl_3 at 70°C.

polar compounds; the gas molecules are not symmetrical, and therefore possess electron-attractive regions (poles) located on the outer valence band of the gas molecule. The strength of the response for the particular challenge gas specie is dependent upon the strength of the polar regions and the molecules ability to bind to the adsorption sites within the CuPc film. The CO challenge gas was undetectable by the CuPc films due to the configuration of the electron valence band. The compactness of the electron valence band for the CO molecule results in a lower affinity for electrons, which is the key for the charge-transfer process to occur between the electron-donating metal-doped phthalocyanine an the electron-accepting challenge gas molecule.

5.4 Responses of Lead Phthalocyanine

Combinations including different thicknesses of the PbPc thin-film, concentrations of the challenge gases, and operating temperature were used to investigate the gas detection capabilities of the CHEMFET. The data from this research indicates that PbPc is sensitive to two of the three challenge gases evaluated: NO₂ and DMMP. Furthermore, the PbPc film coatings manifested the behavior of being sensitive to CH₃OH, CO, C₂HCl₃, and CH₂CHCl. Similar to evaluating the electrical conductivity of CuPc, the PbPc

thin-film's response was evaluated by measuring the dc and ac electrical performance characteristics discussed in Chapter 4.

5.4.1 NO₂ Challenges. Exposures with the NO₂ challenge gas produced significant changes (compared to the baseline response generated by exposing the CHEMFET to filtered air) in the dc electrical resistance of the IGE structure, the gain and phase of the CHEMFET, the CHEMFET's voltage-pulse response in the time and frequency domains, and the CHEMFET's spectral response.

The change in the dc electrical resistance of the IGE structure coated with different thicknesses of the PbPc coating is similar to the response produced by the CuPc film coating. The dc resistance decreased during the exposure of the CHEMFET to NO₂. Figure 5.28 shows the change of the dc resistance for the three different PbPc film thicknesses for the five challenge gas concentrations at the two operating temperatures. Not only did the dc electrical resistance decrease with increasing thin-film thicknesses, it also decreased as the concentrations of the challenge gas were augmented. As noted in the plot, the overall change in the magnitude of the dc electrical resistance is diminished with increasing operating temperature.

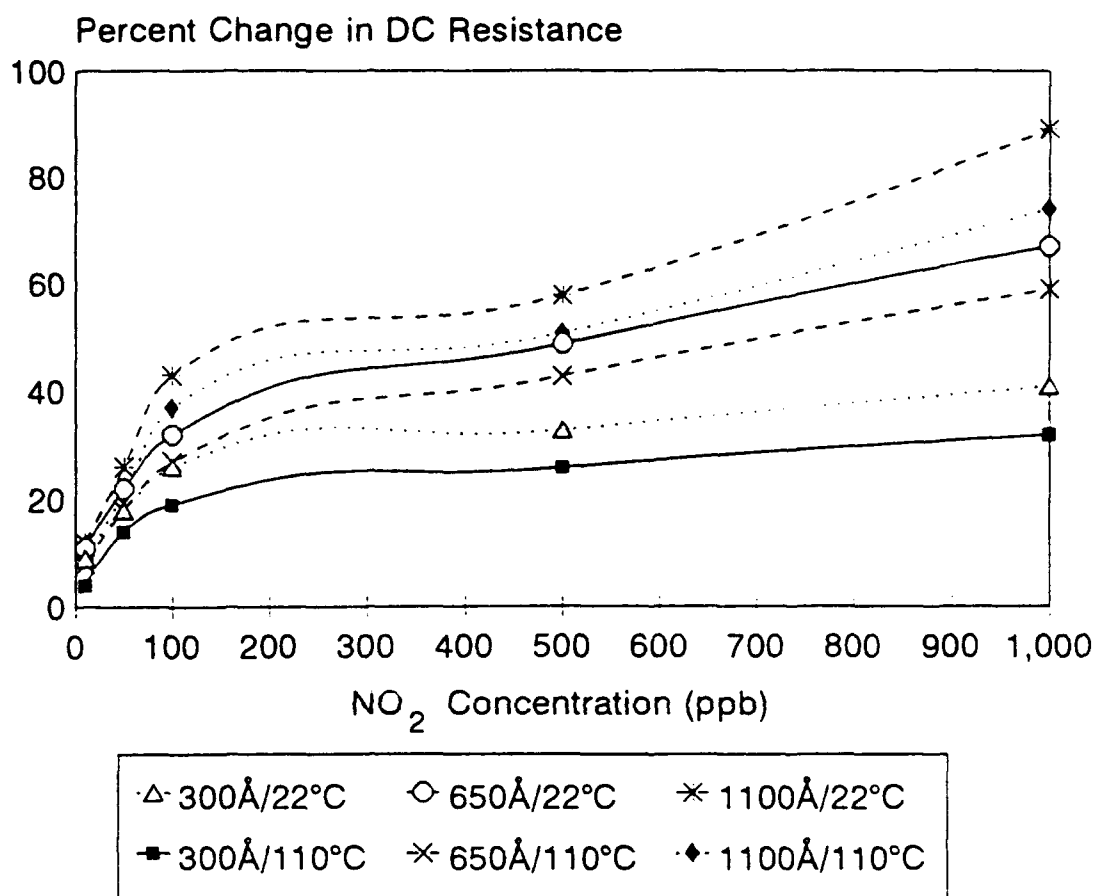


Figure 5.28: Change in DC Resistance of IGE structures coated with PbPc when Exposed to NO₂.

The largest changes in the gain occurred in the low frequency range (i.e., 10 Hz to 10 KHz). The gain varied with the frequency, the thickness of the PbPc film, the concentration of the challenge gas, and the operating temperature. The change of the gain relative to these influencing factors at 10 Hz is depicted in Figure 5.29. At frequencies greater than 10 KHz, the change in the gain is negligible. There is also a negligible change in the gain at high operating temperatures (i.e., 110°C). It is also noted that if either the film thickness or the challenge gas concentration is increased, the change of the gain increases. The change in the phase angle of the PbPc-coated sensing elements displayed similar response characteristics relative to those manifested by the sensing elements coated with CuPc when challenged with NO₂. Figure 5.30 represents the change in the phase of the CHEMFET versus gas concentration at 10 Hz.

The time-domain voltage-pulse response to the NO₂ challenge gas for 22°C and 110°C is shown in Figures 5.31 and 5.32, respectively. When compared to the time-domain response of the CuPc films upon exposure to NO₂ as depicted in Figures 5.5 and 5.6, it is observed that there is a greater change in the amplitude for NO₂ gas exposures to the PbPc films. Also, the reversibility (the ability of the microsensor to return to 90% of its baseline response) is

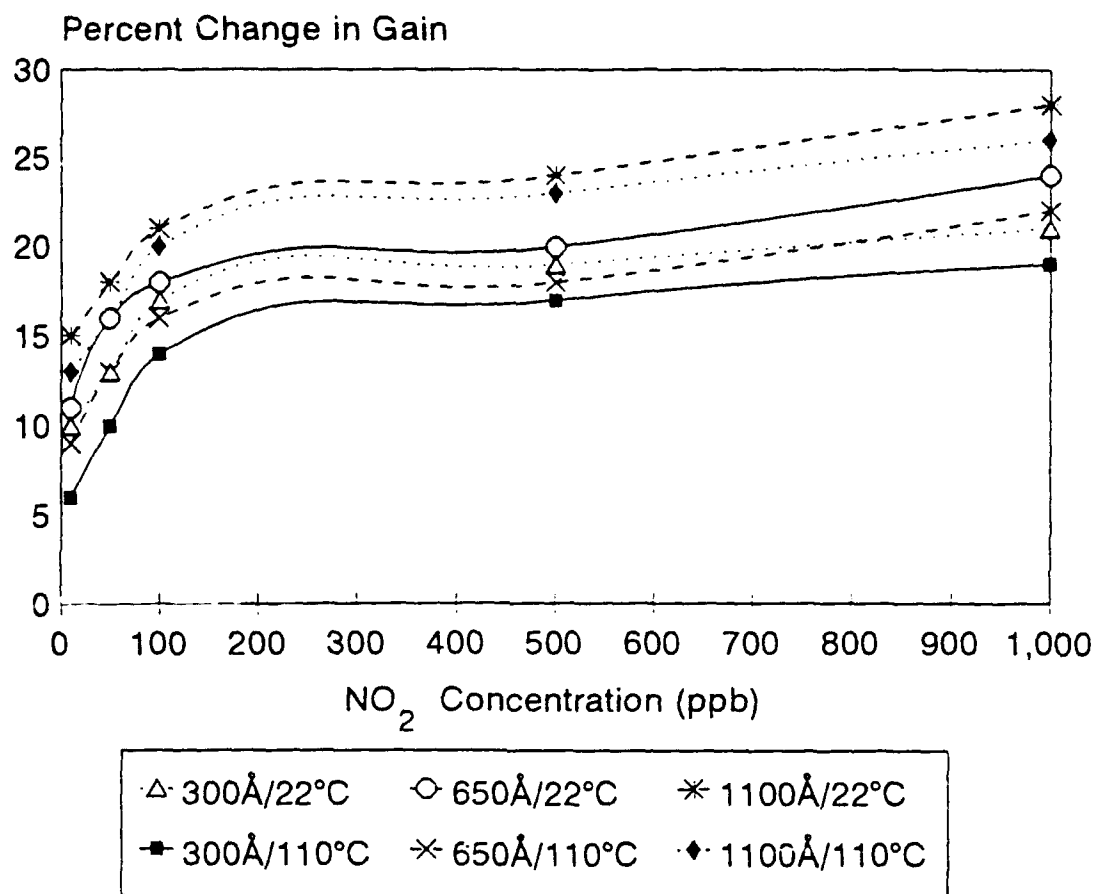


Figure 5.29: Change in Gain at 10 Hz of PbPc CHEMFET when Exposed to NO₂.

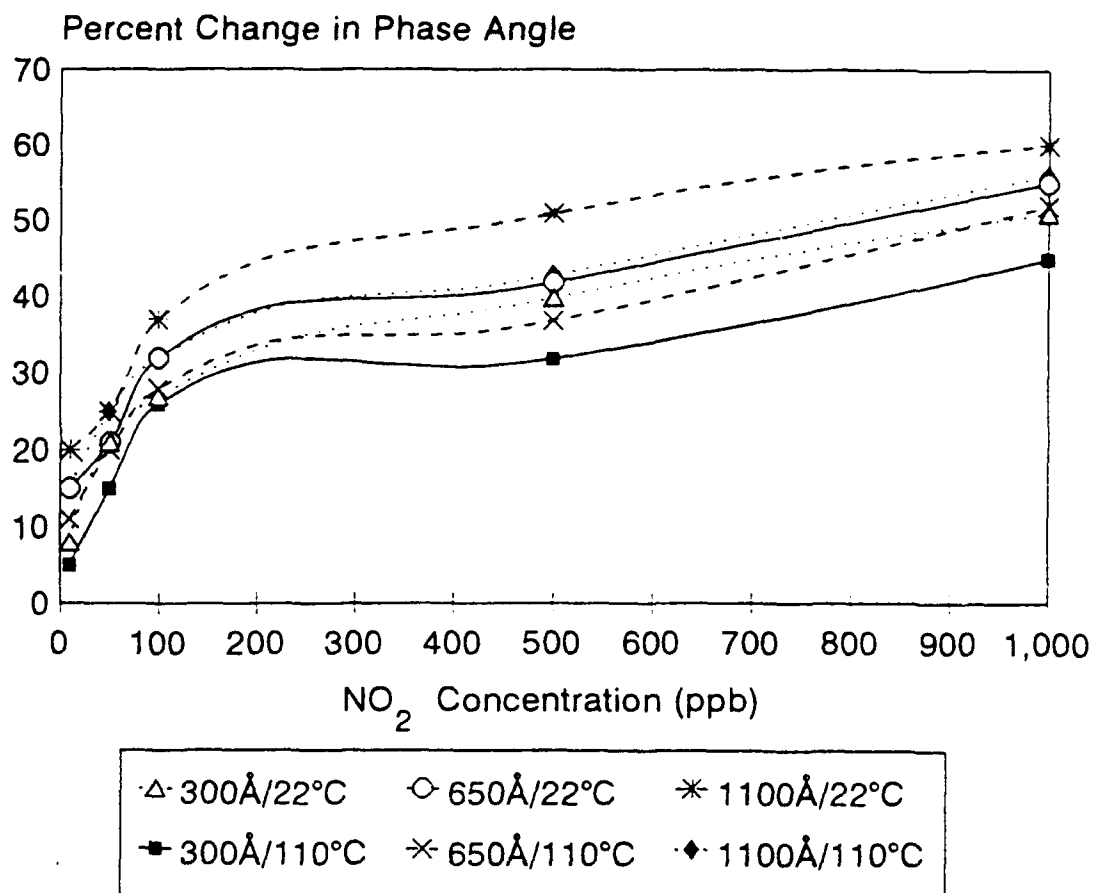
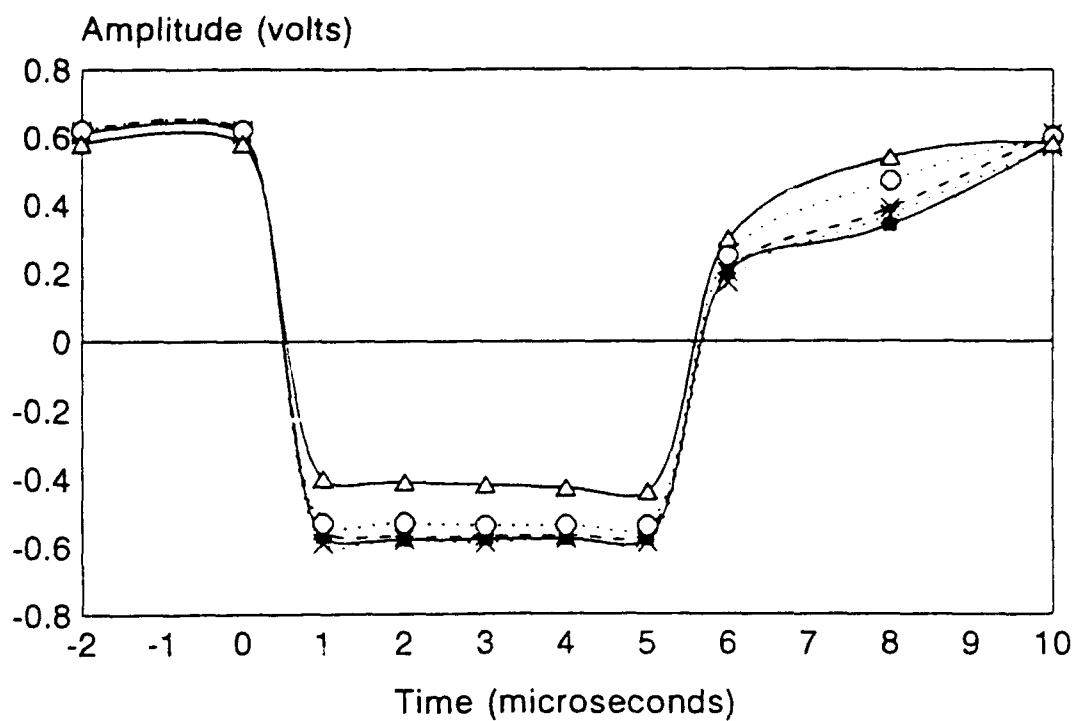


Figure 5.30: Change in Phase Angle at 10 Hz of PbPc CHEMFET when Exposed to NO₂.



NO₂ Concentrations

△ 10 ppb ○ 50 ppb * 100 ppb ■ 500 ppb × 1 ppm

Figure 5.31: Time-Domain Response of PbPc CHEMFET Operated at 22°C when Exposed to NO₂.

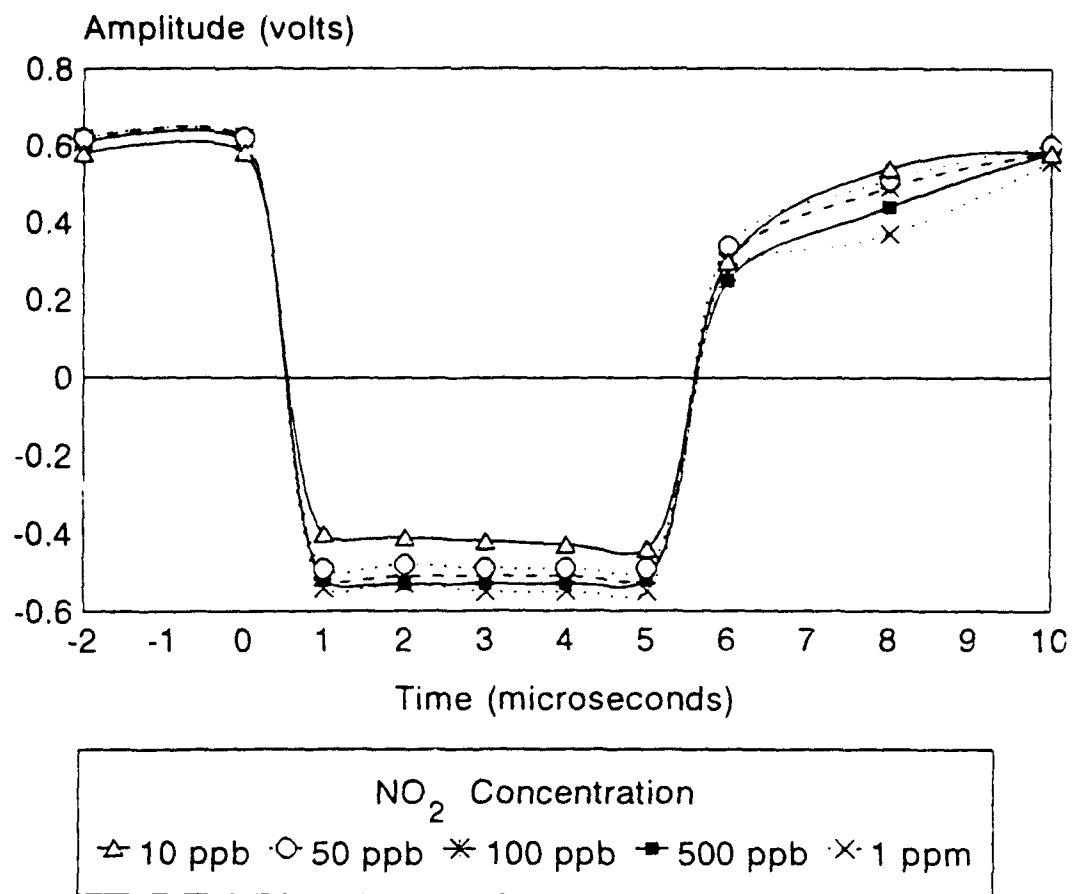


Figure 5.32: Time-domain Response of PbPc CHEMFET Operated at 110°C when Exposed to NO₂.

greater for the PbPc films than the CuPc films. These characteristics indicated that the PbPc films were more sensitive to NO₂ challenge gas than CuPc films.

The spectral response of the PbPc film upon exposure to NO₂ indicated a decrease in the electrical conductivity throughout the measured frequency range of 10 Hz to 1 MHz. Figures 5.33 through 5.35 show the normalized, linearized, difference spectra for the three film thicknesses investigated. As shown by the plots, the slope of the spectral curves is unique for each NO₂ challenge gas concentration. The zero-crossing points are depicted in Table 5.7. The spectral response behavior of the PbPc films upon exposure to NO₂ is similar to the spectral response behavior observed for exposure of the CuPc film to the NO₂ challenge gas. The sampling frequency relative to the zero-crossing points of the normalized difference spectral response still increases as the concentration of the NO₂ challenge gas is increased. Likewise, the value of the sampling frequency also increases as the PbPc film thickness is increased. However, it was observed that the sampling frequency values for the zero-crossing points were significantly greater for the PbPc films when compared to the corresponding values associated with the CuPc films. This characterizes the PbPc films as being more sensitive to NO₂ than the CuPc films.

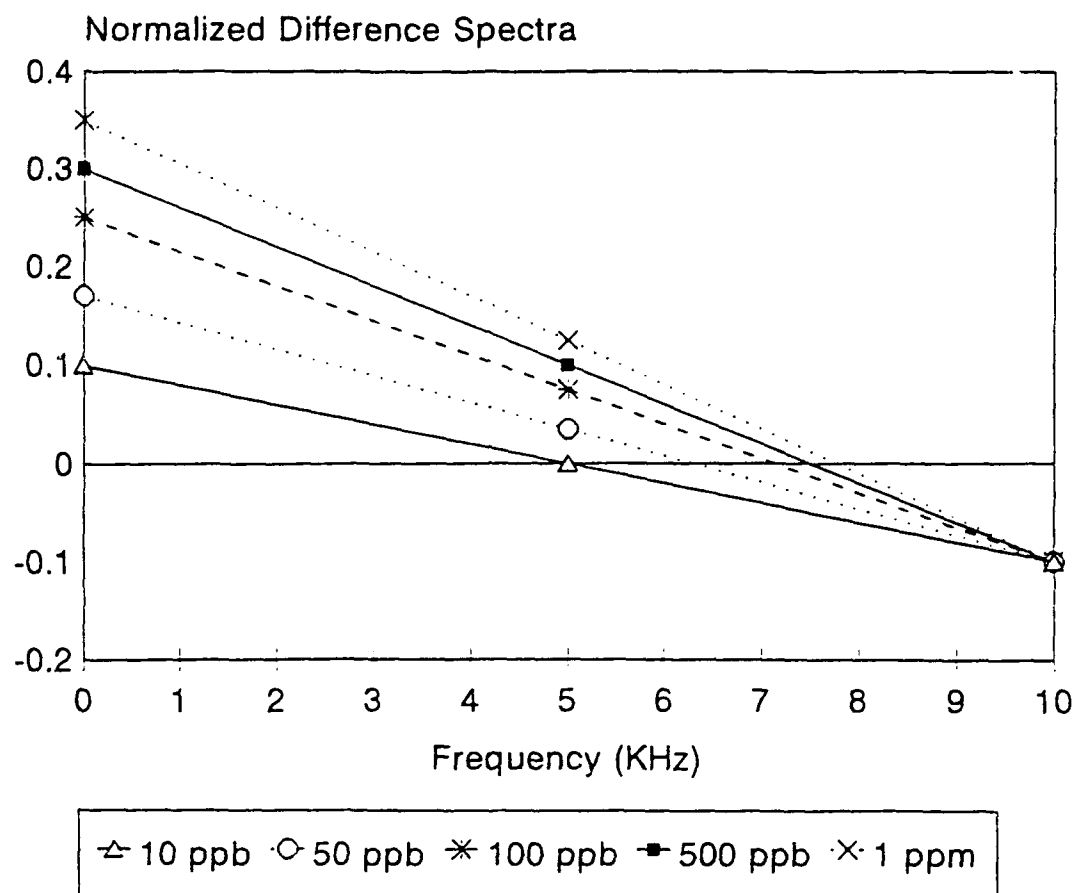


Figure 5.33: Difference Spectral Response of 300 Å Thick PbPc Film when Exposed to NO_2 .

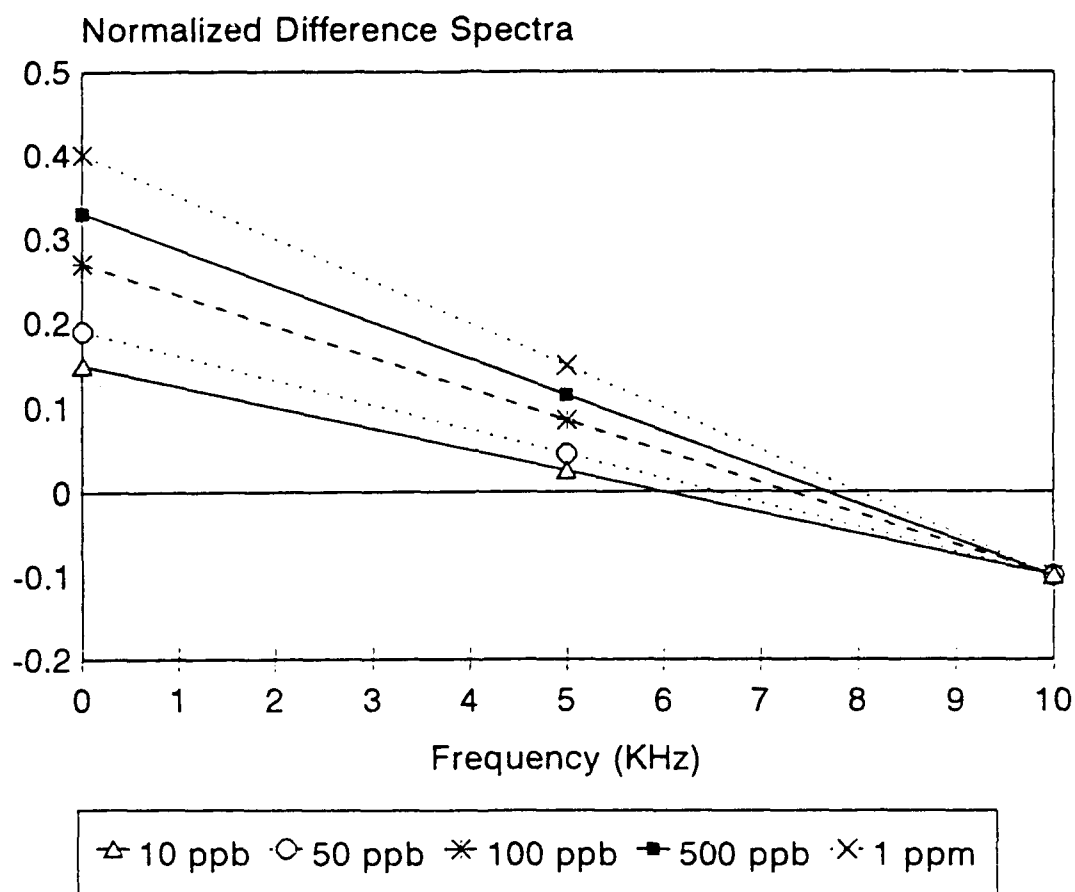


Figure 5.34: Difference Spectral Response of 650 Å Thick PbPc Film when Exposed to NO_2 .

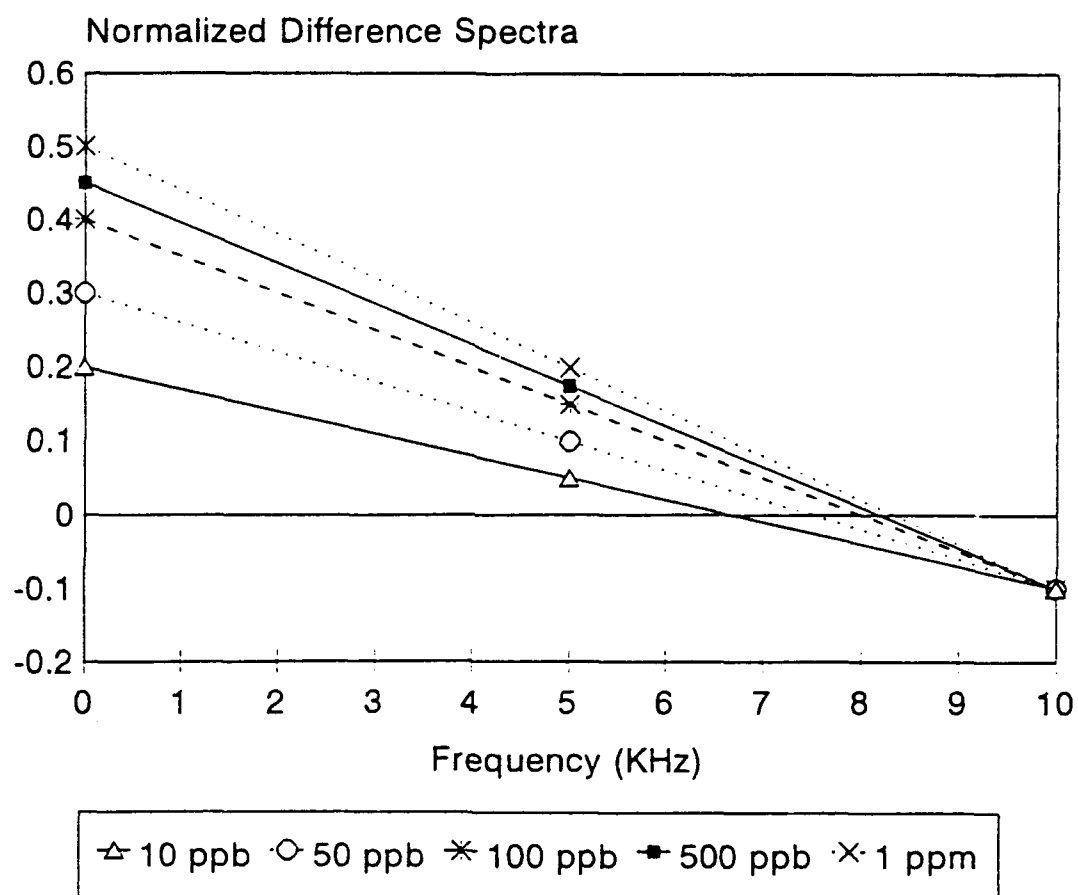


Figure 5.35: Difference Spectral Response of 1100 Å Thick PbPc Film when Exposed to NO_2 .

Table 5.7: Sampled Frequency Values for Zero-Crossing Points of the Normalized Difference Spectra of PbPc when Exposed to NO₂.

| NO ₂ Concentration (ppb) | Thin-Film Thickness Å | Sampling Frequency (KHz) |
|-------------------------------------|-----------------------|--------------------------|
| 10 | 300 | 5.00 |
| | 650 | 6.02 |
| | 1100 | 6.56 |
| 50 | 300 | 6.31 |
| | 650 | 6.53 |
| | 1100 | 7.48 |
| 100 | 300 | 7.12 |
| | 650 | 7.38 |
| | 1100 | 8.02 |
| 500 | 300 | 7.42 |
| | 650 | 7.70 |
| | 1100 | 8.13 |
| 1000 | 300 | 7.90 |
| | 650 | 8.00 |
| | 1100 | 8.30 |

5.4.2 DMMP Challenges. The DMMP challenges produced measurable changes in the dc resistance of the IGE structure and the gain and phase angle of the CHEMFET. No change was observed in the CHEMFET's voltage-pulse response in the time and frequency domains; negligible change was associated with the spectral response of the CHEMFET.

The dc electrical resistance of the IGE structures coated with PbPc decreased while the CHEMFET was exposed to DMMP. The change in the dc electrical resistance varied with the film's thickness, the concentration of the challenge gas, and the operating temperature. It is noted that no change in the dc electrical resistance occurred for DMMP concentrations less than 500 ppb. Figure 5.36 shows the change of the dc resistance for the three different thicknesses of the PbPc films for the three DMMP Challenge gas concentrations at the two operating temperatures. Higher concentrations of DMMP and thicker PbPc film coatings produced a greater change in the dc electrical resistance. The change in the dc electrical resistance response to the DMMP gas decreased as the operating temperature was increased.

When exposed to DMMP, the gain for the CHEMFET displayed a similar, but weaker, pattern to the response revealed by the CuPc thin-films when exposed to DMMP. Similar to the lack of change in dc electrical resistance

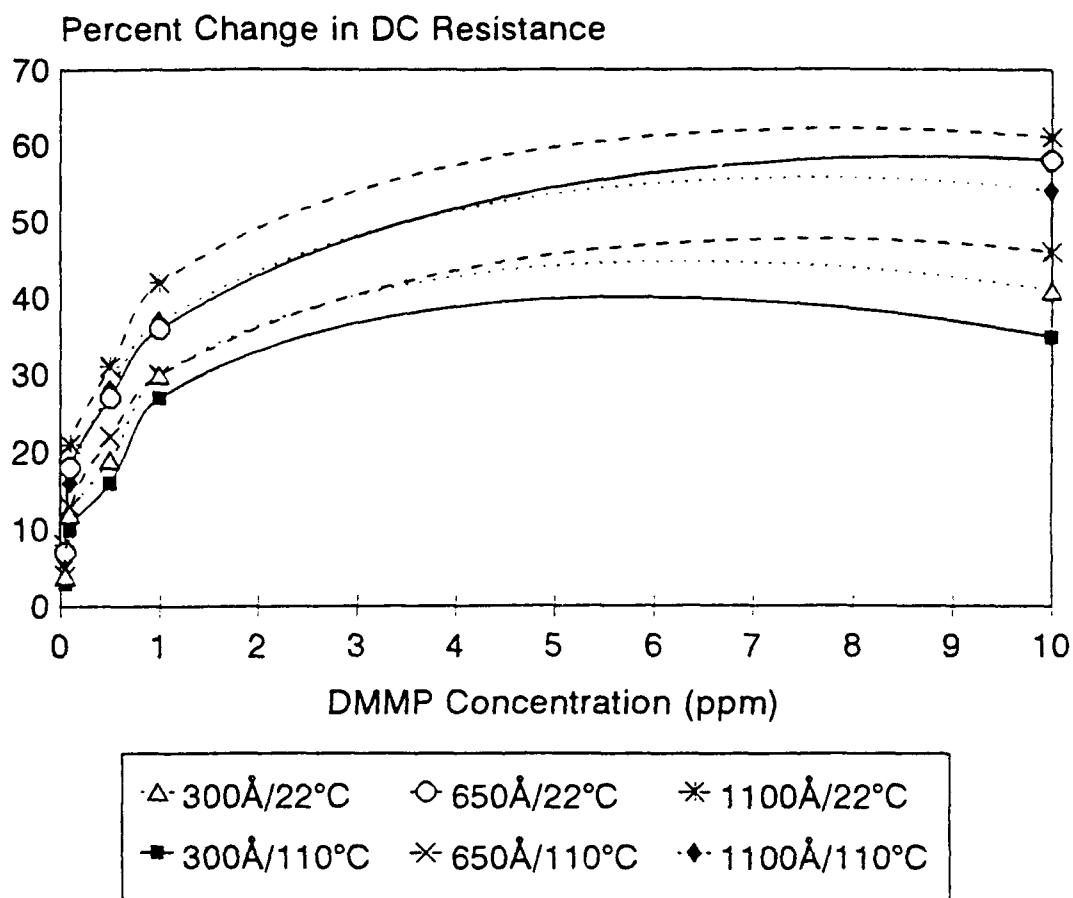


Figure 5.36: Change in DC Resistance of IGE structures coated with PbPc when Exposed to DMMP.

for DMMP exposures at less than 500 ppb, no change in the gain or phase angle was noted for DMMP exposures at less than 500 ppb. Figure 5.37 shows the change of the gain, and Figure 5.38 shows the change in the phase angle of the CHEMFET versus gas concentration at 10 Hz.

The voltage-pulse responses in the time-domain and in the frequency-domain do not provide any information concerning the CHEMFET's detection capability of DMMP.

When exposed to different concentrations of DMMP, the spectral response of the PbPc thin-films did not result in unique curves for the test parameters. The magnitude and the slope of the normalized difference spectra remained unchanged for different concentrations of the challenge gas and different film thicknesses.

The capability of the PbPc-coated sensing elements to detect DMMP is revealed by the collected data. The limited amount of useful data indicates that PbPc films are less sensitive to DMMP than CuPc films which had stronger responses for identical challenge gas concentrations.

5.4.3 BF₃ Challenges. The sensing elements coated with PbPc thin-films and exposed to concentrations of BF₃ did not produced any measurable changes in the electrical characteristics. Unlike that of the CuPc thin-films, the PbPc thin-films did not detect any concentration of BF₃.

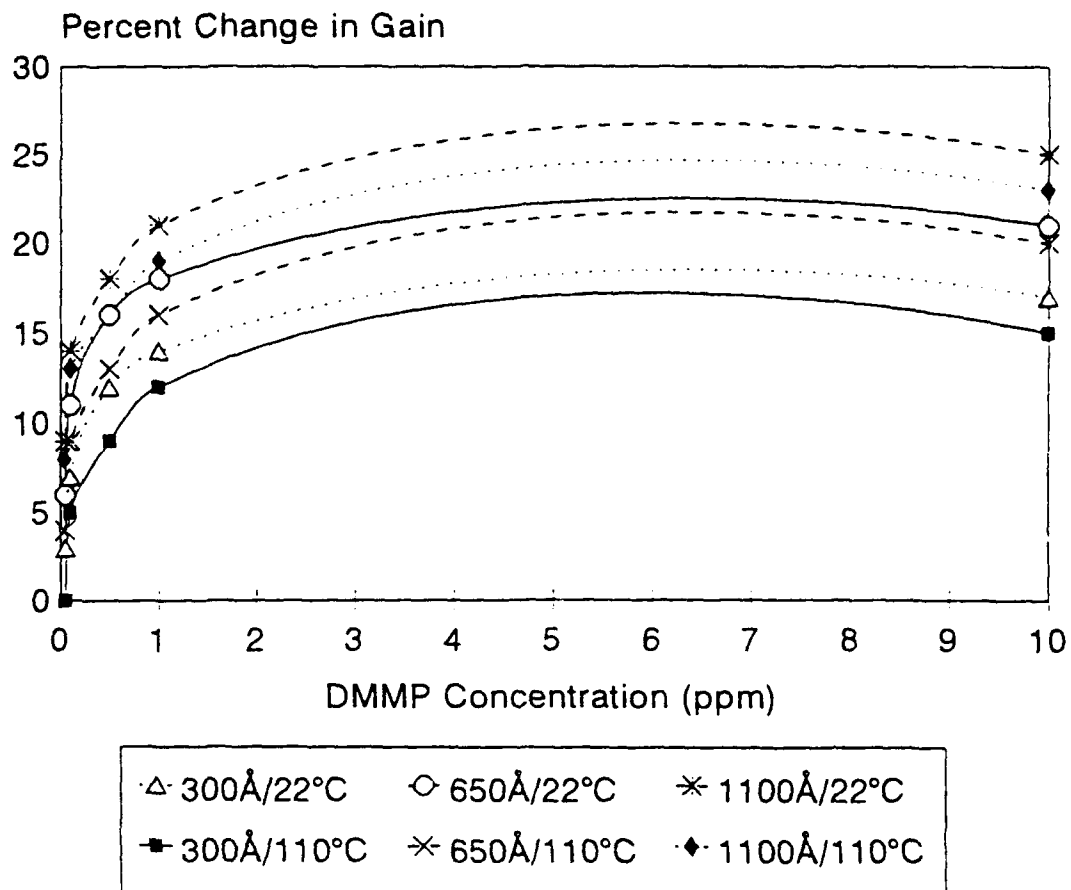


Figure 5.37: Change in Gain at 10 Hz of PbPc CHEMFET when Exposed to DMMP.

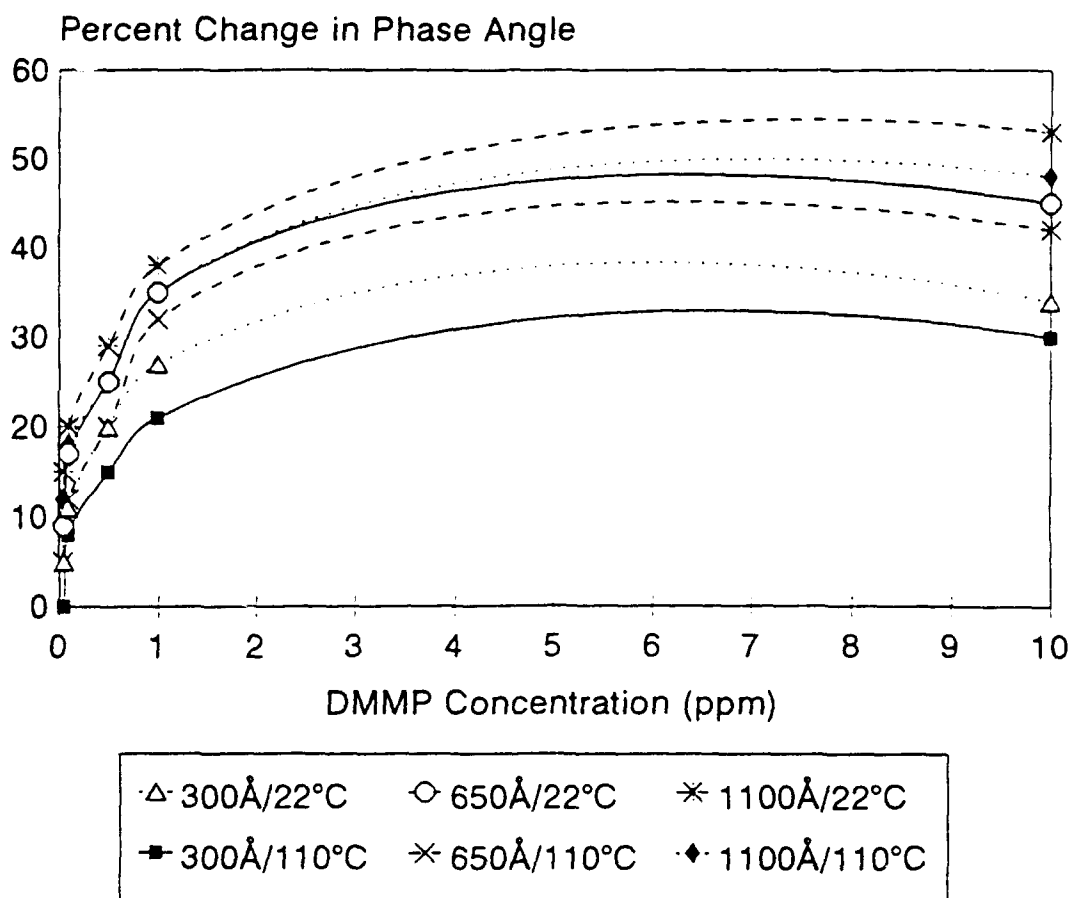


Figure 5.38: Change in Phase Angle at 10 Hz of PbPc CHEMFET when Exposed to DMMP.

5.4.4 Other Gases. CH_3OH , CO , CH_2CHCl , and C_2HCl_3 were only used to screen the detection capabilities of the PbPc-coated CHEMFET. Only dc resistance measurements and gain/phase angle measurements were recorded at an operating temperature of 70°C . These responses were then compared to the results of the CuPc-coated CHEMFET.

Again, the reliability of generating the desired concentrations of CH_2CHCl and C_2HCl_3 is questionable. The accuracy of generating the desired concentrations for CH_3OH and CO was higher since these gases were produced from calibrated permeation tubes. The accuracy of generating the desired concentrations for CH_2CHCl and C_2HCl_3 were improved by heating the injection syringe to 70°C prior to filling it with the desired concentration of the challenge gas. Responses were recorded for all four of the screening challenge gases.

When exposed to CH_3OH and CO , the CHEMFET's response revealed slight changes in the dc resistance and the gain/phase angle. The magnitude of the changes in the dc resistance and gain/phase angle appeared to be functions of the thickness of the film and the challenge gas concentration. For the CH_3OH challenge gas exposures, the increase in the dc electrical resistance relative to the challenge gas concentration and the thin-film thickness is

shown in Figure 5.39. Figures 5.40 and 5.41 show the change in the gain and in the phase angle at 10 Hz, respectively. A much weaker response was measured for CO exposures. The change in the dc electrical resistance, and the changes in the gain and the phase angle of the CHEMFET at 10 Hz are shown in Figures 5.42 through 5.44, respectively.

A comparison of the dc electrical resistance and the gain/phase angle responses between filtered air and CH_2CHCl , and filtered air and C_2HCl_3 , revealed that the electrical properties of the PbPc thin-films undergo a change upon exposure to these challenge gases. The measured electrical characteristics for concentrations of 30 ppb, 100 ppb, and 1 ppm of CH_2CHCl were plotted relative to the film thickness. The change in the dc electrical resistance, and the change in gain and phase angle at 10 Hz are shown in Figures 5.45 through 5.47, respectively. Changes in the dc electrical resistance, and changes in the gain and the phase angle at 10 Hz, are shown in Figures 5.48 through 5.50 for exposures to 10, 50, and 100 ppb of the C_2HCl_3 challenge gas.

A comparison among the electrical characterization responses for the PbPc-coated CHEMFET and the CuPc-coated CHEMFET revealed that for the VOCs investigated, PbPc films were significantly more sensitive to these challenge gases than CuPc films. PbPc films were even able to detect the CO challenge gas at a concentration level of 10 ppm.

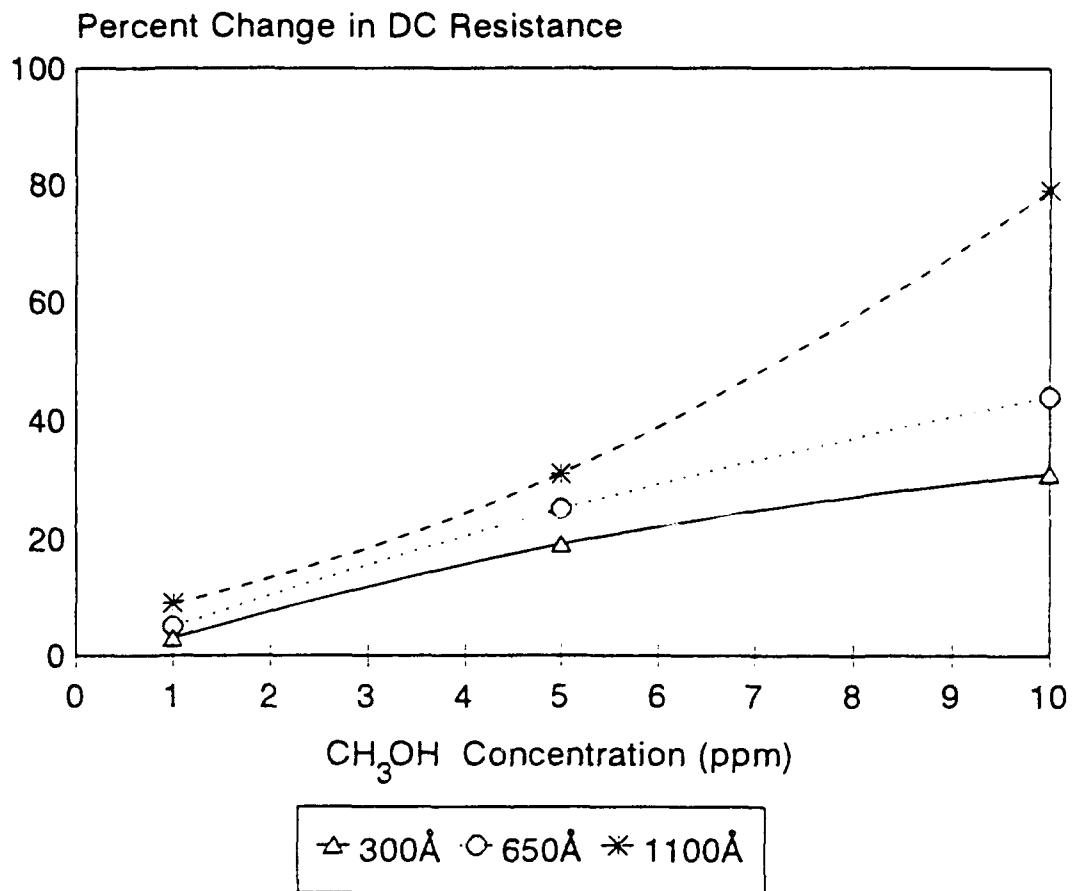


Figure 5.39: Change in DC Resistance of IGE Structures coated with PbPc when Exposed to CH₃OH at 70°C.

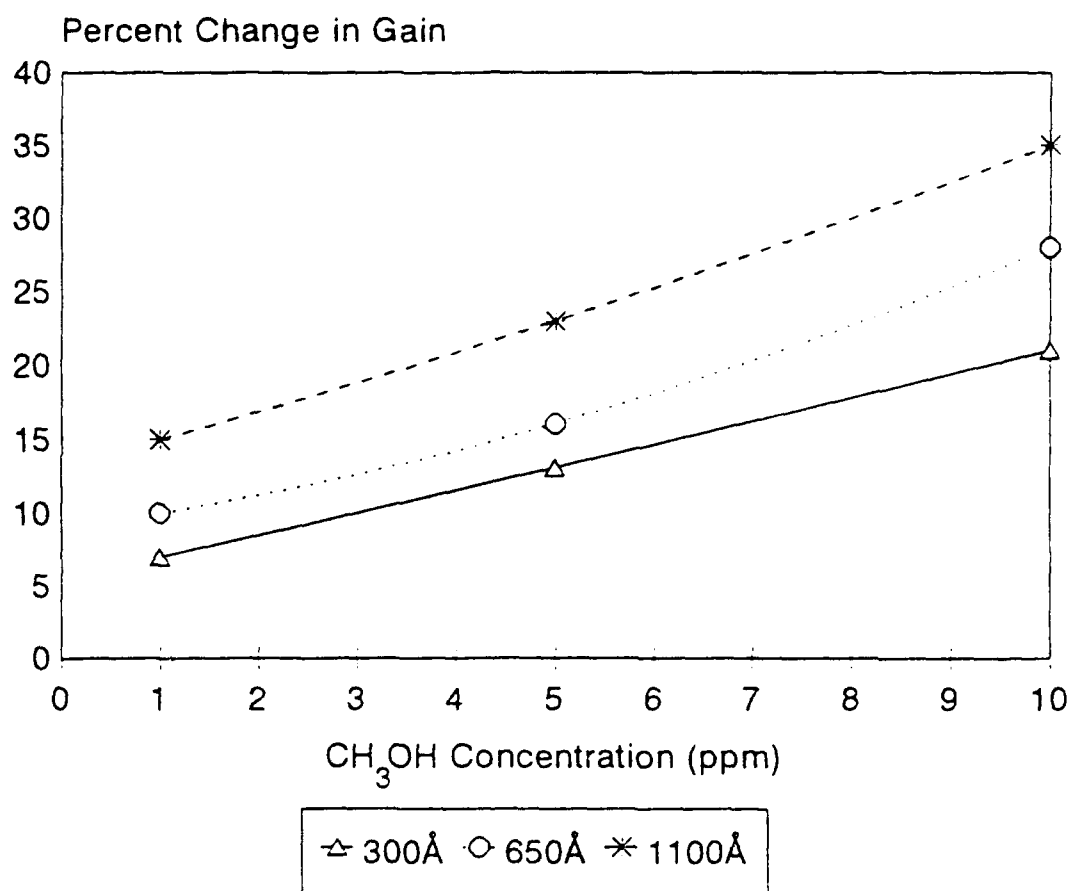


Figure 5.40: Change in Gain at 10 Hz of PbPc CHEMFET when Exposed to CH₃OH at 70°C.

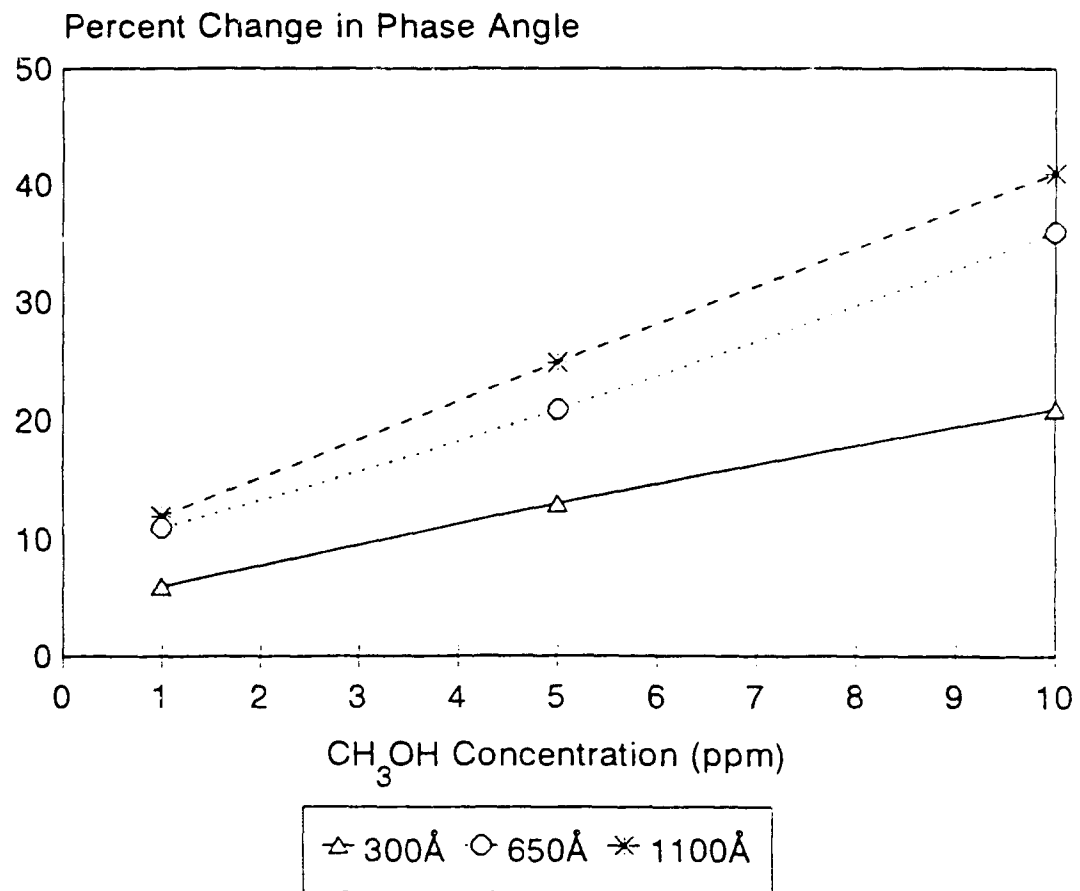


Figure 5.41: Change in Phase Angle at 10 Hz of PbPc CHEMFET when Exposed to CH₃OH at 70°C.

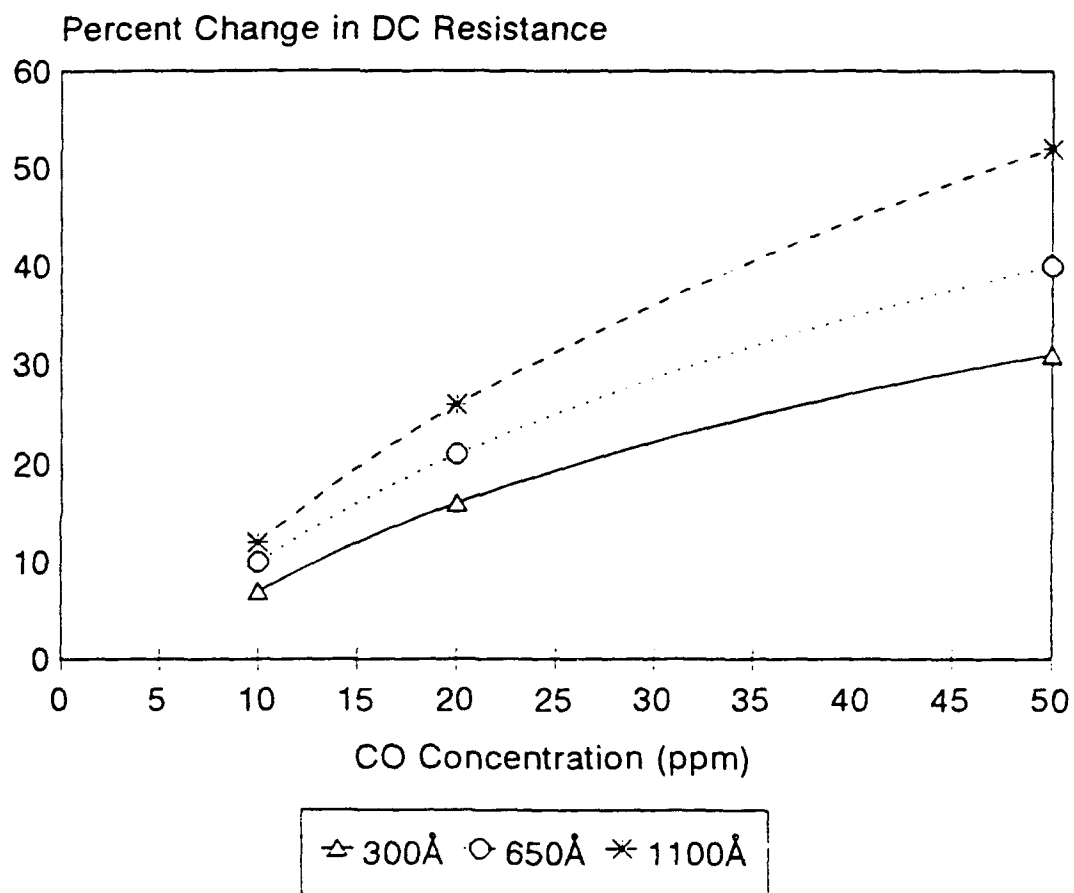


Figure 5.42: Change in DC Resistance of IGE Structures coated with PbPc when Exposed to CO at 70°C.

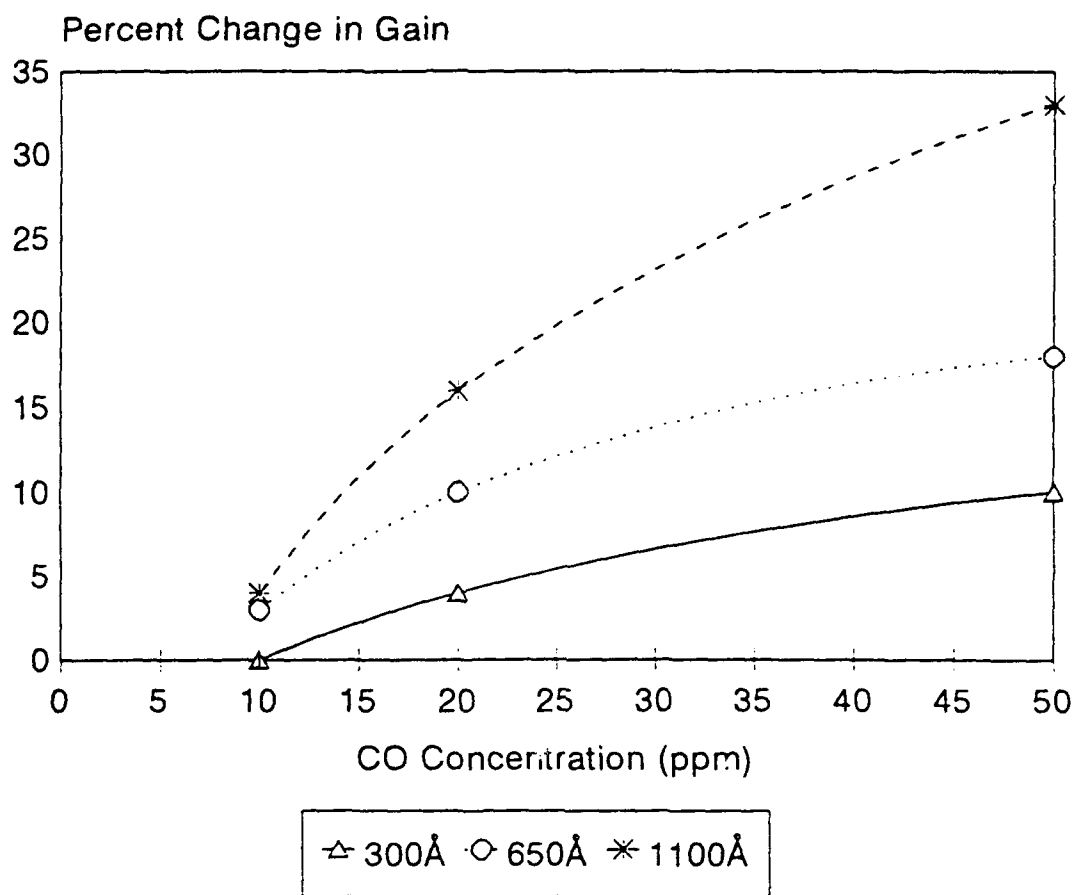


Figure 5.43: Change in Gain at 10 Hz of PbPc CHEMFET when Exposed to CO at 70°C.

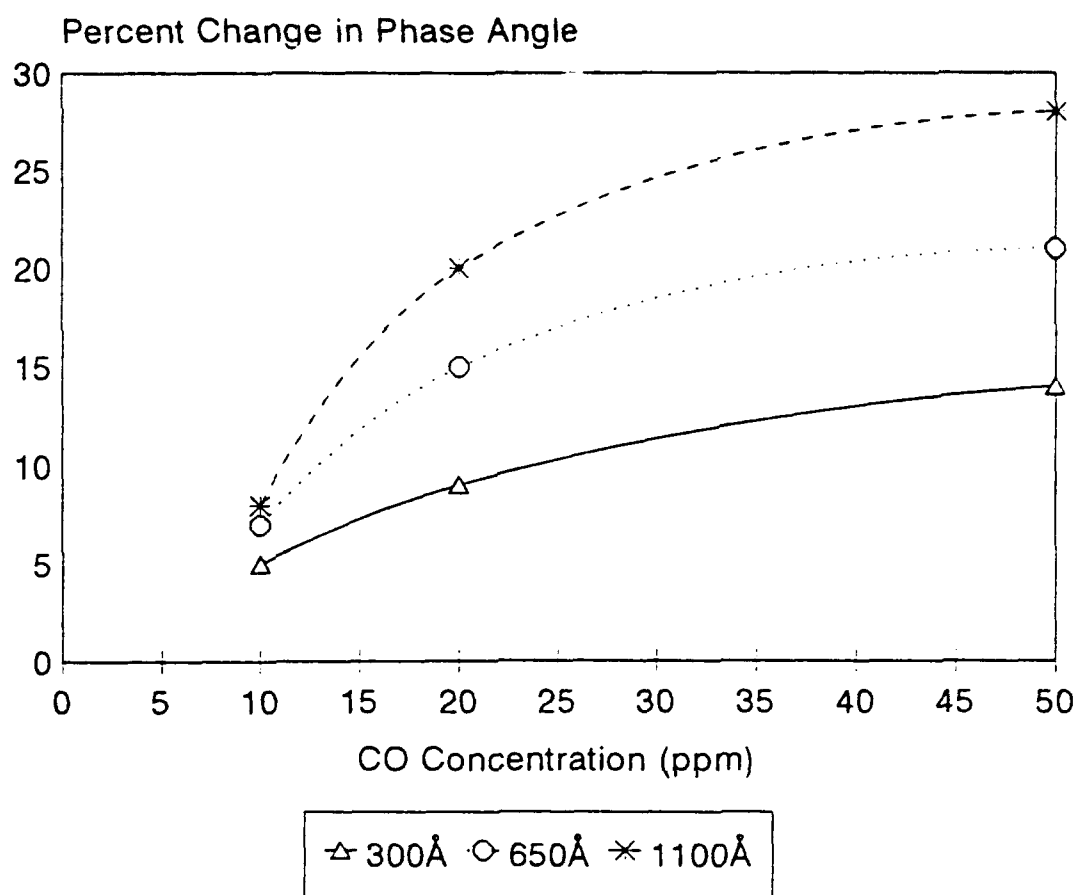


Figure 5.44: Change in Phase Angle at 10 Hz of PbPc CHEMFET when Exposed to CO at 70°C.

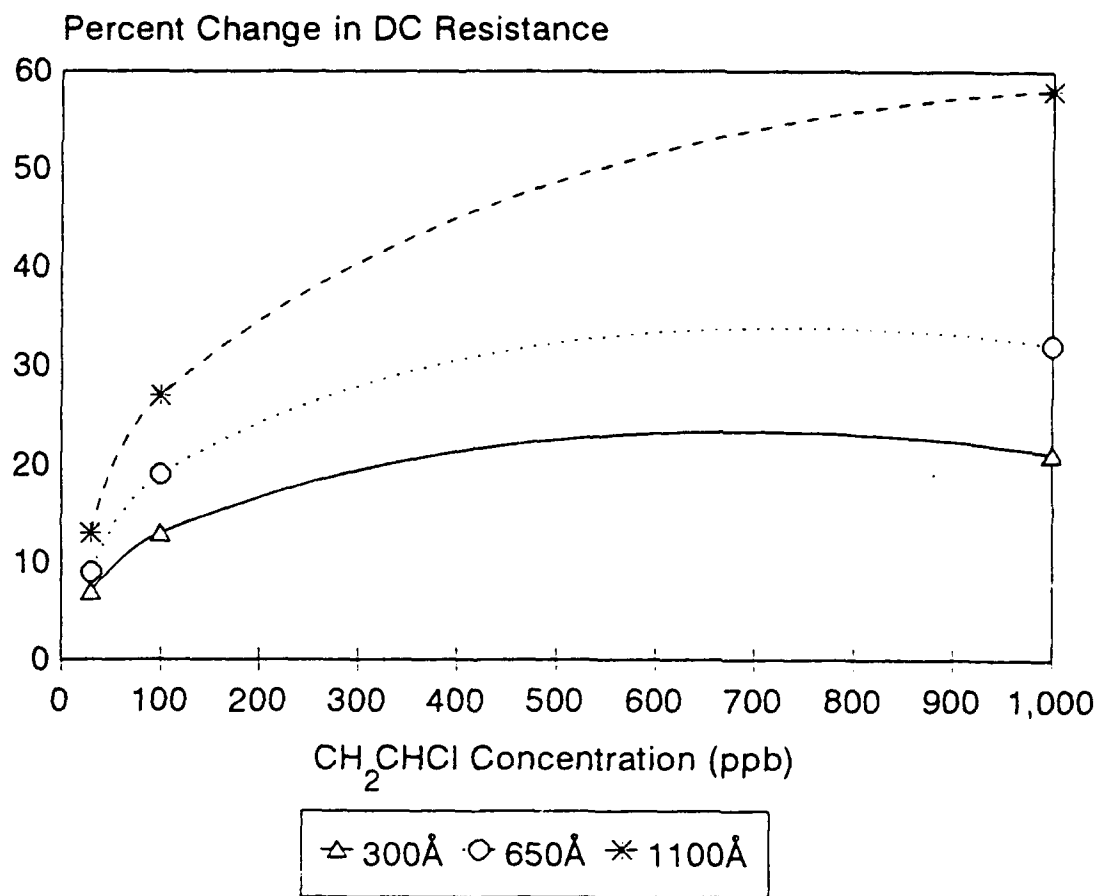


Figure 5.45: Change in DC Resistance of IGE Structures coated with PbPc when Exposed to CH₂CHCl at 70°C.

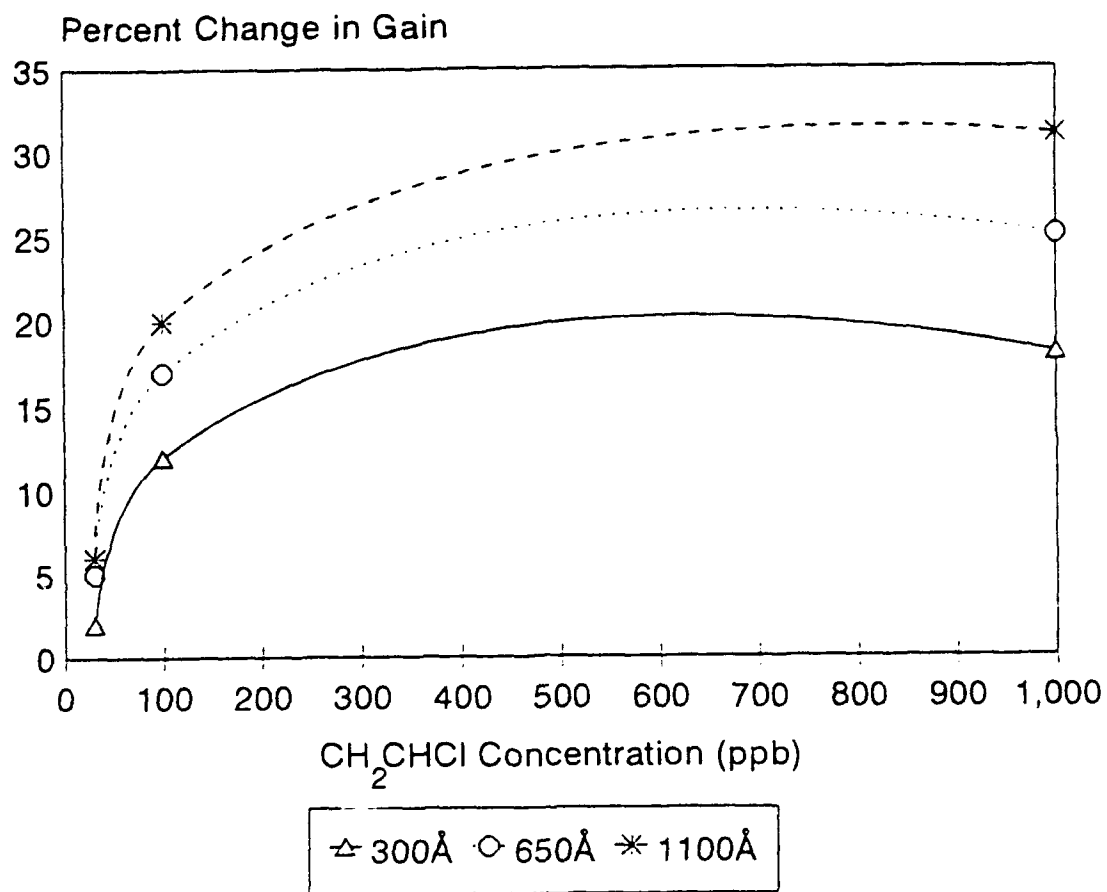


Figure 5.46: Change in Gain at 10 Hz of PbPc CHEMFET when Exposed to CH₂CHCl at 70°C.

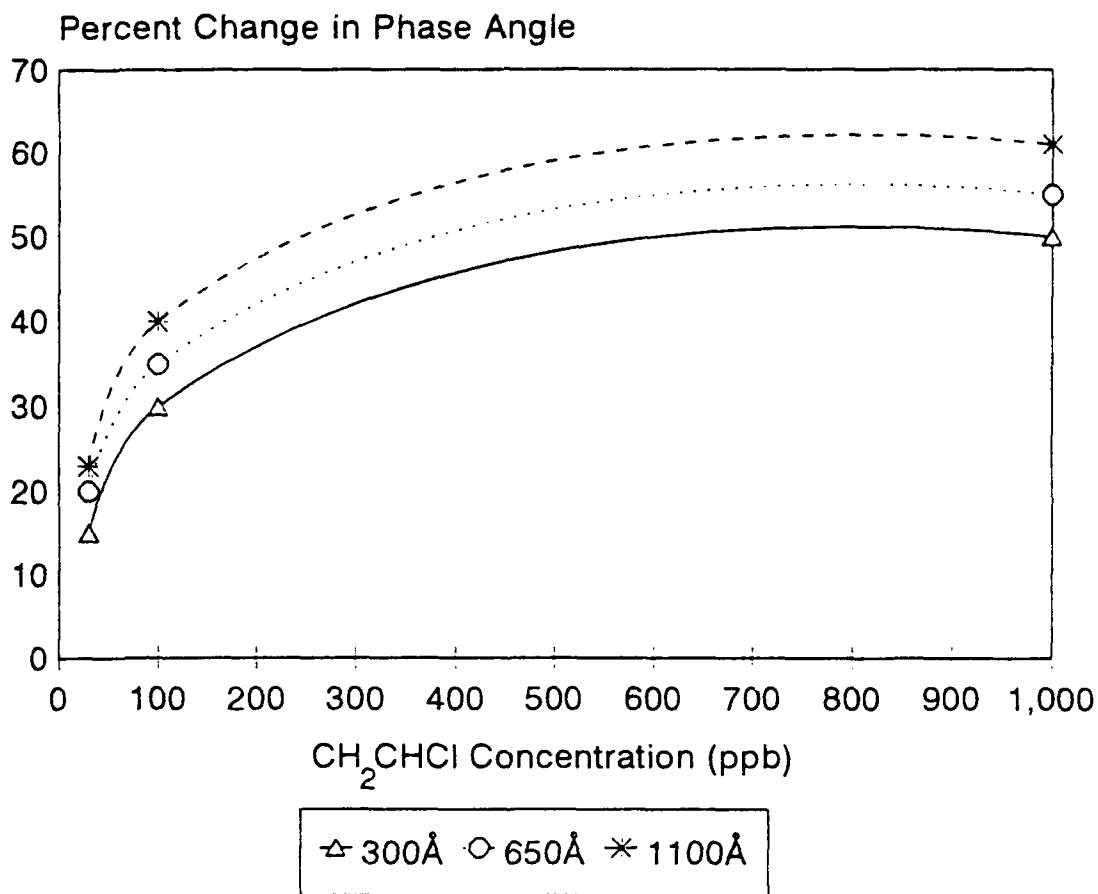


Figure 5.47: Change in Phase Angle at 10 Hz of PbPc CHEMFET when Exposed to CH₂CHCl at 70°C.

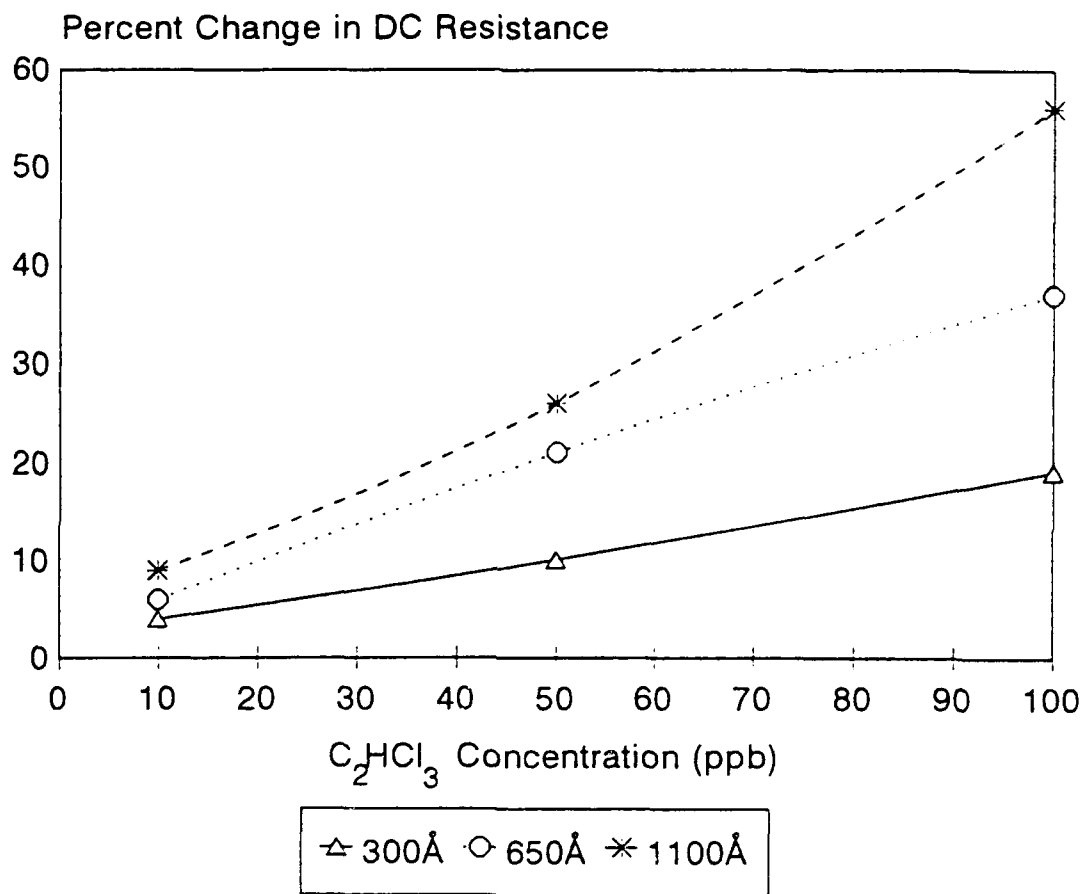


Figure 5.48: Change in DC Resistance of IGE Structures coated with PbPc when Exposed to C_2HCl_3 at 70°C.

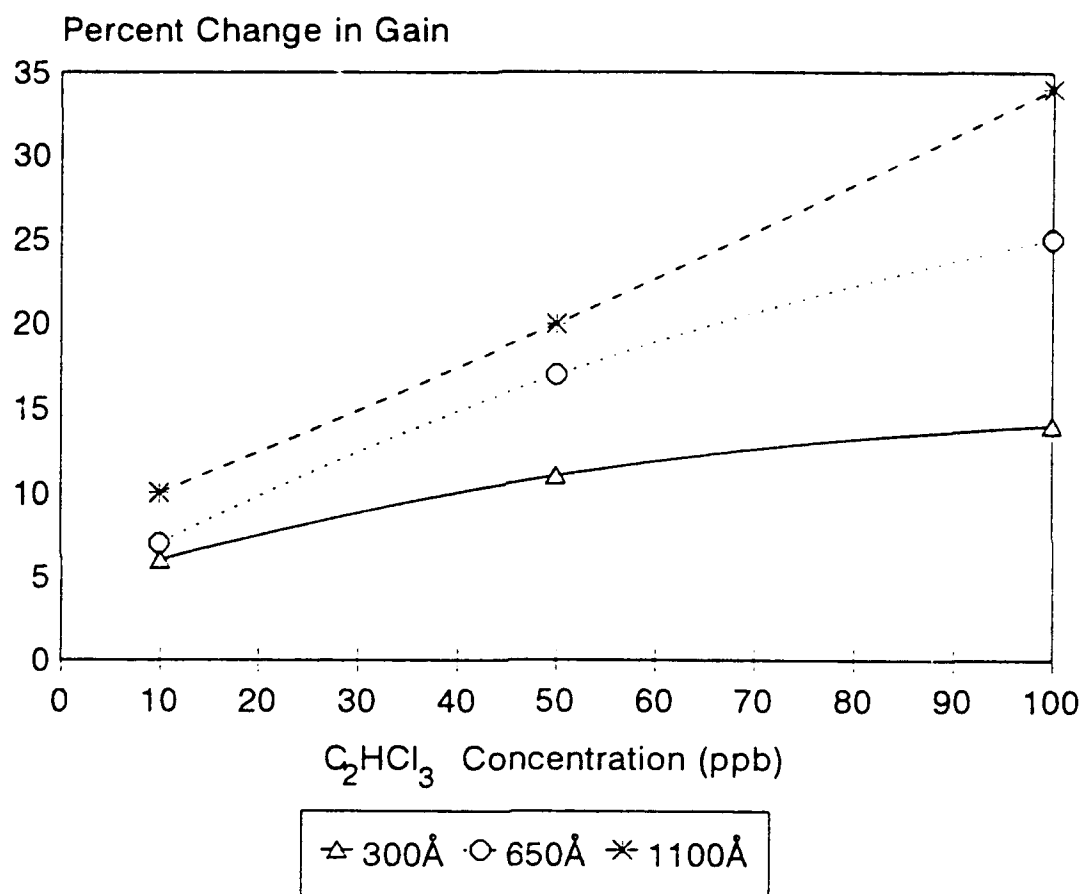


Figure 5.49: Change in Gain at 10 Hz of PbPc CHEMFET when Exposed to C_2HCl_3 at 70°C.

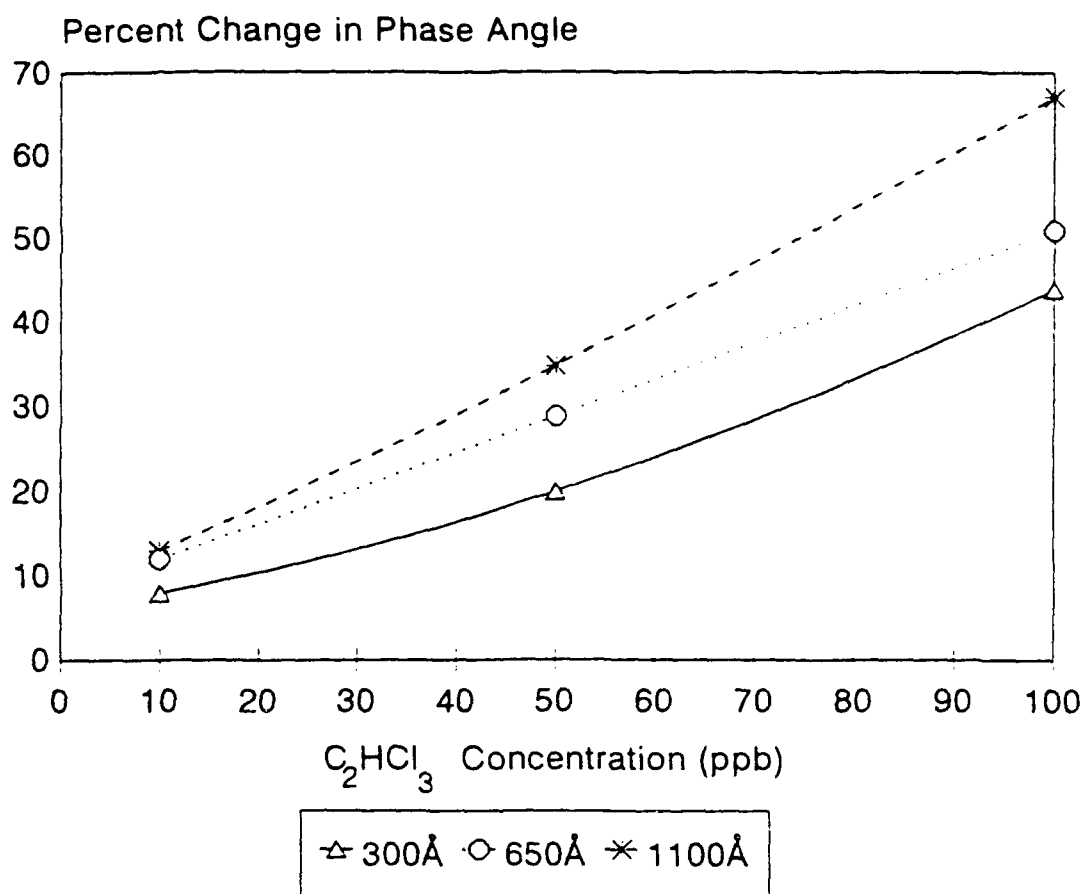


Figure 5.50: Change in Phase Angle at 10 Hz of PbPc CHEMFET when Exposed to C_2HCl_3 at 70°C.

5.5 Sensitivity

The sensitivity of the CHEMFET was determined for each of the challenge gases with respect to the film thickness and type (i.e., CuPc and PbPc). The calculation of the sensitivity involves comparing the data for the mean baseline response relative to the response generated from exposures to the lowest detectable concentration of the challenge gas. Normalized sensitivities were calculated using data gathered for the dc electrical resistance and the gain. From the previous significant literature results contained in Table 2.1, the dc electrical resistance data was used to calculate the sensitivity of the gas microsensor. Similarly, in this investigation, the sensitivities were computed by using the dc electrical resistance data. The gain was also used to calculate the sensitivities, and the results were then compared with the dc electrical resistance sensitivities to determine if a statistical correlation existed between these two sensitivity parameters.

The smallest concentrations of the challenge gases that were detectable for both film types are shown in Table 5.8. The two exceptions are BF_3 and CO. BF_3 was only detected with the CuPc films, and CO was only detected with the PbPc films.

Table 5.8: Challenge Gases and Their Lowest Detectable Concentration for CuPc and PbPc Films.

| Challenge Gas | Lowest Detectable Concentration | Thin-Film Type |
|---------------------------------|---------------------------------|----------------|
| NO ₂ | 10 ppb / 10 ppb | CuPc / PbPc |
| DMMP | 50 ppb / 500 ppb | CuPc / PbPc |
| BF ₃ | 10 ppm / ----* | CuPc / PbPc |
| CH ₃ OH | 1 ppm / 1 ppm | CuPc / PbPc |
| CO | ----* / 10 ppm | CuPc / PbPc |
| CH ₂ CHCl | 30 ppb / 30 ppb | CuPc / PbPc |
| C ₂ HCl ₃ | 10 ppb / 10 ppb | CuPc / PbPc |

* ---- Not detectable

The sensitivities (discussed in Chapter 1 and defined by Equation (1.2)) among the different thicknesses for both film types were calculated. The sensitivities were normalized with respect to the challenge gas and film thickness combination which manifested the greatest response characteristic. For CuPc and PbPc, the film thicknesses of 1000 Å and 1100 Å, respectively, produced the most significant response upon exposure to the NO₂ challenge gas. The normalized sensitivities determined from the dc resistance values for the three thicknesses of CuPc are shown in Figure 5.51. Figure 5.52 shows a similar plot which depicts the normalized sensitivity determined from the recorded gain for each challenge gas. The normalized sensitivities determined from the dc electrical resistance and the gain for the three thicknesses of the PbPc thin-films are shown in Figures 5.53 and 5.54, respectively.

A comparison among these plots supported the previous interpretation of the data (made from the percents of change for the different electrical responses) that the CuPc-coated CHEMFET was more sensitive to DMMP and BF₃ than the PbPc-coated CHEMFET, and that the PbPc films were more sensitive to the NO₂, CH₃OH, CO, CH₂CHCl, and C₂HCl₃ challenge gases. Sensitivities calculated from the dc electrical resistance data and the gain data revealed similar results to the percents of change for these two electrical responses.

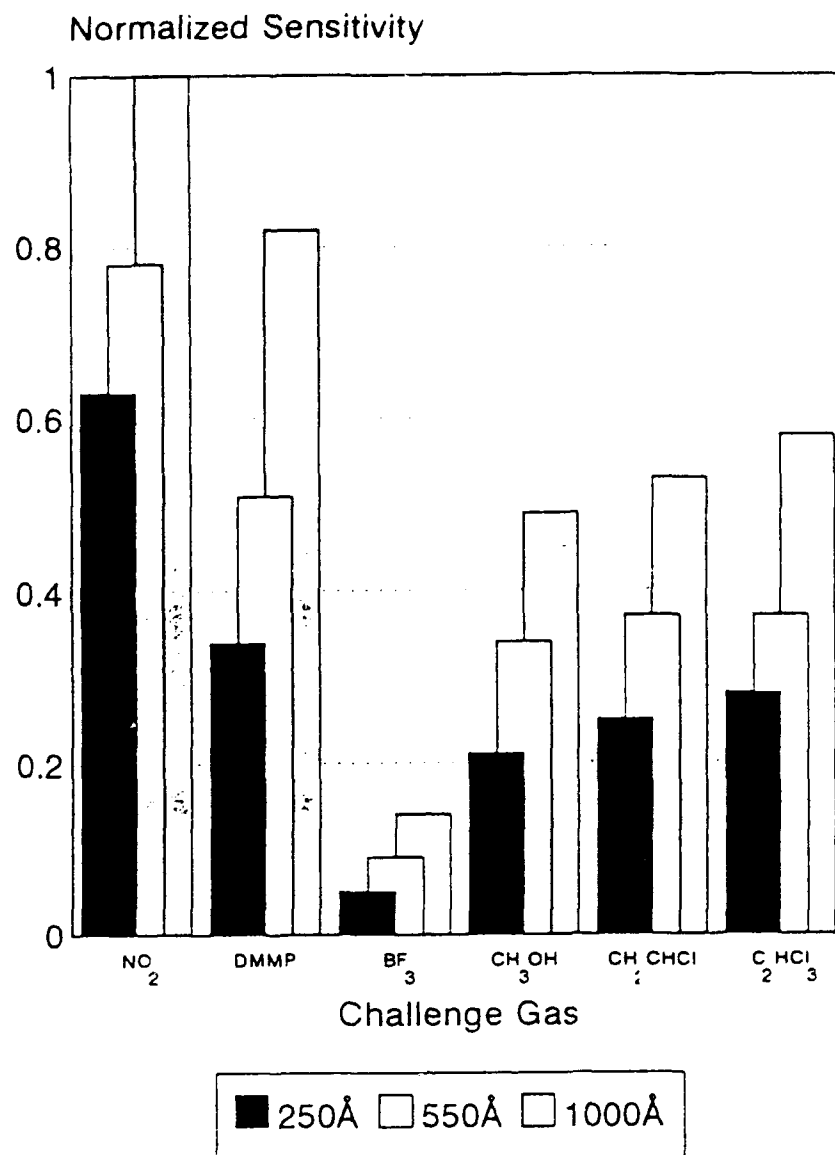


Figure 5.51: Normalized Sensitivities Determined from DC Resistance Values for Three Thicknesses of CuPc.

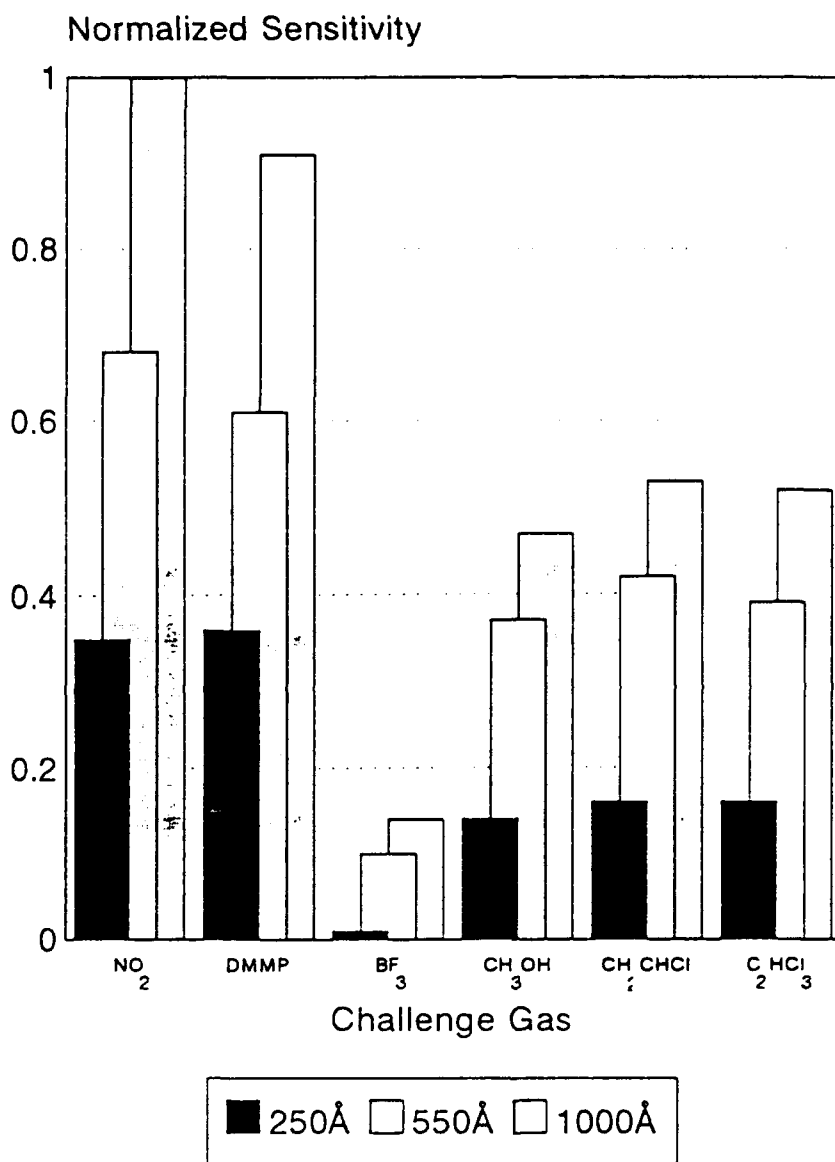


Figure 5.52: Normalized Sensitivities Determined from Gain Values for Three Thicknesses of CuPc.

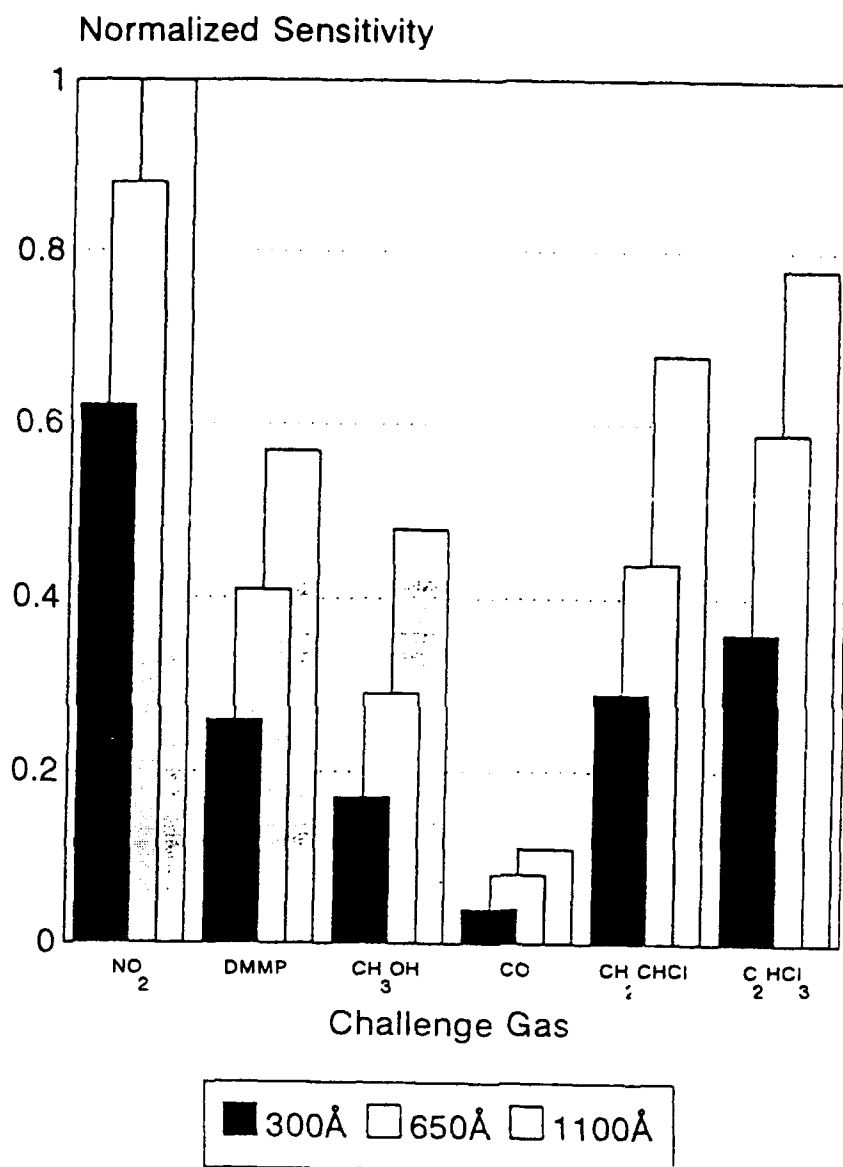


Figure 5.53: Normalized Sensitivities Determined from DC Resistance Values for Three Thicknesses of PbPc.

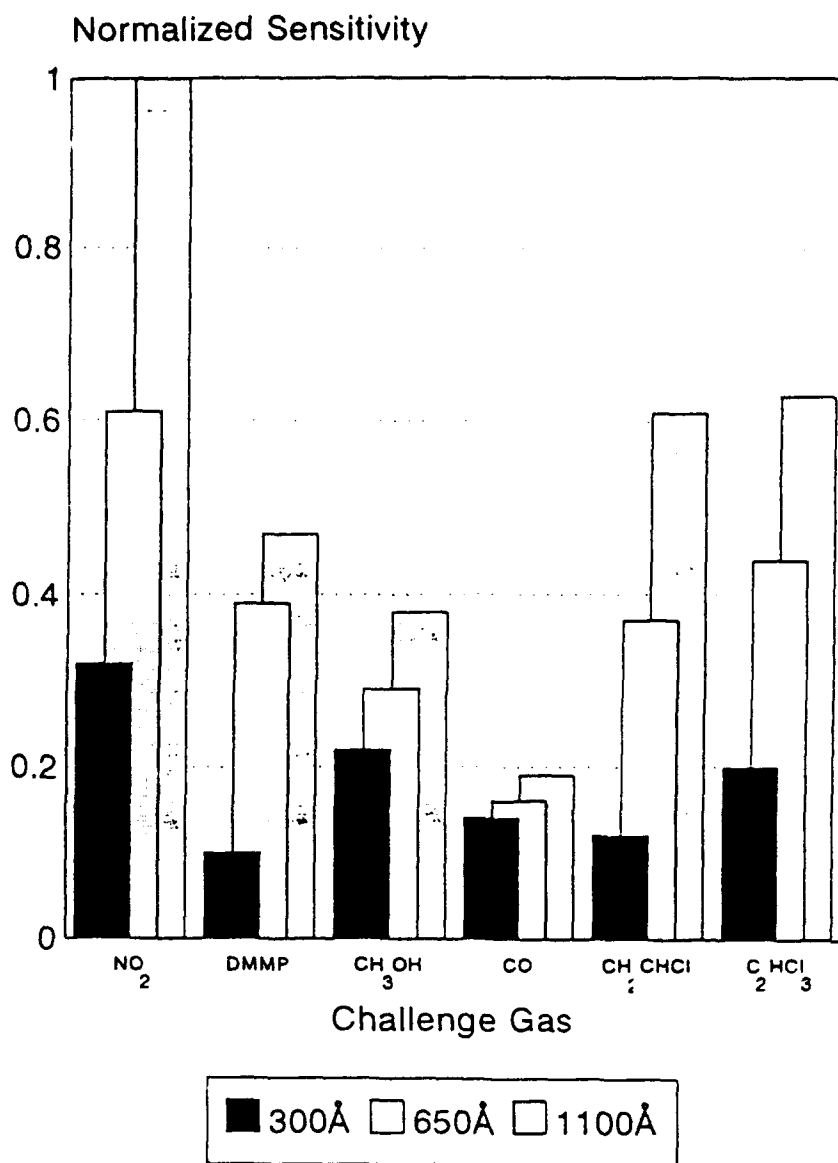


Figure 5.54: Normalized Sensitivities Determined from Gain Values for Three Thicknesses of PbPc.

The trends of the normalized sensitivities calculated from the two sets of data (dc resistance and gain) resemble each other. To determine the relative degree of resemblance, the statistical correlation parameter ($\text{Corr}_{x,y}$) was computed for the dc resistance sensitivity (X) and the gain sensitivity (Y):

$$\text{Corr}_{x,y} = \frac{\text{Cov}_{x,y}}{\sigma_x \sigma_y} \quad (5.1)$$

where $\text{Cov}_{x,y}$ is the covariance of X and Y, and σ_x and σ_y are the X and Y standard deviations. The resulting correlations for the challenge gases are listed in Table 5.9. The resulting correlation parameters ($\text{Corr}_{x,y}$) describe the pseudo-linear relationship between the normalized sensitivities of the dc electrical resistance and the gain measurements; the magnitude of the $\text{Corr}_{x,y}$ parameter suggests a weak relationship for all the challenge gases.

The normalized sensitivities show that thicker films were more sensitive than thinner films. As for the sensitivities of the particular thin-film types, CuPc was more sensitive to the DMMP and BF_3 challenge gases. PbPc was more sensitive to NO_2 , CH_3OH , CO, CH_2CHCl , and C_2HCl_3 .

Table 5.9: Determined Correlations Between Sensitivities.

| Challenge Gas | Thin-Film | Correlation |
|---------------------------------|-----------|-------------|
| NO ₂ | CuPc | 0.22 |
| DMMP | CuPc | 0.31 |
| BF ₃ | CuPc | 0.38 |
| CH ₃ OH | CuPc | 0.35 |
| CH ₂ CHCl | CuPc | 0.29 |
| C ₂ HCl ₃ | CuPc | 0.11 |
| NO ₂ | PbPc | 0.40 |
| DMMP | PbPc | 0.26 |
| CH ₃ OH | PbPc | 0.27 |
| CH ₂ CHCl | PbPc | 0.33 |
| C ₂ HCl ₃ | PbPc | 0.09 |
| CO | PbPc | 0.21 |

5.6 Selectivity

The selectivity of the CHEMFET is characterized by its ability to distinguish between various challenge gases. The challenge gas combinations used to determine the selectivity included: NO_2/DMMP , NO_2/BF_3 , and DMMP/BF_3 . The concentration for each of the challenge gas components for all possible combinations was arbitrarily set at 1 ppm. By using the same concentration for each challenge gas in the mixtures allows for a consistent baseline to be used for comparison. Since the 1000 Å CuPc film and the 1100 Å PbPc film were the most sensitive, the selectivity investigation was limited to these thicknesses for the respective thin-film types.

The normalized difference spectra responses were used to determine the selectivity of a particular challenge gas relative to another challenge gas. Since the slopes of the normalized difference spectral response plots are unique for each challenge gas, this set of data was used to compute the selectivity. The normalized difference spectra response for each combination of the challenge gas mixtures are shown in Figures 5.55 through 5.57. Table 5.10 summarizes the computed selectivity values (defined by Equation (1.3)) for the experimental combinations. The selectivity values relate to the reliability that Gas #2 is being detected when combined with Gas #1 which has a stronger normalized difference spectra response. As noted with the combinations

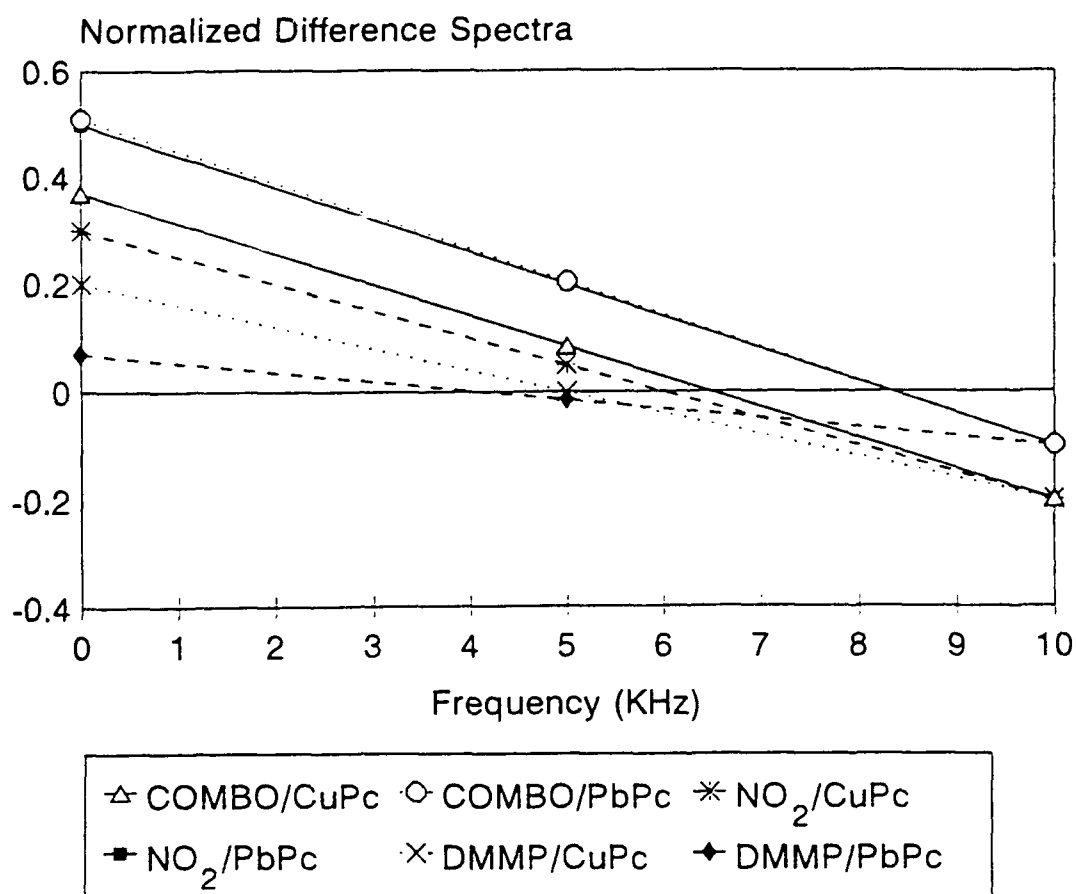


Figure 5.55: Difference Spectral Responses of 1100 Å Thick PbPc Film and 1000 Å Thick CuPc Film when Exposed to the Combination of 1 ppm of NO₂ and 1 ppm of DMMP.

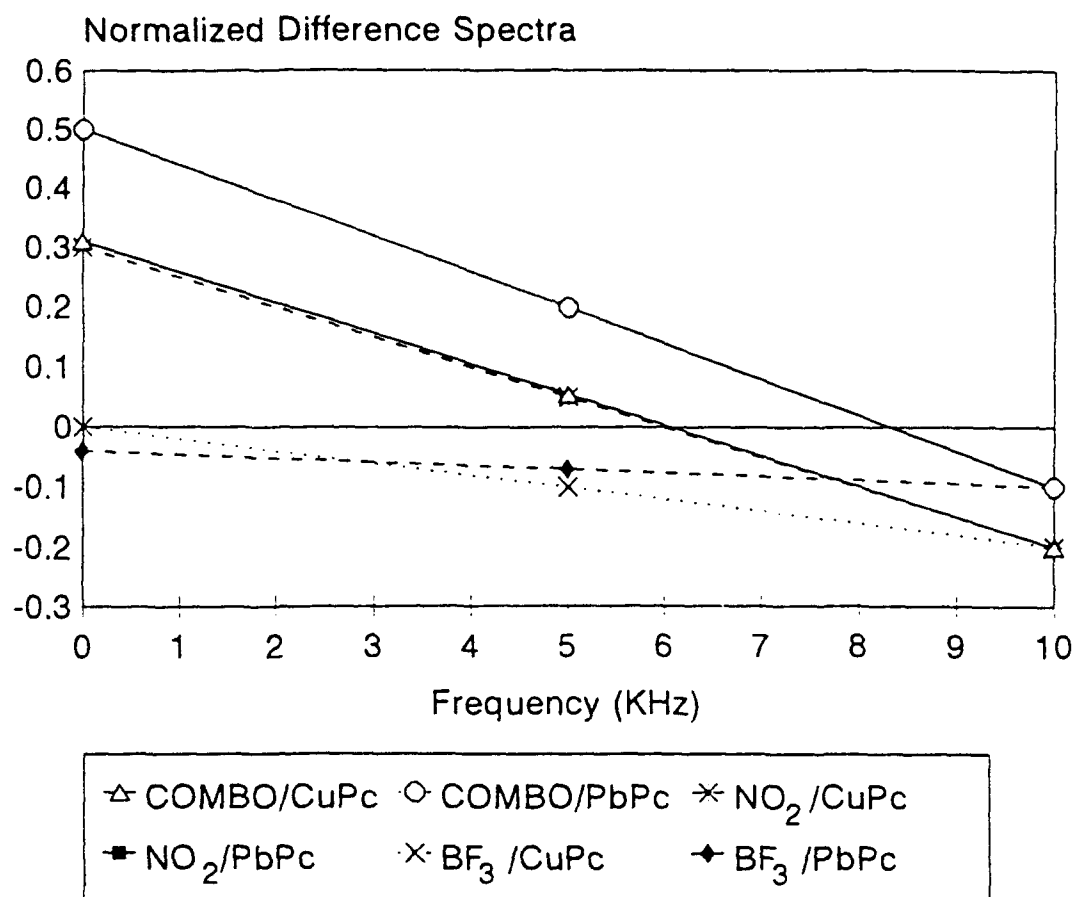


Figure 5.56: Difference Spectral Responses of 1100 Å Thick PbPc Film and 1000 Å Thick CuPc Film when Exposed to the Combination of 1 ppm of NO₂ and 1 ppm of BF₃.

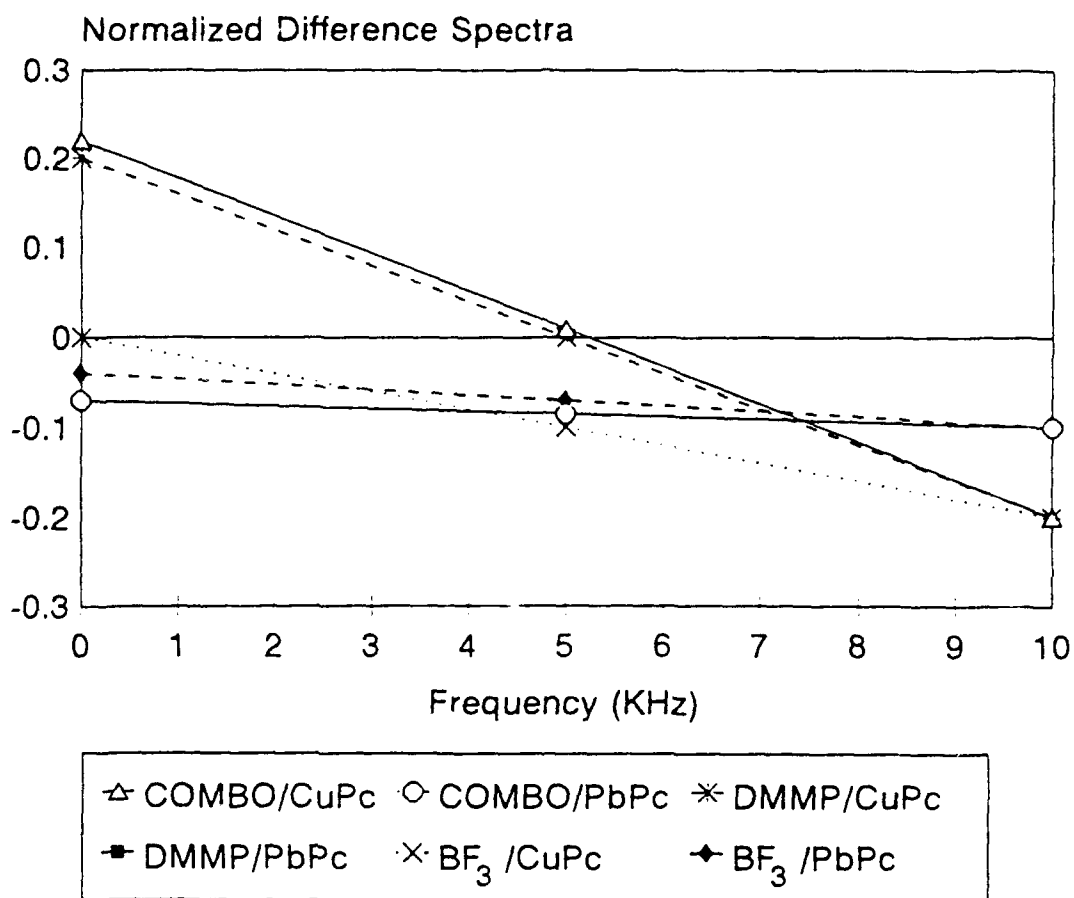


Figure 5.57: Difference Spectral Responses of 1100 Å Thick PbPc Film and 1000 Å Thick CuPc Film when Exposed to the Combination of 1 ppm of DMMP and 1 ppm of BF₃.

Table 5.10: Selectivity of the Challenge Gas Combinations.

| Gas Combination | Thin-Film Type | Slope of Gas #1 ($\times 10^{-5}$) | Slope of Gas #2 ($\times 10^{-5}$) | Slope of Combo ($\times 10^{-5}$) | Selectivity Gas #2 |
|----------------------------------|----------------|--------------------------------------|--------------------------------------|-------------------------------------|--------------------|
| NO ₂ /DMMP | CuPc | 5 | 4 | 5.7 | 0.18 |
| NO ₂ /BF ₃ | CuPc | 5 | 0.2 | 5.1 | 0.50 |
| DMMP/BF ₃ | CuPc | 4 | 0.2 | 4.2 | 1.00 |
| NO ₂ /DMMP | PbPc | 6 | 0.3 | 6.1 | 0.33 |
| NO ₂ /BF ₃ | PbPc | 6 | 0.06 | 6.0 | 0.0 |
| DMMP/BF ₃ | PbPc | 0.3 | 0.06 | 0.3 | 0.0 |

with NO₂ being Gas #1, the selectivity for Gas #2 is low. This behavior is expected since the CHEMFET's response to NO₂ exposures is the most robust when compared to the other challenge gases. Since the original normalized difference spectra were so minute for BF₃, the slightest change in the normalized difference spectra response for the combination of challenge gases would result in a high selectivity value.

5.7 Reversibility

The reversibility of the CHEMFET describes the system's ability to return to 90% of its original state after being exposed to a particular challenge gas. The length of time required for the sensing elements to reach 90% of their original state for the CHEMFET's dc electrical resistance is shown in Tables 5.11 and 5.12 for 22°C and 110°C, respectively. Overall, the time to attain reversibility decreased as the operating temperature was increased from 22°C to 110°C. Furthermore, the reversibility time requirement is lessened as the thickness of the CuPc and PbPc films is reduced.

The relationship between the reversibility and the length of time the sensing elements were exposed to a challenge gas was also investigated. The challenge gas selected for this set of reversibility measurements was NO₂ at a 1 ppm concentration since this challenge gas exhibited

Table 5.11: Reversibility (in seconds) for the Highest Concentration of the Challenge Gases at 22°C.

| Film Type / Thickness | NO ₂ at 1 ppm | DMMP at 10 ppm | BF ₃ at 20 ppm |
|-----------------------|-----------------------------|-------------------|------------------------------|
| CuPc / 250 Å | 870 | 690 | 600 |
| PbPc / 300 Å | 900 | 660 | ---* |
| CuPc / 550 Å | 1110 | 930 | 720 |
| PbPc / 650 Å | 1230 | 810 | ---* |
| CuPc / 1000 Å | 1530 | 1110 | 1020 |
| PbPc / 1100 Å | 1620 | 1050 | ---* |

Table 5.12: Reversibility (in seconds) for the Highest Concentration of the Challenge Gases at 110°C.

| Film Type / Thickness | NO ₂ at 1 ppm | DMMP at 10 ppm | BF ₃ at 20 ppm |
|-----------------------|-----------------------------|-------------------|------------------------------|
| CuPc / 250 Å | 540 | 570 | 420 |
| PbPc / 300 Å | 570 | 570 | ---* |
| CuPc / 550 Å | 660 | 660 | 510 |
| PbPc / 650 Å | 840 | 660 | ---* |
| CuPc / 1000 Å | 1200 | 1080 | 780 |
| PbPc / 1100 Å | 1320 | 1020 | ---* |

*--- Not detectable

the greatest response. The time duration of the challenge gas "plug" delivered to the test chamber, which housed the microsensor, was varied from 2 to 6 minutes. The operating temperature was maintained at 22°C, and only two sensing elements (#7 and #9) were observed, both of which were coated with a 1100 Å thin film of PbPc. The results are depicted in Figure 5.58. Even though the 2-minute duration "plug" of the challenge gas achieved full reversibility the most rapidly, the change in the dc electrical resistance response is not as significant as displayed by the other gas "plugs". On the other hand, the change in the dc electrical resistance for the other four challenge gas "plugs" attain a stable response plateau within 90% of the initial baseline performance response, at which point, any further change in the dc resistance is negligible.

5.8 Summary

Both of the chemically-sensitive thin-film candidates (CuPc and PbPc) were evaluated for their responses to different concentrations of seven challenge gases. The primary gases used consisted of NO₂, DMMP, and BF₃. The performance evaluation of the CHEMFET was conducted with the die isothermally thermostated at 22°C and 110°C. The secondary challenge gases used to establish the detection capability of the CHEMFET included: CH₃OH, CO, CH₂CHCl, and

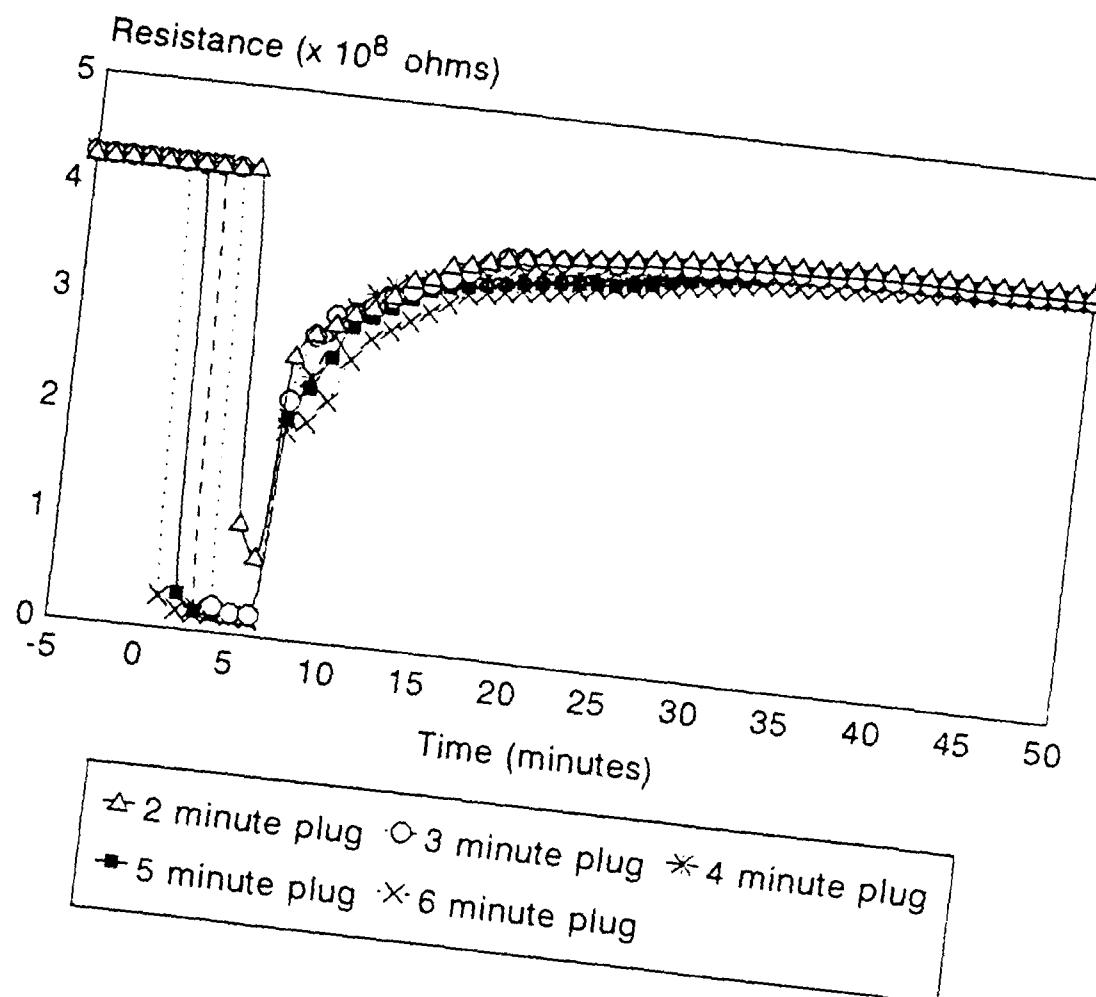


Figure 5.58: Reversibility of PbPc Film of Thickness 1100 Å when Exposed to 1 ppm of NO_2 for Varying Durations.

C_2HCl_3 . These latter challenge gases were monitored while maintaining an operating temperature of 70°C. For exposures to all seven challenge gases, the performance of three film thicknesses for CuPc and PbPc were measured and analyzed.

The purpose of this investigation was to evaluate the sensitivity, selectivity, and reversibility of the CHEMFET. The physical operating parameters were identified which produced the most significant sensitivity, the most significant selectivity, and the most complete degree of reversibility relative to time. Tables 5.13 and 5.14 summarize the sensitivity, selectivity, and reversibility of the CHEMFET coated with CuPc and PbPc films, respectively. The measurable response parameters produced by the CHEMFET included: the dc electrical resistance of the IGE structure, the gain and phase angle of the device, the electrical impedance of the IGE structure, and the CHEMFET's voltage-pulse and difference spectral responses.

The most valuable measurements in this investigation were the dc electrical resistance of the IGE structure and the gain. These two measurement parameters provided the most profound changes and characteristic responses upon exposure to the challenge gases. These measurements were used to compute the sensitivity and reversibility of the CHEMFET relative to the variable operating parameters. Determining the selectivity for the binary challenge gas

Table 5.13: Findings on Sensitivity, Selectivity, and Reversibility for the Investigated CuPc-Coated Microsensor.

| film type/ thickness | gas/ concen. | temp. (°C) | sensit- ivity | select- ivity | revers- ibility |
|-------------------------|---------------------------|---------------|------------------|------------------|--------------------|
| CuPc 250 Å | NO ₂ 10ppb | 22 | 0.06 | | |
| CuPc 250 Å | NO ₂ 50ppb | 22 | 0.10 | | |
| CuPc 250 Å | NO ₂ 100ppb | 22 | 0.15 | | |
| CuPc 250 Å | NO ₂ 500ppb | 22 | 0.21 | | |
| CuPc 250 Å | NO ₂ 1 ppm | 22 | 0.39 | | 870 seconds |
| CuPc 250 Å | DMMP 50ppb | 22 | 0.08 | | |
| CuPc 250 Å | DMMP 100ppb | 22 | 0.14 | | |
| CuPc 250 Å | DMMP 500ppb | 22 | 0.18 | | |
| CuPc 250 Å | DMMP 1ppm | 22 | 0.26 | | |
| CuPc 250 Å | DMMP 10ppm | 22 | 0.32 | | 690 seconds |
| CuPc 250 Å | BF ₃ 50ppb | 22 | --- | | |
| CuPc 250 Å | BF ₃ 100ppb | 22 | --- | | |
| CuPc 250 Å | BF ₃ 1ppm | 22 | --- | | |
| CuPc 250 Å | BF ₃ 10ppm | 22 | 1.15 | | |
| CuPc 250 Å | BF ₃ 20ppm | 22 | 1.56 | | 600 seconds |

Table 5.13: (continued)

| film type/ thickness | gas/ concen. | temp. (°C) | sensit- ivity | select- ivity | revers- ibility |
|-------------------------|---------------------------|---------------|------------------|------------------|--------------------|
| CuPc 550 Å | NO ₂ 10ppb | 22 | 0.12 | | |
| CuPc 550 Å | NO ₂ 50ppb | 22 | 0.19 | | |
| CuPc 550 Å | NO ₂ 100ppb | 22 | 0.27 | | |
| CuPc 550 Å | NO ₂ 500ppb | 22 | 0.46 | | |
| CuPc 550 Å | NO ₂ 1 ppm | 22 | 0.71 | | 1110 seconds |
| CuPc 550 Å | DMMP 50ppb | 22 | 0.10 | | |
| CuPc 550 Å | DMMP 100ppb | 22 | 0.17 | | |
| CuPc 550 Å | DMMP 500ppb | 22 | 0.23 | | |
| CuPc 550 Å | DMMP 1ppm | 22 | 0.30 | | |
| CuPc 550 Å | DMMP 10ppm | 22 | 0.47 | | 930 seconds |
| CuPc 550 Å | BF ₃ 50ppb | 22 | --- | | |
| CuPc 550 Å | BF ₃ 100ppb | 22 | --- | | |
| CuPc 550 Å | BF ₃ 1ppm | 22 | --- | | |
| CuPc 550 Å | BF ₃ 10ppm | 22 | 1.22 | | |
| CuPc 550 Å | BF ₃ 20ppm | 22 | 1.69 | | 720 seconds |

Table 5.13: (continued)

| film type/ thickness | gas/ concen. | temp. (°C) | sensit- ivity | select- ivity | revers- ibility |
|-------------------------|---------------------------|---------------|------------------|------------------|--------------------|
| CuPc 1000 Å | NO ₂ 10ppb | 22 | 0.13 | | |
| CuPc 1000 Å | NO ₂ 50ppb | 22 | 0.21 | | |
| CuPc 1000 Å | NO ₂ 100ppb | 22 | 0.40 | | |
| CuPc 1000 Å | NO ₂ 500ppb | 22 | 0.61 | | |
| CuPc 1000 Å | NO ₂ 1 ppm | 22 | 0.89 | 1.00 | 1530 seconds |
| CuPc 1000 Å | DMMP 50ppb | 22 | 0.15 | | |
| CuPc 1000 Å | DMMP 100ppb | 22 | 0.19 | | |
| CuPc 1000 Å | DMMP 500ppb | 22 | 0.29 | | |
| CuPc 1000 Å | DMMP 1ppm | 22 | 0.40 | 0.18 | |
| CuPc 1000 Å | DMMP 10ppm | 22 | 0.63 | | 1110 seconds |
| CuPc 1000 Å | BF ₃ 50ppb | 22 | --- | | |
| CuPc 1000 Å | BF ₃ 100ppb | 22 | --- | | |
| CuPc 1000 Å | BF ₃ 1ppm | 22 | --- | 0.00 | |
| CuPc 1000 Å | BF ₃ 10ppm | 22 | 1.30 | | |
| CuPc 1000 Å | BF ₃ 20ppm | 22 | 2.63 | | 1020 seconds |

Table 5.13: (continued)

| film type/ thickness | gas/ concen. | temp. (°C) | sensit- ivity | select- ivity | revers- ibility |
|-------------------------|---------------------------|---------------|------------------|------------------|--------------------|
| CuPc 250 Å | NO ₂ 10ppb | 110 | 0.04 | | |
| CuPc 250 Å | NO ₂ 50ppb | 110 | 0.10 | | |
| CuPc 250 Å | NO ₂ 100ppb | 110 | 0.16 | | |
| CuPc 250 Å | NO ₂ 500ppb | 110 | 0.21 | | |
| CuPc 250 Å | NO ₂ 1 ppm | 110 | 0.27 | | 540 seconds |
| CuPc 250 Å | DMMP 50ppb | 110 | 0.05 | | |
| CuPc 250 Å | DMMP 100ppb | 110 | 0.13 | | |
| CuPc 250 Å | DMMP 500ppb | 110 | 0.18 | | |
| CuPc 250 Å | DMMP 1ppm | 110 | 0.24 | | |
| CuPc 250 Å | DMMP 10ppm | 110 | 0.30 | | 570 seconds |
| CuPc 250 Å | BF ₃ 50ppb | 110 | --- | | |
| CuPc 250 Å | BF ₃ 100ppb | 110 | --- | | |
| CuPc 250 Å | BF ₃ 1ppm | 110 | --- | | |
| CuPc 250 Å | BF ₃ 10ppm | 110 | 1.09 | | |
| CuPc 250 Å | BF ₃ 20ppm | 110 | 1.32 | | 420 seconds |

Table 5.13: (continued)

| film type/ thickness | gas/ concen. | temp. (°C) | sensit- ivity | select- ivity | revers- ibility |
|-------------------------|---------------------------|---------------|------------------|------------------|--------------------|
| CuPc 550 Å | NO ₂ 10ppb | 110 | 0.07 | | |
| CuPc 550 Å | NO ₂ 50ppb | 110 | 0.14 | | |
| CuPc 550 Å | NO ₂ 100ppb | 110 | 0.22 | | |
| CuPc 550 Å | NO ₂ 500ppb | 110 | 0.33 | | |
| CuPc 550 Å | NO ₂ 1 ppm | 110 | 0.54 | | 660 seconds |
| CuPc 550 Å | DMMP 50ppb | 110 | 0.10 | | |
| CuPc 550 Å | DMMP 100ppb | 110 | 0.15 | | |
| CuPc 550 Å | DMMP 500ppb | 110 | 0.22 | | |
| CuPc 550 Å | DMMP 1ppm | 110 | 0.28 | | |
| CuPc 550 Å | DMMP 10ppm | 110 | 0.43 | | 660 seconds |
| CuPc 550 Å | BF ₃ 50ppb | 110 | --- | | |
| CuPc 550 Å | BF ₃ 100ppb | 110 | --- | | |
| CuPc 550 Å | BF ₃ 1ppm | 110 | --- | | |
| CuPc 550 Å | BF ₃ 10ppm | 110 | 1.14 | | |
| CuPc 550 Å | BF ₃ 20ppm | 110 | 1.61 | | 510 seconds |

Table 5.13: (continued)

| film type/ thickness | gas/ concen. | temp. (°C) | sensit- ivity | select- ivity | revers- ibility |
|-------------------------|---------------------------|---------------|------------------|------------------|--------------------|
| CuPc 1000 Å | NO ₂ 10ppb | 110 | 0.11 | | |
| CuPc 1000 Å | NO ₂ 50ppb | 110 | 0.18 | | |
| CuPc 1000 Å | NO ₂ 100ppb | 110 | 0.34 | | |
| CuPc 1000 Å | NO ₂ 500ppb | 110 | 0.47 | | |
| CuPc 1000 Å | NO ₂ 1 ppm | 110 | 0.67 | 1.00 | 1200 seconds |
| CuPc 1000 Å | DMMP 50ppb | 110 | 0.13 | | |
| CuPc 1000 Å | DMMP 100ppb | 110 | 0.18 | | |
| CuPc 1000 Å | DMMP 500ppb | 110 | 0.26 | | |
| CuPc 1000 Å | DMMP 1ppm | 110 | 0.36 | 0.18 | |
| CuPc 1000 Å | DMMP 10ppm | 110 | 0.56 | | 1080 seconds |
| CuPc 1000 Å | BF ₃ 50ppb | 110 | --- | | |
| CuPc 1000 Å | BF ₃ 100ppb | 110 | --- | | |
| CuPc 1000 Å | BF ₃ 1ppm | 110 | --- | 0.50 | |
| CuPc 1000 Å | BF ₃ 10ppm | 110 | 1.23 | | |
| CuPc 1000 Å | BF ₃ 20ppm | 110 | 2.13 | | 780 seconds |

Table 5.14: Findings on Sensitivity, Selectivity, and Reversibility for the Investigated PbPc-Coated Microsensor.

| film type/ thickness | gas/ concen. | temp. (°C) | sensit- ivity | select- ivity | revers- ibility |
|-------------------------|---------------------------|---------------|------------------|------------------|--------------------|
| PbPc 300 Å | NO ₂ 10ppb | 22 | 0.09 | | |
| PbPc 300 Å | NO ₂ 50ppb | 22 | 0.18 | | |
| PbPc 300 Å | NO ₂ 100ppb | 22 | 0.26 | | |
| PbPc 300 Å | NO ₂ 500ppb | 22 | 0.33 | | |
| PbPc 300 Å | NO ₂ 1 ppm | 22 | 0.41 | | 900 seconds |
| PbPc 300 Å | DMMP 50ppb | 22 | 0.04 | | |
| PbPc 300 Å | DMMP 100ppb | 22 | 0.12 | | |
| PbPc 300 Å | DMMP 500ppb | 22 | 0.19 | | |
| PbPc 300 Å | DMMP 1ppm | 22 | 0.30 | | |
| PbPc 300 Å | DMMP 10ppm | 22 | 0.41 | | 660 seconds |

Table 5.14: (continued)

| film type/ thickness | gas/ concen. | temp. (°C) | sensit- ivity | select- ivity | revers- ibility |
|-------------------------|---------------------------|---------------|------------------|------------------|--------------------|
| PbPc 650 Å | NO ₂ 10ppb | 22 | 0.11 | | |
| PbPc 650 Å | NO ₂ 50ppb | 22 | 0.22 | | |
| PbPc 650 Å | NO ₂ 100ppb | 22 | 0.32 | | |
| PbPc 650 Å | NO ₂ 500ppb | 22 | 0.49 | | |
| PbPc 650 Å | NO ₂ 1 ppm | 22 | 0.67 | | 1230 seconds |
| PbPc 650 Å | DMMP 50ppb | 22 | 0.07 | | |
| PbPc 650 Å | DMMP 100ppb | 22 | 0.18 | | |
| PbPc 650 Å | DMMP 500ppb | 22 | 0.27 | | |
| PbPc 650 Å | DMMP 1ppm | 22 | 0.36 | | |
| PbPc 650 Å | DMMP 10ppm | 22 | 0.58 | | 810 seconds |

Table 5.14: (continued)

| film type/ thickness | gas/ concen. | temp. (°C) | sensit- ivity | select- ivity | revers- ibility |
|-------------------------|---------------------------|---------------|------------------|------------------|--------------------|
| PbPc 1100 Å | NO ₂ 10ppb | 22 | 0.12 | | |
| PbPc 1100 Å | NO ₂ 50ppb | 22 | 0.26 | | |
| PbPc 1100 Å | NO ₂ 100ppb | 22 | 0.43 | | |
| PbPc 1100 Å | NO ₂ 500ppb | 22 | 0.58 | | |
| PbPc 1100 Å | NO ₂ 1 ppm | 22 | 0.89 | 1.00 | 1530 seconds |
| PbPc 1100 Å | DMMP 50ppb | 22 | 0.08 | | |
| PbPc 1100 Å | DMMP 100ppb | 22 | 0.21 | | |
| PbPc 1100 Å | DMMP 500ppb | 22 | 0.31 | | |
| PbPc 1100 Å | DMMP 1ppm | 22 | 0.42 | 0.33 | |
| PbPc 1100 Å | DMMP 10ppm | 22 | 0.61 | | 1110 seconds |

Table 5.14: (continued)

| film type/ thickness | gas/ concen. | temp. (°C) | sensit- ivity | select- ivity | revers- ibility |
|-------------------------|---------------------------|---------------|------------------|------------------|--------------------|
| PbPc 300 Å | NO ₂ 10ppb | 110 | 0.04 | | |
| PbPc 300 Å | NO ₂ 50ppb | 110 | 0.14 | | |
| PbPc 300 Å | NO ₂ 100ppb | 110 | 0.19 | | |
| PbPc 300 Å | NO ₂ 500ppb | 110 | 0.26 | | |
| PbPc 300 Å | NO ₂ 1 ppm | 110 | 0.32 | | 570 seconds |
| PbPc 300 Å | DMMP 50ppb | 110 | 0.03 | | |
| PbPc 300 Å | DMMP 100ppb | 110 | 0.10 | | |
| PbPc 300 Å | DMMP 500ppb | 110 | 0.16 | | |
| PbPc 300 Å | DMMP 1ppm | 110 | 0.27 | | |
| PbPc 300 Å | DMMP 10ppm | 110 | 0.35 | | 570 seconds |

Table 5.14: (continued)

| film type/ thickness | gas/ concen. | temp. (°C) | sensit- ivity | select- ivity | revers- ibility |
|-------------------------|---------------------------|---------------|------------------|------------------|--------------------|
| PbPc 650 Å | NO ₂ 10ppb | 110 | 0.08 | | |
| PbPc 650 Å | NO ₂ 50ppb | 110 | 0.18 | | |
| PbPc 650 Å | NO ₂ 100ppb | 110 | 0.27 | | |
| PbPc 650 Å | NO ₂ 500ppb | 110 | 0.43 | | |
| PbPc 650 Å | NO ₂ 1 ppm | 110 | 0.59 | | 840 seconds |
| PbPc 650 Å | DMMP 50ppb | 110 | 0.04 | | |
| PbPc 650 Å | DMMP 100ppb | 110 | 0.13 | | |
| PbPc 650 Å | DMMP 500ppb | 110 | 0.22 | | |
| PbPc 650 Å | DMMP 1ppm | 110 | 0.30 | | |
| PbPc 650 Å | DMMP 10ppm | 110 | 0.46 | | 660 seconds |

Table 5.14: (continued)

| film type/ thickness | gas/ concen. | temp. (°C) | sensit- ivity | select- ivity | revers- ibility |
|-------------------------|---------------------------|---------------|------------------|------------------|--------------------|
| PbPc 1100 Å | NO ₂ 10ppb | 110 | 0.09 | | |
| PbPc 1100 Å | NO ₂ 50ppb | 110 | 0.21 | | |
| PbPc 1100 Å | NO ₂ 100ppb | 110 | 0.37 | | |
| PbPc 1100 Å | NO ₂ 500ppb | 110 | 0.51 | | |
| PbPc 1100 Å | NO ₂ 1 ppm | 110 | 0.74 | 1.00 | 1320 seconds |
| PbPc 1100 Å | DMMP 50ppb | 110 | 0.06 | | |
| PbPc 1100 Å | DMMP 100ppb | 110 | 0.16 | | |
| PbPc 1100 Å | DMMP 500ppb | 110 | 0.28 | | |
| PbPc 1100 Å | DMMP 1ppm | 110 | 0.37 | 0.33 | |
| PbPc 1100 Å | DMMP 10ppm | 110 | 0.54 | | 1020 seconds |

combinations could not have been accomplished without the normalized difference spectra responses. Although, a characteristic spectral response was not obtained for BF_3 (compared to the spectral responses gathered for DMMP and NO_2), the resulting normalized difference spectra response provided the necessary information to compute the selectivity of BF_3 .

Chapter 6

6 Conclusions and Recommendations

6.1 Conclusions

An ever increasing interest in protecting, remediating, and restoring the environment has generated a need for advanced monitoring technology. As existing laws are more stringently enforced and new legislation is enacted, enhanced monitoring strategies will be required. Presently, existing analytical instruments have been adapted to perform the monitoring function regardless of their suitability, complexity, and cost. An improved monitoring strategy needs to focus on sensor technology that is able to make *in situ*, repeatable, sensitive, specific, and reliable analyses at a reasonable cost.

The integration of electrical systems and gas sensors have an increasingly vital role. Considering the advances in information processing already achieved with integrated circuits, microelectronic gas-sensors can benefit from integrated circuit process technology. The gas-sensing field can be substantially improved by the power and versatility afforded by integrated circuit technology.

In this study, a symmetrical, two-dimensional array of nine sensing elements was configured on an IC die. The

design of the gas-sensing elements was based on the IGEFET that is serially connected with inverting MOSFET amplifiers. Chemically-sensitive thin-films (i.e., CuPc and PbPc) were deposited on the IGE structure of the sensing elements via vacuum sublimation. The film type and thickness varied for each of the sensing elements. The fabricated CHEMFETs were visually and electrically tested for defects and short circuits.

The electrical performance of the CHEMFET was evaluated with respect to sensitivity, selectivity, and reversibility. The sensitivity, selectivity, and reversibility were affected by several operating parameters, which included: film type, film thickness, challenge gas type, challenge gas concentration, and operating temperature.

The test parameters were investigated over a wide range. The thicknesses and types of the films were systematically varied. The deposited thicknesses of the CuPc films were 250 Å, 550 Å, and 1000 Å; the thicknesses of the PbPc films were 300 Å, 650 Å, and 1100 Å. The gases used to challenge the thin-films consisted of a primary and secondary set of gases. The primary gases were NO₂, DMMP, and BF₃. The secondary gases, only used for screening purposes, included: CH₃OH, CO, CH₂CHCl, and C₂HCl₃. The challenge gas concentrations spanned 10 ppb to 50 ppm. Precise challenge gas concentrations were delivered over a

specified period of time with mass flow controllers. The operating temperatures for investigating the responses to the primary challenge gases were set at 22°C and 110°C. For the secondary challenge gases, only one temperature setting of 70°C was used.

Of the metal-doped phthalocyanine thin-films investigated, CuPc was found to be the most sensitive for detecting DMMP and BF₃. PbPc was found to be the most sensitive to NO₂, CH₃OH, CO, CH₂CHCl, and C₂HCl₃. For both thin-film types, the sensitivity increased as the thickness of the thin-films increased. The sensitivity was reduced at the higher operating temperature. Both metal-doped phthalocyanine films were most sensitive to a 1 ppm concentration of NO₂.

The selectivity of CuPc and PbPc for the binary challenge gas combinations revealed that the CHEMFET has the ability to detect two gases simultaneously. Even though the responses predominantly indicate the presence of a gas which generally has a stronger response, the computation of the selectivity showed that a second gas (at equal concentration to that of the stronger gas) can be detected. PbPc and CuPc were the most selective for NO₂. CuPc was also selective for DMMP and BF₃, which had respective selectivity values of 0.18 and 0.50 when combined with NO₂. PbPc was not selective for BF₃, but this film had was selective for DMMP

with a value of 0.33.

All challenge gas exposures for the film types and their respective thicknesses were reversible at both operating temperatures. To determine the most complete degree of reversibility, the length of time required to attain 90% of the CHEMFET's original baseline state was used. The challenge gas exposures that were less than 3 minutes in duration did not achieve a steady-state response during the time of exposure. Thus, the resulting time of reversibility was deemed to be inaccurate. As the duration of the challenge gas exposures were increased, the reversibility time also increased. In order to achieve a short reversibility, it was necessary to have a short exposure duration, a high operating temperature, and the thinnest possible chemically-sensitive film. CuPc and PbPc exhibited reversibility times twice as rapid for the high operating temperature compared to the low operating temperature.

6.2 Recommendations

This investigation demonstrated that the CHEMFET can be fabricated and evaluated to reveal valuable information concerning the detection of toxic gases. Additional data needs to be measured and recorded to further investigate and identify suitable film types and thicknesses to detect a

wide range of challenge gases. The use of the mass flow controllers enables the user to more precisely control the flow rates of the carrier and diluent gases, as well as the concentrations of the challenge gases. The following courses of action are recommended for future investigations of this field:

1. Evaluate the sensitivity and reversibility of other thin-films including, but not limited to: CoPc, NiPc, MgPc, ZnPc, succinyl chloride (SuCh), succinylcholine chloride (SuClCh), DFPase, 2-Naphthol(β), and L-Histidine Dihydrochloride [8, 20].

2. Modified the gas delivery system to enable formulating gas mixtures consisting of more than two challenge gases.

3. Evaluate the operating temperature of the test chamber. Within the permeation tubes, the emitted challenge gas concentration is determined by an isothermal thermostated water bath. The change in temperature of the test chamber with respect to the permeation tube could cause a change in the desired challenge gas concentration due to condensation.

4. Use calibrated release systems, such as permeation tubes, to ensure accuracy. The utilization of permeation tubes is highly recommended over the use of a syringe, for which problems were observed.

5. Automate the entire challenge gas and electrical characterization system. The measurement and recording of data is automated, but the gas delivery system is essentially under manual control. The mass flow controllers can be automated to release precise rates of flow for a specified period of time.

6. Investigate the behavior of the dc electrical resistance for increasing metal-doped phthalocyanine film thicknesses.

Appendix A

Data Acquisition Software

The programs listed in this section were used to assay and record the electrical measurements from the electrometer, gain/phase analyzer, impedance analyzer, digitizing oscilloscope, and the spectrum analyzer. The program code is PASCAL and was written by Capt John Wiseman [23] and Capt Thomas Jenkins [9]. Modifications were made by the author.

```
(*****)  
(*****)  
(*****)  
  
program gpib;  
  
{$I-}  
{$N+,E+}  
{$M 24000, 0, 655360}  
  
uses Dos, Crt;  
{$I TURBO4.INC}  
  
(*-----*)  
(* This program is for running the HP Gain/Phase *)  
(* Analyzer along with the HP-Spectral Analyzer, *)  
(* HP-O'Scope, Keithley Scanner Switch Matrix, *)  
(* Wavetek Switcher, and the Keithley Electrometer *)  
(*-----*)  
(*-----*)  
(* ----- Switching Matrix Information -----*)  
(* ----- Columns 6 thru 14 - IGEFET outputs-----*)  
(* ----- Row #1 for Gain/Phase Analyzer -----*)  
(* -----Row #3 for Spectral Analyzer-----*)  
(* -----Row #4 for O'Scope-----*)  
(*-----*)  
(* -----Rows 1 and 2 -----*)  
(* -----Columns 1-5 AC Impedance-----*)  
(* -----Columns 1-5 Electrometer-----*)  
(* -----Columns 16-20 G/P Analyzer Input-----*)  
(* -----Columns 21-25 Spectral Analyzer Input--*)  
(* -----Columns 26-30 O'Scope Input -----*)  
(* -----Column 36 Electrometer Voltage Source--*)  
(* -----Column 37 AC Impedance Signals -----*)
```

```

(* -----*)
(* ----- Wavetek Switches -----*)
(* -----Switches 1-11 for AC Impedance-----*)
(* -----Switches 1-11 for Electrometer-----*)
(* ----- Connection to Driven Gate -----*)
(* -----*)

const

  impsw_setup = 'B0371C0371B0372C0372X';
  closewave_for_dc = 'K1CK2CK3CK4CK5CK6CK7CK8CK9CK10CK11CI';
  closekeith_for_dc = 'B0371N0371XB0372N0372XB0361C0361X';
  openkeith_for_imp = 'B0361XN0361XB0371XC0371XB0372XC0372X';
  openwave_for_imp = 'K1OK2OK3OK4OK5OK6OK7OK8OK9OK10CK11CI';

type ExpInfoRec = record
    DIP_ID:integer;
    ExpLogNum:integer;
    FilePrefix:string;
    Gas:string;
    BathTemp:integer;
    FlowRate:integer;
    ChipTemp:integer;
    Humidity:integer;
    FilmType:string;
end;

TimerIndex=(G_P,DCR,PLS,SPE,ADM,TIM);

IGE = 1..9;

String120=string[120];

SAFileRec = record
    IGENUM : byte;
    ElapsedTime: single;
    Data: array [0..400] of integer;
    GasConc: integer;
end;

SABaseRec = record
    SAFreq: array [0..400] of single;
    Message: string;
    Data: array [0..400] of integer;
end;

OSFileRec = record
    IGENUM : byte;
    ElapsedTime : single;
    CH1Preamble: string120;

```

```

        CH2Preamble: string120;
        CH1Data: array [1..500] of integer;
        CH2Data: array [1..500] of integer;
        GasConc:integer;
    end;

GPFileRec = record
    IGENUM : byte;
    ElapsedTime : single;
    Gain: array [1..200] of integer;
    Phase: array [1..200] of integer;
    GasConc: integer;
end;

GPBaseRec = array [1..200] of single;

ImpFileRec = record
    IGENUM : byte;
    ElapsedTime : single;
    ADM: array [1..200] of single;
    Phase: array [1..200] of integer;
    GasConc:integer;
end;

ImpBaseRec = array [1..200] of single;

DCResRec = record
    IGENUM: byte;
    DCBias: integer;
    ElapsedTime: single;
    Resist: single;
    GasConc:integer;
end;

var

HPGainPhase,K706,WaveTek,MyAddr,HPSpectrum,HPScope,K617:integer;
Elapsed_Time_IGE:array [TimerIndex,1..9] of single;
HP4145:integer;
ElapsedTime : single;
DCTimer : single;
SettleTime: single;
stepper, OSMaXInt : integer;
SuperMain, Main, DiskCtr : integer;
IOError : word;
filetest: text;
DCBias : string;
DCBiasVal: single;

```

```

Poll,Stat:      integer;
Controller:     integer;
Query: Char;
Command:       string;
OSSens : string;
OSLimit : Boolean;
ExpInfo:ExpInfoRec;
OSRec : OSFileRec;
InputStr:string;
StrLen:integer;
CommDesc:sdesc;
IGECOUNTER:array [1..4] of IGE;
GasConc, IGECTRDC, prevIGECTRDC : integer;
PrevIGECOUNTER:array [1..4] of IGE;

GPBaseLineData: GPBaseRec;
ImpBaselineData: ImpBaseRec;
SABaselineData: SABaseRec;

Hdr:file of ExpInfoRec;
SABaseFile: file of SABaseRec;
SAFile : file of SAFileRec;
OSFile: file of OSFileRec;
GPFile: file of GPFileRec;
GPBaseFile : file of GPBaseRec;
ImpFile : file of ImpFileRec;
ImpBaseFile : file of ImpBaseRec;
DCResFile : file of DCResRec;
label NextConc;

procedure Beep;
begin
  sound(100);
  delay(100);
  sound(300);
  delay(100);
  sound(500);
  delay(100);
  nosound;
end;{Beep}

procedure OStrig; Forward;
procedure SATrig; Forward;
procedure GPTrig; Forward;

{$I STRCONV.PAS}
{$I 488SUBS.PAS}
{$I TIMERS.PAS}
{$I RRINTR.PAS}
{$I FNHANDL.PAS}

```

```

{$I SWSUBS.PAS}
{$I DCSUBS.PAS}
{$I GPSUBS.PAS}
{$I OSSUBS2.PAS}
{$I SASUBS.PAS}
{$I IMPSUBS.PAS}
{$I INITSUBS.PAS}
{$I NEWDISK.PAS}

begin
  Init;
  SettleTime:=20;
  GetExpInfo(ExpInfo);
  InstrConfig;
  SetTime(0,0,0,0);      {Initialize Timer to zero}
  NewDisk;

  {***** Set-up for Main Segment 1 *****}

  repeat
    for SuperMain := 1 to 1 do begin
      if DiskCtr>2 then begin
        NewDisk;
        DiskCtr:=1;
      end
      else inc(DiskCtr);
      ClrScr;
      Beep;
      write('Enter the Gas Concentration in ppb: ');
      readln(GasConc);
      DCTimer:=Timer+SettleTime;
      Send488(HPGainPhase,'GET1');
      Send488(HPGainPhase,'AOF1; BOF1');
      Send488(Wavetek,CloseWave_For_DC);
      Send488(K706,CloseKeith_For_DC);

      {***** Done with Main 1 Set-up *****}

      for Main:= 1 to 36 do begin
        ClrScr;
        textcolor(lightred);
        writeln('>>>>>> Main 1 at ', Main);
        textcolor(green);
        for stepper:= 1 to 10 do begin
          if DCTimer<Timer then DCResistance;
          case stepper of
            1: SATrig;
            2: GPTrig;
            3: GPWait;
            4: SAWait;

```

```

        5: OStrig;
        6: OSWait;
        7: OSDump;
        8: begin ACOpener; ACCloser; end;
        9: GPDump;
       10: SADump;
    end; {case}
end; {stepper}
end; {Main 1 Loop}
end; {SuperMain}

{***** End of Main Segment 1 *****}

{***** Main Segment 2 *****}

    Goto NextConc;
    Send488(HPGainPhase,'GET2');
    Send488(HPGainPhase,'OPN1');
    Send488(K706, OpenKeith_For_Imp);
    Send488(WaveTek,OpenWave_For_Imp);
    DCOpener; {Open the Last DC Resist Measurement
Switches}
    IGECOUNTER[4]:=9;
    ImpCloser; {Close first set of switches for Impedance
Measurement}
    Delay(30000);

{***** Done With Main Segment 2 Set-up*****}

{***** Main Segment 2 *****}

    if DiskCtr>2 then begin
        NewDisk;
        DiskCtr:=1;
    end
    else inc(DiskCtr);

    ClrScr;
    write('Enter the Gas Concentration in ppb: ');
    readln(GasConc);
    for Main := 1 to 45 do begin
        ClrScr;
        textcolor(lightred);
        writeln('>>>>>>> Main 2 at ', Main);
        textcolor(green);
        ImpTrig;
        SATrig;

        ImpWait;

```



```

    SAwait;
    OStrig;
    OSWait;
    OSDump;

    ACOpener; ACCloser; ImpOpener; ImpCloser;
    ImpDump;
    SADump;

    end; {Main Loop 2};
    DCTimer := Timer + Settletime;
    ImpOpener;
    DCCloser;

{***** End of Main Segment 2 *****}

{***** Query User for More Data Collection ****}

NextConc:Beep;
    writeln('Do You Wish To Collect More Data (Y/N)');
    readln(Query);
    until (Query in ['N','n']);
    assign(filetest,'Header.tmp');
    reset(filetest);
    IOError:=IOResult;
    if IOError=2 then begin
        writeln('New Disk has not been Requested');
        write('Please Reinsert Previous Disk, Press <Enter>
When Ready');
        readln;
    end
    else close(filetest);
end.

```

Appendix B

Supplemental Plots for CuPc/NO₂ Experiments

The plots include dc resistance versus time, gain versus frequency, and the resistance and reactance parts of the impedance versus frequency. The representative film thickness is 1000 Å and the representative challenge gas concentration is 1 ppm.

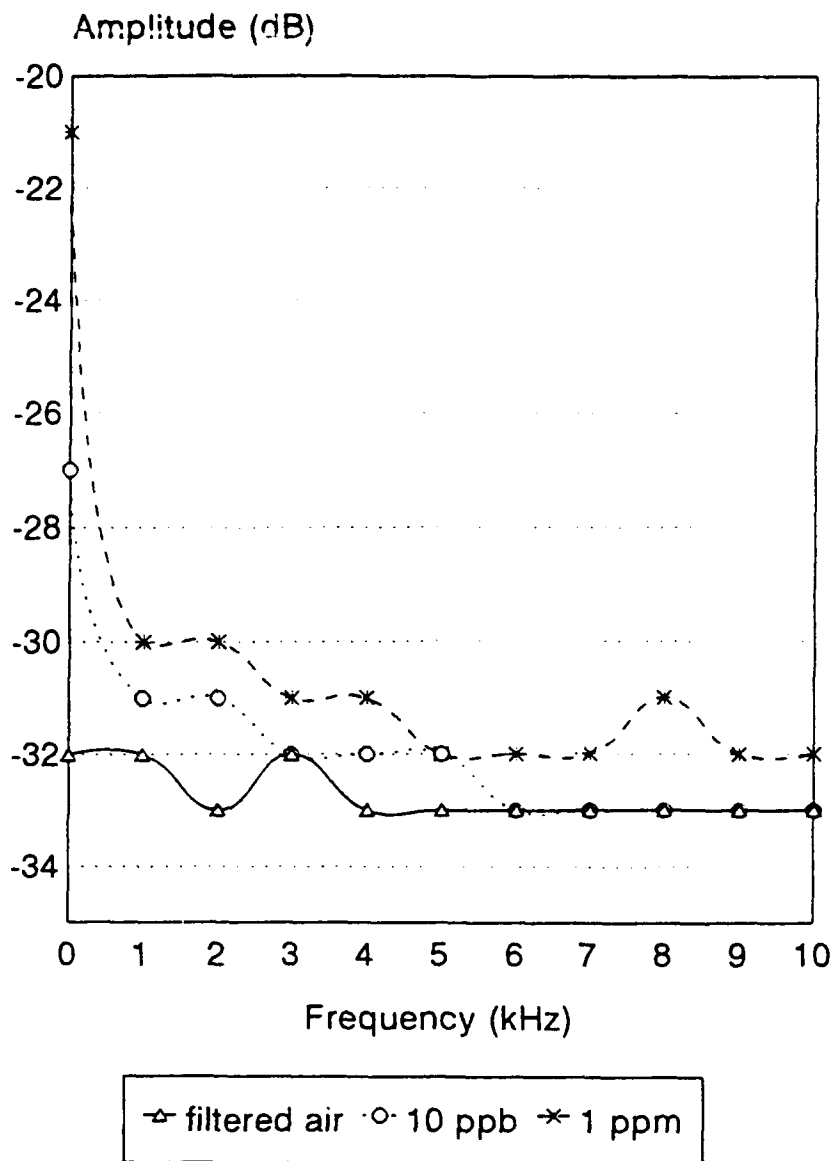


Figure B.1: Low Frequency Response of 1000 Å CuPc Film when Exposed to 10 ppb and 1ppm of NO₂ at 22°C.

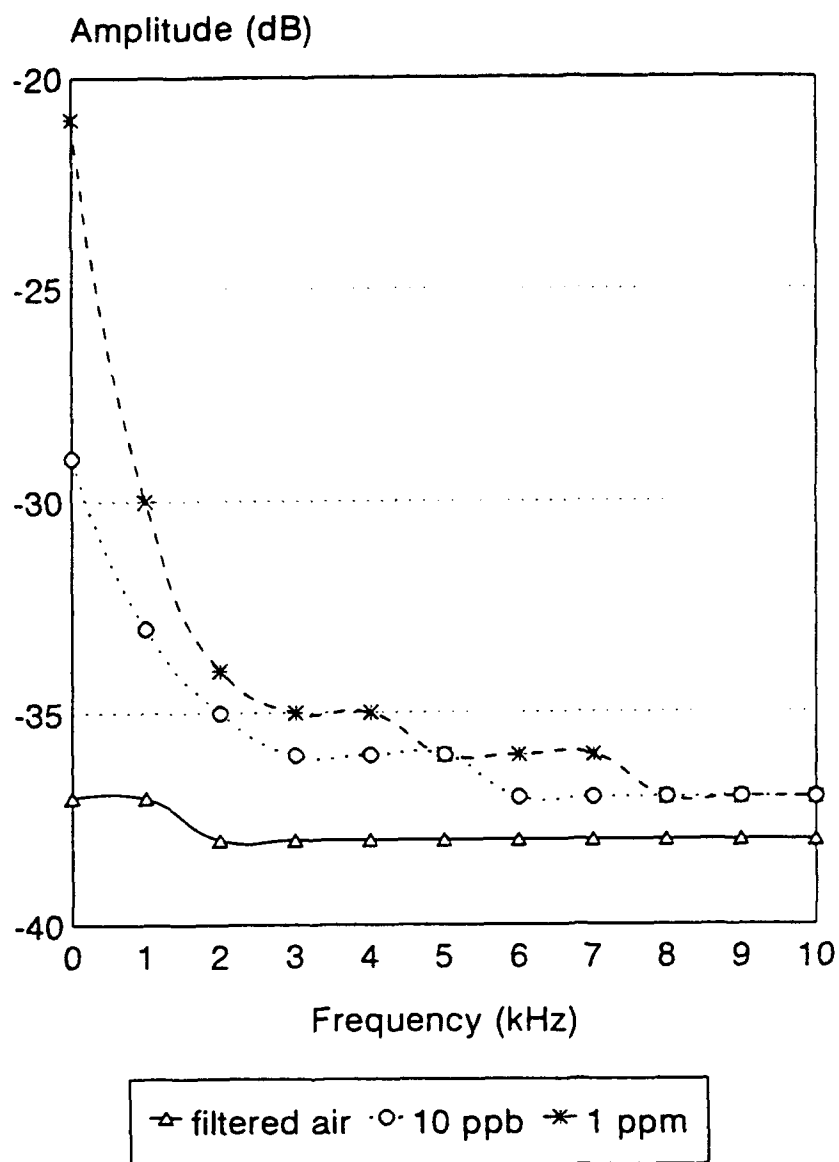


Figure B.2: Low Frequency Response of 1000 Å CuPc Film when Exposed to 10 ppb and 1ppm of NO₂ at 110°C.

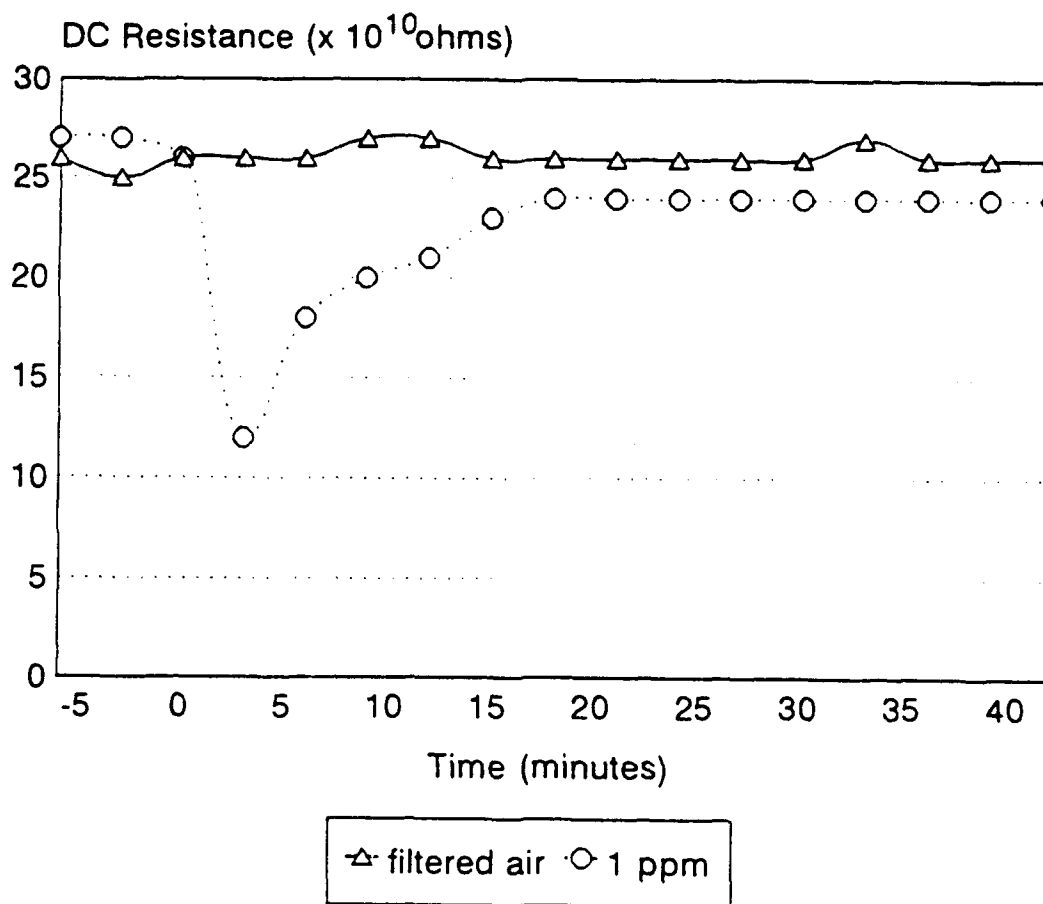


Figure B.3: Resistance versus Time of 1000 Å CuPc Film when Exposed to 1 ppm of NO_2 at 22°C.

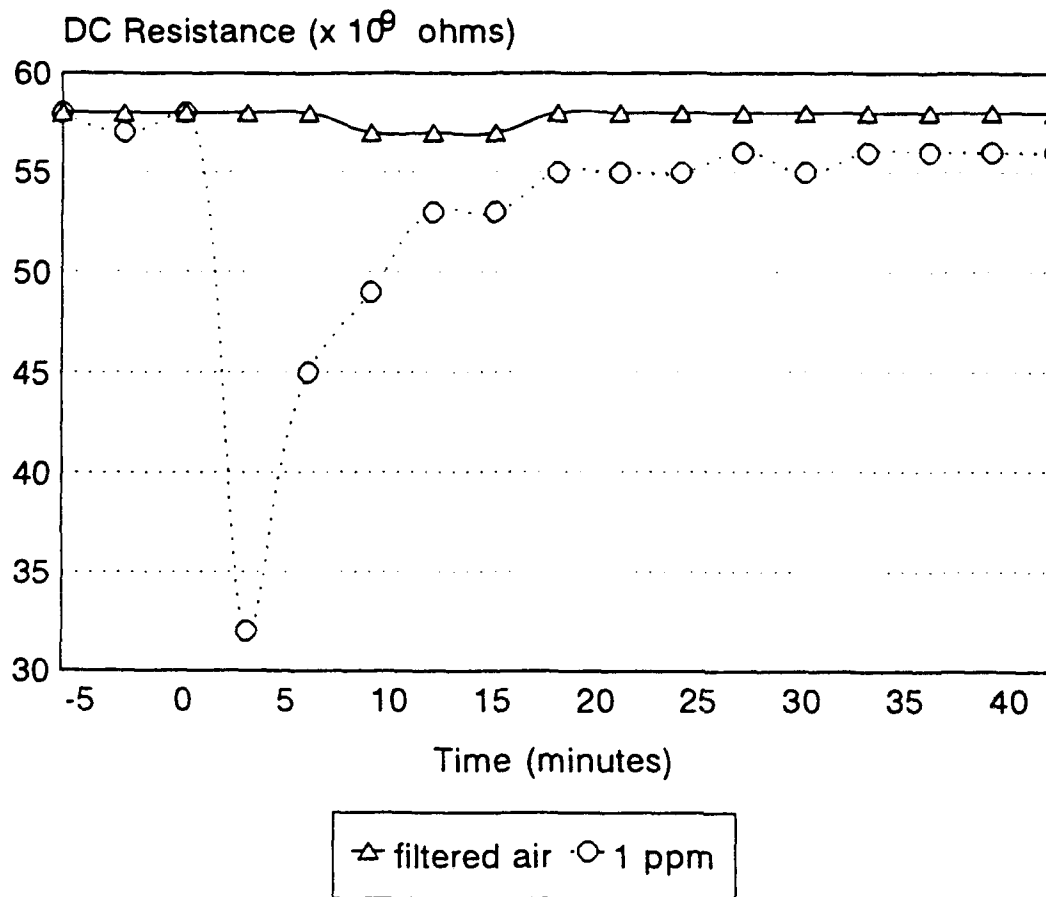


Figure B.4: Resistance versus Time of 1000 Å CuPc Film when Exposed to 1 ppm of NO_2 at 110°C.

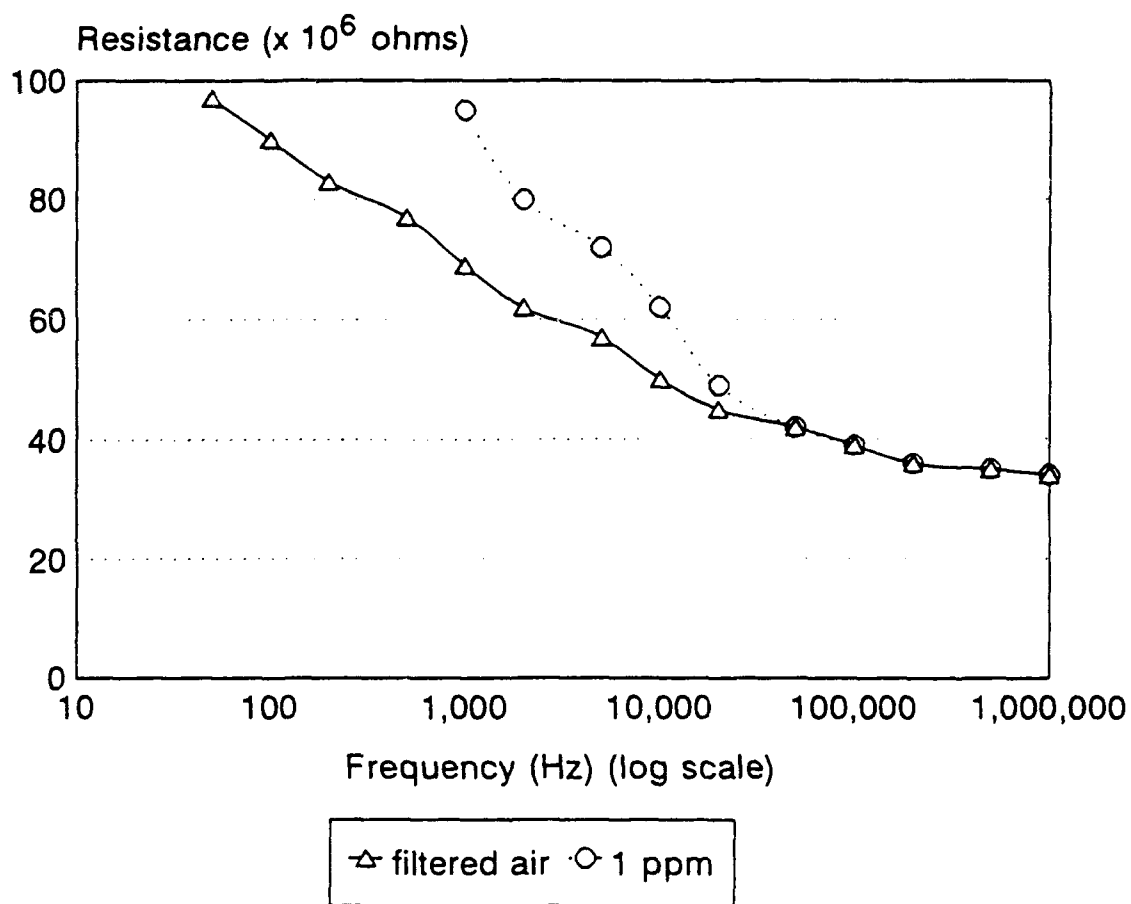


Figure B.5: Resistance Part of the Impedance of 1000 Å CuPc Film when Exposed to 1 ppm of NO_2 at 22°C.

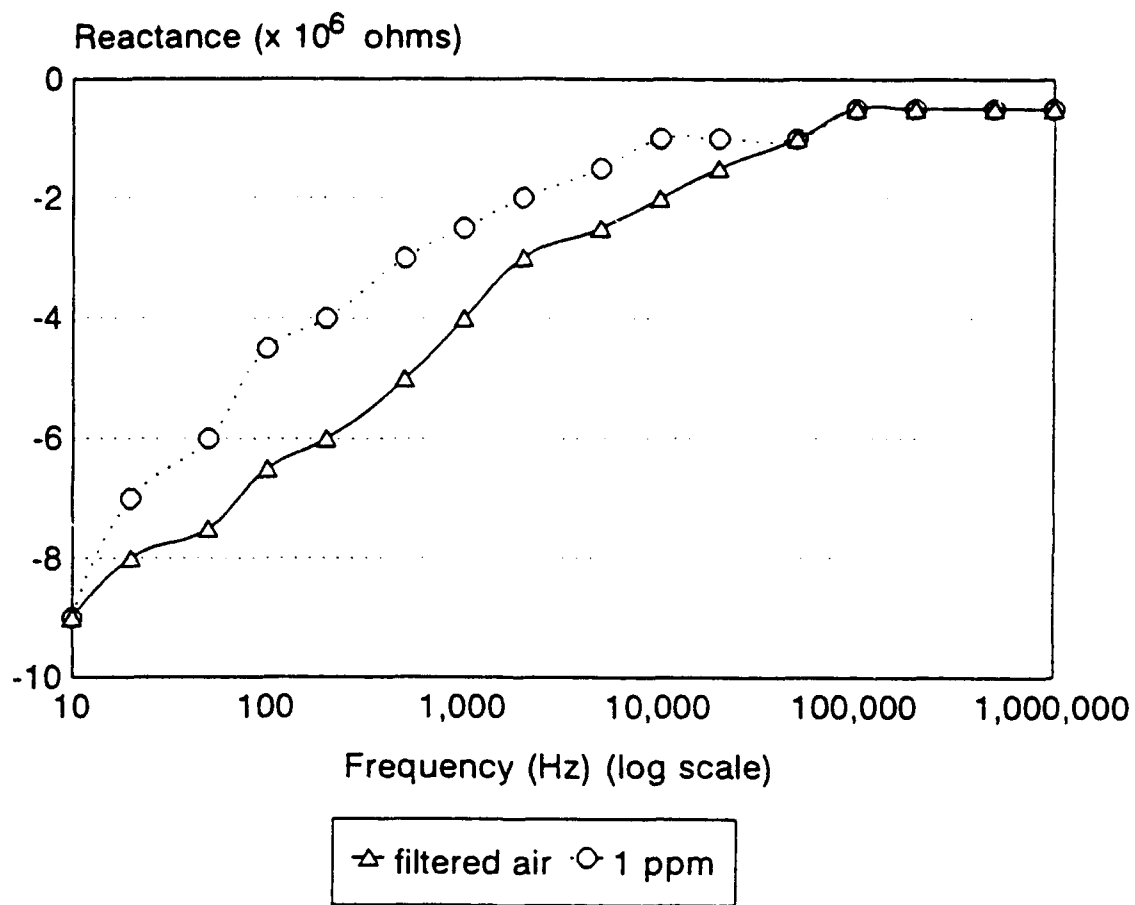


Figure B.6: Reactance Part of the Impedance of 1000 Å CuPc Film when Exposed to 1 ppm of NO_2 at 22°C.

Appendix C

Supplemental Graphs for CuPc/DMMP Experiments

The graphs include dc resistance versus time, gain versus frequency, and the resistance and reactance parts of the impedance versus frequency. The representative film thickness is 1000 Å and the representative challenge gas concentration is 10 ppm.

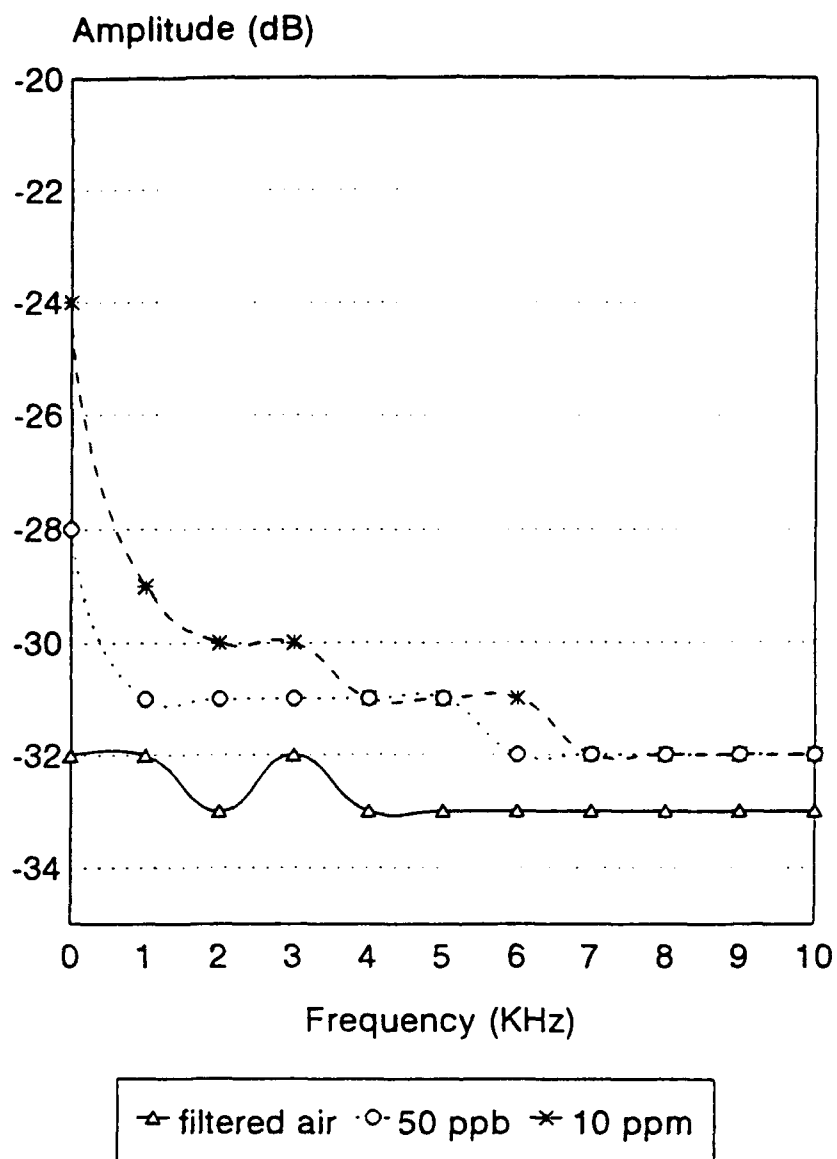


Figure C.1: Low Frequency Response of 1000 Å CuPc Film when Exposed to 50 ppb and 10 ppm of DMMP at 22°C.

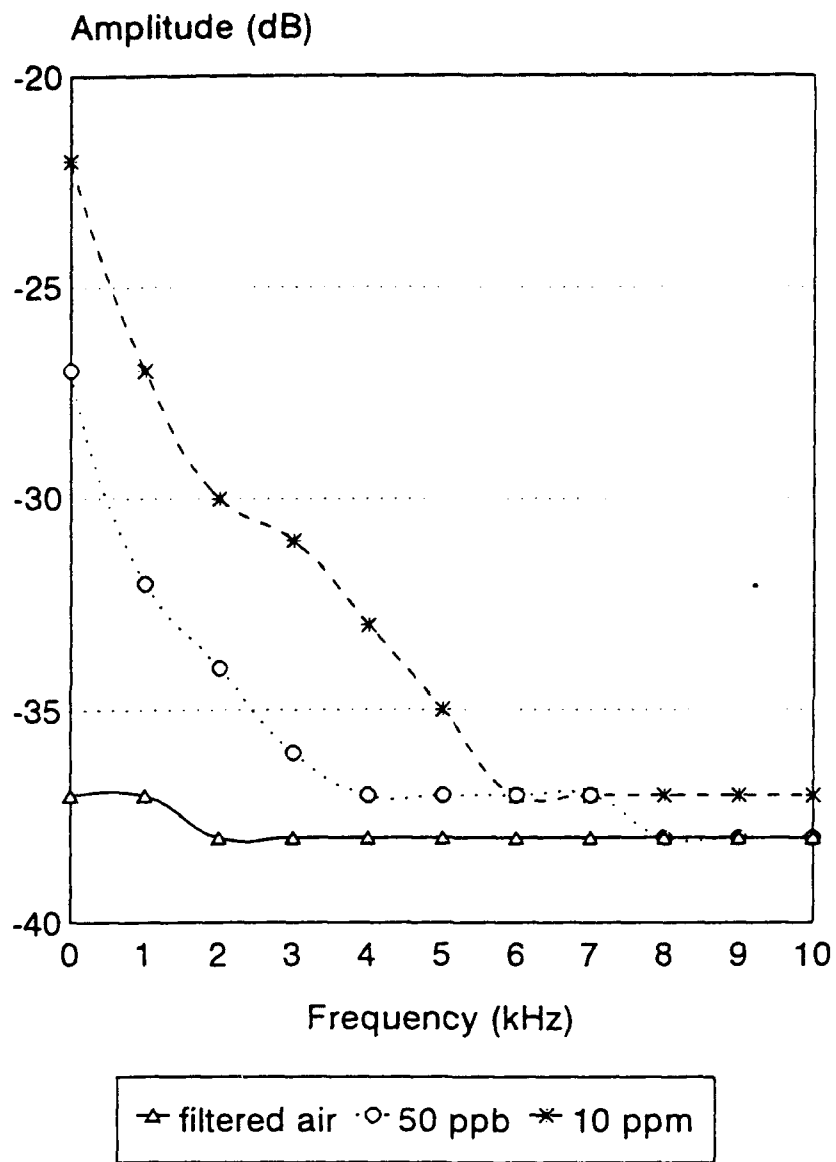


Figure C.2: Low Frequency Response of 1000 Å CuPc Film when Exposed to 50 ppb and 10 ppm of DMMP at 110°C.

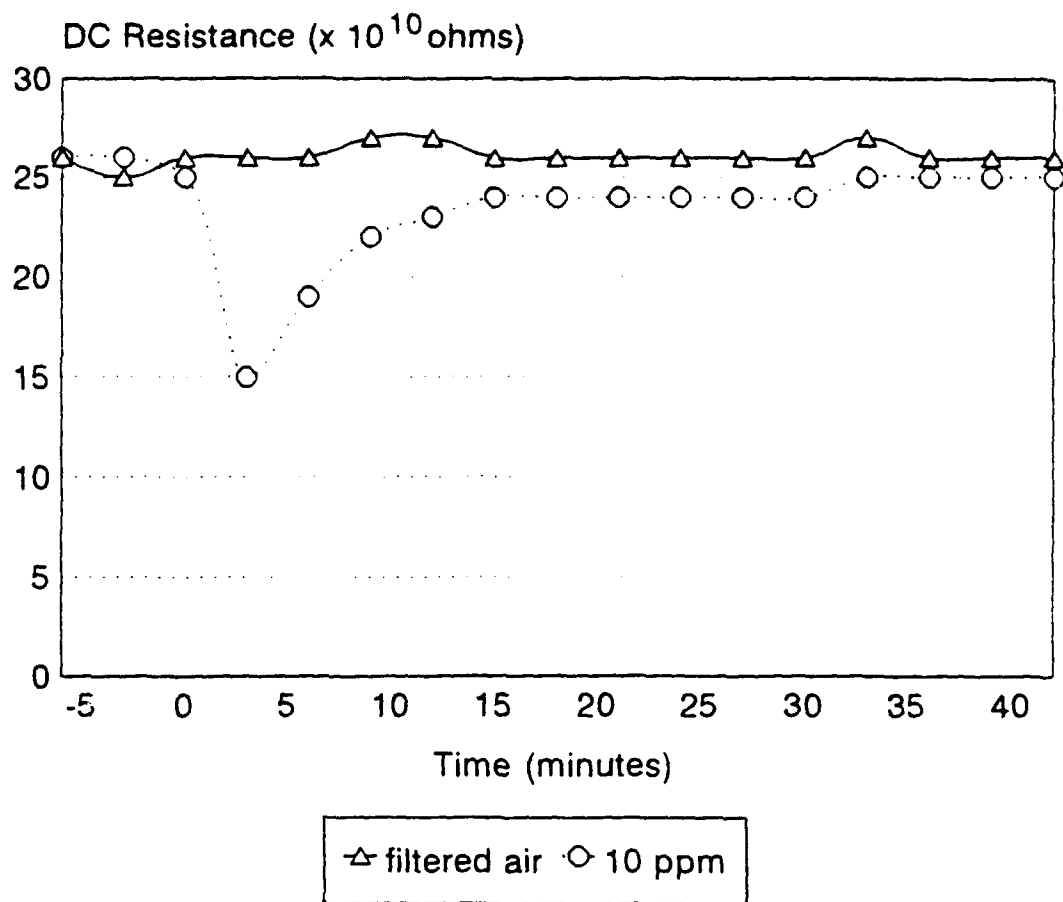


Figure C.3: Resistance versus Time of 1000 Å CuPc Film when Exposed to 10 ppm of DMMP at 22°C.

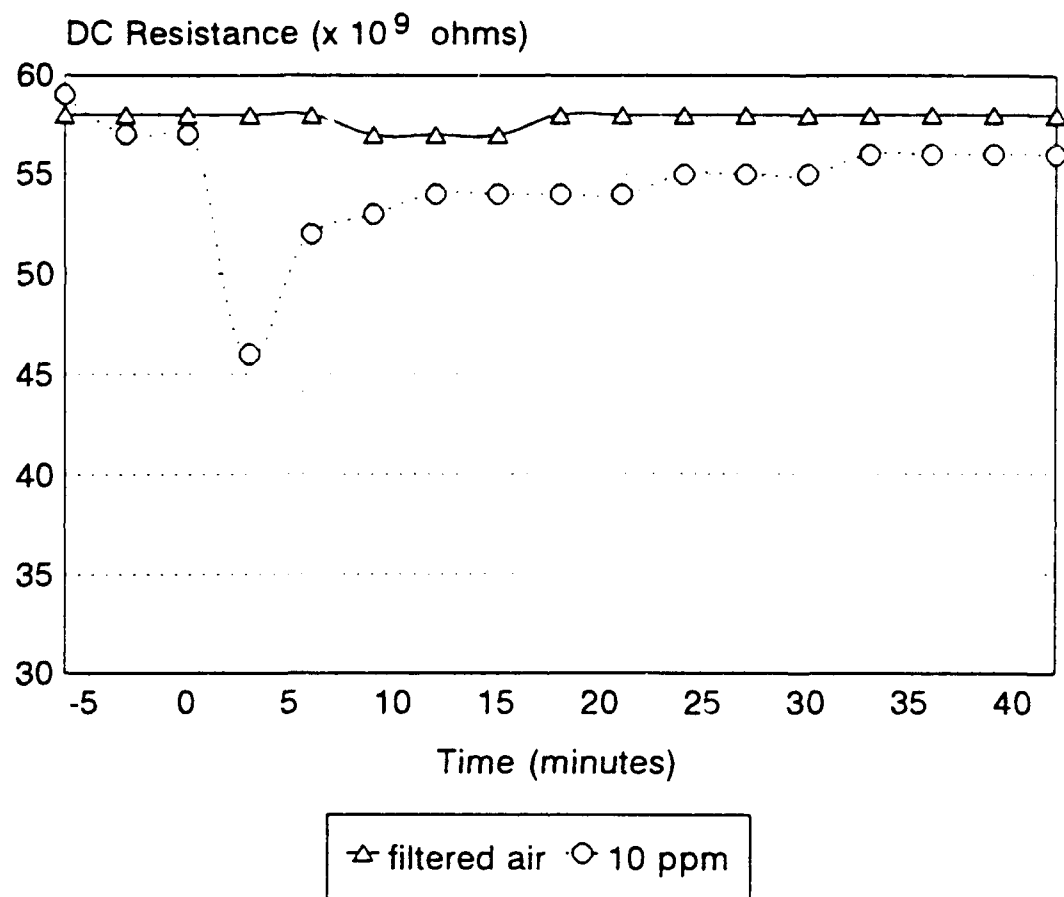


Figure C.4: Resistance versus Time of 1000 Å CuPc Film when Exposed to 10 ppm of DMMP at 110°C.

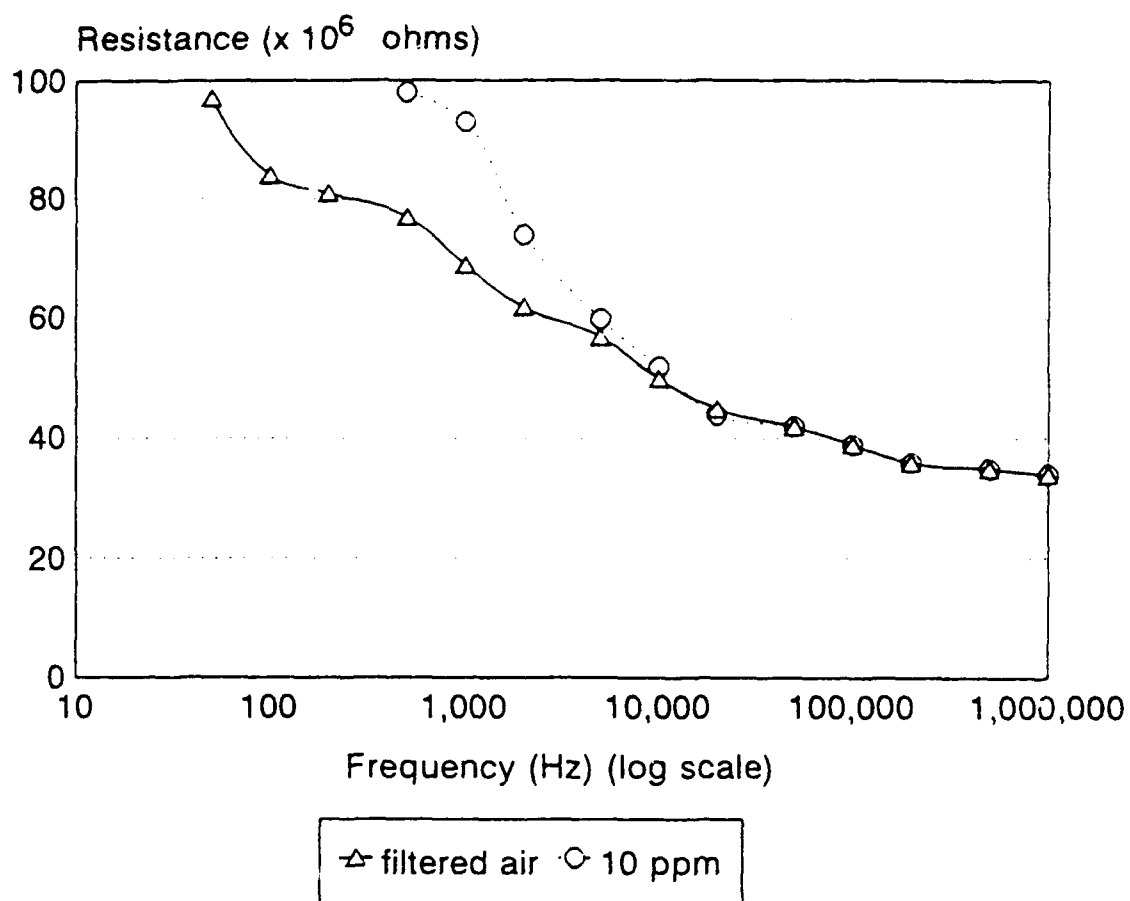


Figure C.5: Resistance Part of the Impedance of 1000 Å CuPc Film when Exposed to 10 ppm of DMMP at 22°C.

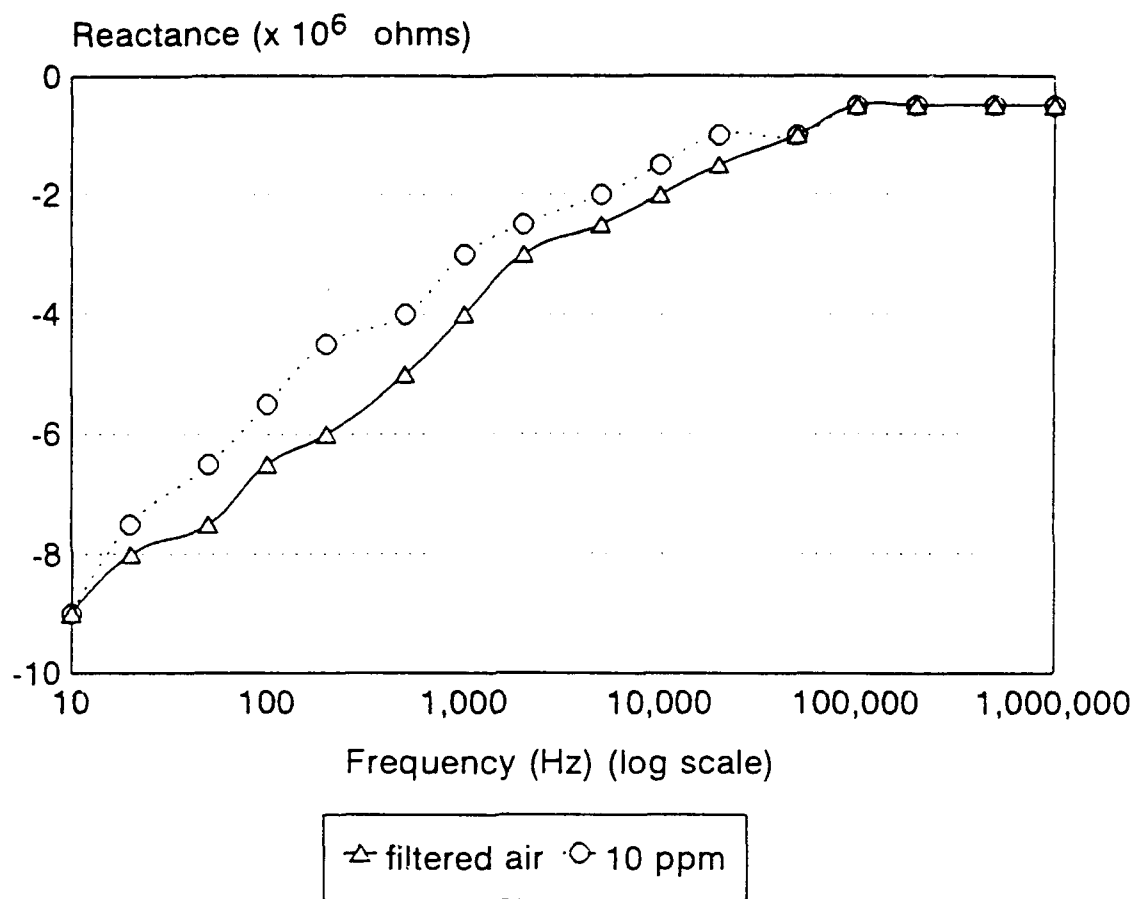


Figure C.6: Reactance Part of the Impedance of 1000 Å CuPc Film when Exposed to 10 ppm of DMMP at 22°C.

Appendix D

Supplemental Graphs for CuPc/BF₃ Experiments

The graphs include dc resistance versus time, gain versus frequency, and the resistance and reactance parts of the impedance versus frequency. The representative film thickness is 1000 Å and the representative challenge gas concentration is 20 ppm.

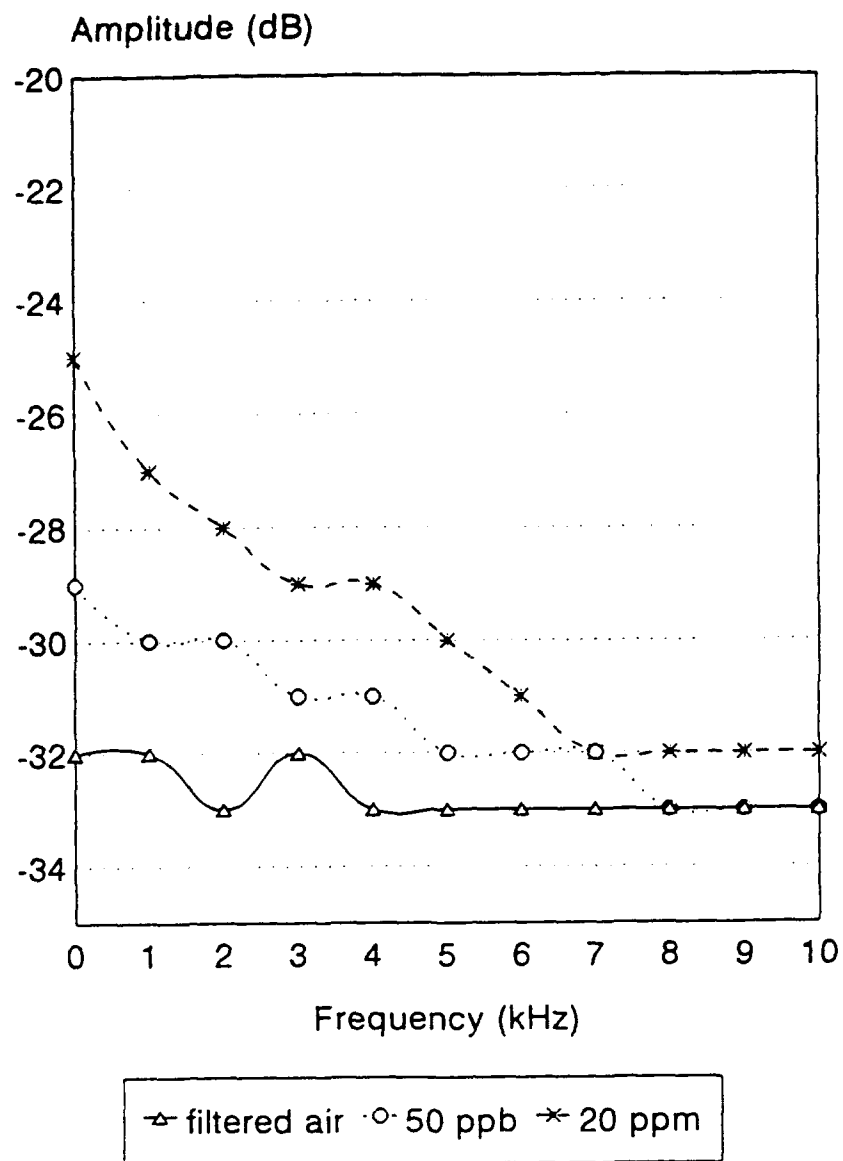


Figure D.1: Low Frequency Response of 1000 Å CuPc Film when Exposed to 50 ppb and 20 ppm of BF_3 at 22°C.

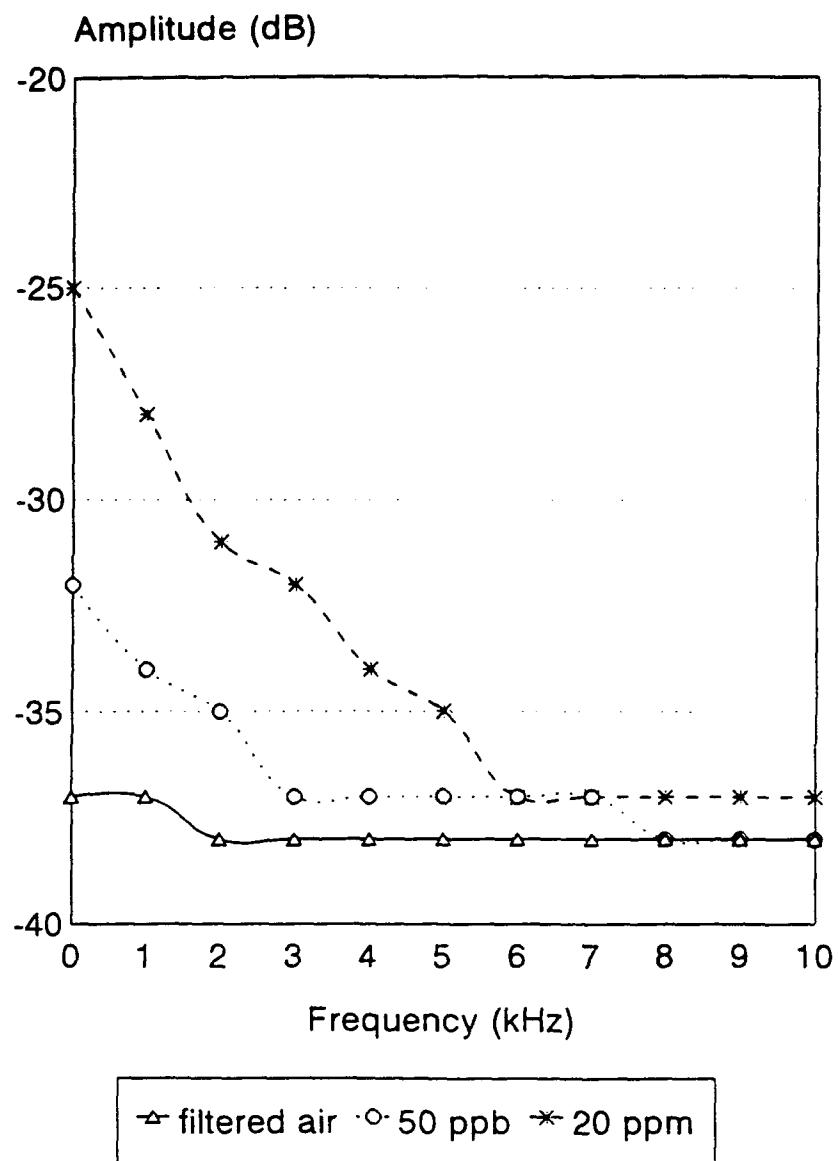


Figure D.2: Low Frequency Response of 1000 Å CuPc Film when Exposed to 50 ppb and 20 ppm of BF_3 at 110°C .

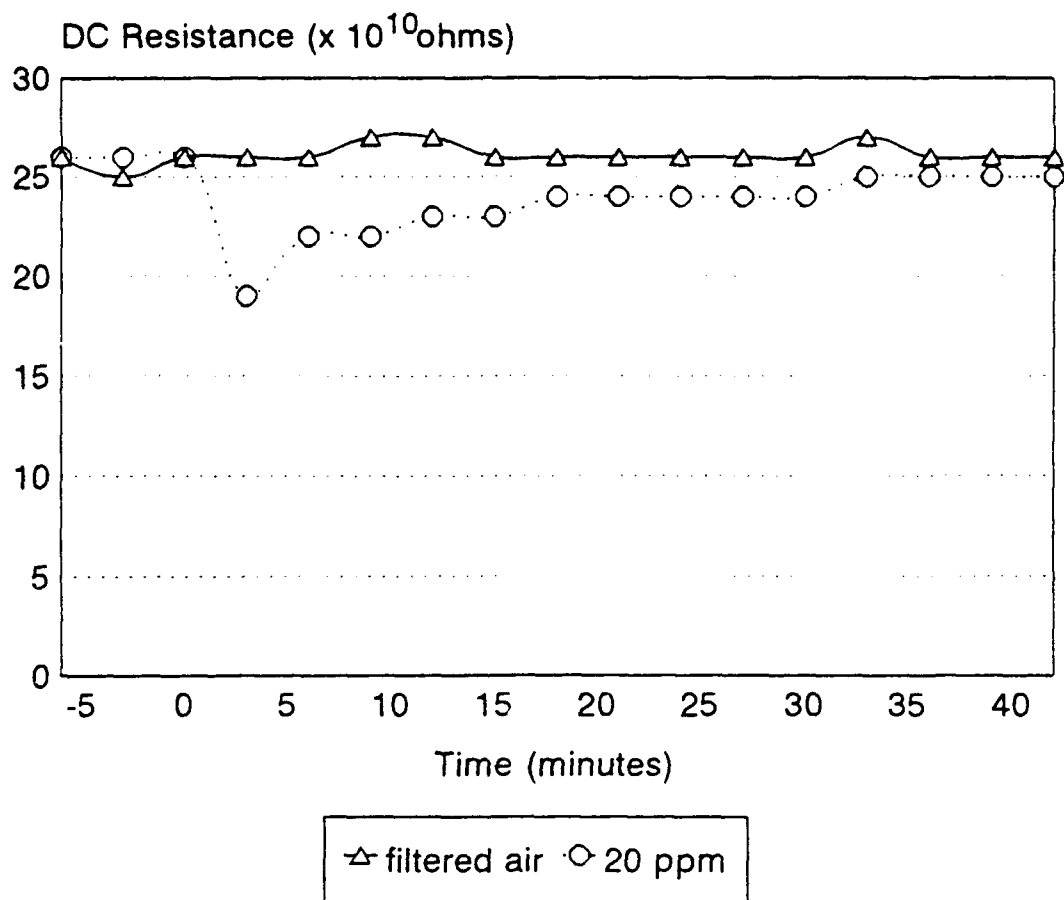


Figure D.3: Resistance versus Time of 1000 Å CuPc Film when Exposed to 20 ppm of BF_3 at 22°C.

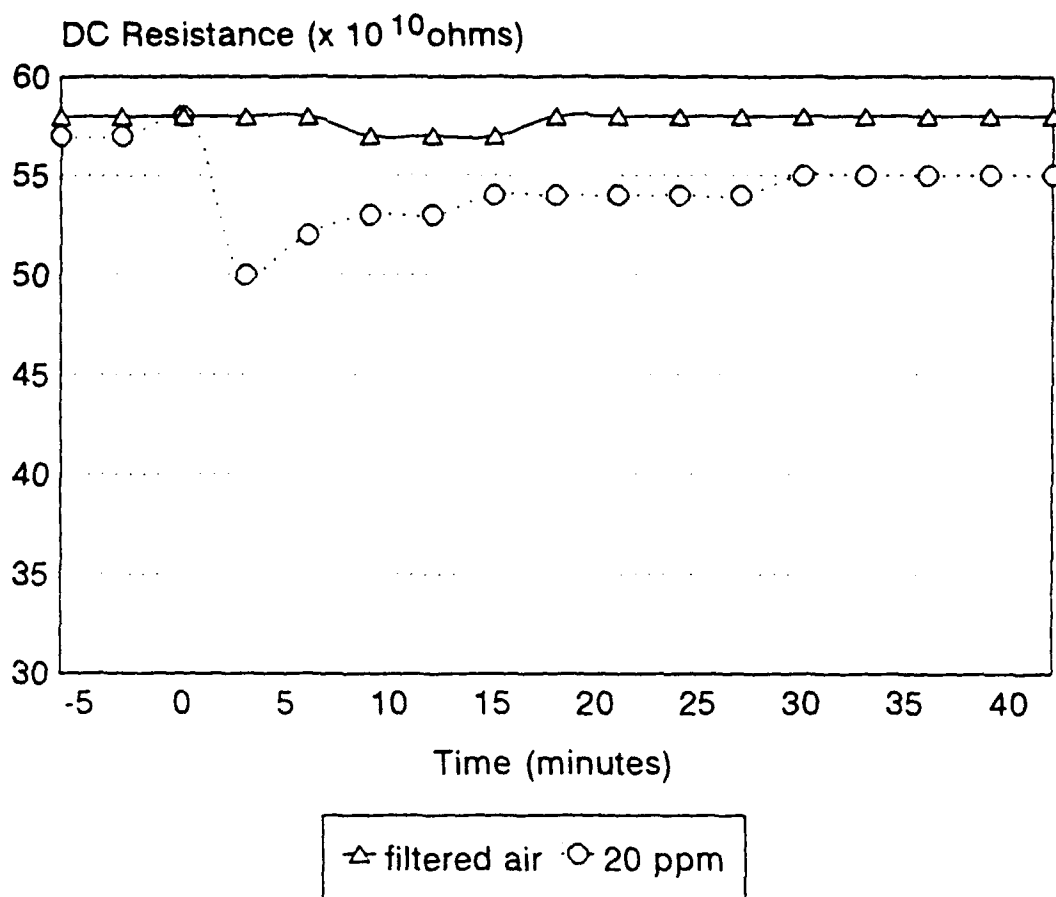


Figure D.4: Resistance versus Time of 1000 Å CuPc Film when Exposed to 20 ppm of BF_3 at 110°C .

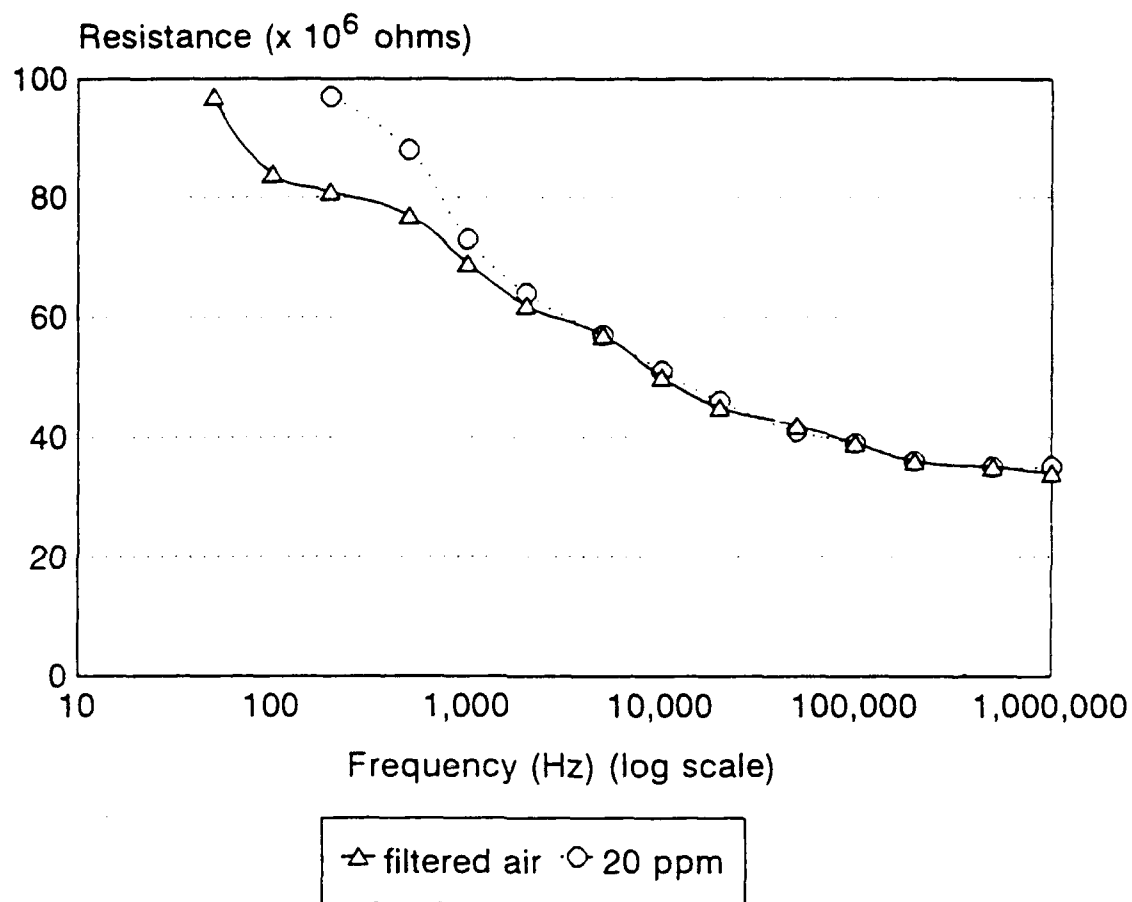


Figure D.5: Resistance Part of the Impedance of 1000 Å CuPc Film when Exposed to 20 ppm of BF_3 at 22°C.

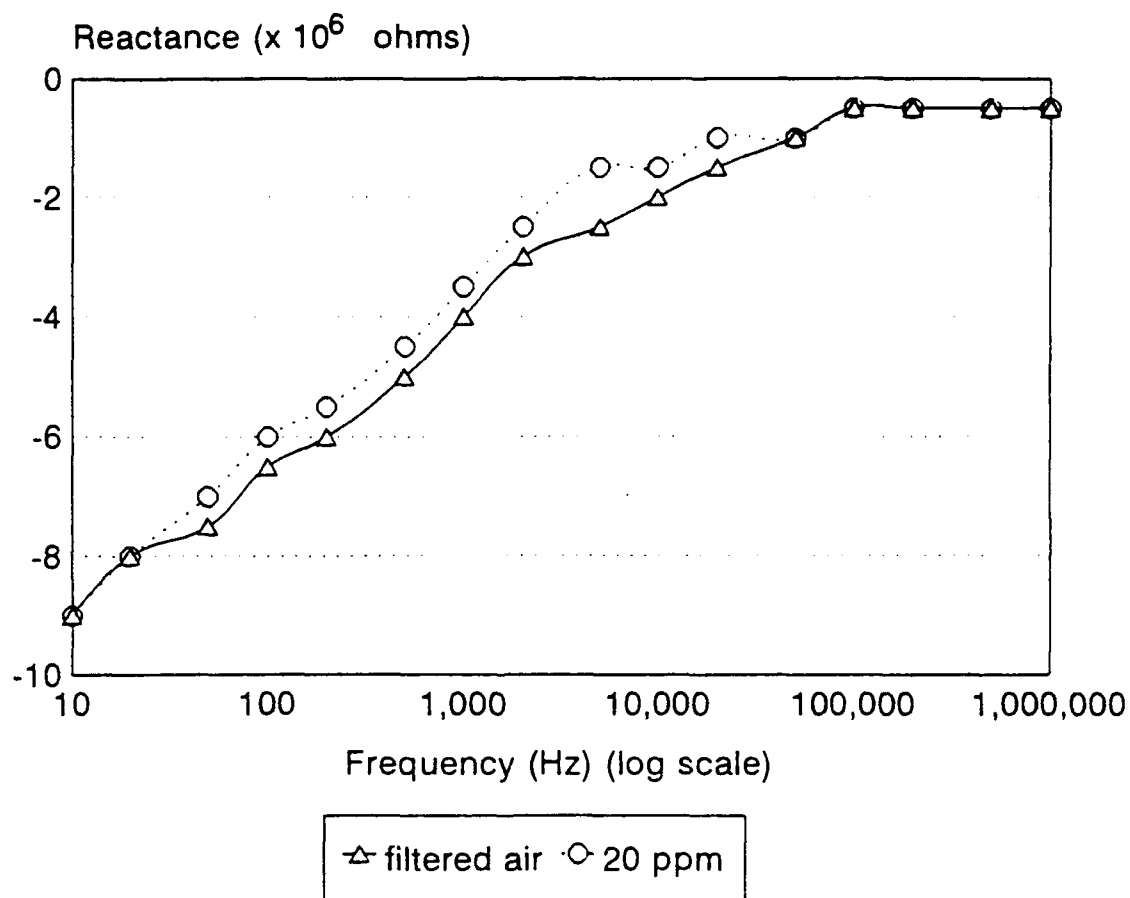


Figure D.6: Reactance Part of the Impedance of 1000 Å CuPc Film when Exposed to 20 ppm of BF_3 at 22°C.

Bibliography

- [1] S. Baker, G. Roberts, and M. Petty. "Phthalocyanine Langmuir-Blodgett Film Gas Detector", IEEE Proceedings. vol. 130, pp. 260-263, October 1983.
- [2] R.A. Beaudet and M. Withers. Test and Evaluation Plan for Chemical Defense Detectors: Generic Test Plan. U.S. Army Research Office, Human Systems Division. Contract DAA G29-81-0100-TCN84-511, May 1985.
- [3] B. Bolto. "Semiconducting Organic Polymers Containing Metal Groups", Organic Semiconducting Polymers. (J. Katon, ed.). New York: Marcel Dekker, Inc., 1968.
- [4] B. Bott and T.A. Jones. "The Use of Multisensor Systems in Monitoring Hazardous Atmospheres", IEEE Proceedings of the Third International Conference on Solid-State Sensors and Actuators Digest of Technical Papers. vol. 21, pp. 81-84, 1985.
- [5] S. Chang and D. Hicks. "Tin Oxide Microsensors", General Motors Research Report. GMR-4954. Electronics Department, General Motors Research Laboratories, Warren, Michigan, February 19, 1985.
- [6] G. Guilbault, Y. Tomita, and E. Kolesar. "A Coated Piezoelectric Crystal for Detection of Organophosphorus Compounds and Pesticides", Sensors and Actuators. vol. 2, pp. 43-47, 1981.
- [7] F. Gutierrez-Monreal and C. Mari. "The Use of Polymer Materials as Sensitive Elements in Physical and Chemical Sensors", Sensors and Actuators. vol. 12, pp. 129-144, 1987.
- [8] C.L. Howe. Characterizing the Sensitivity, Selectivity, and Reversibility of the Metal-Doped Phthalocyanine Thin-Films Used with the Interdigitated Gate Electrode Field-Effect Transistor (IGFET) to Detect Organophosphorus Compounds and Nitrogen Dioxide. MS Thesis, AFIT/GE/ENG/91D-26. Department of Electrical and Computer Engineering, Air Force Institute of Technology (AU), Wright-Patterson AFB, OH, December 1991.

- [9] T.J. Jenkins. Evaluation of Doped Phthalocyanines and a Chemically-Sensitive Field-Effect Transistor for Detecting Nitrogen Dioxide. MS Thesis, AFIT/GE/ENG/89D-18. Department of Electrical and Computer Engineering, Air Force Institute of Technology (AU), Wright-Patterson AFB, OH, December 1989.
- [10] J. Janata. Principles of Chemical Sensors. New York: Plenum Publishing Corp., 1989.
- [11] T.A. Jones and B. Bott. "Gas-Induced Electrical Conductivity in Metal Phthalocyanines", Sensors and Actuators. vol. 9, pp. 27-37, 1986.
- [12] T.A. Jones and B. Bott. "Fast Response Metal Phthalocyanine-Based Gas Sensors", Sensors and Actuators. vol. 17, pp. 467-474, May 1989.
- [13] E.S. Kolesar, Jr. Electronic Detection of Low Concentrations of Organophosphorus Compounds with a Solid-State Device Utilizing Supported Copper and Cuprous Oxide Island Films. PhD Dissertation. University of Texas, Austin, TX, AD-A158181, May 1985.
- [14] E.S. Kolesar, Jr. and J.M. Wiseman. "Interdigitated Gate Electrode Field-Effect Transistor for the Selective Detection of Nitrogen Dioxide and Diisopropyl Methylphosphonate", Analytical Chemistry, vol. 61, pp. 2355-2361, 1989.
- [15] R. Lucklum and B. Mann. "Quartz Microbalance Sensors for Gas Detection", Sensors and Actuators. vol. 4, pp. 499-504, 1991.
- [16] H. Mockert, D. Schmeisser, and W. Gopel. "Lead Phthalocyanine as a Prototype Organic Material for Gas Sensors", Sensors and Actuators. vol. 19, pp. 159-176, 1989.
- [17] J. Murday. "Performance Limits of Chemical Microsensor Technology", Proceedings of the 1986 U.S. Army Chemical Research, Development and Engineering Center Scientific Conference on Chemical Defense Research. vol. 1, AD-B113-947, November 18-21, 1986.
- [18] G. Roberts, J. Batelly, and M. Petty. "Electronic Devices Incorporating Stable Phthalocyanine Langmuir-Blodgett Films", Electronics and Optics. vol. 2, pp. 113-123, July 1985.

- [19] E. Schiede and G. Guilbault. "Piezoelectric Detectors for Organophosphorus Compounds and Pesticides", Analytical Chemistry. vol. 44, pp. 1764-1768, September 1972.
- [20] J.E. Shin. Evaluation of Chemically-Sensitive Field-Effect Transistors for the Detection of Organophosphorus Compounds. MS Thesis, AFIT/GE/ENG/89D-47. Department of Electrical and Computer Engineering, Air Force Institute of Technology (AU), Wright-Patterson AFB, OH, December 1989.
- [21] P.W. Smith. "Cholinesterase Inhibition in Relation to Fitness to Fly," Aerospace Medicine. vol. 39, pp. 754-758, July 1968.
- [22] Y. Syrkin and M. Dyatkina. Structure of Molecules and the Chemical Bond. (M. Partridge and D. Jordan, trans.). New York: Dover Publications, 1964.
- [23] J.M. Wiseman. Investigation of the Impedance Modulation of Thin Films with a Chemically-Sensitive Field-Effect Transistor. MS Thesis, AFIT/GE/ENG/88D-61. Department of Electrical and Computer Engineering, Air Force Institute of Technology (AU), Wright-Patterson AFB, OH, December 1988.
- [24] H. Wohltjen and W. Barger. "Chemical Microsensors for Vapor Detection," Proceedings of the IEEE Solid-State Sensor Conference. vol. 3, pp. 42-43, 1984.
- [25] H. Wohltjen, G. Heiland, and W. Barger. "A Vapor Sensitive Chemiresistor Fabricated with Planar Microelectrodes and a Langmuir-Blodgett Organic Semiconductor Film", IEEE Transactions on Electron Devices. vol. 32, pp. 1170-1174, July 1985.
- [26] M.J. Willett. "Spectroscopy of Surface Reactions", Techniques and Mechanisms in Gas Sensing. (P.T. Moseley, J.O.W. Norris, and D.E. Williams, eds.). pp. 63-107, 1991.
- [27] B. Bott and S.C. Thorpe. "Metal Phthalocyanine Gas Sensors", Techniques and Mechanisms in Gas Sensing. (P.T. Moseley, J.O.W. Norris, and D.E. Williams, eds.). pp. 139-160, 1991.
- [28] E.S. Kolesar, Jr. "A Novel Toxic Gas Microsensor", ChemTech. vol. 22, pp. 504-510, 1992.

- [29] E.S. Kolesar, Jr. and J.M. Wiseman. "Selective Detection of Nitrogen Dioxide and Diisopropyl Methylphosphonate with an Interdigitated Gate Electrode Field-Effect Transistor", Sensors and Actuators. vol. 5, pp. 37-46, 1991.
- [30] E.S. Kolesar, Jr., J. Wiseman, T. Jenkins, A. Moosey, J. Shin, C. Brothers, and T. Graham. "Integrated Circuit Microsensor for Selectively Detecting Nitrogen Dioxide and Diisopropyl Methylphosphonate", Sensors and Actuators. vol. 220, pp. 30-37, 1992.
- [31] M. Prudenziati and B. Morten. "Thick-Film Sensors: an Overview", Sensors and Actuators. vol. 10, pp. 65-82, 1986.
- [32] G. Heiland and D. Kohl. "Problems and Possibilities of Oxidic and Organic Semiconductor Gas Sensors", Sensors and Actuators. vol. 8, pp. 227-233, 1985.
- [33] S.L. Rose-Pehrsson and D.B. Ballantine. "Data Analysis of Surface Acoustic Wave Device Coating Responses Using Pattern Recognition Methods", Proceedings of the 1986 US Army Chemical Research, Development and Engineering Center Scientific Conference on Chemical Defense Research. US Army Armament, Munitions & Chemical Command, Aberdeen Proving Ground, MD, June 1987.
- [34] I. Harvey, G.S.V. Coles, and J. Watson. "The Development of an Automatic Test Chamber for the Characterization of Gas Sensors", Sensors and Actuators. vol. 16, pp. 393-405, 1989.
- [35] C.P. Brothers. Evaluation of an Interdigitated Gate Electrode Field-Effect Transistor for Detecting Organophosphorus Compounds. MS Thesis, AFIT/GE/ENG/90D-07. Department of Electrical and Computer Engineering, Air Force Institute of Technology (AU), Wright-Patterson AFB, OH, December 1990.
- [36] S.A. Krutovertsev, S.I. Sorokin, A.V. Zorin, Y.A. Letuchy, and O.Y. Antonova. "Polymer Film-Based Sensors for Ammonia Detection", Sensors and Actuators. vol. B7, pp. 492-494, 1992.
- [37] S. Kanefusa and M. Nitta. "The Detection of H₂ Gas by Metal Phthalocyanine-Based Gas Sensors", Sensors and Actuators. vol. B9, pp. 85-90, 1992.

- [38] A.W.J. Cranny, J.K. Atkinson, P.M. Burr, and D. Mack. "A Comparison of Thick and Thin-Film Gas-sensitive Organic Semiconductor Compounds", Sensors and Actuators. vol. B4, pp. 169-174, 1991.
- [39] A. Heilmann, M. Muller, C. Hamonn, V. Lantto, and H. Torvela. "Gas Sensitivity Measurements on NO₂ Sensors Based on Lead Phthalocyanine Thin Films", Sensors and Actuators. vol. B4, pp. 511-513, 1991.
- [40] J.E. Darby, R.J. McIlroy, G. Revell, S.C. Thorpe, and A. Wilson. "Effect of Electron Acceptor Gases on Lead Oxide and Lead Phthalocyanine Thin Films: A Comparative Study", Sensors and Actuators. vol. B3, pp. 157-160, 1991.
- [41] J. Unwin and P.T. Walsh. "An Exposure Monitor for Chlorinated Hydrocarbons Based on Conductometry Using Lead Phthalocyanine Films", Sensors and Actuators. vol. 18, pp. 45-57, 1989.
- [42] A. Wilson and R.A. Collins. "Electrical Characteristics of Planar Phthalocyanine Thin Film Gas Sensors", Sensors and Actuators. vol. 12, pp. 389-403, 1987.
- [43] J.D. Wright. "Gas Adsorption on Phthalocyanines and its Effects on Electrical Properties", Progress in Surface Science. vol. 31, pp. 1-60, 1989.
- [44] Instrumentation Manual for Mass Flow Controllers and Mass Flow Meters. Tylan General, Torrance, California, 1991.
- [45] H. Wohltjen and A. Snow. "The Selective Detection of Vapors Using Surface Acoustic Wave Devices," IEEE Proceedings of the Third International Conference on Solid-State Sensors and Actuators Digest of Technical Papers. vol. 1, pp. 66-70, 1985.
- [46] T.A. Temofonte and K.F. Schoch. "Phthalocyanine Semiconductor Sensors for Room-Temperature ppb Level Detection of Toxic Gases", Journal of Applied Physics. vol. 65, pp. 1350-1355, February 1989.
- [47] J. Watson. "A Note on the Electrical Characterization of Solid-State Gas Sensors", Sensors and Actuators. vol. B8, pp. 173-177, 1992.

Vita

Lieutenant Neal T. Hauschild was born 12 November 1969 in Corvallis, Oregon. He graduated from West Springfield High School in Springfield, Virginia in 1988. He attended Duke University, where he participated in the Air Force Reserved Officer Training Corps. He graduated in May 1992 and received the degree of Bachelor of Science in Electrical Engineering and the degree of Bachelor of Science in Biomedical Engineering. He was commissioned in the United States Air Force in May 1992. He entered the School of Engineering, Air Force Institute of Technology in July 1992.

Permanent Address: 8817 Newport Ct
Springfield, VA 22153

REPORT DOCUMENTATION PAGE

Form Approved
OMB No 0704-0188

Public reporting burden for this collection of information is estimated to average 1 hour per response, including the time for reviewing instructions, searching existing data sources, gathering and maintaining the data needed, and completing and reviewing the collection of information. Send comments regarding this burden estimate or any other aspect of this collection of information, including suggestions for reducing this burden, to Washington Headquarters Services, Directorate for Information Operations and Reports, 1215 Jefferson Davis Highway, Suite 1204, Arlington, VA 22202-4302, and to the Office of Management and Budget, Paperwork Reduction Project (0704-0188), Washington, DC 20503.

| | | | | |
|----------------------------------------------------------------------------------------------------------------------------------------------------------------------------------------------------------------------------------------------------------------------------------------------------------------------------------------------------------------------------------------------------------------------------------------------------------------------------------------------------------------------------------------------------------------------------------------------------------------------------------------------------------------------------------------------------------------------------------------------------------------------------------------------------------------------------------------------------------------------------------------------------------------------------------------------------------------------------------------------------------------------------------------------------------------------------------------------------------------------------------------------------------------------------------------------------------------------------------------------------------------------------------------------------------------------------------------------------------------------------------------------|----------------------------------------------------------|---------------------------------------------------------|----------------------------------------------------------------|--|
| 1. AGENCY USE ONLY (Leave blank) | | 2. REPORT DATE September 1993 | 3. REPORT TYPE AND DATES COVERED Master's Thesis | |
| 4. TITLE AND SUBTITLE INVESTIGATION OF THE SENSITIVITY, SELECTIVITY, AND REVERSIBILITY OF THE CHEMFET TO DETECT NITROGEN DIOXIDE, DIMETHYL METHYLPHOSPHONATE AND BORON TRIFLUORIDE | | | 5. FUNDING NUMBERS | |
| 6. AUTHOR(S) Neal T. Hauschild, Second Lieutenant, USAF | | | | |
| 7. PERFORMING ORGANIZATION NAME(S) AND ADDRESS(ES) Air Force Institute of Technology, WPAFB OH 45433-6583 | | | 8. PERFORMING ORGANIZATION REPORT NUMBER AFIT/GE/ENG/93S-10 | |
| 9. SPONSORING / MONITORING AGENCY NAME(S) AND ADDRESS(ES) Dr. Dave Erwin Armstrong Laboratory (AL/OERD) Brooks AFB, TX 78235 | | | 10. SPONSORING / MONITORING AGENCY REPORT NUMBER | |
| 11. SUPPLEMENTARY NOTES | | | | |
| 12a. DISTRIBUTION / AVAILABILITY STATEMENT Approved for public release; distribution unlimited | | | 12b. DISTRIBUTION CODE | |
| 13. ABSTRACT (Maximum 200 words) This study investigated the sensitivity, selectivity, and reversibility of a chemically-sensitive field-effect transistor (CHEMFET) gas microsensor. Various physical operating parameters were tested to determine which produced the most significant sensitivity, selectivity, and reversibility which were computed from response changes generated from electrical conductivity modulations when exposed to challenge gases. The variable operating parameters included: thin-film material, film thickness, challenge gas specie, challenge gas concentration, and operating temperature. Copper phthalocyanine and lead phthalocyanine were used as thin films to detect the following challenge gases: nitrogen dioxide, dimethyl methylphosphonate, boron trifluoride, methanol, carbon monoxide, vinyl chloride, and trichloroethylene. Tests revealed that copper phthalocyanine was the most sensitive to dimethyl methylphosphonate and boron trifluoride, whereas lead phthalocyanine was the most sensitive to the remaining challenge gases. The CHEMFET was selective to the binary challenge gas combinations. The films were most selective for nitrogen dioxide. The CHEMFET was fully reversibly, and the time duration for full reversibility increased with increasing challenge gas concentrations and increasing time of exposure. | | | | |
| 14. SUBJECT TERMS | | | 15. NUMBER OF PAGES 259 | |
| | | | 16. PRICE CODE | |
| 17. SECURITY CLASSIFICATION OF REPORT Unclassified | 18. SECURITY CLASSIFICATION OF THIS PAGE Unclassified | 19. SECURITY CLASSIFICATION OF ABSTRACT Unclassified | 20. LIMITATION OF ABSTRACT UL | |

GENERAL INSTRUCTIONS FOR COMPLETING SF 298

The Report Documentation Page (RDP) is used in announcing and cataloging reports. It is important that this information be consistent with the rest of the report, particularly the cover and title page. Instructions for filling in each block of the form follow. It is important to *stay within the lines* to meet optical scanning requirements.

Block 1. Agency Use Only (Leave blank).

Block 2. Report Date. Full publication date including day, month, and year, if available (e.g. 1 Jan 88). Must cite at least the year.

Block 3. Type of Report and Dates Covered. State whether report is interim, final, etc. If applicable, enter inclusive report dates (e.g. 10 Jun 87 - 30 Jun 88).

Block 4. Title and Subtitle. A title is taken from the part of the report that provides the most meaningful and complete information. When a report is prepared in more than one volume, repeat the primary title, add volume number, and include subtitle for the specific volume. On classified documents enter the title classification in parentheses.

Block 5. Funding Numbers. To include contract and grant numbers; may include program element number(s), project number(s), task number(s), and work unit number(s). Use the following labels:

| | |
|----------------------|------------------------------|
| C - Contract | PR - Project |
| G - Grant | TA - Task |
| PE - Program Element | WU - Work Unit Accession No. |

Block 6. Author(s). Name(s) of person(s) responsible for writing the report, performing the research, or credited with the content of the report. If editor or compiler, this should follow the name(s).

Block 7. Performing Organization Name(s) and Address(es). Self-explanatory.

Block 8. Performing Organization Report Number. Enter the unique alphanumeric report number(s) assigned by the organization performing the report.

Block 9. Sponsoring/Monitoring Agency Name(s) and Address(es). Self-explanatory.

Block 10. Sponsoring/Monitoring Agency Report Number. (If known)

Block 11. Supplementary Notes. Enter information not included elsewhere such as: Prepared in cooperation with...; Trans. of...; To be published in... When a report is revised, include a statement whether the new report supersedes or supplements the older report.

Block 12a. Distribution/Availability Statement. Denotes public availability or limitations. Cite any availability to the public. Enter additional limitations or special markings in all capitals (e.g. NOFORN, REL, ITAR).

DOD - See DoDD 5230.24, "Distribution Statements on Technical Documents."

DOE - See authorities

NASA - See Handbook NHB 2200.2.

NTIS - Leave blank.

Block 12b. Distribution Code.

DOD - Leave blank.

DOE - Enter DOE distribution categories from the Standard Distribution for Unclassified Scientific and Technical Reports.

NASA - Leave blank.

NTIS - Leave blank.

Block 13. Abstract. Include a brief (*Maximum 200 words*) factual summary of the most significant information contained in the report.

Block 14. Subject Terms. Keywords or phrases identifying major subjects in the report.

Block 15. Number of Pages. Enter the total number of pages.

Block 16. Price Code. Enter appropriate price code (*NTIS only*)

Blocks 17. - 19. Security Classifications. Self-explanatory. Enter U.S. Security Classification in accordance with U.S. Security Regulations (i.e., UNCLASSIFIED). If form contains classified information, stamp classification on the top and bottom of the page.

Block 20. Limitation of Abstract. This block must be completed to assign a limitation to the abstract. Enter either UL (unlimited) or SAR (same as report). An entry in this block is necessary if the abstract is to be limited. If blank, the abstract is assumed to be unlimited.